Dispersion Polymerisations in Supercritical Carbon Dioxide for the Production of Core-Shell Particles

Kristoffer Konrad Kortsen, BSc, MSc, AMRSC





Thesis submitted to the University of Nottingham for the degree of Doctor of Philosophy

September 2022

Declaration

All work presented in this Thesis is the original work of the author, with the exception of results referenced to other sources. It has not been submitted as part of any other degree or professional qualification.

Signed:…… Date: …30/09/2022……

Kristoffer Konrad Kortsen

Abstract

Polymer additives are an essential part of the plastics industry. Impact modifiers are a class of additives widely used to improve impact resistance of typically brittle plastics. However, they are currently produced in water but sold as a dry powder, necessitating a very energy intensive spray-drying process. This thesis reports on the exploration of using CO_2 as the rection medium to produce impact modifiers, as this will allow the drying step to be bypassed, reducing overall energy costs by over 90%.

While polymerisations had been conducted in $scCO_2$ previously, three large questions appeared towards assessing the suitability of this solvent in producing impact modifiers. Firstly, reactions in $scCO_2$ have been difficult to monitor, so could we develop a more accessible monitoring method? secondly, what are the limits of the system and what are the effects of changing reaction conditions in $scCO_2$? Finally, impact modifiers are polymer particles with intricate core-shell morphology, so could we develop a synthesis method to achieve this morphology in $scCO_2$?

These questions were addressed one-by-one in this thesis. Firstly, using a novel sampling cylinder, a method was developed that allowed for the reliable on-line monitoring of a wide range of polymerisations. The sampling cylinder also helped to assess the effect of varying reactor conditions real time. It was discovered that, beyond conventional reactor loading effects, the pressure of the reactor affects particle size. Finally, the gained insights of kinetics and control were exploited to synthesise the first ever core-shell particles in $scCO_2$. While a very narrow operating window was determined, the fundamental understanding gained in this work showed it was possible to make core-shell particles with controlled domain ratios and sizes.

Acknowledgements

First of all, I would like to thank Professor Steve Howdle for bringing me to the UK and giving me the opportunity to complete this work in Nottingham. I would also like to thank Dr Sofie Sannen and Dr Harald Braun, from Kaneka Belgium NV, for funding the project and handpicking me to lead it. When I first started a placement at Kaneka in 2017, I could not even have imagined ending up where I am today, and it's all thanks to Sofie's belief in me!

A special thank you goes to Dr Vincenzo Taresco, who has been a better post doc and mentor than I could ever have dreamed of. His positive attitude and insistence that my work was good, really drove my project and ambitions throughout.

I'd also like to thank everyone in the workshops, and in particular Rich Wilson. I've taken a lot of Rich's time during my PhD with high-pressure issues and hairbrained ideas, but hopefully he has enjoyed it as much as I have.

A big thank you goes out to all my collaborators, both within the university and beyond. Working with brilliant minds is essential to a successful project and it has taught me so much more than I can express here.

I'd also like to thank everyone who's come through our B10 lab. Whether it was a 1-day visit or an entire PhD, you all contributed to an unforgettable workplace! I met a lot of people during my time in Nottingham, and while I leave the place with a heavy heart, I have gained some true friends that will stay with me for the rest of my life.

Finally, thanks to the mom, dad, Obbi, Olli, and Hat. 🤗

Publications related to this work

Chapter 3

1. K. Kortsen, A.A.C. Pacheco, J.C. Lentz, V. Taresco, S.M. Howdle, **On-line polymerisation monitoring in $scCO_2$: a reliable and inexpensive sampling method in high pressure applications**, The Journal of Supercritical Fluids, (2020) 105047, https://doi.org/10.1016/j.supflu.2020.105047.

2. A.A.C. Pacheco, A.F. da Silva Filho, K. Kortsen, M.W.D. Hanson-Heine, V. Taresco, J.D. Hirst, M. Lansalot, F. D'Agosto, S.M. Howdle, **Influence of structure and solubility of chain transfer agents on the RAFT control of dispersion polymerisation in $scCO_2$**, Chemical Science, 12 (2021) 1016-1030, https://doi.org/10.1039/D0SC05281G.

Chapter 4

3. Kortsen, K.; Fowler, H. R.; Jacob, P. L.; Krumins, E.; Lentz, J. C.; Souhil, M. R. A.; Taresco, V.; Howdle, S. M., **Exploiting the tuneable density of scCO2 to improve particle size control for dispersion polymerisations in the presence of poly(dimethyl siloxane) stabilisers**, *European Polymer Journal, (*2022) 111108, https://doi.org/10.1016/j.eurpolymj.2022.111108.

Symbols and abbreviations

AA	Acrylic Acid
ACOMP	Automatic Continuous On-Line Monitoring of Polymerisations
AFM	Atomic Force Microscopy
AIBN	2,2'-azobis(isobutyronitrile)
AIM	Acrylic Impact Modifier
AMA	Allyl Methacrylate
ATRP	Atom Transfer Radical Polymerisation
BA	Butyl Acrylate
BMA	Butyl Methacrylate
BzA	Benzyl Acrylate
CCTP	Catalytic Chain Transfer Polymerisation
$CDCl_3$	Deuterated Chloroform
CFC	Chlorofluorocarbon
CL	Caprolactone
CO_2	Carbon Dioxide
CPDT	2-Cyano-2-Propyl Dodecyl Trithiocarbonate
CRP	Controlled Radical Polymerisation
CTA	Chain Transfer Agent
Đ	Dispersity

D_2O	Deuterated Water
D_3	Hexamethylcyclotrisiloxane
DLS	Dynamic Light Scattering
DMA	Dynamic Mechanical Analysis
DMAEMA	Dimethylaminoethyl Methacrylate
DMSO-d_6	Deuterated Dimethyl Sulfoxide
d_n	Number Average Particle Diameter
DSC	Differential Scanning Calorimetry
d_v	Volume Average Particle Diameter or De Brouckere Mean
DVB	Divinylbenzene
EGDMA	Ethylene Glycol Dimethyl Acrylate
EPDM	Ethylene Propylene Diene Monomer
eROP	Enzymatic Ring-Opening Polymerisation
FRP	Free Radical Polymerisation
FTIR	Fourier-Transform Infrared Spectroscopy
G’	Storage Modulus
G’’	Loss Modulus
GC	Gas Chromatography
GPC	Gel Permeation Chromatography
HEMA	2-Hydroxyethyl Methacrylate

HPLC	High Pressure Liquid Chromatography
IR	Infrared
J_{crit}	Critical Chain Length
k_d	Rate Constant of Decomposition
k_i	Rate Constant of Initiation
k_p	Rate Constant of Propagation
k_t	Rate Constant of Termination
k_{tc}	Rate Constant of Termination by Combination
k_{td}	Rate Constant of Termination by Disproportionation
$k_{tr,M}$	Rate Constant of Radical Transfer to Monomer
MAA	Methacrylic Acid
MBA	N,N'-methylenebisacrylamide
MMA	Methyl Methacrylate
M_n	Number Average Molar Mass
M_w	Weight Average Molar Mass
nBuLi	N-Butyllithium
NIPAM	N-isopropylacrylamide
NMP	Nitroxide-Mediated Radical Polymerisation
NMR	Nuclear Magnetic Resonance spectroscopy
Novozym-435	Candida Antarctica Lipase B Immobilized on Acrylic Resin

P_c	Critical Pressure
PDMS	Poly(Dimethyl Siloxane)
PDMS-MA	Methacrylate Terminated Poly(Dimethyl Siloxane)
PMMA	Poly(Methyl Methacrylate)
PS	Polystyrene
PSD	Particle Size Distribution
PTFE	Polytetrafluoroethylene
RAFT	Reversible Addition-Fragmentation Chain Transfer
RMS	Root Mean Square
ROP	Ring-Opening Polymerisation
R_p	Rate of Polymerisation
RPM	Rotation Per Minute
SAXS	Small Angle X-Ray Scattering
$scCO_2$	Supercritical Carbon Dioxide
SCF	Supercritical Fluid
SEM	Scanning Electron Microscopy
St	Styrene
T_c	Critical temperature
TEM	Transmission Electron Microscopy
THF	Tetrahydrofuran

ToF-SIMS	Time-of-Flight Secondary Ion Mass Spectrometry
UV	Ultraviolet
V-70	2,2’-azobis(4-methoxy-2,4-dimethylvaleronitrile)
VOC	Volatile Organic Compound
X_{calc}	Calculated Conversion
X_{exp}	Experimentally Measured Conversion
Z_{mer}	Critical Chain Length
α	Partition Coefficient
σ	Standard Deviation

Contents

Declaration i

Abstract ii

Acknowledgements iii

Publications related to this work iv

Symbols and abbreviations v

Contents x

Chapter 1 Introduction 1

1.1 Overview 2

1.2 Polymer structures 3

1.3 Polymer synthesis 4

1.3.1 Free radical polymerisation (FRP) 9

1.3.1.1 Decomposition 10

1.3.1.2 Initiation 11

1.3.1.3 Propagation 12

1.3.1.4 Termination 12

1.3.1.5 Radical transfer 13

1.3.2 Controlled radical polymerisation (CRP) 14

1.4 Polymerisation medium 15

1.4.1 Bulk polymerisation 16

1.4.2 Solution polymerisation 16

1.4.3 Heterogeneous polymerisation 17

1.4.3.1 Emulsion polymerisation 17

1.4.3.2 Dispersion polymerisation 18

1.4.3.3 Precipitation polymerisation 20

1.5 Supercritical fluids 20

1.5.1 Supercritical CO_2 21

1.5.2 Polymerisation in $scCO_2$ 22

1.5.2.1 Homogeneous polymerisations in $scCO_2$ 22

1.5.2.2 Heterogeneous polymerisations in $scCO_2$ 23

1.5.2.3 Dispersion polymerisation in $scCO_2$ 24

1.6 Polymer additives 25

1.6.1 Impact modifiers 26

1.7 Summary and Thesis aims 28

Chapter 2 Instrumental and Analytical Methods 31

2.1 Overview 32

2.2 High pressure equipment 32

2.2.1 Carbon dioxide pump 32

2.2.1.1 Standard operating procedure 33

2.2.1.2 Emergency shutdown procedure 34

2.2.2 High-pressure set-up 35

2.2.3 MK III high-pressure autoclave 37

2.2.3.1 Standard operating procedure 38

2.2.3.2 Emergency shutdown procedure 39

2.2.4 Liquid addition under high pressure 41

2.2.4.1 Standard operating procedure 41

2.2.4.2 Emergency shutdown procedure 42

2.2.5 High pressure fixed volume view cell 43

2.2.5.1 Standard operation procedure 44

2.2.5.2 Emergency shutdown procedure 46

2.2.6 High-pressure sampling set-up 46

2.2.6.1 Standard operating procedure 47

2.3 Analytical methods 51

2.3.1 Gel permeation chromatography (GPC) 51

2.3.2 Nuclear magnetic resonance spectroscopy (NMR) 51

2.3.3 Scanning electron microscopy (SEM) 53

2.3.4 Differential scanning calorimetry (DSC) 54

2.3.5 Dynamic light scattering (DLS) 55

2.3.6 Dynamic mechanical analysis (DMA) 55

2.3.7 Transmission electron microscopy (TEM) 56

2.3.8 Time-of-flight secondary ion mass spectrometry (ToF-SIMS) 57

2.3.9 Atomic force microscopy (AFM) 57

2.3.10 NanoIR 58

Chapter 3 On-line Polymerisation Monitoring in Supercritical Carbon Dioxide . 59

3.1 Overview 60

3.2 Introduction 60

3.2.1 Monitoring polymerisations in conventional solvents 61

3.2.2 Monitoring polymerisations in $scCO_2$ 66

3.2.3 Polymerisation kinetics 68

3.2.3.1 Reaction description 68

3.2.3.2 Kinetics of heterogeneous polymerisations 69

3.3 Aims and objectives 71

3.4 Experimental 71

3.4.1 Materials 71

3.4.2 HPLC initiated free radical dispersion polymerisation of MMA 72

3.4.3 RAFT controlled dispersion polymerisation of MMA 73

3.4.4 Free radical dispersion polymerisation of styrene 74

3.4.5 Free radical precipitation polymerisation of acrylic acid 75

3.4.6 Enzymatic ring-opening polymerisation of caprolactone 75

3.4.7 Monitoring methods 76

3.4.7.1 Quench and measure method 76

3.4.7.2 Sampling pipe method 76

3.4.7.3 Sampling cylinder method 78

3.5 Results and discussion 81

3.5.1 Batch free-radical dispersion polymerisation of MMA 81

3.5.1.1 Kinetic modelling 87

3.5.2 Sampling pipe method 95

3.5.3 Sampling cylinder method 100

3.5.3.1 Setup testing 100

3.5.3.2 On-line monitoring of the free-radical dispersion polymerisation of MMA 103

3.5.3.3 Monitoring of a range of reaction systems 114

3.6 Conclusions 123

Chapter 4 Improving Reactor Conditions and Exploiting the Tuneable Density of $scCO_2$ in Free Radical Dispersion Polymerisations 125

4.1 Overview 126

4.2 Introduction 126

4.2.1 Stabilising dispersion polymerisations 127

4.2.2 The importance of agitation 129

4.2.3 The effect of component concentrations and reactor loading 132

4.2.4 Effect of solvent/antisolvent strength 133

4.2.4.1 Mixed solvent systems 133

4.2.4.2 Mixed solvent systems with $scCO_2$ 134

4.2.4.3 Pressure influence in $scCO_2$ dispersions 134

4.3 Aims and objectives 135

4.4 Experimental 136

4.4.1 Materials 136

4.4.2 One step dispersion polymerisation in $scCO_2$ 137

4.4.3 HPLC initiated dispersion polymerisation in $scCO_2$ 138

4.4.4 Two step dispersion polymerisation in $scCO_2$ 139

4.4.5 Solubility measurement in fixed volume viewcell 141

4.4.6 PDMS-MA synthesis through anionic polymerisation 141

4.4.7 Free radical dispersion polymerisation of styrene 142

4.5 Results and discussion 143

4.5.1 Agitation effects 143

4.5.2 Loading Limits of dispersion polymerisation of MMA 153

4.5.2.1 Single stage loading limit 155

4.5.2.2 Ultimate loading limit 159

4.5.3 Influence of pressure on the dispersion polymerisation of MMA 160

4.5.3.1 Solubility of commercial PDMS-MA (10 kDa) at 65 °C 160

4.5.3.2 MMA dispersion polymerisation with commercial PDMS-MA (10 kDa) 162

4.5.3.3 Influence of stabiliser chain length 173

4.5.3.4 Expanding the attainable particle size range 177

4.5.4 Dispersion polymerisation of styrene with PDMS-MA stabiliser 178

4.5.4.1 Cosolvent effect on polymerisation kinetics 182

4.5.4.2 Effect of pressure on particle size control 183

4.5.4.3 Loading limit of polymerisation 184

4.6 Conclusions 186

Chapter 5 Production of Core Shell Particles for Impact Modification 188

5.1 Overview 189

5.2 Introduction 189

5.2.1 Structure and applications of core-shell particles 190

5.2.1.1 Core-shell particles as impact modifiers 192

5.2.2 Core-shell particle synthesis in $scCO_2$ 194

5.3 Aims and objectives 196

5.4 Experimental 197

5.4.1 Materials 197

5.4.2 Free radical dispersion polymerisation of styrene with DVB 198

5.4.3 Redispersion of PS particles in $scCO_2$ 198

5.4.4 Preparation of PS:PMMA core-shell particles in $scCO_2$ 199

5.5 Results and discussion 200

5.5.1 PS:PMMA Core-shell particle synthesis 200

5.5.2 Varying shell thickness 209

5.5.2.1 Alternative analysis methods 223

5.5.3 Varying core size and material 226

5.5.4 The addition of crosslinking to core-shell particles 230

5.5.5 The use of alternate monomers in core-shell particles 234

5.6 Conclusions 241

Chapter 6 Conclusions and Future Work 243

6.1 Conclusions 244

6.2 Future work 247

Appendix 249

Chapter 7 References 269

Chapter 1

Introduction

1.1 Overview

Worldwide production of polymers is continuously increasing, even during economic and manufacturing downturns.[1] This trend is expected to continue in the coming decades, despite concerns about the environmental impact of plastics.[2] within the growing market for polymers, environmental concerns are influencing business and policy decisions, driving research into environmentally friendly materials and production processes.[3, 4] One avenue for environmental impact improvement of polymer production is the replacement of currently used solvents with greener alternatives, such as supercritical fluids.[5-7] Supercritical carbon dioxide ($scCO_2$) in particular, is a promising green solvent with potential to replace water and oil based solvents used currently in commercial polymerisation processes.[8, 9]

First, this work will present an overview of polymers and their production methods, focussing in on the production of polymer particles in heterogeneous systems. An introduction to supercritical fluids and producing polymers within this medium will then be given. Subsequent chapters will display a detailed study into free radical dispersion polymerisations in $scCO_2$, with the aim of improving control and understanding of the process. Finally, the improved understanding and control over the system will be exploited to reproduce current commercial products in a green solvent. A detailed discussion of more specific topics and aims will be given at the beginning of each chapter.

1.2 Polymer structures

Polymers find a wide range of applications both in industrial and consumer-oriented applications. This includes simple polymeric materials used in the plastic industry, as well as more complex specialty polymers utilised in pharmaceutical, medical and space applications, among many.[10]

Polymers are built up of long chains of covalently bound monomer units. Several monomer types can be combined in one polymer to form so called copolymers (Figure 1.1), showing a range of interesting characteristics. This research project will initially focus solely on homopolymers, constructed from a single monomer type.[11]

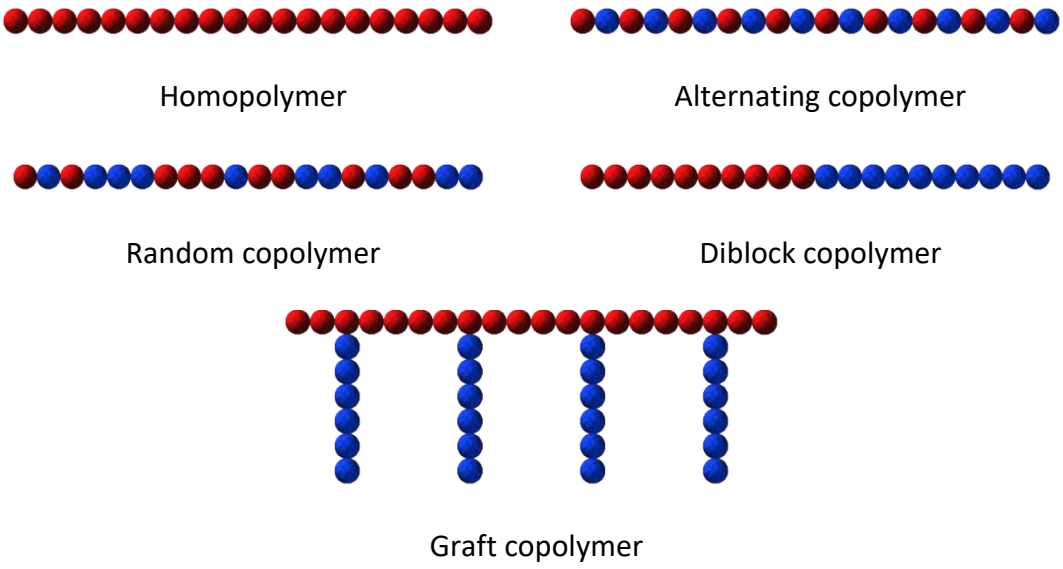


Figure 1.1 Schematic representation of various polymer structures that can be formed. Red and blue spheres represent different monomer molecules.

Polymer materials contain vast amounts of polymer chains with varying amounts of monomer units, resulting in an array of molar masses. To describe the overall chain length or molecular weight of a polymer product, a molar mass distribution is described using average molecular weights and dispersity values. The most common

averages used for polymer sample description are the number average molar mass (M_n) and mass average molar mass (M_w). M_n, shown in Equation 1.1 below, is the arithmetic average of individual chain masses. M_w, shown in Equation 1.2, is a weighted average of individual chain masses, favouring larger polymer chains over shorter chains. Dispersity (Đ) is a measure of the uniformity of a polymer product and is calculated using Equation 1.3. If all chains in a sample are of the exact same length, all averages will be identical and a dispersity of 1 will be achieved. In practice however, this is not achieved due to the statistical nature of the polymerisation process.[11]

$$M_n = \frac{\sum M_i N_i}{\sum N_i}$$

Equation 1.1

$$M_w = \frac{\sum {M_i}^2 N_i}{\sum M_i N_i}$$

Equation 1.2

$$Đ = \frac{M_w}{M_n}$$

Equation 1.3

1.3 Polymer synthesis

Polymer chains are generally formed through two different polymerisation mechanisms, namely step-growth or chain-growth polymerisation.[11]

In the step-growth mechanism, some monomers react to form dimers. These dimers can react with additional monomer units to form trimers and with other dimers to

form tetramers. This mechanism will continue to occur, resulting in the formation of oligomers. To actually form polymer chains through this mechanism, larger oligomer chains have to combine. This only occurs after most of the monomer has been used, meaning that very high conversion is required to form a high molecular weight polymer (Figure 1.2). Ideal monomers for this mechanism must carry functional groups that can react with each other, for example an alcohol and a carboxylic acid.[11]

Chain-growth polymerisation occurs through an initiator, containing an active centre such as a cation, an anion or a radical. This active centre will react with a susceptible monomer unit, forming an active centre on the monomer. This activated monomer can then react with another monomer to form a dimer, which can then add another monomer to form a trimer. This very fast monomer addition quickly results in the formation of polymer chains, even at lower conversion (Figure 1.2).

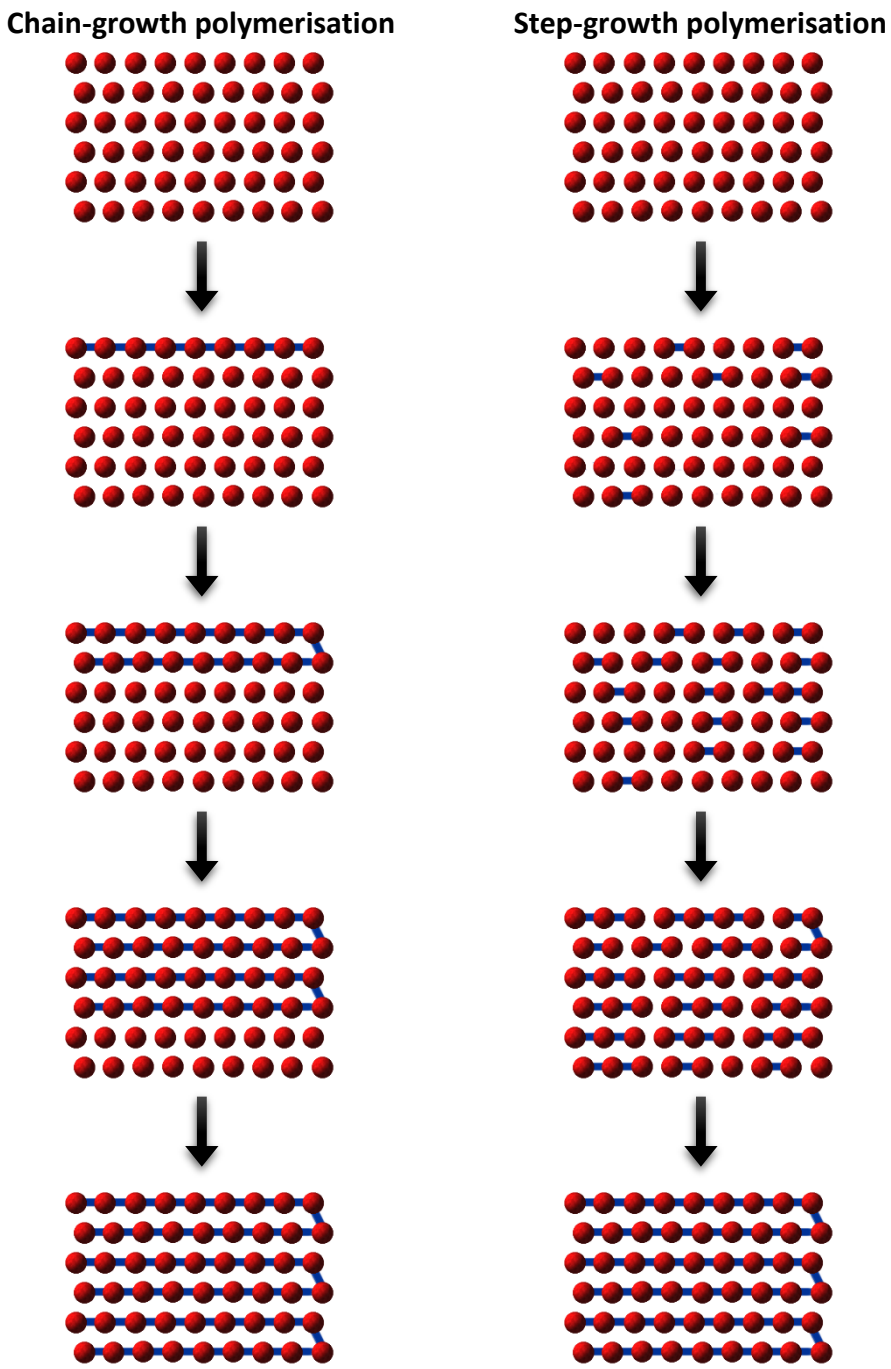


Figure 1.2 Schematic comparison of step-growth versus chain-growth polymerisation, showing the different method of forming polymer chains.

Compared to the step-growth mechanism, chain-growth provides a far easier way of achieving high molecular weight polymers (Figure 1.3).[11]

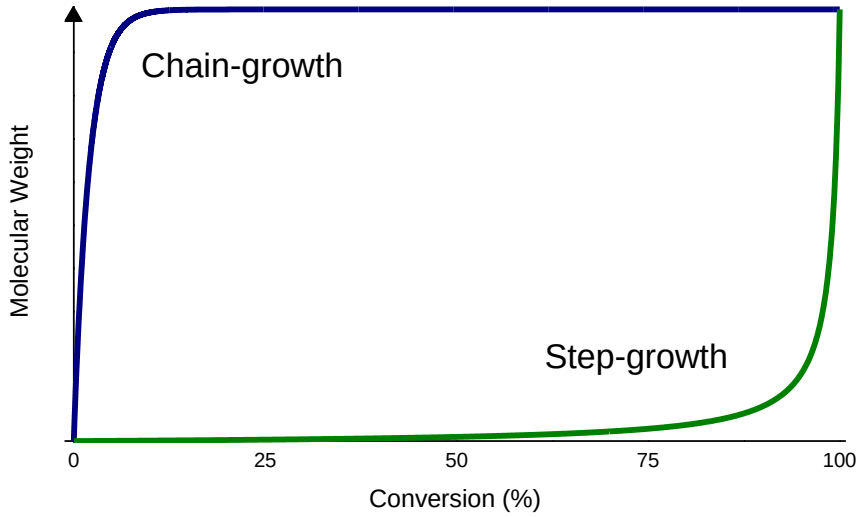


Figure 1.3 Schematic representation of typical molecular weight trends during a polymerisation reaction progressing by chain-growth (blue) and step-growth (green).

Chain-growth polymers require the use of an initiator that will be built into the beginning of every polymer chain. The stepwise addition of monomer units requires the monomer to possess a viable structure, classically a carbon-carbon double bond.[11] The double bond of methyl methacrylate (MMA) (Figure 1.4), is ideally suited to participate in a chain-growth polymerisation.

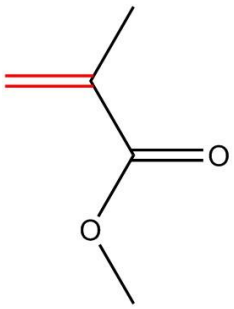


Figure 1.4 Chemical structure of methyl methacrylate, with the polymerising double bond highlighted in red.

Chain-growth polyadditions can occur via anionic, cationic or radical intermediates.[11] The utilised intermediate type depends on several factors, including monomer species, desired product specification and reaction conditions. A styrene monomer is

able to stabilise all three reaction intermediates (Figure 1.5), due to the resonance structures accessible through the attached benzene ring.[11]

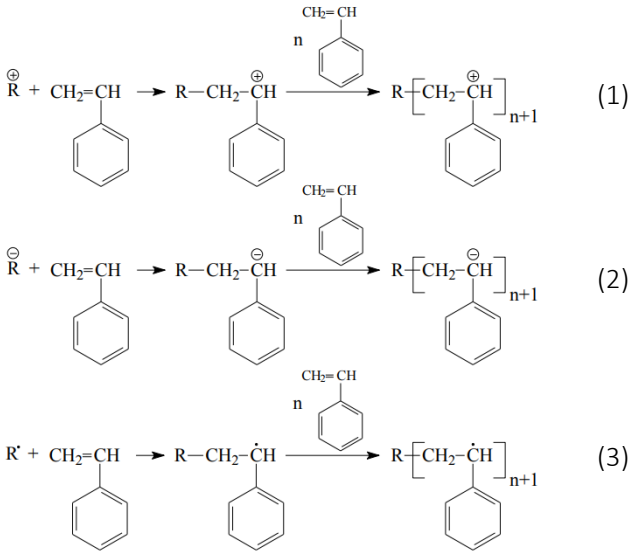


Figure 1.5. Intermediate structures formed during styrene polymerisation, for cationic (1), anionic (2) and radical (3) polymerisations. All three intermediate structures are stabilised due to the benzene ring, attached to the active carbon.[11]

Cationic polymerisations result in the formation of a carbocation propagating species (Figure 1.5(1)). The monomer used for this must therefore be sufficiently stable in this intermediate form to allow polymerisation.[11] If the carbocation is insufficiently stabilised, its lifetime will be too short to allow chain extension. An MMA carbocation is severely destabilised by the electron withdrawing ester group, meaning it cannot partake in a cationic polyaddition reaction.

Anionic polymerisations proceed via carbanion intermediates (Figure 1.5(2)). A monomer able to stabilise this structure is therefore required to allow for polymerisations. MMA is ideal for this, as its carbanion structure is both inductively stabilised by the ester group and mesomerically stabilised (Figure 1.6). The main downside of anionic polymerisation of MMA is that specific conditions (temperature, solvent, initiating ion) are required to supress side-reactions. Due to this, an anionic

polyaddition is generally avoided in industrial poly(methyl methacrylate) (PMMA) production.[11]

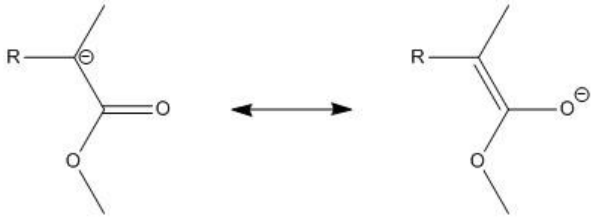


Figure 1.6 Mesomeric stabilisation of methyl methacrylate anion, formed during anionic polymerisation.

Radical polyadditions produce highly reactive radical intermediates (Figure 1.5(3)). The non-discriminatory nature of radicals, means most vinyl monomer types will be suitable for this reaction type.[11] Its relative simplicity and ease of reaction, makes it the preferred polymerisation type in industry. It is also the reaction type that will be utilised during this research project.

1.3.1 Free radical polymerisation (FRP)

In free radical polymerisations, six steps are generally distinguished: decomposition, initiation, propagation, two types of termination and radical transfer (Scheme 1.1), and each step will be summarised below.[11, 12]

$$I \xrightarrow{k_d} 2R^{\cdot} \quad (1)$$

$$R^{\cdot} + M \xrightarrow{k_i} RM_1^{\cdot} \quad (2)$$

$$RM_n^{\cdot} + M \xrightarrow{k_p} RM_{n+1}^{\cdot} \quad (3)$$

$$RM_n^{\cdot} + RM_m^{\cdot} \xrightarrow{k_{tc}} RM_{n+m}R \quad (4)$$

$$RM_n^{\cdot} + RM_m^{\cdot} \xrightarrow{k_{td}} RM_n + RM_m \quad (5)$$

$$RM_n^{\cdot} + M \xrightarrow{k_{tr,M}} RM_n + M_1^{\cdot} \quad (6)$$

Scheme 1.1 General equations of free radical polymerisation. (1) Decomposition, (2) initiation, (3) propagation, (4) termination by combination, (5) termination by disproportionation, (6) radical transfer. I = initiator molecule, M = monomer, M_x = polymer chain of length x, R = initiator decomposition product.[12]

1.3.1.1 Decomposition

In the first step of a free radical polymerisation, radicals are formed that go on to start the polymerisation reaction. The simplest way of producing radicals is through homolytic scission, the simple decomposition of a molecule to form two radical initiators. This can be achieved either by heat induction or photochemical induction.[11] The radical initiator 2,2'-azobis(isobutyronitrile) (AIBN) is a widely used radical forming initiator and is a reliable source of radicals for polymerisations.[13-15] This azo compound decomposes with heat, resulting in the formation of two free radicals and nitrogen gas (Figure 1.7).

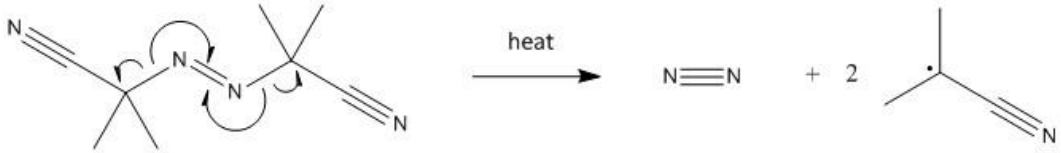


Figure 1.7 Decomposition of 2,2'-azobis(isobutryronitrile) (AIBN) induced by the addition of heat, resulting in the formation of nitrogen and two radical molecules.

Decomposition rate and radical flux will increase with increasing temperature for heat induced initiators such as AIBN. Additionally, the radical flux decreases exponentially as initiator molecules decompose, described by the initiator half-life, the typical time it takes for half of the initiator to decompose in a specific polymerisation system. The half-life value will be dependant on a range of factors such as the temperature, the initiator used, and solvents in the system. More intricate radical generation methods are possible, for example the use of redox chemistry. Although this redox initiation allows for a higher and more constant flux of radicals, it does require the use several interacting compounds in an initiator system.[11, 15]

1.3.1.2 Initiation

In the initiation step, a formed radical reacts with a monomer to form a new radical species, where the radical is located on the monomer unit (Figure 1.8). Depending on the stability of the formed radical, this reaction can be significantly slower than further propagation steps. Initiation efficiency is very dependent on the reaction medium, as radicals are fast reacting and will tend to react with the first susceptible species they encounter.[11]

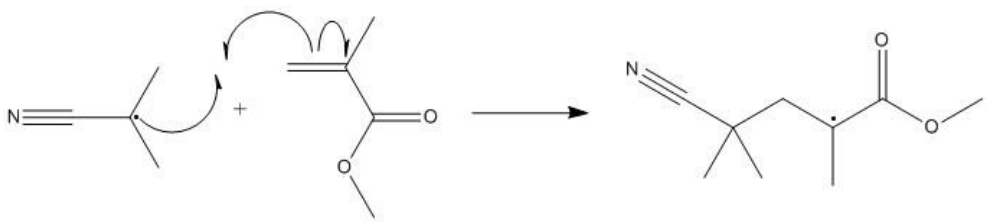


Figure 1.8 Initiation of methyl methacrylate by a radical formed from 2,2'-azobis(isobutyronitrile) decomposition.

1.3.1.3 Propagation

During propagation, successive monomer units are bound to the growing chain. The active radical centre is transferred to the newly acquired monomer unit upon attachment, meaning that the radical stability is unchanged throughout, unlike during initiation (Figure 1.9). The efficiency of this propagation is again dependent on the chemical environment of the radical and therefore heavily influenced by the reaction medium.[11]

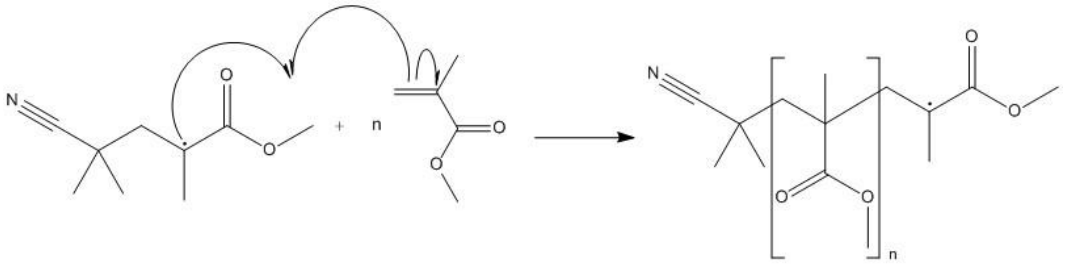


Figure 1.9 Propagation of an active methyl methacrylate polymer chain. The degree of polymerisation is given by n.

1.3.1.4 Termination

Termination occurs when two radical species react with one another. This can occur either by disproportionation or recombination (Figure 1.10). Disproportionation results in the formation of one saturated polymer chain and one polymer chain with an unsaturated chain end. Recombination results in the formation of a carbon-carbon bond between the two growing chains, summing their molar masses in a polymer chain containing an initiator unit on both ends. Clearly, the method of termination can have a great effect on the molecular weight of the final polymer, as recombination results in significantly longer chains than disproportionation.[11]

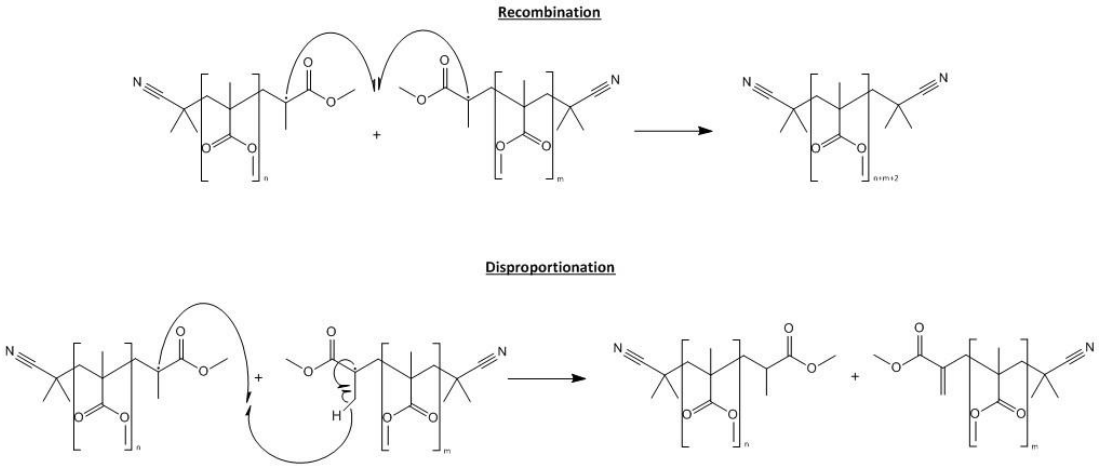


Figure 1.10 Termination reactions of active methyl methacrylate polymer chains, by recombination and by disproportionation. Showing that longer chains are formed by recombination, compared to disproportionation.

As can be seen in Figure 1.10, the mode of termination will influence the terminal end-group present on the polymer chain. This difference in the amount of initiator based end groups can be used to determine the occurrence of the two termination methods.[13]

1.3.1.5 Radical transfer

Beyond termination, chain propagation can also be halted by a radical transfer reaction occurring, for example to a monomer unit (Figure 1.11). This reaction results in a propagating chain transferring the radical function to a monomer unit, stopping the polymer chain from extending further.[11] The resulting monomer radical will proceed to react, meaning reactivity is not lost, but average chain length is reduced. Other forms of radical transfer, to another polymer chain for example, can result in branching rather than chain length reduction.

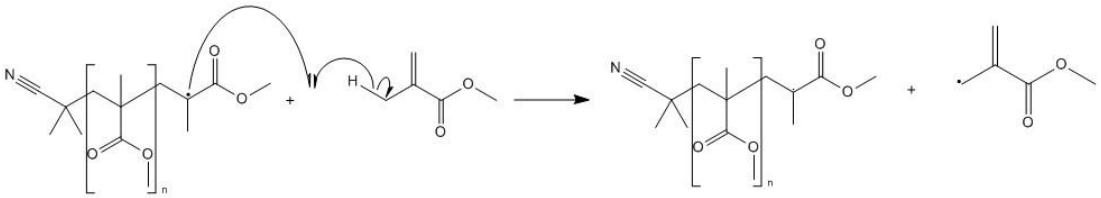


Figure 1.11 Radical transfer reaction from an active methyl methacrylate polymer chain to a monomer unit, forming a terminated polymer chain and a reactive monomer radical.

1.3.2 Controlled radical polymerisation (CRP)

Controlled radical polymerisations (also called reversible deactivation radical polymerisations) are a subset of FRP that allow for additional control over polymer architecture and composition, often through the use of chain transfer agents (CTAs). The use of CTAs allows for the mimicking of living polymerisation conditions, first described by Szwarc in 1956.[16] A living polymerisation is described as a chain polymerisation from which termination and irreversible chain transfer are absent, resulting in a polymer chain end that is always available for propagation. Various methods of CRP have been developed including catalytic chain transfer polymerisation (CCTP),[17] nitroxide-mediated radical polymerisation (NMP),[18, 19] atom transfer radical polymerisation (ATRP),[20, 21] and reversible addition-fragmentation chain transfer (RAFT) polymerisation.[17, 22-24]

The main differentiator between FRP and CRP reactions is the progression of molecular weight with monomer conversion. A living polymerisation shows a linear growth in molecular weight as monomer is converted, and successful CRPs show the same behaviour (Figure 1.12).[25] Secondly, in a CRP, all initiation must occur quickly and in the early stages of polymerisation, to allow all chains to grow at the same time. In FRP on the other hand, initiation occurs throughout, with new polymer chains

being formed continuously until monomer is fully consumed. The exertion of control upon growing polymer chains does mean that polymer chains are mostly in a dormant state, resulting in far slower polymerisation times for CRP compared to FRP.[17]

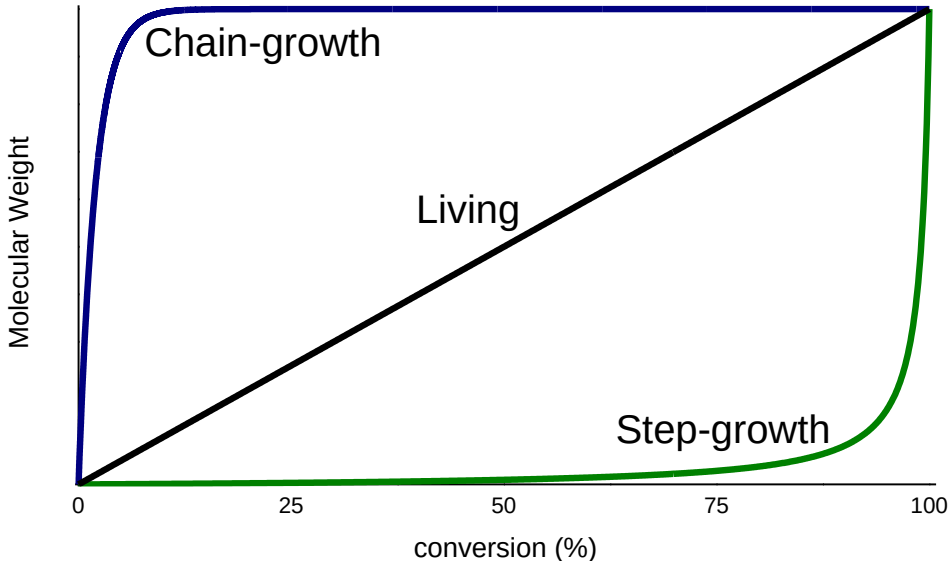


Figure 1.12 Schematic representation of typical molecular weight trends during a polymerisation reaction progressing by chain-growth (blue), step-growth (green), and living (black) polymerisation.

CRP allows for sequential and controlled addition of different monomer types, enabling the production of copolymers with defined architecture, such as block and brush copolymers.[17]

1.4 Polymerisation medium

Due to the indiscriminate nature of radical reactivity, the physical surrounding of an active radical in radical polyadditions is very important.[11] If the radical is surrounded by monomer, a polymer chain will quickly form. However, if radicals are in close

proximity, termination will dominate. Consequently, tailoring the polymerisation medium is essential to allow for radical polymerisation control.

1.4.1 Bulk polymerisation

The simplest medium to use is simply the monomer itself. This method allows for high monomer concentrations surrounding a radical, resulting in the possibility of achieving high molecular weights and fast polymerisation reactions. This does however introduce a significant issue, namely the Trommsdorf effect. As polymer content increases during the reaction, the viscosity of the medium increases. This reduces the diffusion rate of radicals, resulting in a decreased termination as radicals are less likely to meet. This auto-accelerates the polymerisation reaction, further reducing diffusion and termination. This effect is of significant importance for industry, where the increased heat production of such a runaway reaction brings significant explosion risk.[11]

1.4.2 Solution polymerisation

To avoid significant viscosity increases during polymerisation, the monomer can be dissolved in a solvent. This also allows for a more stable and efficient heat dissipation throughout the reaction. A severe downside of using a solvent is the decrease in monomer concentration around the propagating radicals. This results in a slower reaction and a lower molecular weight in the final polymer for free radical polymerisations. It can also be difficult to find a suitable solvent that allows all components to dissolve throughout polymerisation. Due to these limitations, a homogeneous solution is rarely used for radical polymerisations.[11]

1.4.3 Heterogeneous polymerisation

To combine the advantages of polymerisations in solution, while maintaining the reaction speeds and product specifications of bulk polymerisations, several “tricks” can be implemented utilising heterogeneous solutions. A short description of a few relevant techniques will follow.

1.4.3.1 Emulsion polymerisation

Many commonly used monomers, including MMA, are very poorly soluble in water.[26] A mixture of monomer and water will readily phase separate. By adding an amphiphilic compound, called a surfactant, hydrophobic monomer droplets can be stabilised within the water phase. Stirring this mixture results in a heterogeneous solution called an emulsion, a large water phase with undissolved monomer droplets and surfactant micelles throughout. Radical initiators are generally soluble in water, resulting in radicals being located in the water phase. A very small amount of monomer will be soluble in the water phase, allowing small oligomers to be formed from the created radicals. These short chains can then enter an existing micelle or be surrounded by surfactant, forming a new micelle. Large monomer droplets will keep resupplying the water phase with monomer that will then allow monomer to diffuse into surfactant micelles. Polymerisation will continue to occur in an active micelle until a second radical enters, causing termination (Figure 1.13).[27] Emulsion polymerisation has the advantage of polymerising in solution, with heat dissipation and low viscosity guaranteed by the large water phase. It combines this with the advantage of actually polymerising in closed micelles, with high monomer concentration and efficient radical isolation.[27] By isolating every radical in micelles,

radical termination is avoided, allowing for high molecular weights despite the high overall radical concentrations required for higher reaction rates. This highly desired combination of high reaction rate, high molecular weight and controllability, means emulsion polymerisation is used extensively in industrial polymer production.[27]

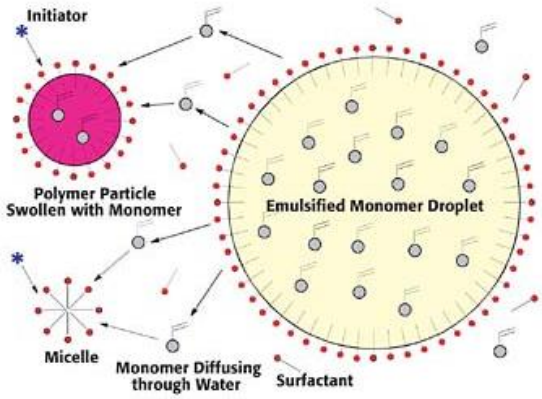


Figure 1.13 Schematic overview of the emulsion polymerisation mechanism, showing various structures present in the polymerisation system.[28]

This reaction technique produces 0.05 – 1 µm-sized particles. Micron-sized polymer particles have a wide variety of applications but require modification of a simple emulsion polymerisation that produces smaller particles. This is often achieved by using seeded emulsion polymerisation, a process that uses a previously created polymer particle as a starting point to grow further. Although this is used widely in industry, it does require additional steps to produce desired particles.

1.4.3.2 Dispersion polymerisation

Unlike emulsion polymerisation, dispersion polymerisation consists of a reaction medium that is a good solvent for the monomer but is still a poor solvent for the forming polymer. Initially this means that the monomer solvent mixture is a homogeneous solution. In this homogeneous solution, the initiator will form radicals and proceed to grow the polymer chain. When the growing chain reaches a critical

chain length (J_{crit}[11, 29] or Z_{mer}[30]), it is no longer soluble in the solvent and will phase separate. A suitable surfactant is used to stabilise the precipitating polymer chains, forming a heterogeneous solution. The surfactant is essential to avoid aggregation of the insoluble particles, allowing spherical particles to be formed. The available monomer can also migrate into the newly created polymer phase, allowing polymerisation to continue in the polymer phase as well as the solvent phase (Figure 1.14).[31] Ultimately this results in discrete polymer particles of 100 nm to 10 µm in diameter, larger than particles produced by emulsion polymerisation.[7] Due to the ability to form this specific particle size range, one step dispersion polymerisation is a promising alternative to seeded emulsion polymerisations, depending on desired particle size.

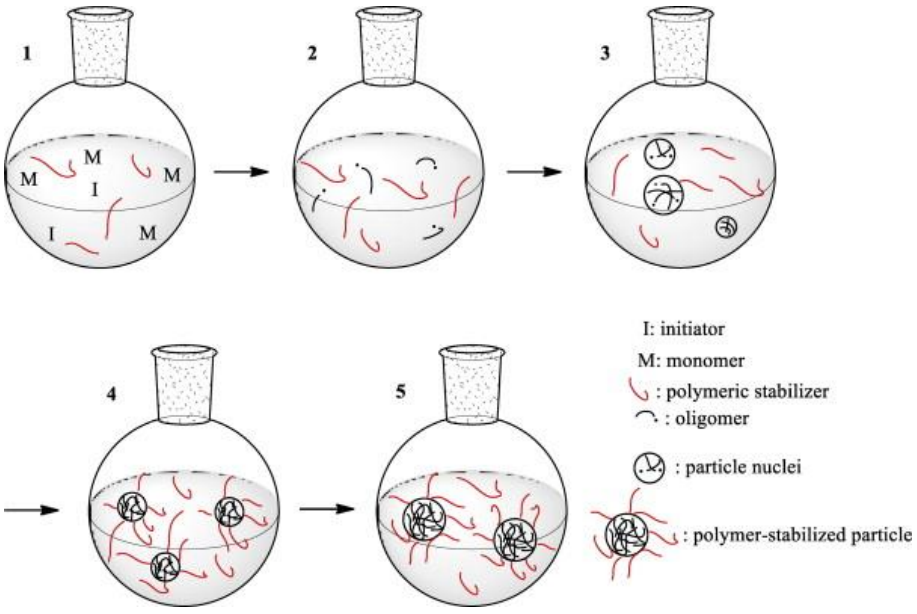


Figure 1.14 Schematic overview of the dispersion polymerisation mechanism. 1) Homogeneous solution before polymerisation, 2) homogeneous solution with soluble oligomer chains, 3) heterogeneous solution with insoluble oligomer chains dispersed, 4) heterogeneous solution with growing polymer chains stabilised by the stabiliser, 5) heterogeneous solution of dispersed polymer particles stabilised by stabiliser.[7]

1.4.3.3 Precipitation polymerisation

Unlike emulsion and dispersion polymerisations, precipitation polymerisations do not require the use of a stabiliser compound. As with a dispersion polymerisation, the monomer and initiator are initially soluble in solvent. When the growing polymer chain in a precipitation reaches the Z_{mer} length and becomes insoluble, it is allowed to coalesce and form a precipitated phase in the absence of stabiliser. Depending on the polymer formed, the solvent used, and the agitation of the system, the agglomerated polymer can form stable particles, though often with less defined morphology than other heterogeneous polymerisation methods.[27, 32]

1.5 Supercritical fluids

With growing environmental concerns influencing business and policy decisions globally, research into environmentally friendly production processes are of great interest.[3, 4] Current industrial polymer production processes often use water as the main solvent, generally resulting in contamination of the reaction solvent through the use of volatile organic compounds (VOCs) and chlorofluorocarbons (CFCs).[15, 33] This results in contaminated waste water streams, with negative consequences for the environment, oceans and availability of drinking water. Additionally, water must be removed from the final product, in cost and energy intensive drying processes, further increasing the negative environmental impact.[9, 15] As environmental impact becomes a more pressing concern, the interest in alternative solvents is increasing.[3] Alternative solvent systems could alleviate water contamination issues, reduce energy costs and reduce the impact on the environment. Additional advantages, such

as novel products and properties, may even be found by using suitable alternatives to water.

The use of supercritical fluids (SCFs) is also of great interest, as it allows the combination of several desired properties. SCFs allow for the solvation of many compounds, while possessing diffusion coefficients similar to the gas phase.[9] To attain an SCF, a characteristic critical temperature and pressure must be reached (Figure 1.15).[8]

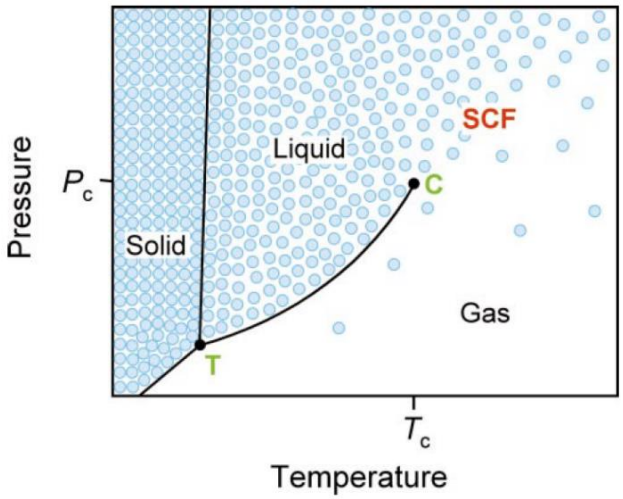


Figure 1.15. Schematic pressure-temperature phase diagram for a pure component showing the supercritical fluid (SCF) region. The triple point (T) and critical point (C) are marked. The blue circles represent the variation in density of the substance in the different regions of the phase diagram. Note that the density varies continuously between the liquid state and the gas state, providing that the liquid-gas equilibrium line (T-C) is not crossed.[8]

1.5.1 Supercritical CO_2

Carbon dioxide (CO_2), generally known as a pollutant,[3, 4] is a promising candidate as an alternative solvent, combining considerable environmental advantages[34] with the desired properties of SCFs described above.[8, 9, 35, 36] It is a cheap, non-flammable and environmentally friendly solvent[34], with an easily attainable supercritical point.[8] The

supercritical point is reached at relatively mild conditions, with a T_c of 31.1 °C and a P_c of 73.8 bar.[8, 9] Avoiding extreme temperatures or pressures is an essential factor both in limiting cost and assuring safety of use. This supercritical CO_2 ($scCO_2$) is a good solvent for a wide range of monomers, making it an intriguing candidate to replace water in traditional industrial polymerisations.

A further advantage of using $scCO_2$ as the polymerisation medium, is found after the reaction is complete. When returning to atmospheric conditions, CO_2 will revert to the gas phase. This results in a solvent free polymer product, without the need for an energy intensive drying process. This is a large cost saving, which could compensate for the increased cost associated with the initial pressure generation when compared to traditional industrial processes.

1.5.2 Polymerisation in $scCO_2$

Several different polymerisation reactions have been carried out in $scCO_2$, including free radical chain growth, cationic chain growth, thermal ring-opening, transition metal catalysis and melt phase condensation polymerisations.[8]

1.5.2.1 Homogeneous polymerisations in $scCO_2$

Many initial studies of polymerisations in $scCO_2$ focused on homogeneous polymerisations.[14] Amorphous fluoropolymers showed good solubility under mild conditions and were the first polymers to be produced in $scCO_2$.[8] DeSimone *et al.* reported the first successful homogeneous free radical polymerisation in $scCO_2$ in 1992.[37] Amorphous fluoropolymers such as poly(1H,1H – perfluorooctyl acrylate) were synthesised in $scCO_2$ using AIBN (50 % w/v monomer, 59.4 °C, 207 bar, 48 h).[14]

A range of fluorinated acrylates, methacrylates and fluoroalkyl-derived styrene monomers have been polymerised or copolymerised homogeneously in $scCO_2$.[8, 9] Homogeneous free radical polymerisation of styrene in $scCO_2$ was achieved by Beuermann *et al.* [38] High pressure and low conversion ensured the reaction remained homogeneous and only low molecular weight polymer was synthesised.

1.5.2.2 Heterogeneous polymerisations in $scCO_2$

The poor solubility of most common high molecular weight polymers in $scCO_2$ at reasonable temperature and pressure conditions, makes $scCO_2$ an ideal solvent for heterogeneous polymerisations.[9, 39, 40] Most common and industrially important vinyl monomers, such as MMA, are highly soluble in $scCO_2$, while the corresponding polymers are poorly soluble.[8, 9, 39]

Precipitation polymerisations have been performed successfully for a wide range of monomers. The precipitation polymerisation of acrylic acid in $scCO_2$ was reported by Romack *et al.*[41] This polymerisation was performed at pressures ranging from 125 to 365 bar and showed that pressure within this range did not noticeably influence the molecular weight, molecular weight distribution or particle morphology. Precipitation polymerisations of MMA and styrene have been performed, with molecular weight being controlled through the use of transfer agents.[9]

Emulsion polymerisations in $scCO_2$ have been used for the synthesis of biodegradable polyesters. The copolymerisation of lactide and glycolide to form poly(lactide-co-glycolide) with poly(1,1-dehydroperfluorooctyl acrylate) as a stabiliser was reported by Hile *et al.*[42]

1.5.2.3 Dispersion polymerisation in $scCO_2$

As a nonpolar molecule, $scCO_2$ is a good solvent for MMA but not for PMMA, meaning it is ideally suited for dispersion polymerisations.[6, 43] In 1994 the first free radical dispersion polymerisation in $scCO_2$ was reported by DeSimone *et al.*[44] the use of poly(1,1-dehydroperfluorooctyl acrylate) as a stabiliser allowed for high conversion (>90%) and high molecular weight (190-325 kDa) PMMA to be produced under mild conditions (65 °C, 204 bar). SEM analysis showed that uniform spherical particles were formed with an average diameter of 1.2-2.5 µm.[45] Another example of fluorinated stabiliser, used successfully under similar conditions, is the carboxylic acid terminated poly(hexafluoropropylene oxide), commercially known as Krytox 157FSL [DuPont].[46] It was found that the Krytox 157FSL stabilised reaction did not require intense agitation to maintain a successful dispersion at mild conditions (65 °C, 130 bar) in $scCO_2$.[47]

An alternative to fluorinated stabiliser compounds can be found in siloxane-based surfactants. There are a wide range of poly(siloxanes) that are able to stabilise dispersion polymerisations in $scCO_2$.[8] The synthesis of high molecular weight PMMA via dispersion polymerisation in $scCO_2$ using methacrylate terminated poly(dimethylsiloxane) (PDMS-MA) and AIBN was first reported by Shaffer *et al.* in 1996.[48] This PDMS-MA stabiliser macromolecule is also used for MMA dispersion polymerisations in $scCO_2$ by Howdle *et al.*[35, 49-51] The methacrylate terminal end group can participate in polymer propagation, with Howdle *et al.* showing 5-15% of the stabiliser grafting into the formed polymer.[49] Alternative end-group terminations on PDMS stabilisers, such as vinyl[52] or glycidyl methacrylate[53] end groups, have also

proven to allow successful dispersion reactions to occur for MMA. The PDMS end group's grafting affinity will however influence the stabiliser efficiency in a dispersion polymerisation.[7] PDMS based stabilisers with 2 functionalised end groups, such a divinyl terminated PDMS[54], also result in a successful MMA dispersion polymerisation. Alternative silicon based stabilisers, including [poly((bicyclo[2.2.1]hept-5-en-2-yl)triethoxysilane)][55], have also shown to successfully stabilise MMA dispersion polymerisations under similar conditions.

1.6 Polymer additives

Throughout the plastics industry, materials are added to "pure" polymer materials in order to improve product quality and induce desirable properties, known as polymer additives.[56] Additive systems for the polymer industry were built on previous knowledge gained from the rubber industry,[57] and the additive market has since overtaken the field expanding into other application areas beyond plastics.[58] Additives for polymers perform a range of roles in a plastic product often split into two categories; modifying specific properties (mechanical strength, colour, transparency, heat or UV resistance, conductivity, bacterial resistance) and modifying processing characteristics (curing, miscibility, ductility, mouldability, lubriciousness and slippiness, recyclability).[58] Polymer additives often convey several benefits at once. For example carbon black is widely used as a pigment, but also functions as a light shield, as a conductivity enhancer, and as a reinforcement.[58] While many pigment and filler additives are small molecules, additives for processability enhancement or mechanical strength alteration can be polymers themselves.[59] Polymeric polymer additives can deliver a range of property and processability

enhancements, though detailed polymer knowledge is required to understand the effect of macromolecules in a complex plastic mixture.

1.6.1 Impact modifiers

An example of polymeric polymer additives that provide improved mechanical properties are impact modifiers. The goal of impact modifiers is to compensate for inherent brittleness, or temperature induced embrittlement, notch sensitivity, and crack propagation. The mechanism for this relies on incorporating a polymeric component that can absorb the energy of an impact and disperse it.[58] This is mainly achieved by introducing nanometric rubbery particles throughout a plastic matrix. Impact modifying particles are able to deform under stress by internal cavitation (Figure 1.16), avoiding the propagation of stress throughout the sample, delaying the onset of crazing and subsequent stress fracturing in the polymer matrix.[60-63]

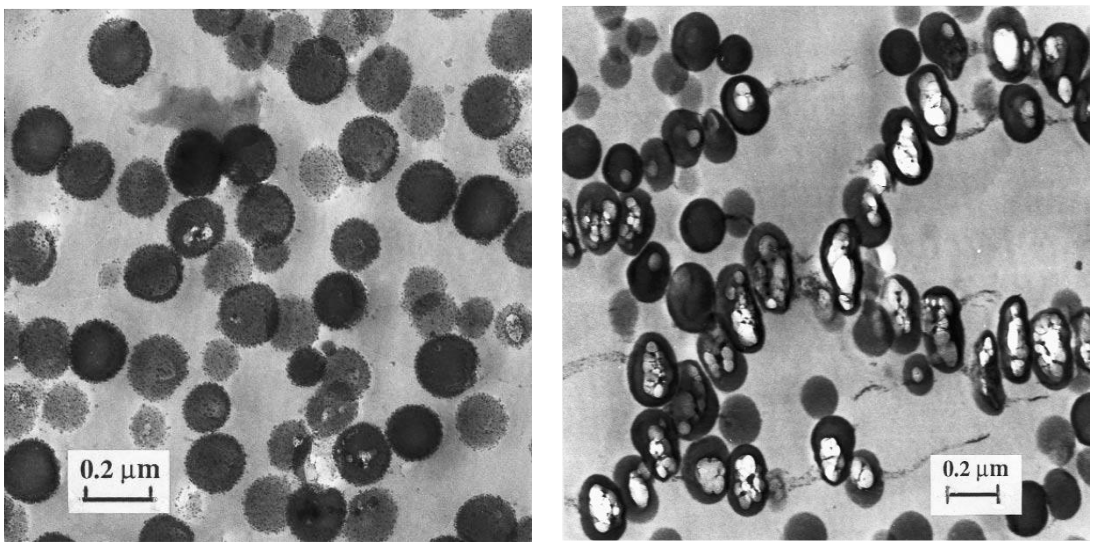


Figure 1.16 Cross-sections of poly(styrene-co-acrylonitrile) tensile bar with poly(butylacrylate) impact modifier particles. Left: tensile bar without impact damage. Right: tensile bar after fracture failure, showing cavitation of the rubber particles, dilatation bands, and crazing.[60]

The role of cavitation within impact modifier particles is highlighted in Figure 1.17, where cavitation is shown to delay the occurrence of a brittle break failure.[64, 65] Cavitated impact modifier particles allow for a ductile yield to occur, causing the material to stretch under stress. Without cavitation, crazes propagate through the matrix, resulting in a brittle break. Slow deformation of a plastic sample, was used to induce cavitation, which subsequently showed improved resistance to brittle break upon impact, highlighting the mechanism of rubbery particle impact modification.[65]

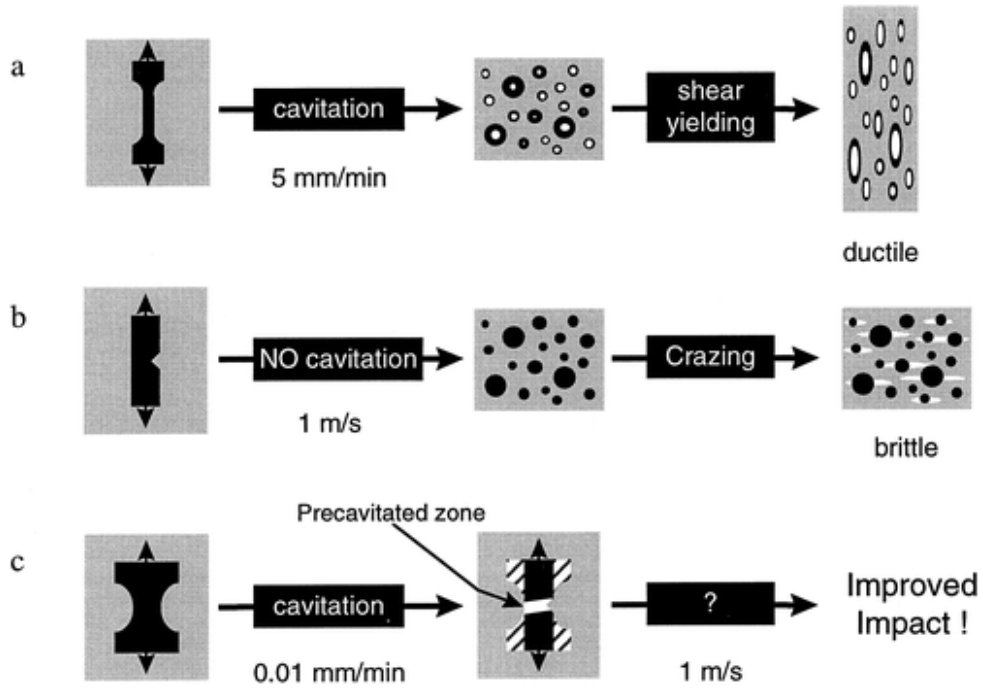


Figure 1.17 Schematic representation of the relation between the mechanical test, the mode of microscopic deformation, and the macroscopic toughness of resins containing impact modifier particles: (a) tensile, (b) impact deformation, and (c) a combined test in which a sample is pre-deformed in the tensile test prior to impact testing.[64]

While a range of polymer particles can provide impact modification, dispersion within a polymer matrix can be a challenge. The addition of a compatibilising polymeric layer onto the impact modifier particle is usually required to assure the particle incorporates evenly into the matrix (Figure 1.18).[27] The production of this core-shell

type particle typically requires a multi-stage heterogeneous polymerisation conducted in an aqueous or organic solvent.[27, 66]

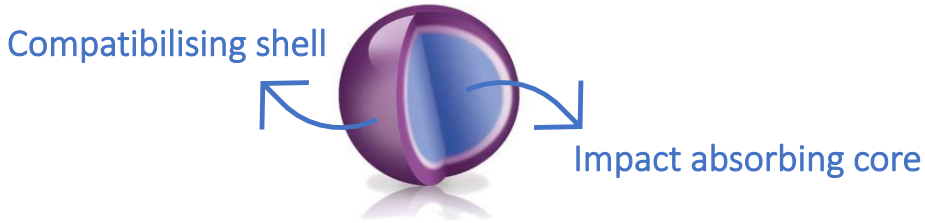


Figure 1.18 typical structure of a core-shell impact modifier, consisting of an impact modifying core and a compatibilising polymer shell that is soluble in the target matrix.

1.7 Summary and Thesis aims

This introduction has detailed the fundamentals of polymers and polymer synthesis, with a focus on polymerisation media and particle production. The use of $scCO_2$ as a green solvent alternative was highlighted, showcasing the range of polymerisations already possible in this solvent. The overall aim of this work is to explore the production of impact modifying core-shell particles in $scCO_2$, therefore an initial introduction into polymer additives and impact modification was given.

Chapter 2 outlines the equipment and analytical techniques utilised throughout this work.

Chapter 3 (Figure 1.19) first outlines reaction monitoring in conventional solvents and typical kinetics descriptions of heterogeneous polymerisations. The lack of equivalent monitoring capability in $scCO_2$ is then framed. A novel and reliable monitoring system for polymerisations in $scCO_2$ is then developed to address this shortcoming, through the on-line collection of a representative reaction sample. This sampling system is tested on a range of known polymerisations, displaying its versatile applicability. A kinetic description of the free radical dispersion polymerisation of MMA is developed

from the acquired monitoring data, giving a better insight into the polymerisation mechanism and locus.

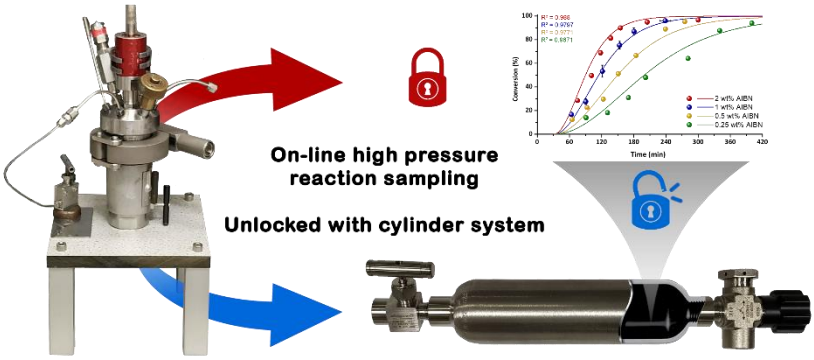


Figure 1.19 graphical abstract of Chapter 3, highlighting the sampling cylinder system developed for on-line reaction monitoring in $scCO_2$ and the kinetic insights this has unlocked.

Chapter 4 (Figure 1.20) builds on the knowledge gained in chapter 3 to further optimise free radical dispersion polymerisations in $scCO_2$. The effect of component concentrations and solvent strength on dispersion polymerisations is analysed. The uniquely variable density of supercritical fluids is exploited to unlock a different way of controlling particle size in a dispersion, ultimately leading to a vast expansion of the attainable particle size range.

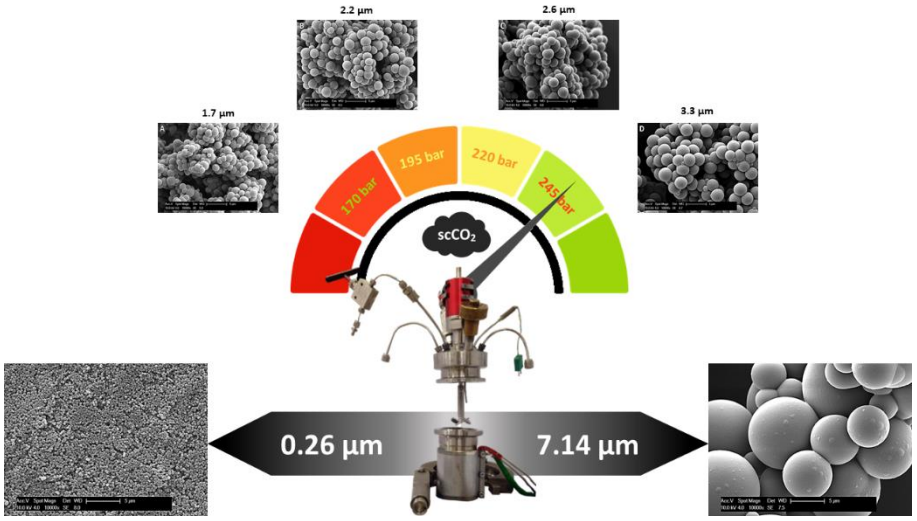


Figure 1.20 Graphical abstract of Chapter 4, highlighting the effect of pressure on particle size and the attainable particle size range in the free radical dispersion polymerisation of MMA.

Finally, chapter 5 (Figure 1.21) shows the exploitation of the gained knowledge to produce true core-shell polymer particles in $scCO_2$ for the first time. Particles of varying size and layer thickness are explored and analysed in detail. The possibilities and limitations of the core-shell polymerisation technique are explored, giving a clear framework for future avenues of research and a path towards their commercial future.

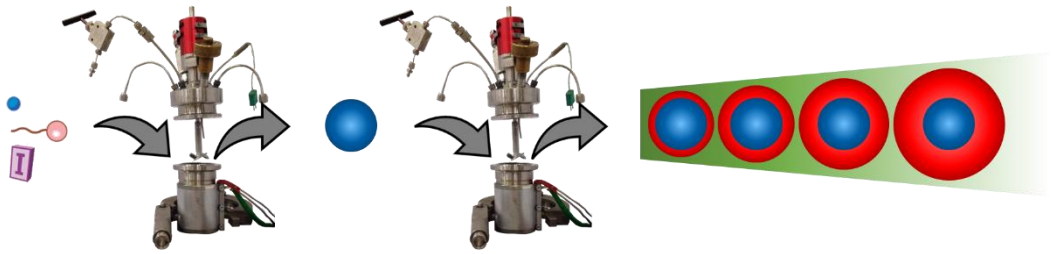


Figure 1.21 Graphical abstract of Chapter 5, highlighting the first ever production of core-shell particles in $scCO_2$ and the ability to produce particles with varied feature size.

Chapter 2

Instrumental and Analytical Methods

2.1 Overview

The aim of this work is to use CO_2 as a green solvent alternative for the synthesis of polymeric particles. The use of CO_2 as a solvent necessitates working at elevated pressures, using bespoke equipment. This chapter will outline the equipment used to work with $scCO_2$, and their standard operating procedures essential for safe working. Following this, analytical techniques used for characterisation throughout the thesis are described.

2.2 High pressure equipment

Before proceeding, it is important to note that working with high pressure equipment requires extensive in-person training. The description of equipment and procedures that follows is not a substitute for training and is only intended as information to understand the work performed.

2.2.1 Carbon dioxide pump

For all high-pressure experiments, liquid carbon dioxide was introduced from a cylinder (Air Products and Chemicals Inc., SCF grade 5.5, 99.9995 %) at a pressure of ~55 bar, to a PM-101 high pressure pump (NWA, Germany) (*Figure 2.1*). Incoming CO_2 pressure was monitored by the first pressure dial, and CO_2 was guided through a refrigerated condenser to guarantee liquid phase CO_2 filled the pump. The dual piston pump was driven by compressed air at ~4 bar, ensuring the CO_2 is compressed to required reaction pressures of up to 300 bar, and output pressure was monitored via a second dial.

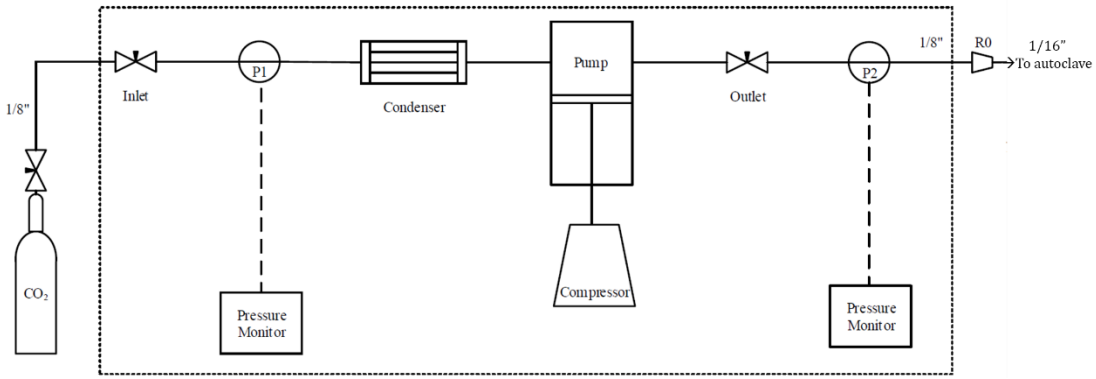


Figure 2.1 Schematic of high-pressure pump system used to deliver CO_2 from cylinder to autoclave setup.

2.2.1.1 Standard operating procedure

1. Check that all of the valves on the front face of the pump are closed and the line around the lab is isolated by closing the isolation tap (*Figure 2.2*).
2. Connect the compressed air into the inlet fitting on the back of the pump with a minimum pressure of 3 bar (labelled as air inlet). This can be done using either the compressor or air cylinder depending on use. Standard work uses the compressor, flushing uses the air cylinder.
3. Connect the CO_2 cylinder *via* the brass (NPT) fitting. Do not open cylinder yet.
4. Switch on the pump and leave it to cool for 1 hour.
5. Open the cylinder, fully open minus a quarter turn.
6. Fully open, minus a quarter turn, the input valve which is on the left side of the front pump panel (anti-clockwise to open). The pressure gauge should read ~55 bar.
7. Fully open and turn back a quarter the output valve on the right side of the front pump panel.

8. Control the maximum output pressure by turning the black knob on the front pump panel (labelled air pressure). To increase the pressure, turn clockwise, but be aware that there is a lag between opening the knob and the pressure increasing, so take time to monitor the increase.
9. Open isolation tap to deliver CO_2 towards the autoclaves.

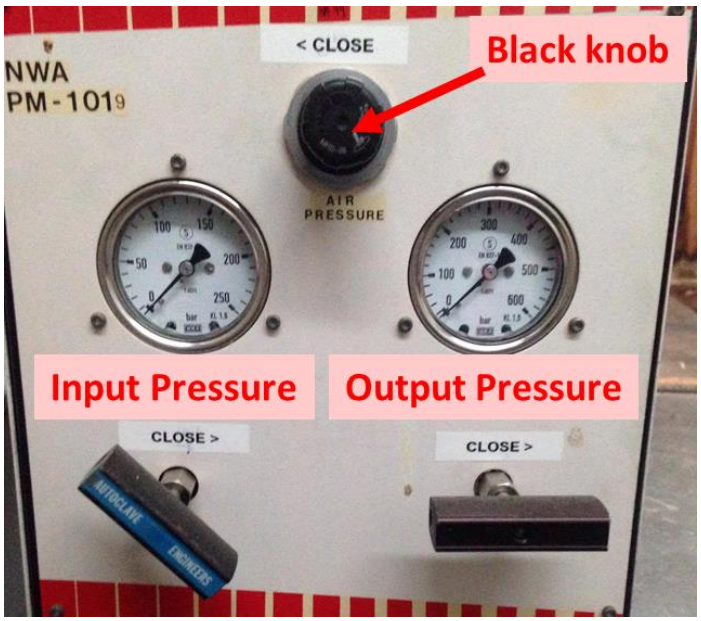


Figure 2.2 front face of NWA PM-101 pump, showing pressure monitors and control valves.

2.2.1.2 Emergency shutdown procedure

1. Close the black knob on the front pump panel by turning anticlockwise, which will cause an audible release of residual pressure.
2. Close the output pressure valve on the right-hand side of the pump front panel (*Figure 2.2*).
3. Close the input pressure valve on the left-hand side of the pump front panel.
4. Close gas cylinder.

2.2.2 High-pressure set-up

The high-pressure setup was connected to the CO_2 pump via a series of HiP valves, Swagelok SS316 tubing, and unions (*Figure 2.3*). Each high-pressure setup consisted of 2 autoclave systems with electronic pressure and temperature monitoring.

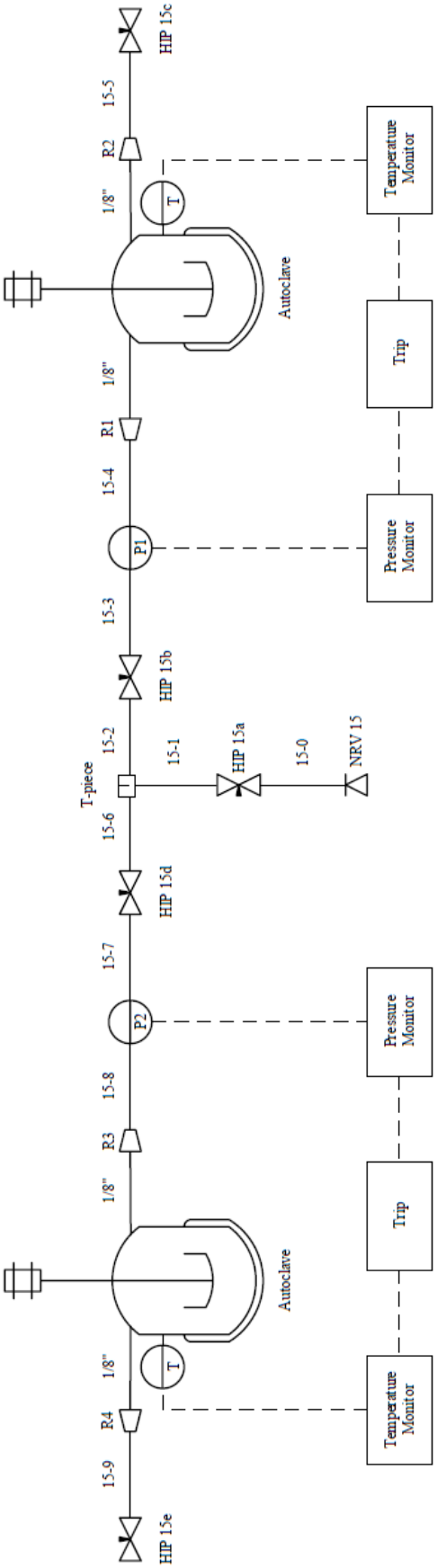


Figure 2.3 Schematic of an individual high-pressure set-up, NRV 15 connects to the CO_2 pump (Figure 2.1).

2.2.3 MK III high-pressure autoclave

All high-pressure polymerisations were conducted using bespoke high-pressure reactors (autoclaves), designed and produced at the University of Nottingham (Figure 2.4). The maximum working pressure was 300 bar, while the maximum working temperature is dependent on the type of rubber seal used for assembly (typically 105 °C).

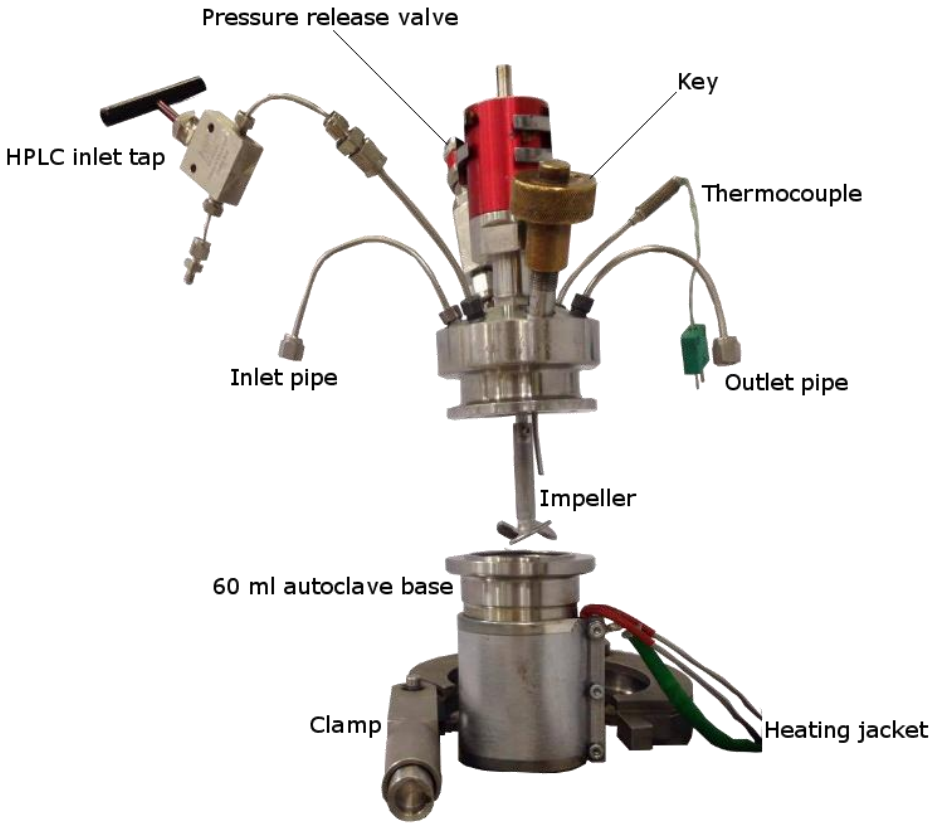


Figure 2.4 MKIII high-pressure autoclave, produced at the University of Nottingham.

Each autoclave consists of two main sections, the head and the base. Head and base are sealed by an O-ring (typically ethylene propylene diene monomer, EPDM), placed between the matching faces and held together by a stainless-steel clamp. The clamp is secured using a custom key that sits in the head during operation. The autoclave head also features the required ports for CO_2 addition, CO_2 release, reagent addition, and contains an internal thermocouple (SS316 sheathed K-type, RS Components, 1.5

mm diameter) for temperature monitoring and heating control. The thermocouple is connected to an external heating jacket (Watlow) surrounding the base, controlled to ± 1°C using a Cal 3200 digital heating controller (RS Components). Pressure is monitored using a quartz piezoelectric transducer (max. 345 bar, RDP Electronics), providing a digital read out in pounds-per-square-inch on an in-house built monitor. A connected electronic trip will disconnect heating in case of pressure exceeding a set value. Furthermore, the head contains a Swagelok SS-4R3A proportional relief valve, that will release pressure in the event of the system exceeding 300 bar.

A magnetically coupled stirrer shaft is located centrally in the autoclave head, with an attached impeller extending into the autoclave base. The stirring is driven by an IKA Eurostar digital motor at 50-2000 RPM.

2.2.3.1 Standard operating procedure

1. An EPDM O-ring was placed in the body, then the head and body clamped together. The clamp was tightened using the safety key which was then screwed into the head. The inlet and outlet pipes were attached and tightened (reducing unions R1 and R2, *Figure 2.3*), then the heating jacket was secured around the body.
2. The setup was leak tested by pressurising to ~50 bar by opening HIP 15a and HIP 15b, keeping HIP 15c closed (*Figure 2.3*). All fittings were checked for leaks with 'Snoop' (Sigma Aldrich).
3. If required, the autoclave was vented to ambient pressure through HIP 15c and any leaking fittings adjusted. (Fittings were never tightened under pressure).

4. Steps 2 and 3 were repeated until no leaks were visible, then any remaining gas was vented until the autoclave was at atmospheric pressure.
5. In order to remove residual oxygen the key was removed, HIP 15c closed and CO_2 flowed through the open key hole at ~2 bar for 30 minutes (HIP 15a and HIP 15b partially open).
6. A monomer solution was added through the open keyhole against the positive pressure of CO_2 to ensure no oxygen entered the vessel. The key was then screwed in and the pressure was raised to ~50 bar.
7. The stirrer was switched on and the CO_2/monomer solution mixed while the internal thermocouple and heating band were connected to the control box and set to the desired temperature with the pressure monitored throughout.
8. The autoclave was allowed to reach its final temperature and the pressure was increased to desired conditions by slow addition of CO_2.
9. After the desired reaction time, the autoclave was cooled by switching off and removing the heating band allowing the temperature to drop to ambient.
10. Once at ambient, the CO_2 was vented into the fume hood by opening HIP 15c.
11. Once at ambient temperature and pressure, the safety key was removed, reducing unions R2 and R3 disconnected, the clamp opened, and the product collected.

2.2.3.2 Emergency shutdown procedure

Ensure that the pressure monitor always remains on throughout this procedure and that the temperature is monitored by means of the internal thermocouple. This procedure should be carried out behind blast shields and whilst wearing full face shield protection

1. Set the heating box to 0 °C and unplug the heating jacket.
2. Carefully remove the heating jacket and allow the autoclave to cool to room temperature.
3. Remove the heating jacket, then place the autoclave in a dry ice/acetone bath until the temperature is lowered (*NO LOWER THAN -50 °C*, as the O-ring will fail below this temperature) and the pressure is as close to ambient pressure as possible.
4. If the pressure is less than 4 bar, loosen the key slowly to release the residual pressure. Do not fully remove the key until the autoclave reaches ambient pressure. Ensure that the pressure is released into the back of the fume hood, away from face.
5. If the pressure is above 4 bar, carefully loosen R2 (*Figure 2.3*) one full rotation on the 1/8” side. If this is unsuccessful in releasing the pressure, sequentially loosen one full rotation the autoclave engineer fittings in the head of the autoclave (except the inlet fitting). Each joint should not be loosened more than one full rotation. When pressure is below 4 bar, loosen the key slowly to release the residual pressure.
6. If the pressure is still not released seek help from the workshop.
7. Once the key has been removed allow the autoclave to warm to room temperature.
8. Undo the clamp and carefully remove it.
9. Open the autoclave.

2.2.4 Liquid addition under high pressure

The in-house developed MKIII high-pressure autoclave features a connection for the addition of liquid reagents whilst under pressure. This extra port in the autoclave head is built up of Swagelok tubing with a straight taper seal non-rotating stem needle valve (HiP 15-11AF1) (*Figure 2.4*), that can be connected to a HPLC pump (Jasco PU-4180) (*Figure 2.5*) through 1/16" Swagelok tubing.

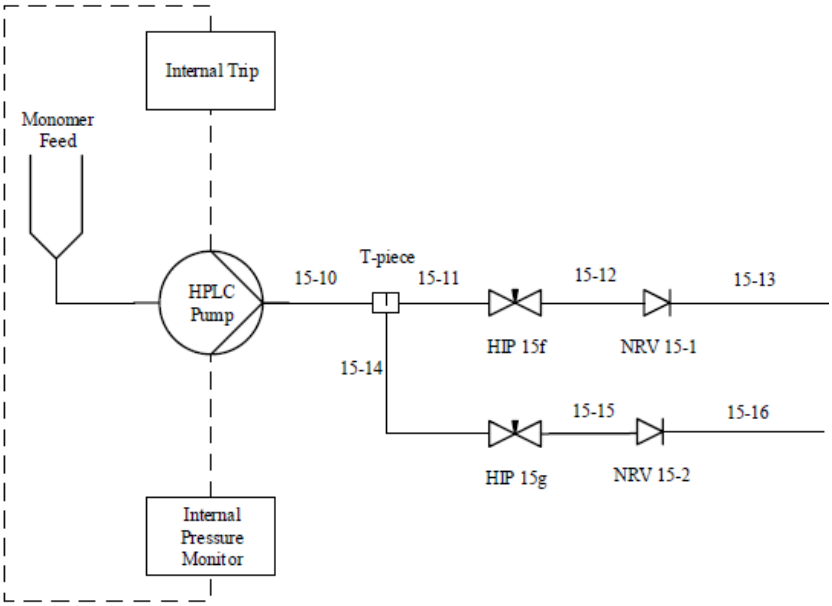


Figure 2.5 Schematic of Jasco PU-4180 HPLC pump set-up. 15-13 and 15-16 connect to their respective autoclave in the used high-pressure set-up (Figure 2.3), through the HPLC inlet tap connection (Figure 2.4).

2.2.4.1 Standard operating procedure

1. The initial state of the pump/autoclave should be with the HPLC line open only to the active autoclave side (HIP 15g or HIP 15f), and with the HPLC pump disconnected from the autoclave at 15-33 or 15-16 (*Figure 2.5*).
2. Flush the HPLC pump with acetone prior to liquid addition.
3. Flush the HPLC pump with the liquid being injected. Ensure that enough is used to displace all acetone in the tubing.

4. Connect HPLC outlet line (15-13 or 15-16, *Figure 2.5*) to the addition port on the autoclave.
5. Set pumping speed to 1-5 ml/min and begin pumping with the HPLC inlet tap closed. Pressure will build in the HPLC pump, which can be monitored from the display.
6. Continue pumping until the pump pressure matches the pressure inside the autoclave. (Note the liquid level in the HPLC pump syringe)
7. Open the HPLC inlet tap on the autoclave head, note that the pressure in the autoclave on the HPLC pump display do not change.
8. Set the desired pump rate and engage the HPLC pump.
9. Once the desired amount has been added, stop the HPLC pump and close the HPLC inlet tap in the autoclave head, sealing the autoclave from the HPLC pump.
10. Open the purge valve on the HPLC pump to release the pressure in the HPLC addition system.
11. Disconnect the HPLC outlet line (15-13 or 15-16, *Figure 2.5*). The tubing still contains addition liquid, so open in a fume hood slowly and be aware of any hazards of the materials.
12. Note the pressure inside autoclave, as this has increased with the addition of material. Do not add more CO_2 at this point as a pressure increase lag may occur.
13. Flush HPLC pipes with a suitable solvent, typically acetone, to the added liquid from the HPLC pump set-up.

2.2.4.2 Emergency shutdown procedure

1. Stop pump.

2. Close the HPLC inlet tap on autoclave to seal the autoclave set-up from the HPLC pump set-up.
3. Open the purge valve on the HPLC pump to release the pressure from the pump.
4. Switch off pump at mains.
5. Restart HPLC pump and replace all liquid in the set-up with acetone.

2.2.5 High pressure fixed volume view cell

To study the behaviour of compounds under high pressure conditions, a fixed volume view cell with a volume of ~100 ml was utilised. The in-house designed set-up retains many of the features of the MKIII high-pressure autoclave, but possesses two autoclave heads, each clamped to the central body (*Figure 2.6*). Both heads contain a sapphire window with a Teflon spacer and EPDM O-ring, for visible inspection under high-pressure conditions.

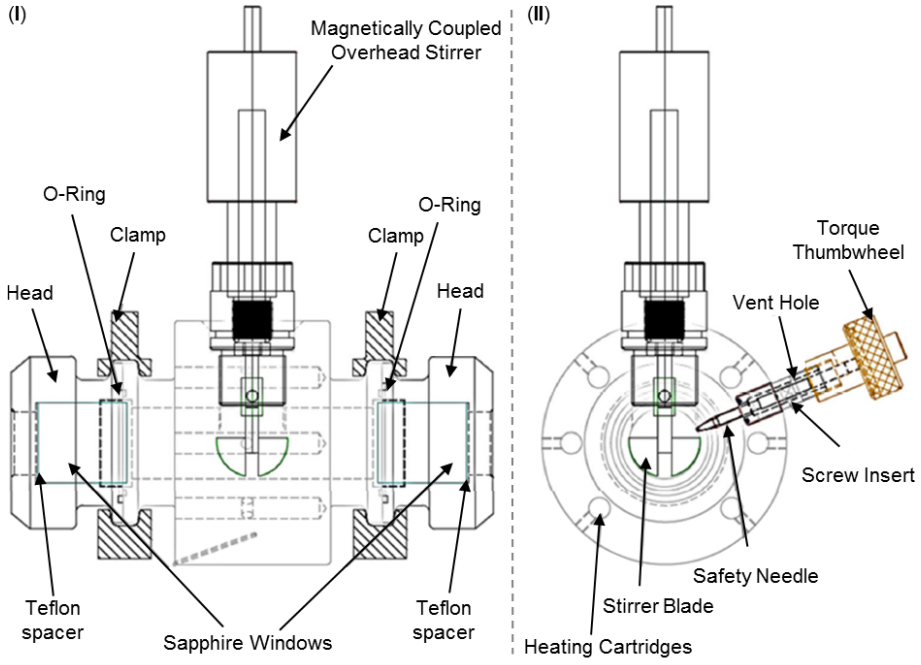


Figure 2.6 Schematic representation of the high-pressure fixed volume viewcell

The view cell is fixed into a purpose-built stand with safety shield, and is held in place using a clamp system (*Figure 2.7*).

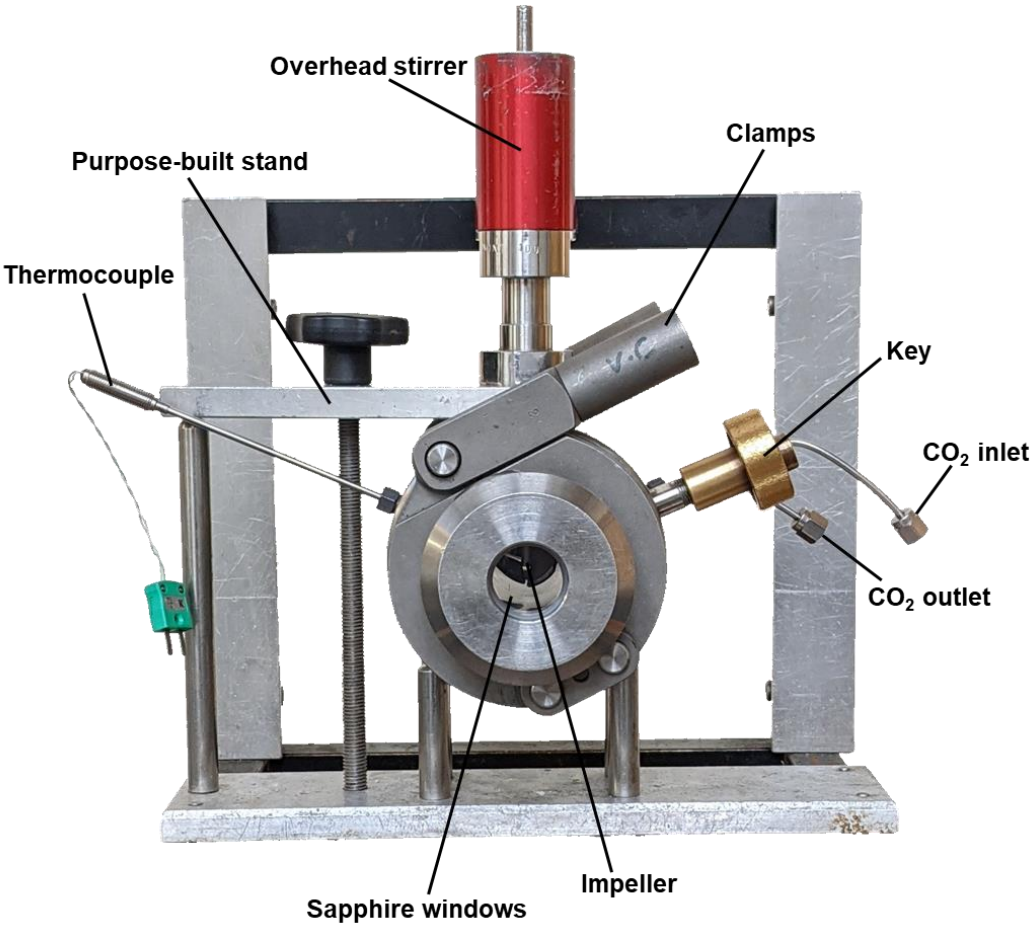


Figure 2.7 Image of fixed volume view cell set-up showing the body clamped into a purpose-built stand with safety shield.

2.2.5.1 Standard operation procedure

1. Insert the sapphire windows into the two heads, first placing the teflon spacer, followed by the window with an EPDM O-ring. Be sure to keep the head on a level surface and insert the sapphire window slowly, keeping it straight at all times.
2. Place O-rings at either end of the autoclave body
3. tighten all fittings in the body before fitting the rear head and clamp
4. Charge the cell with the sample under investigation via the open front end.
5. Check that the stirrer, heating cartridges, pressure transducer monitor, temperature controller, and thermocouples are all connected.
6. Fit the front head with an EPDM O-ring and clamp.

7. Insert the transparent safety shield into the view cell stand.
8. Slowly add CO_2 up to 100 bar in order to leak test the set up. Check all fittings for leaks with 'snoop'.
9. If required, vent the cell through the outlet tap and adjust any leaking fittings. Never tighten fittings while the cell is under pressure!
10. Repeat step 8 after adjusting fittings. Vent any remaining gas until the cell is at atmospheric pressure.
11. Purge the autoclave with a flow of CO_2, at 2-4 bar for 30 min in order to remove residual oxygen
12. Fit and hand tighten the key
13. Add CO_2 up to 50 bar and engage the stirring
14. Turn on the heating to the desired temperature.
15. Allow the autoclave to reach its final temperature. Monitor the pressure in the vessel constantly throughout this process!
16. Once the temperature has been reached, add CO_2 up to a final pressure of $\leq$300 bar. Note that this process will cause the cell to cool slightly, so allow the temperature to stabilise after each addition of CO_2.
17. After the desired observations have been made, turn off the heating and disconnect the heating element. Allow the cell to cool to room temperature, monitoring the temperature through the thermocouple.
18. After allowing the autoclave to cool to ambient temperature, vent CO_2 slowly into the fume hood. Once at ambient pressure, remove the key, disassemble the set-up, and clean the cell.

2.2.5.2 Emergency shutdown procedure

1. Switch of heating cartridges through the temperature control box and unplug the heating elements. Ensure that the pressure monitor always remains on throughout this procedure.
2. Allow the cell to cool to room temperature while monitoring the temperature by means of the internal thermocouple.
3. Loosen the knurled thumbwheel key slowly to release the residual pressure. Ensure that the pressure is released in the opposite direction to your body.
4. If the pressure is still not released seek help from the workshop.
5. Once the cell is at ambient pressure, remove the key, disassemble the set-up, and clean the cell.

2.2.6 High-pressure sampling set-up

To study kinetic behaviour of polymerisations in the MKIII high-pressure autoclave, a high-pressure sampling set-up was developed and used (*Figure 2.8*). The details of its design and implementation will follow in Chapter 3, while the standard operating procedure is outlined below.

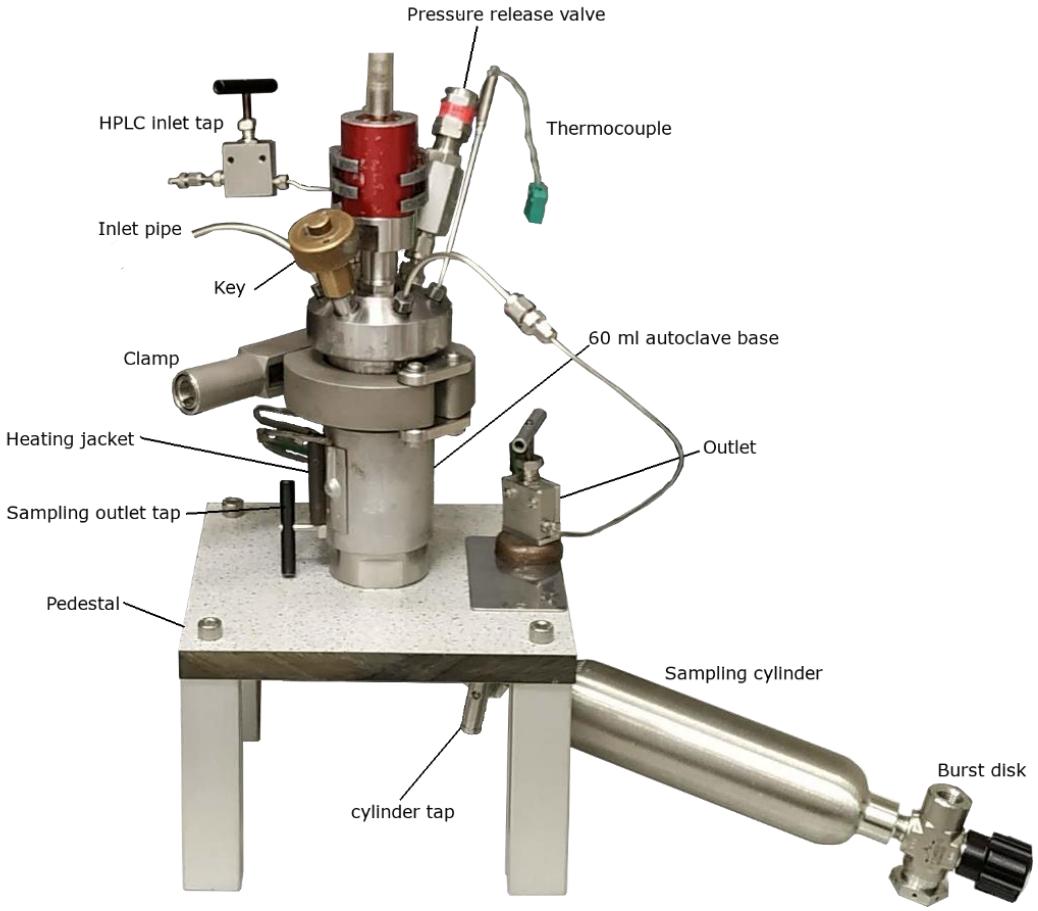


Figure 2.8 MKII high-pressure autoclave with high-pressure sampling set-up.

2.2.6.1 Standard operating procedure

1. Familiarise yourself with the standard operating procedure of the MKIII high-pressure autoclave before proceeding.
2. Attach the heating band by removing the screws and sliding it over the sampling outlet tap. Reinsert the screws and tighten the heating band above the sampling outlet tap, but below the clamp lip of the base.
3. Place an O-ring in the autoclave base, attach the required stirrer and assemble the autoclave. Place the autoclave on the pedestal, assuring the sampling outlet is accessible.
4. Ensure the autoclave is clamped firmly in place, then attach and tighten all the fittings and overhead stirrer.

5. Pressurise the setup to a minimum of 50 bar in order to leak test the set up. Check all fittings for leaks with 'snoop', including the sampling outlet and tap.
6. If leaks are found, vent the autoclave through the outlet tap and adjust any leaking fittings. **Never tighten fittings while the cell is under pressure!** Repeat leak test before proceeding.
7. Vent any remaining gas until the cell is at atmospheric pressure.
8. Purge the autoclave with a flow of CO_2, at ~2 bar for 30 min to remove residual oxygen.
9. Charge the autoclave with reactants through the keyhole, inset the key and hand tighten.
10. Fill the autoclave with CO_2 to ~50 bar.
11. Ensure that the internal thermocouple and heating jacket are plugged in. Set the heating to 50 °C and allow autoclave to reach this temperature. Increase the pressure slowly to 120 bar before setting the heating to 65 °C. *(If using different temperatures consult more experienced people in the lab).*
12. Allow the autoclave to reach its final temperature. Monitor the pressure in the vessel constantly throughout this process!
13. Once the temperature has been reached, top up the autoclave to its final pressure. *Note that this process will cause the cell to cool slightly, so allow the temperature to stabilise after each addition of CO_2.*
14. Fill out the "overnight reaction card" with appropriate reactants, conditions and hazards and leave clearly visible.
15. To take a sample
    a. Detach the cylinder tap from the sampling cylinder.

b. Assure that the bonnet valve tap on the burst disk is closed.

c. Add 5 ml of a deuterated solvent to the sampling cylinder using a syringe.(*this amount is dependent on your sample pipe length. 0.5 ml per cm of pipe gives a clear NMR signal*)

d. Attach the cylinder tap to the cylinder, hand tightening the joint firmly. (*Teflon tape is not required to seal the joint*) make sure that the cylinder tap is closed!

e. Add CO_2 to the system, raising the pressure by 20-25 bar.

f. Attach a partially hollow sampling pipe (*Figure 2.9*) to the sampling outlet, using a 3/8" spanner (autoclave engineer). Tighten the joint firmly, using your other hand to keep the autoclave stable. **Be aware that the autoclave is warm, so wear a heat resistant glove if needed!**



Figure 2.9 Partially hollow sampling pipe, used to flush sampling exit prior to sample collection.

g. Open the sample outlet tap a few full turns. The pressure will drop ~1 bar.

h. After a few seconds, close the sample outlet tap.

i. Detach the sampling pipe from the autoclave using the 3/8" spanner. **Be aware that the autoclave is warm, so wear a heat resistant glove if needed!**

j. Attach the autoclave engineer fitting of the sampling cylinder pipe to the sampling outlet, using a 3/8" spanner. Tighten the joint firmly, using your

other hand to keep the autoclave stable. **Be aware that the autoclave is warm, so wear a heat resistant glove is needed!**

k. **Confirm that the cylinder tap is closed!** At this point all taps throughout the setup should be shut.

l. Open the sample outlet tap a few full turns. The pressure will quickly drop by 10-15 bar, causing a drop in temperature. It will immediately begin to recover again.

m. After a few seconds, close the sample outlet tap.

n. With the autoclave sealed again, fully open the cylinder tap. The sample will spray into the cylinder and a very short hiss can be heard (like opening a cola bottle).

o. Detach the autoclave engineer fitting of the sampling cylinder from the sampling outlet using the 3/8" spanner. **Be aware that the autoclave is warm, so wear a heat resistant glove if needed!**

p. Pour the cylinder content into a vial, through the sampling cylinder tap and pipe.

q. Detach the cylinder tap and clean the cylinder system thoroughly before drying it well.

16. If further samples are required, repeat the step 15.

17. After the desired reaction time, set the heating box to 0 °C and unplug the heating band to prevent further heating. Allow the cell to cool to a subcritical temperature, monitoring the temperature by means of the internal thermocouple.

18. After allowing the autoclave to cool vent the CO_2 into the fume hood.

19. **If the autoclave is blocked follow the emergency shutdown procedure for the MKIII high-pressure autoclave setup (see section 2.2.3.2).** Never attempt to vent through the sampling exit!
20. Once at ambient temperature and pressure, remove the key; undo the Swagelok fittings in the fume hood, remove the clamp, open the autoclave, and collect the product.

2.3 Analytical methods

2.3.1 Gel permeation chromatography (GPC)

Molar masses and molar mass distributions was determined through gel permeation chromatography (GPC). During this work, GPC was performed with THF (HPLC grade, Fisher Scientific, stabiliser free) as the eluent at room temperature using two Agilent PL-gel mixed-C columns in series with a flow rate of 1 ml min^{-1}. Sample detection was achieved using a multiangle light scattering detector and differential refractometer. The system was calibrated using narrow dispersity PMMA standards(10 EasiVials covering an M_n of 1 090 to 538 500 g/mol).

2.3.2 Nuclear magnetic resonance spectroscopy (NMR)

Nuclear magnetic resonance spectroscopy (NMR) is a useful tool to confirm the identity of compounds containing NMR active nuclei. In this work ^1H NMR was used to identify monomer to polymer conversion.

Samples were dissolved in a suitable deuterated solvent ($CDCl_3$, D_2O or DMSO-d_6) and analysed using a Bruker DPX 400 MHz spectrometer. Chemical shifts were assigned in parts per million (ppm) and referenced to the residual protonated solvent peak of

the solvent. All spectra were obtained at ambient temperature (22 ± 1 °C). MestReNova 14.0.1 copyright 2019 (Mestrelab Research S.L.) was used for analysing all spectra.

An annotated spectrum of a PMMA/MMA mixture is shown in Figure 2.10. From this, conversion of MMA was determined using Equation 2.1 . the proton peak at 6.09 ppm was used to represent MMA throughout the thesis, while the peaks at 5.55 and 3.74 ppm are annotated for clarity.

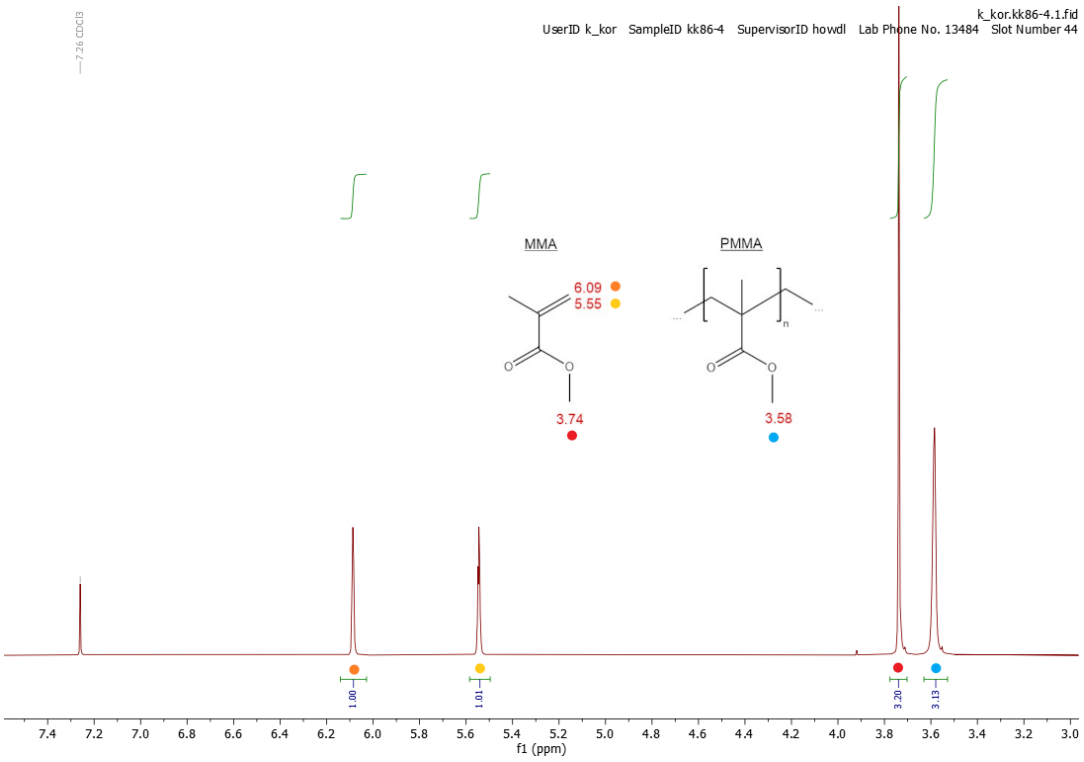


Figure 2.10 Annotated ^{1}H NMR of a PMMA and MMA mixture in $CDCl_3$. With the yellow and orange dot representing a single hydrogen on MMA, the red dot representing 3 hydrogens of MMA, and the blue dot representing 3 hydrogens of PMMA. A residual protonated solvent peak of $CHCl_3$, used to reference the spectrum, can be seen at 7.26 ppm. Conversion of MMA into PMMA was calculated by dividing the blue peak value by the sum of the blue peak value and 3 times the orange peak value.

$$x_{MMA} = \frac{I_{blue(3.58\ ppm)}}{I_{blue(3.58\ pp)} - 3 * I_{orange(6.09\ ppm)}} * 100\%$$

Equation 2.1

2.3.3 Scanning electron microscopy (SEM)

Scanning electron microscopy (SEM) is widely used for particle morphology determination at the nanometre and micrometre scale. In SEM, a focussed electron beam is fired at a sample in an ultrahigh vacuum chamber (to prevent electron scattering on air particles). Back-scattered electrons are emitted from the sample and registered as an electronic signal by a detector. After amplification, this signal is converted into a grey-scale image.

Polymer powder samples were mounted on aluminium SEM stubs using carbon tape or redispersed in hexane and deposited on a glass slide prior to mounting on carbon tape. To avoid charge build-up in the sample, a platinum coating was applied to the samples prior to SEM imaging. The coated particle samples were then imaged using a FEI Phillips XL30 SEM. The image analysis software Fiji(ImageJ) was used to analyse product morphology and feature size from obtained images. The reliability of this particle sizing method was verified by repeat analysis of several SEM images and several prepared samples, and consistent results were observed. As in previous publications employing this method,[35, 55, 67-69] 100 particles was found to be sufficient to obtain reliable particle size data for such monodisperse particle populations.

PSD is a measure used widely to describe the uniformity of spherical polymer particles and powders.[6, 8, 9] The PSD is determined as the ratio of the volume average diameter (d_v), also known as the De Brouckere mean, and the number average

diameter (d_n).[70-73] The equations used to determine the particle diameter mean values and PSD are shown below (Equation 2.2 – Equation 2.4).

$$d_n = \frac{\sum d_i n_i}{\sum n_i}$$

Equation 2.2

$$d_v = \frac{\sum {d_i}^4 n_i}{\sum {d_i}^3 n_i}$$

Equation 2.3

$$PSD = \frac{d_v}{d_n}$$

Equation 2.4

2.3.4 Differential scanning calorimetry (DSC)

Thermal properties of polymer materials can be measured using differential scanning calorimetry (DSC), including melting points, crystallisation points, and glass transition temperatures. The technique monitors the difference in heat flow rate between the sample and a reference during heating and cooling. DSC typically requires an initial heating cycle to remove thermal history of the sample prior to the measurement of thermal properties.

Polymer thermal properties were investigated by DSC using a TA Instruments Q2000, at a heating rate of 20 °C/min in the temperature range of -20 to 200 °C. Hermetic pans and lids (TA Instruments, Brussels, Belgium) were used for the analysis of the samples, using empty pans as the reference. The DSC cell was constantly purged with nitrogen gas at a flow rate of 50 ml/min.

2.3.5 Dynamic light scattering (DLS)

Dynamic light scattering (DLS) is a technique that is used to determine the size and size distribution of nanoparticles in a suspension. In DLS, a laser is shot through a sample, particles will scatter the incident light, and the scattered light is collected. As particles move in suspension, due to Brownian motion, the scattered light provides information regarding the speed at which they are diffusing, which is inversely related to the size of the particles.

DLS was performed using a Malvern Zetasizer Helix at 25 °C using a 633 nm (4 mW) wavelength laser. The scattered light was detected at an angle of 173°. Particles were suspended in heptane at a concentration of 0.25 mg/ml. The mixture was homogenised by sonication prior to analysis.

2.3.6 Dynamic mechanical analysis (DMA)

As with DSC, dynamic mechanical analysis (DMA) provides information about the thermal properties of polymer materials. The technique analyses the temperature dependence of the storage modulus (G') and the loss modulus (G''), representing the elasticity and viscosity of the sample respectively. Thermal transitions can be observed as transitions in the moduli and as peak maxima in the moduli derived tan δ (Equation 2.5). the main advantage of DMA over DSC, is that measurements are performed without an initial heating cycle to remove thermal history, allowing for the observation of morphological effects.

$$\tan\delta = \frac{G''}{G'}$$

Equation 2.5

DMA was performed using a Triton Technologies dynamic mechanical analyser (now Mettler Toledo DMA1, Columbus, OH, USA) using the powder pocket accessory. The use of this attachment allowed for direct measurement of the synthesised powder with no further sample preparation required. Approximately 40 mg of sample was packed into a powder pocket and mounted in single cantilever bending geometry. Samples were analysed at a relevant temperature range between −100 and 250 °C, at 1 and 10 Hz frequency, at a heating rate of 3 °C/min. The T_g was recorded as the peak temperature of the tan δ trace obtained at 10 Hz or the change maximum of the storage modulus (G') when the tan δ peak was not sufficiently clear.

2.3.7 Transmission electron microscopy (TEM)

Transmission electron microscopy (TEM) is an imaging technique similar to SEM. Instead of detecting back scattered electrons, as in SEM, TEM relies on the detection of transmitted through the sample. This requires thin sections of sample to be prepared, but can give detailed morphological information not accessible with SEM.

TEM images were captured using a FEI Tecnai G2 12 Biotwin at an accelerating voltage of 100 kV. Samples were prepared by embedding particles in an epoxy resin (Agar 100) at 50 °C for 48 hours prior to slicing 100 nm thick sections using an RMC Powertome microtome equipped with a Diatome diamond knife. Sections were captured on a 400-mesh copper grid and stained for 2-4 hours with Ruthenium vapour to induce image contrast. Ruthenium vapour was generated in a sealed container by combining 12.4 mg of $RuCl_3$ with 4.2 mg of $NaIO_4$ in 1 ml of H_2O. after staining, the solution is quenched with an excess of corn oil.

2.3.8 Time-of-flight secondary ion mass spectrometry (ToF-SIMS)

Time-of-flight secondary ion mass spectrometry (ToF-SIMS) is an analysis technique that allows for surface sensitive mass spectroscopy, giving chemical information about a samples surface. By sputtering a sample with a focussed ion beam, the surface can be dislodged. The released ions can then be analysed for their molecular composition, revealing the molecular or polymeric make-up of the surface. By sequentially sputtering and analysing, data can be gathered about thechemical makeup under the surface. Depth profile data were obtained using a ToF-SIMS IV instrument (ION-TOF GmbH, Münster, Germany). The measurements were performed in non-interlaced mode with 1 frame of analysis followed by 1 frame of sputter. The primary ion beam used for analysis was a bismuth liquid metal ion gun (Bi_3^+) operated at 25 keV (pulsed target current of around 1 pA) and an argon gas cluster (Ar_{1700}^+, 10 keV) was used as the sputter source for depth profiling. Sputtering was performed over an area of 500 µm × 500 µm, with the central 200 µm × 200 µm area analysed at a 256 × 256 pixel resolution. Positive ion data were collected, and the profiling data were analysed using SurfaceLab 7 software (IONTOF GmbH).

2.3.9 Atomic force microscopy (AFM)

Atomic Force Microscopy (AFM) is a type of microscopy that analyses a sample through a probe to observe the sample surface. By tapping the probe onto the surface, the hardness of the sample at that point can be measured. Measurements were conducted on a Dimension FastScan AFM (Bruker Corporation), working in PeakForce quantitative nanomechanical property (PF-QNM) mode in air with an

RTESPA-150 silicon probe (spring constant = 2.44 N m^{-1}). Samples were prepared by dispersing 20 mg of polymer in 2 ml of heptane, sonicating to assure full dispersion, then spin coating the solution onto a silicon wafer or glass slide at 1500 rpm. Residual solvent was allowed to evaporate overnight, prior to AFM analysis of the deposited particles.

2.3.10 NanoIR

Samples found to be suitable for AFM were sent to Bruker (Karlsruhe, Germany) for NanoIR analysis, a technique that combines AFM and IR spectroscopy to acquire high resolution chemical information.[74] This technique allows for the resolution of AFM microscopy to be combined with the chemical information gained from IR. In practice, this allows for the nanometre scaled chemical mapping of a sample surface. Measurements were conducted using a Bruker nanoIR3-s with FASTspectra QCL laser source in tapping mode. AFM topography was used to check surface quality and identify particles, followed by photothermal AFM-IR imaging at different locations (point spectra) within the sample area. Subsequent IR chemical imaging at fixed wavenumbers was conducted to create band ratio images.

Chapter 3

On-line Polymerisation Monitoring in Supercritical Carbon Dioxide

3.1 Overview

Supercritical carbon dioxide ($scCO_2$) is a promising alternative to traditional solvents, combining considerable environmental advantages[34] with the enhanced solvation and diffusivity properties of SCFs.[8, 9, 35, 36] It is a cheap, non-flammable and environmentally friendly solvent,[34] with an easily attainable critical point at relatively mild conditions (T_c = 31.1 °C and P_c = 73.8 bar).[8, 9] But despite the potential benefits, barriers remain to its wider industrial use.

Safe, large scale, industrial polymerisations rely heavily on consistent on-line monitoring of reaction progression, something that is easily achieved in traditional solvents through a wide range of techniques.[15, 30, 75-78] Reactions in $scCO_2$ however, are more complicated to monitor due to the elevated pressure present in sealed systems, complicating the implementation of typical monitoring systems and increasing the cost significantly. This chapter will describe the design and implementation of a tailored sampling system capable of providing on-line monitoring in $scCO_2$ in a cheap and reliable manner. The system will be tested against a range of polymerisations and adapted to suit a range of conditions, showcasing the robust potential of the system for industrial applications. The kinetic profile of a typical dispersion polymerisation in $scCO_2$ will also be analysed, to gain further insight into the mechanism and allow for a thorough description of the system.

3.2 Introduction

The monitoring of polymerisation reactions has both fundamental and applied motivations. On a fundamental level, monitoring of various reaction characteristics

can resolve underlying reaction mechanisms and reveal ways in which a reaction deviates from what is thought to occur ideally. On a more practical level, monitoring allows for the optimisation of reaction conditions on a lab scale. This information ultimately leads to safe efficiency gains in industrial reactors, with optimised resource use and subsequent emission reductions.[30]

The reliable kinetic description of a polymerisation reaction is essential for its safe commercial implementation. The determination of kinetic properties of a polymerisation reaction relies on two essential factors. Firstly, it requires a reliable method of monitoring, allowing the reaction progress to be tracked throughout. Secondly, it requires a comprehensive description of all reactions occurring in the system during polymerisation. In traditional solvents used widely in industry, a robust kinetic description is determined on a lab scale, using a range of techniques tailored to the system and the data needs. This kinetic information is then used to guide reaction scale-up and implement safe and reliable monitoring throughout the process. In $scCO_2$ however, reliable and accessible monitoring on the lab scale has so far been a barrier to kinetic data acquisition and any potential industrial future of the system.

3.2.1 Monitoring polymerisations in conventional solvents

Polymer characteristics such as molecular weight, chain length distribution, conformation, spatial dimensions, viscosity, and many others, can affect macroscopic polymer properties such as tensile strength, rheological properties, material processability, impact resistance, crystallinity, etc. The final application of a produced polymer will determine the suitable polymer characterisation method that gives the

desired information. A wide range of off-line polymer characterisation techniques have been translated into on-line polymerisation monitoring systems on an industrial scale.[30] While many polymer properties can be of interest for on-line monitoring, and can be determined through a range of analytical techniques tailored to the type of reaction and the reactor setup, polymerisation progress for kinetic analysis is widely described in terms of monomer to polymer conversion and molecular weight.[11, 15, 30, 75]

Spectroscopic techniques, such as IR, Raman, NMR, etc., are used extensively for on-line monitoring and control of solution-based processes in different fields.[30] In the polymer field however, spectroscopic techniques are most commonly used for offline analysis of a final product.[30, 79-83] There are very few examples of direct in-line or on-line monitoring and control of large scale polymerisation processes, with most usage focussing on processing of polymer resin, not the actual polymerisation stage.[30, 84, 85] Reported applications of spectroscopic techniques for on-line polymerisation tracking in literature are exclusively for small scale lab-scale reactors, mainly due to fouling issues that occur in large scale systems.[30] Fouling is not an issue on a lab-scale, as the spectrometer probe can be between successive experiments. Additionally, the sensitivity to fluctuations and vibrations of spectrometers will disturb the collection of spectral data and the performance of calibration models at large scale plant sites.[30] The wide and varied use of spectroscopic techniques on the lab scale[75], does however provide valuable insights in polymerisation systems, and often leads to offline spectroscopic product analysis at the industrial scale.[30]

Calorimetry, conductivity, densimetry, and rheological measurements are all non-invasive indirect measurement methods that can be used for on-line polymerisation monitoring. They are sometimes referred to as in-line monitoring systems. Indirect monitoring methods measure a state or physical property in a reactor, that is linked back to reaction progress through kinetic models in real time.[30] The main advantage of these techniques is the non-invasive nature, the rapidity of feedback, and the low cost. They do however require previous knowledge of the reaction, and they can only be used if there is a large enough change in the physical property or state that is being probed. For example, a clear and measurable change in heat capacity is needed to be able to use calorimetry for reaction monitoring, while many heat contributions can be present in a typical semibatch polymerisation reactor (Figure 3.1). The overall heat generated in the reactor can be monitored but separating the different sources of heat can be challenging. Additionally, separate reactions occurring simultaneously are impossible to distinguish. While non-invasive indirect monitoring is essential for safety and quick feedback, it is insufficient by itself to completely monitor a polymerisation reactor.[30]

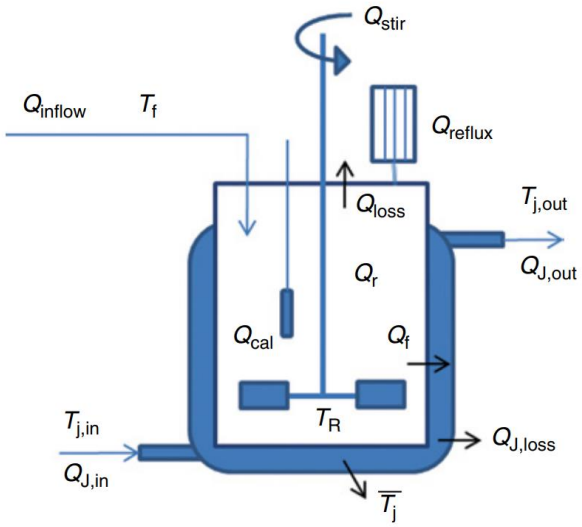


Figure 3.1 Schematic of a semibatch stirred tank reactor with indication of the heat contributions.[30]

The most detailed and information rich method of polymerisation monitoring is through offline analysis of an on-line obtained sample. A sample of an ongoing polymerisation can be analysed thoroughly, often through SEC/GPC, gas chromatography, and light scattering techniques, to determine component concentrations and polymer characteristics. The two main drawbacks of reaction sampling are assuring a representative sample is obtained and the delay between sample collection and analysis.[30] Heterogeneous systems can offer a challenge in terms of consistent sample collection, and data must be correlated with other monitoring methods to assure accuracy. In commercial systems, delayed sample analysis is often mitigated by using integrated sampling and measuring systems that are then considered fully on-line.[30, 75, 86] An example of this is a rapid GPC system connected to a polymerisation reactor for rapid monitoring of molecular weight progression during polymerisation (Figure 3.2).[86]

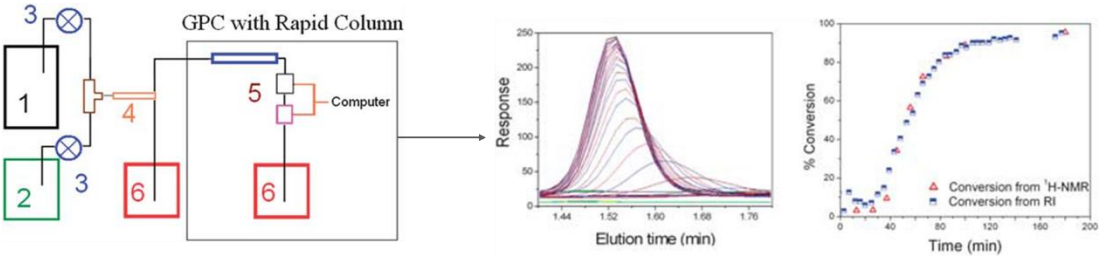


Figure 3.2 Setup of on-line rapid GPC instrumentation and typical data output. With (1) reactor, (2) solvent, (3) HPLC pumps, (4) injection loop, (5) detectors, and (6) waste.[75, 86]

Automatic continuous on-line monitoring of polymerisations (ACOMP) is a principle based on the continuous withdrawal of small sample volumes from an ongoing reaction, followed by dilution and analysis in a series of flow through detectors.[30, 75, 78, 87, 88] It is an expansion upon the sample and analyse methods described previously, and it allows the direct feedback of data on reaction control. A wide array of detectors can be incorporated into an ACOMP setup, including light scattering, differential refractive index, ultraviolet/visible absorption, viscosity, conductivity, and ^{1}H NMR[88] among many others.[30] The continuous recording of kinetic data and polymer properties can then be used to feed back into polymerisation control, for example to control the feedstock addition in a semi-batch polymerisation. For example, ^{1}H NMR and UV were used to track monomer conversion of acrylamide, sodium acrylate, and styrene sulfonate by McAfee *et al*. (Figure 3.3). The higher reactivity of styrene sulfonate would mean the formation of large gradients in the copolymerisation, but the ACOMP system was used to control the feedstock addition and maintain a constant polymer composition throughout the formed polymer.[88]

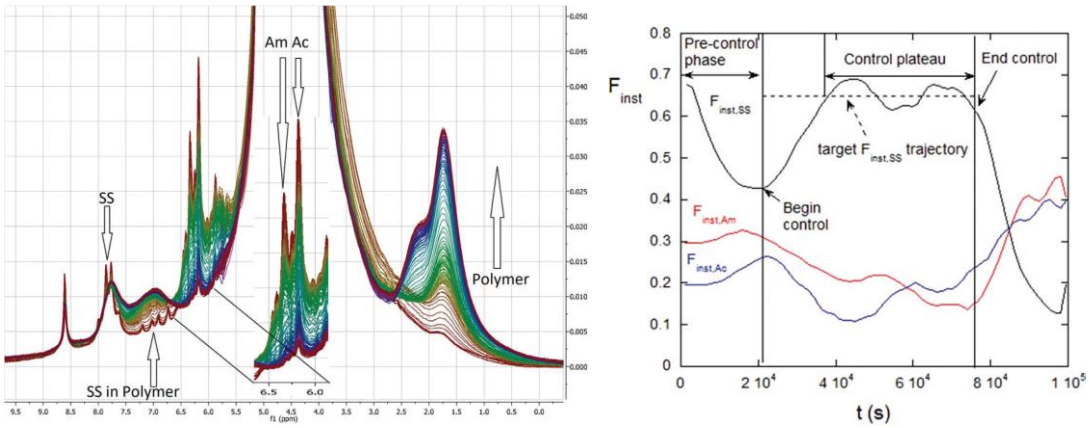


Figure 3.3 (left) Sample ^{1}H NMR spectra from the terpolymerisation of styrene sulfonate (SS), acrylamide (Am), and sodium acrylate (Ac). (right) Instant fractions of monomers during polymerisation, showing the fast consumption of SS, and the feedstock control system able to maintain a constant fraction during polymerisation.[88]

3.2.2 Monitoring polymerisations in $scCO_2$

While the tracking of an ongoing polymerisation reaction in traditional solvents can be achieved with a wide range of techniques,[30] reactions in $scCO_2$ are more complicated to monitor due to the elevated pressure present in sealed systems. Spectroscopic techniques can be used in $scCO_2$, but require bespoke and specialised equipment, capable of withstanding the high system pressures, and because of this the use of on-line spectroscopic techniques for polymerisations in $scCO_2$ is currently limited.

FTIR has been used to monitor the precipitation polymerisation of acrylic acid in $scCO_2$.[89] While the viability of the technique was confirmed by comparing polymerisation results in $scCO_2$ to the atmospheric polymerisation in toluene and model fittings, the widespread use of IR in $scCO_2$ is hampered by the costly and precise setup required.

Raman spectroscopy, another technique used widely for on-line monitoring of polymerisations,[90] has also been implemented in $scCO_2$ reaction monitoring.[91] As with IR spectroscopy, Raman spectroscopy requires the incorporation of an optical fible into the body of the reactor for incident light interaction with the reaction medium. While Raman spectra can be captured at location of the incident light, avoiding the need for a fixed path length or second window,[92] the overall cost of such a setup forms a barrier to widespread implementation.

Turbidimetry, unlike static or dynamic light scattering,[93, 94] is not sensitive to multiple scattering disruptions and can therefore be used for the monitoring of strongly scattering suspensions as found in $scCO_2$ polymerisations.[95] While this can provide on-line polymerisation monitoring at initial stages of a polymerisation, it does require costly apparatus to allow line-of-sight through the reaction medium.[96-99]

An on-line (or in-line) monitoring technique that does not require the incorporation of windows or probes into the $scCO_2$ reactor setup is power compensation calorimetry.[29, 51, 100, 101] Polymerisation progress can be tracked by monitoring the power required to maintain system temperature at the desired level. When a sufficiently exothermic polymerisation reaction occurs, less power will be needed to maintain reactor temperature and power output can then be correlated to polymerisation progress. Despite the accurate data this method can provide, the efficacy is very dependent on the thermal properties of the reaction and molecular data is lacking. The setup is also scale sensitive, as calorimetry is generally less applicable to large scale systems due to the sensitivity to other heat and loss factors.

Polymerisation reactions at atmospheric pressure are most widely monitored by sampling a known volume from the reactor at regular intervals, and analysing this offline or through integrated on-line sample and analyse systems.[90] This technique can also be applied to polymerisations in $scCO_2$, but the reaction setup must be modified to allow for this. The autoclave requires a needle valve exit to allow for sampling, as described by Thurecht and co-workers.[102] Polymer conversion can then be followed via for example ^{1}H NMR measurement, comparing the polymer concentration to residual monomer concentration.[35] While simply collecting a sample from a needle valve exit can provide a reliable sample, the major problem is that volatile components will be lost, resulting in erroneous results. Additionally, the method of sample collection introduces sharp pressure fluctuations, that can have a detrimental impact on the ongoing reaction. It is important to assure representative sample collection, that doesn't affect the ongoing polymerisation. On-line sampling is generally considered the most comprehensive and reliable polymerisation monitoring method.[30]

3.2.3 Polymerisation kinetics

Next to monitoring of an ongoing polymerisation, a kinetic description of the reaction is essential to predict reaction outcomes and understand anomalous behaviour.

3.2.3.1 Reaction description

In free radical polymerisations, six separate reactions can be distinguished: decomposition, initiation, propagation, two types of termination and radical transfer to monomer, as shown in Scheme 3.1.[11, 12]

$$I \xrightarrow{k_d} 2R^{\cdot} \quad (1)$$

$$R^{\cdot} + M \xrightarrow{k_i} RM_1^{\cdot} \quad (2)$$

$$RM_n^{\cdot} + M \xrightarrow{k_p} RM_{n+1}^{\cdot} \quad (3)$$

$$RM_n^{\cdot} + RM_m^{\cdot} \xrightarrow{k_{tc}} RM_{n+m}R \quad (4)$$

$$RM_n^{\cdot} + RM_m^{\cdot} \xrightarrow{k_{td}} RM_n + RM_m \quad (5)$$

$$RM_n^{\cdot} + M \xrightarrow{k_{tr}} RM_n + M_1^{\cdot} \quad (6)$$

Scheme 3.1 General equations of free radical polymerisation. (1) Decomposition, (2) initiation, (3) propagation, (4) termination by combination, (5) termination by disproportionation, (6) radical transfer. I = initiator molecule, M = monomer, M_x = polymer chain of length x, R = initiator decomposition product, k_d = dissociation rate constant, k_i = initiation rate constant, k_p = polymerisation rate constant, k_{tc} = termination by recombination rate constant, k_{td} = termination by dissociation rate constant, k_{tr} = radical transfer to monomer rate constant.[12]

The accuracy of this description is limited to a one phase homogeneous system, where component concentrations do not vary throughout the mixture. It will need to be expanded upon to describe the reaction possibilities within a dispersion system where multiple phases are present.

3.2.3.2 Kinetics of heterogeneous polymerisations

A heterogeneous dispersion polymerisation system is characterised by two separate phases, a continuous phase dominated by the chosen solvent and a dispersed phase consisting mainly of the formed polymer.[7] Both phases can contain all reaction components in varying concentration, resulting in the reactions shown in Scheme 3.2.[12, 103]

$$I \xrightarrow{k_{d,j}} 2R^{\cdot} \quad (1)$$

$$R^{\cdot} + M \xrightarrow{k_{i,j}} RM_1^{\cdot} \quad (2)$$

$$RM_n^{\cdot} + M \xrightarrow{k_{p,j}} RM_{n+1}^{\cdot} \quad (3)$$

$$RM_n^{\cdot} + RM_m^{\cdot} \xrightarrow{k_{tc,j}} RM_{n+m}R \quad (4)$$

$$RM_n^{\cdot} + RM_m^{\cdot} \xrightarrow{k_{td,j}} RM_n + RM_m \quad (5)$$

$$RM_n^{\cdot} + M \xrightarrow{k_{tr,j}} RM_n + M_1^{\cdot} \quad (6)$$

Scheme 3.2 General equations of free radical polymerisation in a two-phase system. (1) Decomposition, (2) initiation, (3) propagation, (4) termination by combination, (5) termination by disproportionation, (6) radical transfer. I = initiator molecule, M = monomer, M_x = polymer chain of length x, R = initiator decomposition product, k_d = dissociation rate constant, k_i = initiation rate constant, k_p = polymerisation rate constant, k_{tc} = termination by recombination rate constant, k_{td} = termination by dissociation rate constant, k_{tr} = radical transfer to monomer rate constant, j=phase (j=1 indicates the continuous phase, j=2 represents the polymer-rich dispersed phase).

To resolve the reactions of Scheme 3.2, it is essential to know where reactions are occurring within the system. During the early stage of a dispersion reaction, polymerisation only occurs in the continuous phase, as it is the only phase present.[96] When the growing polymer chains reach a critical chain length (J_{crit}[11, 29] / Z_{mer}[30]), characteristic of the polymer and solvent under investigation, it will precipitate out of solution and be stabilised by the present stabiliser, forming the dispersed phase. Depending on specific solubility and mobility, the reacting components present in the continuous phase can diffuse into the dispersed phase, allowing for polymerisation to occur in both phases. The locus of polymerisation is dependent on the component partitioning between the continuous and dispersed phase.[104-106]

3.3 Aims and objectives

The goal of the research presented here is to develop a reliable and widely applicable sampling method for supercritical fluid reactions, that could be directly comparable to on-line monitoring techniques used for atmospheric polymerisations throughout research and industy.[30, 75, 107, 108] With reactor sampling being at the core of on-line monitoring and ACOMP systems, a reliable sampling method is essential for the commercial application of $scCO_2$ as a solvent for polymerisations.

Using the dispersion polymerisation of MMA as a proof-of-concept reaction, a reliable, simple, and inexpensive sampling system will be developed. The polymerisation kinetics will be determined by successive batch reactions, and the accuracy of the sampling system will be assessed against this. The system will then be utilised to demonstrate the predictive nature of the kinetic data, in a quick and efficient manner.

Further to this, the sampling method will be tested in a range of polymerisations to showcase the ease of applying the novel method to a range of different reaction systems.

3.4 Experimental

3.4.1 Materials

Methyl methacrylate (MMA, 99 %) was obtained from Mitsubishi Chemical. 2,2'-Azobis(isobutyronitrile) (AIBN, 98 %) was purchased from Molekula. Methacrylate terminated polydimethylsiloxane (PDMS-MA, 150-200 cSt, 10 000 g/mol) was

acquired from Fluorochem. 2-cyano-2-propyl dodecyl trithiocarbonate (CPDT, 97 %), styrene (99 %), acrylic acid (AA, 99 %) and 2-Hydroxyethyl methacrylate (HEMA, 97 %) were purchased from Sigma-Aldrich. ε-Caprolactone (CL, 99 %) was obtained from Fisher Scientific. Novozym-435 (Candida Antarctica lipase B immobilized on acrylic resin) was kindly donated by Novozymes A/S, Denmark. Carbon dioxide (CO_2, SCF grade 5.5, 99.9995 %) was obtained from Air Products and Chemicals Inc. All chemicals were used as received.

3.4.2 HPLC initiated free radical dispersion polymerisation of MMA

Batch type dispersion polymerisations were carried out in an in-house built high-pressure reaction vessel with an internal volume of 60 ml (max. operating conditions: 120 °C, 380 bar), detailed in section 2.2.3. To control the start time of the polymerisation, initiator was added though a JASCO LC-4000 HPLC pump attached to the reaction vessel, described in section 2.2.4.

All reactions were conducted with MMA (9.36 g, 10 ml), PDMS-MA stabiliser (5 wt% relative to MMA, 0.468 g) and AIBN initiator (0.25-2 wt% relative to MMA, 23.4-187.2 mg). Oxygen is a known inhibitor for polymerisation reactions, as it reacts with formed radicals, stopping all chain propagation.[109] All solutions used in the polymerisation process were therefore degassed to avoid oxygen contamination. MMA, PDMS-MA and AIBN were all degassed by bubbling with argon in separate vials for 30 minutes. During this time, the autoclave was flushed with CO_2 at 2-3 bar, venting through the keyhole. After 30 minutes of degassing, MMA (7.5 ml, 7.02 g) was added to the PDMS-MA vial and this mixture was injected into the autoclave

through the keyhole against a positive flow of CO_2. The key was then inserted into the autoclave, sealing it off from the atmosphere. At this point CO_2 was added, pressurising the system to 50 bar. Heat was then applied through the heating jacket, bringing the temperature to 65 °C. CO_2 was then added until the system pressure reached 200 bar. As the AIBN initiator is a solid powder, it cannot be added to the autoclave without solvent. A stock solution of 0.3744 g AIBN in 10 ml MMA is used to pump in the desired amount of initiator (0.0936 g). Before connecting the HPLC pump to the autoclave, the pipe system is first rinsed by pumping acetone through to the autoclave connection. Following this, the MMA/AIBN stock solution is pumped through, pushing out the acetone. When the piping is filled with the stock solution, the pipe is connected to the HPLC inlet tap of the autoclave, shown in section 2.2.3. With the autoclave inlet tap closed, pressure in the HPLC pump is built up by pumping in stock solution at a slow rate. The pressure of the HPLC pump is brought to reaction pressure, meaning that opening the inlet tap will not cause any liquid movement. The flow rate of the HPLC pump was set to 1 ml/min. The inlet tap was then opened, and the pump was engaged. The desired amount of AIBN, along with 2.5 ml of MMA, was added after 2.5 minutes of pumping at 1 ml/min. after this time, the pump was stopped, and the inlet tap was closed. The pressure was then raised to 220 bar by adding CO_2, if needed. The end of the initiator injection was chosen as the starting point of the reaction.

3.4.3 RAFT controlled dispersion polymerisation of MMA

The reaction was conducted with MMA (0.1 mol, 10 g), PDMS-MA stabiliser (5 wt% relative to MMA, 0.5 g) and AIBN initiator (0.085 mmol, 28 mg) and the chain transfer

agent 2-cyano-2-propyl dodecyl trithiocarbonate (CPDT) (0.17 mmol, 59 mg) in a 60 ml high pressure autoclave. All reagents were kept on ice and degassed by bubbling with argon for 30 minutes. During this time, the autoclave was flushed with CO_2 at 2-3 bar, venting through the keyhole. After 30 minutes, the reactants were injected into the autoclave through the keyhole against a positive flow of CO_2. The key was then inserted into the autoclave, sealing it off from the atmosphere. At this point CO_2 was added, pressurising the system to 50 bar. Heat was then applied through the heating jacket, bringing the temperature to 65 °C. CO_2 was then added until the system pressure reached 275 bar. The moment the reaction temperature was reached was chosen as the starting point of the reaction.

3.4.4 Free radical dispersion polymerisation of styrene

The reaction was conducted with styrene (9.09 g, 10 ml), PDMS-MA stabiliser (20 wt% relative to styrene, 1.818 g) and AIBN initiator (2 wt% relative to styrene, 181.8 mg) in a 60 ml high pressure autoclave. Styrene and PDMS-MA with AIBN were degassed by bubbling with argon in separate vials for 30 minutes. During this time, the autoclave was flushed with CO_2 at 2-3 bar, venting through the keyhole. After 30 minutes, styrene (10 ml, 9.09 g) was added to the PDMS-MA and AIBN and this mixture was injected into the autoclave through the keyhole against a positive flow of CO_2. The key was then inserted into the autoclave, sealing it off from the atmosphere. At this point CO_2 was added, pressurising the system to 50 bar. Heat was then applied through the heating jacket, bringing the temperature to 65 °C. CO_2 was then added until the system pressure reached 245 bar. The moment the reaction temperature was reached was chosen as the starting point of the reaction.

3.4.5 Free radical precipitation polymerisation of acrylic acid

The reaction was conducted with acrylic acid (2 g) and AIBN initiator (1.5 wt% relative to acrylic acid, 30 mg) in a 60 ml high pressure autoclave. Acrylic acid with AIBN was degassed by bubbling with argon in a glass vial for 30 minutes. During this time, the autoclave was flushed with CO_2 at 2-3 bar, venting through the keyhole. After 30 minutes, the acrylic acid and AIBN mixture was injected into the autoclave through the keyhole against a positive flow of CO_2. The key was then inserted into the autoclave, sealing it off from the atmosphere. At this point CO_2 was added, pressurising the system to 50 bar. Heat was then applied through the heating jacket, bringing the temperature to 62 °C. CO_2 was then added until the system pressure reached 160 bar. The moment the reaction temperature was reached was chosen as the starting point of the reaction.

3.4.6 Enzymatic ring-opening polymerisation of caprolactone

The reaction was conducted with CL (4 g, 35 mmol), HEMA (0.18 g, 1.40 mol) and Novozym-435 (0.4 g, 10 wt% relative to the caprolactone) in a 60 ml high pressure autoclave. HEMA and CL were loaded into the autoclave base, while Novozym beads were placed into a wire mesh cage affixed to the stirrer shaft described in previously.[110] The autoclave was degassed using a flow of CO_2 (3 bar, 15 min) through the keyhole, before being sealed and pressured to 50 bar. Heat was then applied through the heating jacket up to 65 °C. CO_2 was then added until the system pressure

reached 207 bar. The moment the reaction temperature was reached was chosen as the starting point of the reaction.

3.4.7 Monitoring methods

3.4.7.1 Quench and measure method

Batch polymerisations were carried out following the procedure detailed in section 3.4.2. Successive reactions were halted by submerging the autoclave in an ice-water bath (Figure 3.4), cooling the system to subcritical temperatures within a minute. The pressure was then slowly released, and the product was analysed for conversion and molecular weight, in line with the methodology used across the research field previously.[40, 53, 111-113] This was done to establish a reference baseline for expected conversion values.

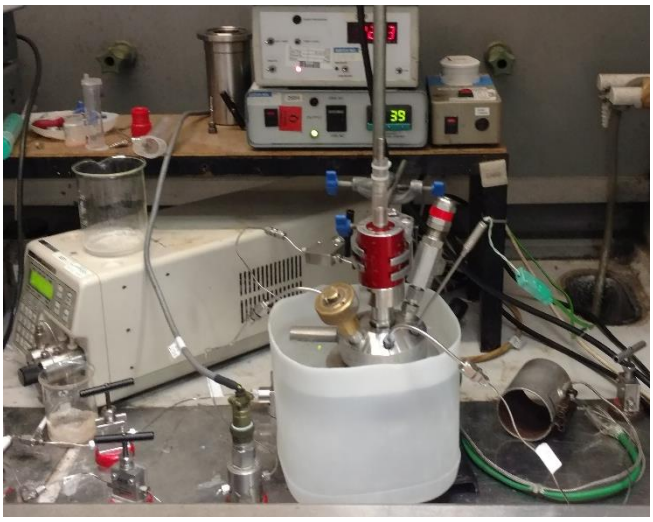


Figure 3.4 High pressure autoclave submerged in water and ice bath, to quickly cool the polymerising system.

3.4.7.2 Sampling pipe method

Batch polymerisations were carried out following the procedure detailed in section 3.4.2, using the sampling autoclave shown in section 2.2.6. Sampling was achieved

using a partially hollow pipe (Figure 3.5). To acquire a sample from an ongoing polymerisation, the sampling pipe was screwed into the bottom of the sampling autoclave, using an autoclave engineer fitting. With the fitting sealed tightly, the sampling tap was opened fully, and the sampling pipe was exposed to the polymerising system. At this point a slight pressure drop of approximately 0.5 bar was observed, confirming that the additional volume of the sampling pipe is part of the system. After 5 seconds the tap was closed again, sealing the sampling pipe from the system. The sampling pipe was then unscrewed, releasing pressure, and producing a short hiss as CO_2 is released from the pipe. A small amount of monomer and polymer will be left in the sampling pipe. The pipe was then submerged in deuterated chloroform in a small vial, dissolving the sample for ^1H NMR characterisation (see heading 2.3.2). After cleaning and drying, the sampling pipe can again be used to extract another sample. CO_2 was not added to the system after sampling, as the pressure drop was considered insignificant.

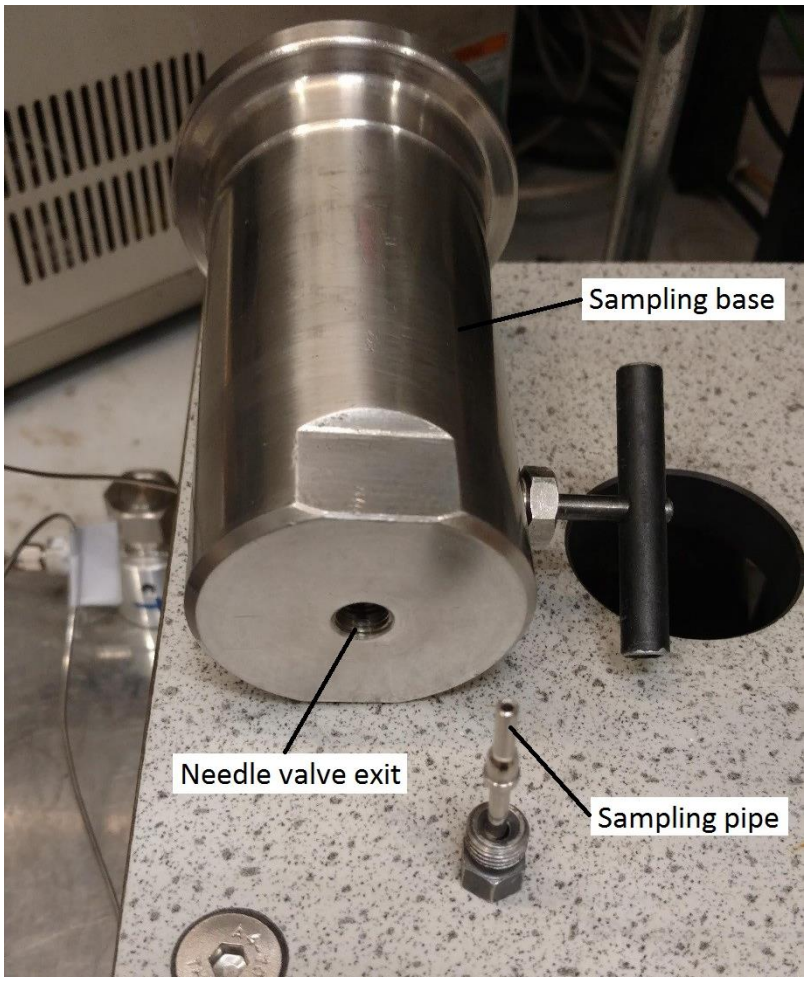


Figure 3.5 Sampling autoclave base, showing the needle valve exit in the bottom of the base, with partially hollow sampling pipe.

3.4.7.3 Sampling cylinder method

Polymerisations were carried out following the procedure detailed in section 3.4.2, using the sampling autoclave shown in section 2.2.6. The sampling cylinder system is attached to the sampling autoclave via the needle valve exit with 7 cm of ⅛ inch steel tubing (internal volume of 0.18 cm^3) and an autoclave engineer fitting (Figure 3.6).

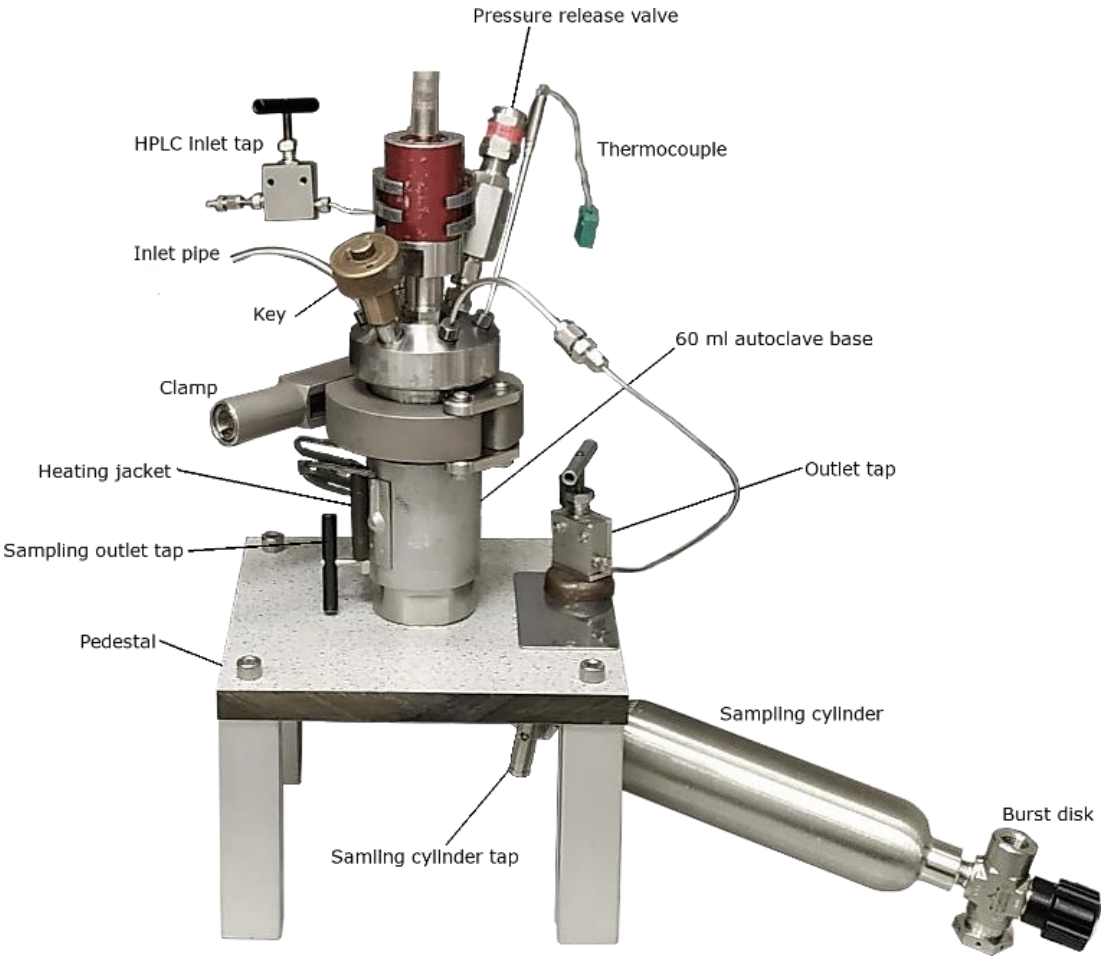


Figure 3.6 60 ml Sampling autoclave setup on a pedestal, with sampling cylinder system attached to sampling exit.

The sampling cylinder system consists of a straight needle valve tap, a 150 ml stainless steel PTFE coated stainless steel cylinder and an angled needle valve tap with rupture disk (rating: 2850±150 psi @ 20 °C), all purchased from Swagelok (Figure 3.7).

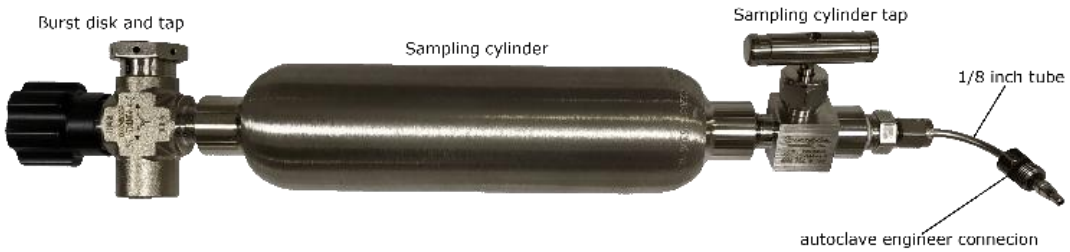


Figure 3.7 Cylinder system used to obtain on-line samples during monitoring experiments. Swagelok product codes: burst disk and tap: SS-16DKM4F4-A-2, sampling cylinder: 36L-50DF4-150-T, sampling cylinder tap: SS-20VM4-F4.

Prior to sample acquisition, the sampling cylinder was loaded with a deuterated solvent (5 ml). If required, an internal standard can be added to the solvent. A deuterated solvent was used so that the obtained mixture could be analysed directly by NMR, but basic lab solvents can also be used. The cylinder system was then attached to the sampling outlet using the Autoclave Engineer connection. With all taps closed firmly, CO_2 was added to the autoclave to increase the internal pressure by 15 bar. The sampling outlet tap was then opened, filling the ⅛ inch tube with approximately 0.18 ml of autoclave content and causing the overall pressure to drop by 15 bar. The sampling tap was closed after 5-10 seconds, resealing the autoclave from the sampling setup. After closing the sampling outlet tap, the sampling cylinder tap was opened. The contents of the high pressure ⅛ inch tube releases directly into the cylinder chamber, where it is captured into the deuterated solvent. The cylinder system was then detached from the autoclave and the sample – dissolved in the chosen deuterated solvent – was recovered by pouring the content back through the ⅛ inch tube into a glass vial. The recovered solution was analysed for conversion and molecular weight. The joint between the sampling cylinder and the sampling cylinder tap was opened, and the cylinder system was rinsed thoroughly with a good solvent for the polymerisation product and dried before repeating the procedure to obtain

the next sample. A cylinder volume of 150 ml was chosen to allow for the capture of a high-pressure sample while keeping the final cylinder pressure below 2 bar.

3.5 Results and discussion

This section will focus on the development of an on-line monitoring system for polymerisations in $scCO_2$ and comparing its reliability to the cumbersome offline method. Reaction progress of the dispersion polymerisation of MMA was followed using both off-line and on-line monitoring methods. NMR and GPC analyses were used to assess the reliability of novel systems, and the data were analysed with kinetic modelling. The on-line monitoring system was then utilised for a range of polymerisations and reactions to test its universal applicability.

3.5.1 Batch free-radical dispersion polymerisation of MMA

A known and reliable method of achieving conversion data at several points during a polymerisation reaction, is by interrupting the reaction and analysing the formed product. This was done following the autoclave quench and measure method (section 3.4.7.1). This batch approach was used to establish a reliable reaction progression curve, despite the requirement of a large number of individual experiments. successive polymerisations were conducted with 1 wt% AIBN and 5 wt% PDMS-MA relative to MMA and were quenched by crash cooling at 30-minute reaction time intervals, up to 240 minutes, based on the approximate total reaction time known from previous research and literature.[52, 55, 67, 103, 114] Experiments were repeated 3 times at timepoints where significant change was still occurring (30 to 150 minutes),

to assure reproducibility of the data. The products were analysed by NMR for conversion and GPC for molecular weight averages (Table 3.1).

Table 3.1 Results of batch polymerisation reactions quenched by crash cooling at 30-minute intervals.

Reaction time (min)	Conversion (%)[a]	M_n (kDa)[b]	M_w (kDa)[b]	Đ[b]	Product consistency	Yield (%)
30	2.6	20	37	1.88	Liquid	-
30	2.6	19	48	2.59	Liquid	87.4
30	2.9	20	43	2.11	Liquid	86.4
60	10.7	33	89	2.72	Liquid	-
60	9.1	35	87	2.46	Liquid	-
60	8.5	28	73	2.59	Liquid	89.2
90	29.1	65	183	2.83	Viscous liquid	-
90	22.3	49	157	3.18	Viscous liquid	-
90	26.6	58	173	2.99	Viscous liquid	-
120	52.5	86	254	2.95	Cloudy gel	-
120	51.2	85	248	2.92	Cloudy gel	-
120	52.3	93	252	2.72	Cloudy gel	-
150	84.8	133	323	2.43	powder	70.7
150	85.1	120	318	2.65	Powder	72.7
150	85.9	124	313	2.52	Powder	71.4
180	93.2	167	346	2.06	Powder	83.1
210	94.9	158	334	2.11	Powder	85.4
240	96.0	168	343	2.04	Powder	85.3

a – determined via ^{1}H NMR (section 2.3.2), b – determined via GPC (section 2.3.1)

Graphically, the conversion as a function of reaction time shows a distinct sigmoidal progression (Figure 3.8). This is what would be expected for a dispersion polymerisation with high reactivity in the dispersed phase. As the dispersed phase grows in volume, the polymer production in this phase becomes more pronounced. This causes an acceleration in the observed polymerisation rate, in turn growing the dispersed phase even quicker. As monomer is consumed and higher conversion is reached, polymerisation will then slow down due to the reduced availability of monomer. The observed conversion trend is as expected from literature, both in terms of reaction duration and a clear sigmoidal progression,[103] which is typical of a

dispersion polymerisation with significant polymerisation occurring in the dispersed particle phase of the system.[12, 106]

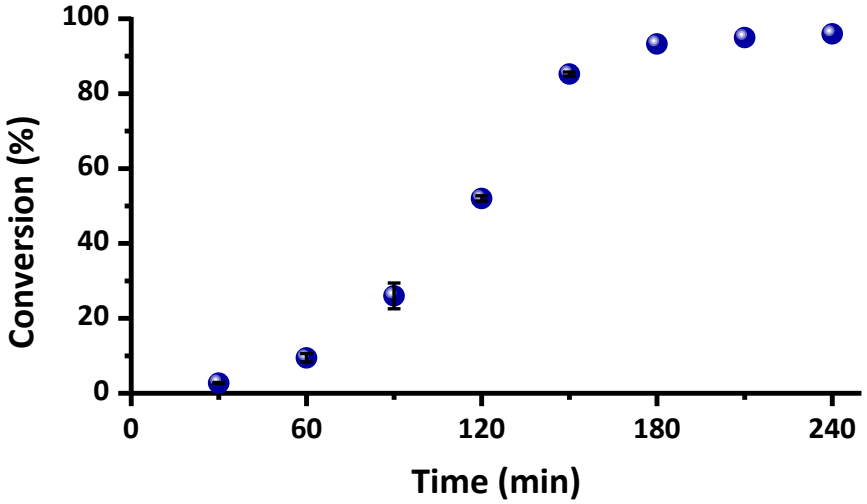


Figure 3.8 Conversion of MMA as a function of reaction time from sequential batch reactions quenched by crash cooling. Error bars represent the standard deviation of experimental conversion from 3 separate reactions. Reaction conditions: 10 ml of MMA, 0.468 g of PDMS-MA, 93.6 mg of AIBN, 220 bar and 65 °C.

The molecular weight progression as a function of conversion showed a constant rise (Figure 3.9), as has been observed previously.[103, 104, 111] The observed increase in molecular weight as polymerisation progresses is not what is seen for a typical free radical chain-growth polymerisation in solution. Common free-radical chain-growth polymerisations will quickly reach an average molecular weight that will remain constant during further polymerisation, as discussed in chapter 1. This is due to the average chain length that can be reached by growing polymer chains within the polymerising system, which depends on the immediate surroundings of a propagating radical.[11] the majority of polymerisations in solution do not involve a significant change in the surroundings of the radical as polymerisation progresses, meaning molecular weight averages do not change with increasing monomer conversion. Further polymerisation simply results in more polymer chains of the

same average length.[11] Large changes in radical surroundings can occur in bulk polymerisations, resulting in the Trommsdorf effect, which occurs when diffusion mobility is severely decreased due to high polymer concentration, resulting in a decrease in termination probability. Reduced termination will result in progressively longer chains being formed and the average molecular weight sharply increasing during further polymerisation.[11, 27]

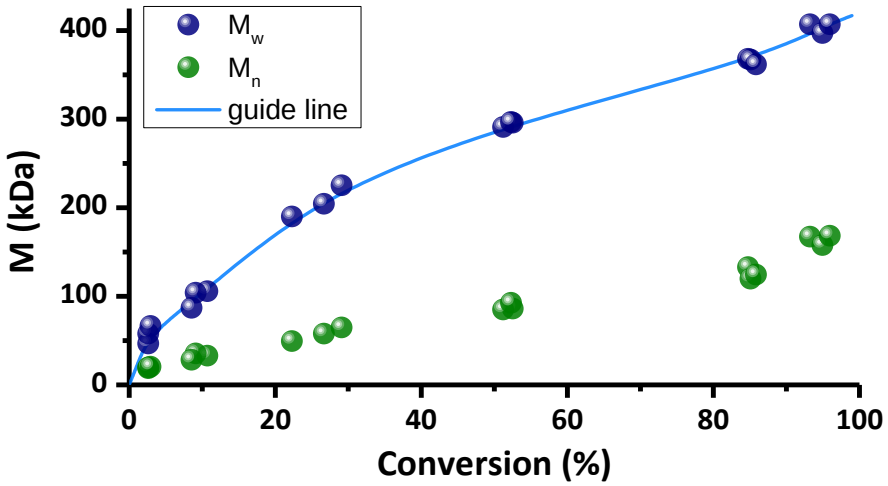


Figure 3.9 Mass-average molar mass in function of conversion from sequential batch reactions quenched by crash cooling, with a guideline to further highlight the increase in molecular weight in function of reaction time. Error bars represent the standard deviation on data from 3 separate reactions. Reaction conditions: 10 ml of MMA, 0.468 g of PDMS-MA, 93.6 mg of AIBN, 220 bar and 65 ℃.

For the MMA dispersion polymerisation under investigation, GPC results show chains are on average growing longer as the reaction progresses. This is caused by an overall reduction in diffusive mobility around propagating radicals. This reduced mobility is further indication that chains are growing within the dispersed polymer rich phase that is being formed, where diffusive mobility is far lower than in the continuous supercritical phase. As the dispersed particles grow larger, polymerisation within the dispersed phase becomes more dominant, resulting in a continuous increase in

molecular weight averages. This trend is seen clearly in for the dispersion polymerisation of MMA, where an initial sharp increase in molecular weight is followed by a continuous gradual increase up to 85% conversion (Figure 3.9). Beyond 85% conversion, a sharpened increase in molecular weight is seen, indicating that the Trommsdorf effect is occurring due to mobility within the dispersed phase reducing further, mimicking the effect typically seen in bulk polymerisations. This is in agreement with literature descriptions of dispersion polymerisations with the dispersed phase as the main locus of polymer production and a gelling effect occurring within this phase at high conversion.[12, 96]

The constant increase in average molar mass is caused by the shift of the main polymerisation locus towards the growing dispersed phase, where longer chains are formed. This occurs because of the higher monomer concentration in the dispersed phase compared to the continuous phase, as well as restricted movement of the growing chains due to gelation in the growing particles.

The yield of most polymerisations, the percentage of mass added to the autoclave that was recovered after the reaction, was found to be ≥ 85% (Table 3.1), with some material being lost within the autoclave tubing and attached to the steel walls. For the polymerisations stopped after 150 minutes, only ~72% of the original mass was recovered. After 150 minutes, the product visually appeared to be a dry powder, but it is likely that a significant amount of monomer was still present. To recover the powder, it was collected on filter paper and transferred into a vial, before analysis via NMR was conducted to determine conversion. It is suspected that monomer was lost

during the venting and collecting procedure, artificially inflating the conversion data at 150 minutes.

The final product, after 4 hours of reaction time, was a free-flowing white powder, consisting of discrete spherical particles with a diameter of 2566 ± 471 nm. Particle sizing was determined from several SEM images by encircling 100 particles and determining the average diameter (Figure 3.10).

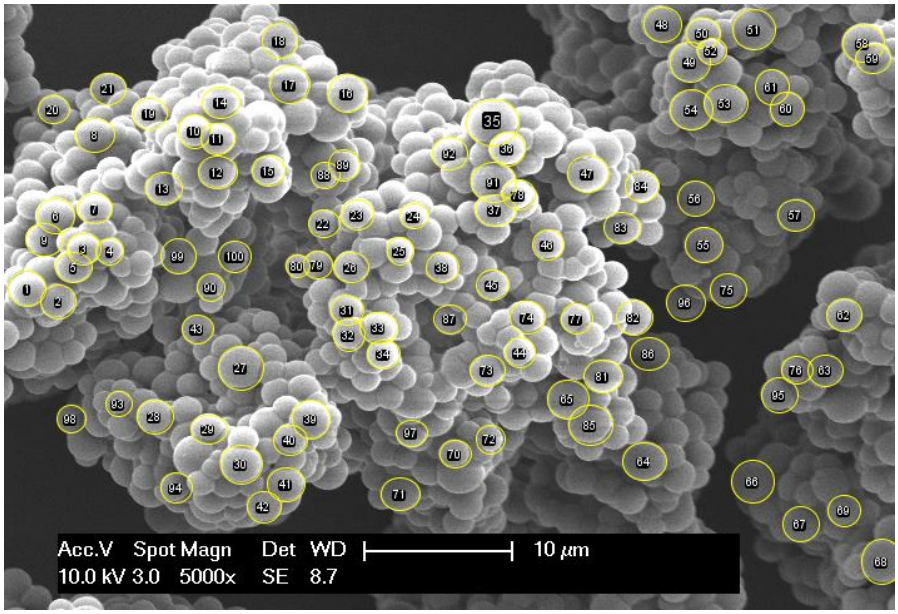


Figure 3.10 SEM image of PDMS-MA stabilised PMMA particles formed after 240 minutes of reaction time, showing distinct spherical morphology with an average particle diameter of 2566 ± 471 nm. Yellow circles were used to determine the average particle diameter in Fiji(ImageJ).

The reliability of this particle sizing method was verified by repeat analysis of several SEM images on several prepared samples, and no significant variation in outcome was observed. As in previous publications employing this method,[35, 55, 67-69] 100 particles was found to be sufficient to obtain reliable and reproducible particle size data for such monodisperse particle populations.

3.5.1.1 Kinetic modelling

The goal of kinetic modelling was to obtain a reaction description that was robust enough to predictably describe the polymerisation system, while maintaining maximum simplicity. This model can then be used to test the alternate monitoring systems and can be used to predict reaction outcomes under different conditions.

3.5.1.1.1 One phase kinetic model

Kinetic modelling of the conversion data obtained from batch polymerisations (Table 3.1) was first attempted using a simple one phase polymerisation model suited for some dispersion polymerisations.[115] The rate constants for the reactions shown in Scheme 3.3 were taken into consideration for this model.

$$I \xrightarrow{k_d} 2R^{\cdot} \quad (1)$$

$$RM_n^{\cdot} + M \xrightarrow{k_p} RM_{n+1}^{\cdot} \quad (2)$$

$$RM_n^{\cdot} + RM_m^{\cdot} \xrightarrow{k_{tc}} RM_{n+m}R \quad (3)$$

$$RM_n^{\cdot} + RM_m^{\cdot} \xrightarrow{k_{td}} RM_n + RM_m \quad (4)$$

$$RM_n^{\cdot} + M \xrightarrow{k_{tr}} RM_n + M_1^{\cdot} \quad (5)$$

Scheme 3.3 Considered equations for polymerisation kinetics analysis in the one phase model. (1) Decomposition, (2) propagation, (3) termination by combination, (4) termination by disproportionation, (5) radical transfer. I = initiator molecule, M = monomer, M_x = polymer chain of length x, R = initiator decomposition product, k_d = dissociation rate constant, k_p = polymerisation rate constant, k_{tc} = termination by recombination rate constant, k_{td} = termination by dissociation rate constant, k_{tr} = radical transfer to monomer rate constant.[115]

It was assumed that rate constants were independent of chain length, as the direct environment of an active polymer radical is unaffected by chain length. From the reactions shown in Scheme 3.3, rate Equation 3.1 to rate Equation 3.4 were determined.

$$\frac{\delta}{\delta t} I(t) = -k_d I(t)$$

Equation 3.1

$$\frac{\delta}{\delta t} \sum_{n=0}^{\infty} M_n^{\cdot}(t) = 2k_d I(t) - (k_{tc} + k_{td}) * \sum_{n=0}^{\infty} M_n^{\cdot\,2}(t)$$

Equation 3.2

$$\frac{\delta}{\delta t} M(t) = -\left(k_p + k_{tr}\right) * \sum_{n=0}^{\infty} M_n^{\cdot}(t) * M(t)$$

Equation 3.3

$$\frac{\delta}{\delta t} \sum_{n=0}^{\infty} M_n(t) = \left(\frac{1}{2} k_{tc} + k_{td}\right) * \sum_{n=0}^{\infty} M_n^{\cdot\,2}(t) + k_{tr} * \sum_{n=0}^{\infty} M_n^{\cdot}(t) * M(t)$$

Equation 3.4

To resolve this set of equations, it was assumed that a constant concentration of radicals was present at all times in the polymerisation system, known as the steady-state principal. This steady-state principal is a widely accepted approximation, used to solve kinetic equations in polymer systems.[116, 117] As discussed in the introduction, thermal initiators like AIBN decay into radicals in a non-linear fashion, meaning there will be an ever-decreasing radical concentration in the reaction. The applicability of the steady-state approximation loses validity when reaction time begins to exceed the radical half-life time. The half-life of AIBN in $scCO_2$ at 65 °C is known to be approximately 24.5 hours,[14] well above the reaction times under investigation here.

The equation set could therefore be simplified, resulting in Equation 3.5 to Equation 3.7:

$$I(t) = I(0) * e^{-k_d t}$$

Equation 3.5

$$\sum_{n=0}^{\infty} M_n^{\cdot}(t) = \sqrt{\frac{2k_d I(0)}{k_{tc} + k_{td}}} * e^{-0.5 k_d t}$$

Equation 3.6

$$M(t) = M(0) e^{-2\left(k_p + k_{tr}\right) * [\sum_{n=0}^{\infty} M_n^{\cdot}(0) - \sum_{n=0}^{\infty} M_n^{\cdot}(t)]/k_d}$$

Equation 3.7

From literature, the dissociation rate constant k_d of AIBN in $scCO_2$ is known at the employed reaction conditions .[14] Additionally the propagation to chain transfer ratio, $\frac{k_p}{k_{tr}}$, and the ratio of the different termination modes, $\frac{k_{tc}}{k_{td}}$, have been determined in literature.[13, 103, 118] The remaining unknown variables were the propagation rate k_p and the termination by combination rate constant k_{tc}. From Equation 3.7, the amount of monomer in the system at any given time could be found. This was then used to determine the conversion at time t by using Equation 3.8. The amount of polymer formed could also be found from the amount of monomer used by solving Equation 3.9.

$$x(t) = \frac{|M(t) - M(0)|}{M(0)} * 100\%$$

Equation 3.8

$$polymer\ yield\ = |M(t) - M(0)| * 0.06\ l * 100.12\ g/mol$$

Equation 3.9

This calculated conversion (Equation 3.8) was then plotted as a function of time and compared to experimental values. The variables k_p and k_{tc} were varied to achieve

the best possible overlap between experimental conversion measurements and the plot of Equation 3.8.

To quantify the accuracy of the modelled conversion, the root mean square (RMS) error was employed. The RMS error was calculated by comparing all measured conversions (x_{exp}) to calculated conversions (x_{calc}) at a given time using Equation 3.10. This error was minimised across all experiments to find the most accurate values for k_p and k_{tc} and to gauge the applicability of the model for the polymerisation.

$$RMS\ error = \sqrt{\sum (x_{exp} - x_{calc})^2}$$

Equation 3.10

To compensate for an initial nucleation phase and any impurities delaying polymerisation, an induction period was included in the model. During the induction phase, the polymer propagation rate is assumed to be zero. In reality, the induction phase involves polymerisation in the continuous phase to form the disperse polymer phase. This approximation is needed, because the one phase model only accounts for one constant polymerisation locus, meaning initial polymerisation must be assumed to be zero.[103, 104] The less reactive phase is therefore ignored in this approximation. The induction time was also varied to minimise RMS error.

The one phase kinetic model was applied to the collected conversion data of batch polymerisations (Table 3.1). A best fit, with minimal RMS error, was overlaid onto the experimental data (Figure 3.11).

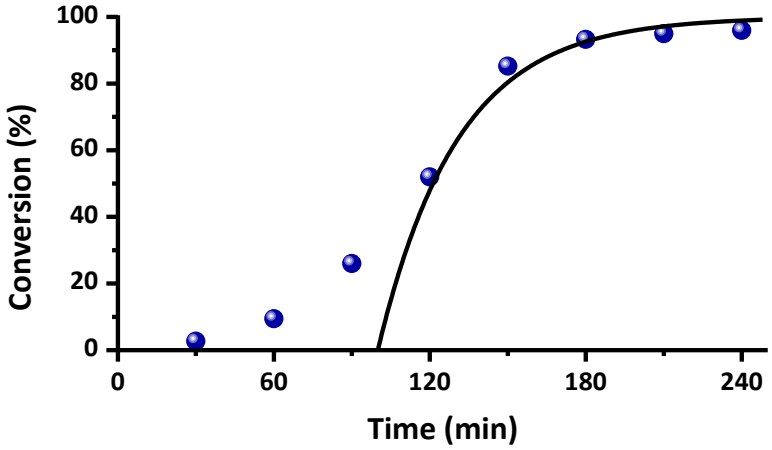


Figure 3.11 One phase kinetic model of conversion as a function of time, fitted to experimental conversion data from quenching experiment results detailed in Table 3.1. Induction period = 100 min, $k_p = 800\ \frac{l}{mol*s}$, $k_{tc} = 50000\ \frac{l}{mol*s}$.

The one phase approximation used for kinetic modelling could not be fitted to the experimental data due to the oversimplified limitations used in the model. The one phase model can only account for a continuous decrease in conversion rate as monomer is consumed. While this approximation can work for dispersion polymerisations,[115-117] The polymerisation of MMA in $scCO_2$ showed a more pronounced acceleration phase in the conversion progression, that occurs as the dispersed phase grows. The large difference in polymerisation rate between the continuous and dispersed phase for this reaction then results in the observed sigmodal conversion progression. By introducing an induction period of 100 minutes into the model fitting, the initial acceleration was avoided and fitting of the later conversion progress could be attempted. The introduction of this induction period however, resulted in the model predicting 0% conversion after 90 minutes, while experimentally it was measured to be 26%. This large error is intrinsic to the one phase model, meaning this model could not be fitted reliably to the MMA polymerisation in $scCO_2$ and a more robust model was required.

3.5.1.1.2 Sigmoidal kinetic model

Building on the basis of the one phase kinetic model and work by Mueller *et al.*,[12, 103, 111] a sigmoidal model was developed to determine the rate constants in Scheme 3.3. This type of model was first developed by Barret and Thomas,[106] and showed excellent predictive modelling for dispersion polymerisations with sigmoidal conversion progression. The sigmoidal model assumes all polymerisation occurs in the dispersed polymer particle phase, which is what was observed during the batch polymerisation reactions. The known literature values for k_d, $\frac{k_p}{k_{tr}}$ and $\frac{k_{tc}}{k_{td}}$ [13, 103, 118] were again used for the sigmoidal modal development, resulting in two unknown rate constants k_p, the propagation rate constant of the reaction, and k_t, the overall termination rate constant (Equation 3.11).

$$k_t = k_{tc} + k_{td}$$

Equation 3.11

The polymerisation rate (R_p) of a bulk polymerisation is described by Equation 3.12. By assuming a constant partition coefficient (α) of the monomer across the dispersed and continuous phase, the R_p of a dispersion polymerisation can be described by Equation 3.13. V is the volume of the dispersed phase.

$$R_p = [M] * k_p * \sqrt{(\frac{R_i}{k_t})}$$

Equation 3.12

$$R_p = \alpha * [M] * k_p * \sqrt{(\frac{V * R_i}{k_t})}$$

Equation 3.13

Applying the steady-state principal to Equation 3.13, and assuming the volume of the dispersed phase is directly proportional to the amount of polymer formed, conversion progression can be expressed using Equation 3.14 for the change in conversion (x) as a function of time and Equation 3.15 for the overall reaction rate constant.

$$\frac{d}{dt}x = k \cdot \sqrt{x} \cdot (1 - x)$$

Equation 3.14

$$k = \alpha \cdot \sqrt{[M]_0 \cdot [I] \cdot V_p \cdot k_i} \cdot \frac{k_p}{\sqrt{k_t}}$$

Equation 3.15

The initial component concentrations $[M]_0$ and $[I]$ were separated from k, to obtain the reduced rate constant k' that encapsulates the individual reaction rate constants and unknown values associated with the system.

$$k' = \frac{k}{\sqrt{[M]_0 \cdot [I]}} = \alpha \cdot \sqrt{V_p \cdot k_i} \cdot \frac{k_p}{\sqrt{k_t}}$$

Equation 3.16

The initial polymerisation in the continuous phase is not accounted for in this model, so this was compensated for with the addition of an induction phase where no apparent conversion occurs, as described previously in the one phase model. The conversion at reaction time t can then be determined using Equation 3.17, incorporating an induction time t_0 and using the overall pseudo first order rate constant k.

$$x(t) = \begin{cases} 0\,, & t \le t_0 \\ \left(\frac{e^{kt} - e^{kt_0}}{e^{kt} + e^{kt_0}}\right)^2, & t > t_0 \end{cases} \quad with \quad k = k' * \sqrt{[M]_0 * [I]}$$

Equation 3.17

The exponential formula shown in Equation 3.17 results in a sigmoidal conversion progression in function of time, with the fitting variables t_0 and k'. This equation was fitted to the experimental conversion data (Table 3.1) by varying t_0 and k' to minimise the RMS error value. Taking into account that the conversion at 150 minutes was artificially high a best fit was found (Figure 3.12).

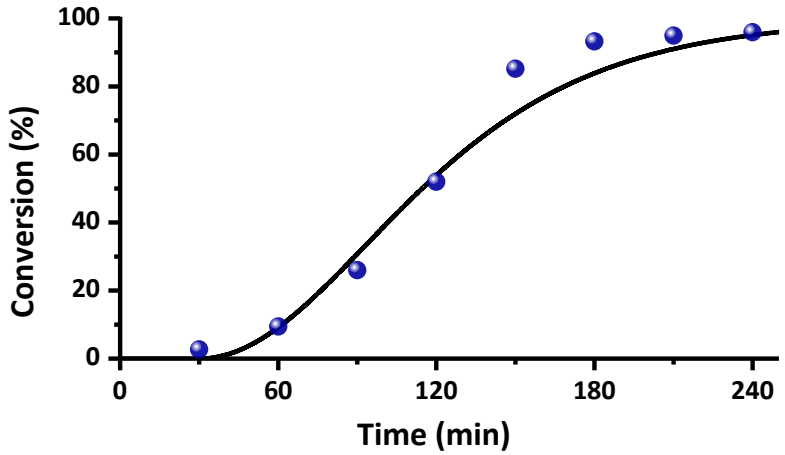


Figure 3.12 Sigmoidal kinetic model of conversion as a function of time, fitted to the conversion data from batch MMA free radical dispersion polymerisations detailed in Table 3.1. conversion data at 150 minutes was assumed to be too high, so was ignored in model fitting. Reaction conditions: 10 ml of MMA, 0.468 g of PDMS-MA, 93.6 mg of AIBN, 220 bar and 65 ℃. Model fitting variables: $t_0 = 1800\ s$, $k' = 2.85 * 10^{-3}\ M^{-1}s^{-1}$.

The sigmoidal kinetic model was able to approach the experimental results closely, with a far smaller RMS error than for the one phase kinetic model. The remaining errors intrinsically part of the modelling method, are during the initial nucleation phase of the reaction and during later stages where the Trommsdorf effect occurs. The sigmoidal model does not include polymerisation occurring in the continuous phase, resulting in an error during the initial nucleation phase. The model also cannot account for polymerisation rate increases induced due to mobility reduction. The model error during the initial nucleation phase was compensated for by including an

induction period of 30 minutes. This initial induction phase will also compensate for any inhibitor present in the system. With all chemicals used as received, there will be a range of inhibitor and stabiliser compounds present that can delay onset of polymerisation. While some initiator will be lost to reactions with these compounds, it is not expected to have noticeable effects on the model beyond the induction period as 90 percent of AIBN is still present after 4 hours of reaction time (based on a half-life time of 24.5 hours in $scCO_2$ at 65 °C[14]).

In summary, a very time and material demanding approach requiring eighteen separate reactions was used to acquire a robust kinetic baseline. Our aim below is to show that this could be done better.

3.5.2 Sampling pipe method

While many on-line monitoring options are expensive and require specific setups, a readily available direct sampling approach from a single needle valve exit has been trialled previously by Thurecht *et al*.[102] within the group.

Three experiments were conducted using the sampling autoclave setup, under the polymerisation conditions (10 ml MMA, 5 wt% PDMS-MA, 1 wt% AIBN) used previously for the batch experiments. Reactions were halted after approximately 4 hours and allowed to cool naturally before the formed powder was recovered and analysed. Final results of the polymerisation reactions are shown in Table 3.2, confirming that a PMMA powder of high conversion was formed. SEM showed that the expected PMMA particles were formed, and that sampling with the sampling pipe method had no adverse effect on the reaction outcome.

Table 3.2 Results of 3 identical polymerisation reactions conducted in the sampling base setup with sampling pipe.

Entry	Reaction time (min)	Conversion (%)[a]	M_n (kDa)[b]	M_w (kDa)[b]	Đ[b]	Product consistency	Yield (%)
1	230	98.2	105	355	3.38	Powder	89.1
2	240	90.4	139	387	2.79	Powder	82.0
3	240	96.6	161	406	2.53	Powder	85.4

a – determined via ^{1}H NMR (section 2.3.2), b – determined via GPC (section 2.3.1)

Reaction samples were obtained during polymerisation at regular intervals using the sampling pipe method described in section 3.4.7.2. The acquired samples were analysed for conversion using ^{1}H NMR and molecular weight averages using GPC (Table 3.3). The conversion results were plotted as a function of reaction time (Figure 3.13).

Table 3.3 Sample results of polymerisation reactions monitored using the sampling pipe method. Reaction conditions: 10 ml of MMA, 0.468 g of PDMS-MA, 93.6 mg of AIBN, 220 bar and 65 °C.

Reaction time (min)	Conversion (%)[a]	M_n (kDa)[b]	M_w (kDa)[b]	Đ[b]
10	24.1	-	-	-
13	6.3	-	-	-
20	13.0	-	-	-
23	33.5	16	26	1.69
30	58.3	15	30	1.98
30	77.2	28	58	2.05
33	84.8	21	47	2.28
40	86.3	16	54	3.27
43	82.1	23	65	2.88
45	80.5	36	99	2.76
50	85.7	18	55	2.96
53	81.6	26	79	2.99
60	79.3	54	155	2.85
60	79.2	21	56	2.72
63	87.1	31	96	3.13
70	82.6	24	70	2.85
73	83.7	43	136	3.15
75	88.6	68	192	2.82
83	82.3	48	153	3.22
88	83.4	33	115	3.53
90	89.9	66	191	2.91
93	85.4	55	177	3.23
103	85.9	41	137	3.34
118	82.7	52	165	3.17
120	95.6	79	232	2.93
123	89.3	92	310	3.38
138	91.5	63	241	3.84
150	98.1	91	266	2.92
153	94.4	68	254	3.76
158	95.0	79	274	3.49
180	98.6	79	246	3.12
183	96.1	84	305	3.63
188	95.0	80	282	3.52
230	98.2	143	316	2.21
240	90.4	139	387	2.79
240	96.6	161	366	2.28

a – determined via ^{1}H NMR (section 2.3.2), b – determined via GPC (section 2.3.1)

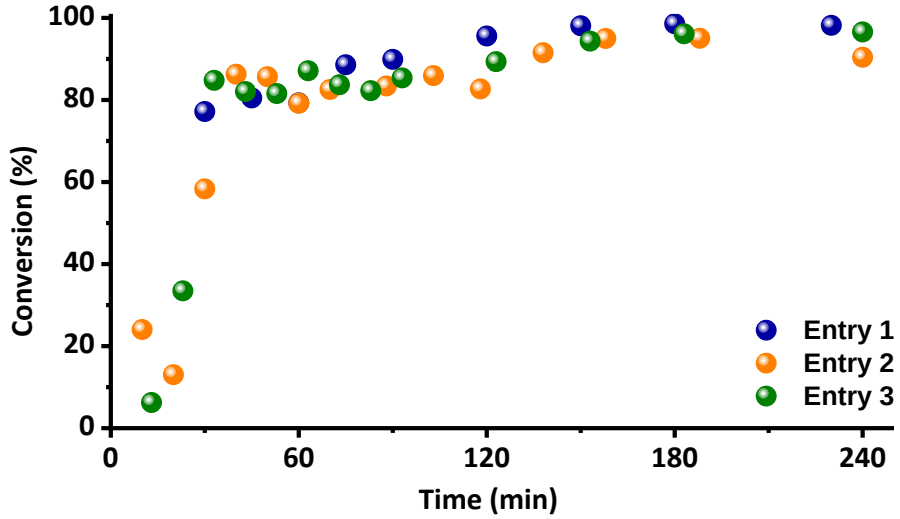


Figure 3.13 Conversion as a function of time for sampling pipe experiments (Table 3.2). Conversion measured via ^{1}H NMR (section 2.3.2) of acquired autoclave samples and of the final powder product (last measurement point).

The measured conversion progression was consistent across the three repeat experiments using the sampling pipe system. However, comparison with the previously determined sigmoidal trend, showed that the observations are erroneous (Figure 3.14), with the shaded area highlighting the large difference in results.

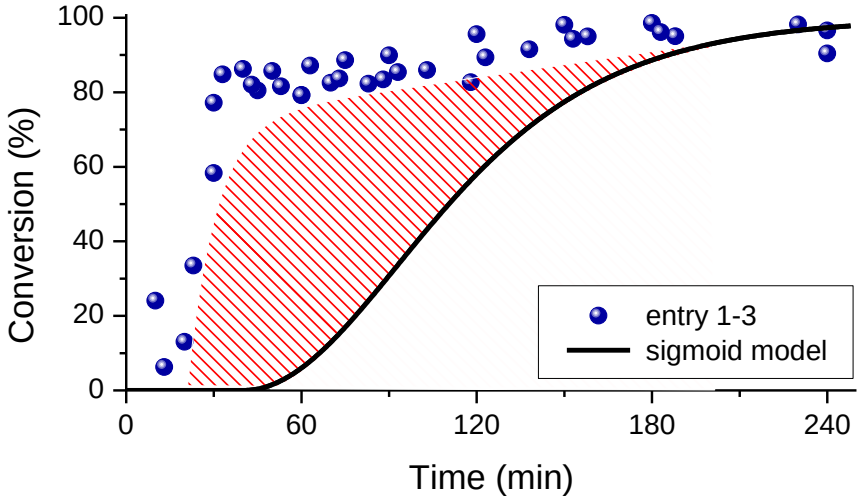


Figure 3.14 Conversion as a function of time for sampling pipe experiments (Table 3.2) compared to the sigmoidal model fitted to batch experiments (Figure 3.12). The shaded area highlights the large difference in conversion measurements, despite identical reaction conditions and product outcomes.

An explanation for the erroneously high conversion results was found in the sampling process itself. When the ongoing reaction is collected in the sampling pipe, it is still at reaction conditions. When the sampling pipe is then unscrewed to obtain the sample, pressure is immediately released. During this process, the volatile monomer present in the pipe dissipates from the sample. As the ^{1}H NMR analysis technique relies on the comparison of MMA and PMMA concentration to describe conversion (section 2.3.2), MMA loss resulted in artificially high conversion measurements throughout.

To confirm the loss of monomer from sampling pipe, GPC analysis was performed on all acquired samples. As GPC only measures polymer chains and not monomer, results were not influenced by loss of MMA in the sample. GPC Results showed a consistent increase in molecular weight averages during polymerisation, similar to observations made during the quenching experiments (Figure 3.15).

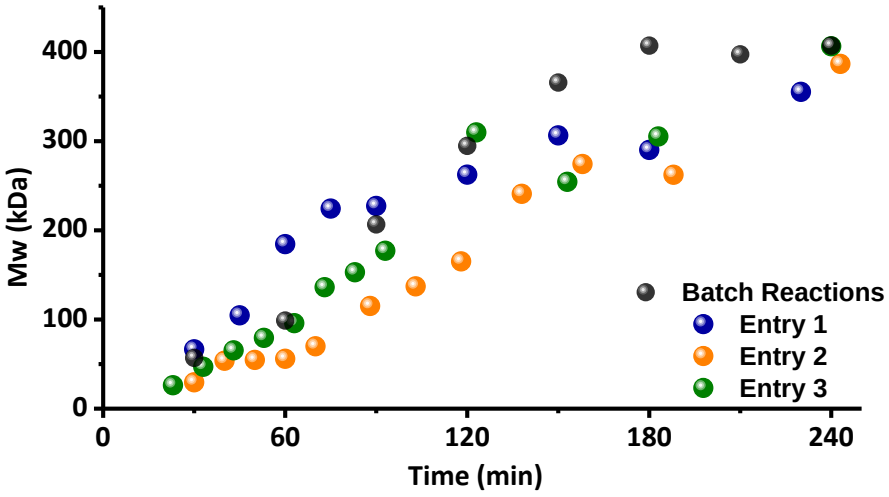


Figure 3.15. Mass average molar mass as a function of reaction time for sampling pipe experiments detailed in Table 3.2, and quench experiments detailed in Table 3.1. A continuous increase in molecular weight was observed for both experimental methods.

While the sampling pipe experiments did not afford reliable conversion data, representative molecular weight data was acquired. The molecular weight data could however not be analysed in function of conversion, limiting the usefulness of the technique for kinetic purposes.

3.5.3 Sampling cylinder method

Due to the consistent loss of monomer, on-line monitoring with the sampling pipe method proved inadequate. To alleviate the issue a novel sampling system was designed and implemented, where volatile monomer could be captured despite the intense pressure drop experienced when sampling at reaction conditions. To keep costs low, the choice was made to avoid moving parts that could be used to slowly expand a sample volume, such as syringe pumps or manual pressure generators.

The cylinder system (Figure 3.7) was constructed to ensure no volatile compounds could be lost during sample expansion, but still allow for the immediate pressure release of the sample when desired. The basic concept of the setup was to allow the intense pressure-drop to occur in a sealed volume, as any nebulised monomer would still be contained. A solvent was then added to this sealed volume to aid in capturing the monomer. A fixed sample volume is obtained with the sample size being determined by the length of tubing used to connect the cylinder to the sampling base (Figure 3.6).

3.5.3.1 Setup testing

Before using the newly assembled system for high pressure sample acquisition, it was tested for reliability and impact using only CO_2. The reactor was brought to reaction

conditions of 65 °C and 250 bar and the sampling cylinder was attached (Figure 3.6). CO_2 was sampled by opening the sampling tap for 5 seconds, before resealing it, and the pressure drop was monitored (Figure 3.16). Pressure in the sampling pipe was released into the cylinder by opening the high pressure Swagelok tap. As only CO_2 was present in the cylinder, the pressure was released by opening the angled tap with burst disk. The cylinder taps were then resealed, and sampling could be repeated.

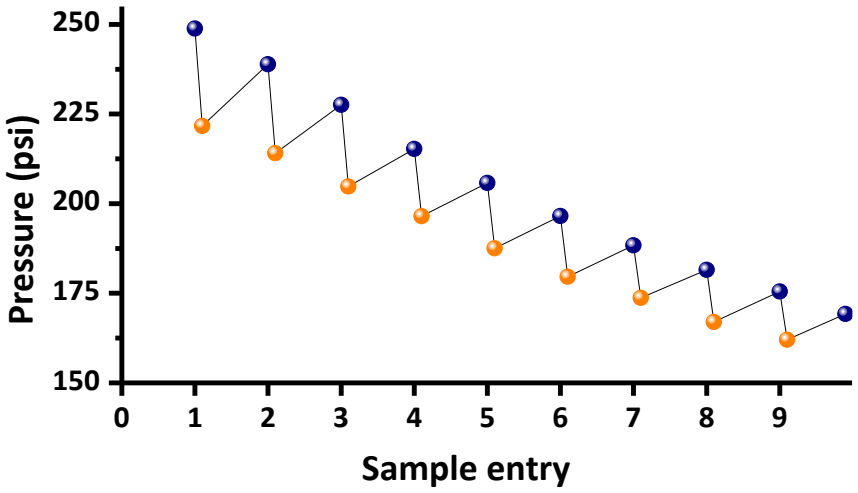


Figure 3.16 Observed pressure progression during consecutive samplings of $scCO_2$, using the sampling cylinder setup attached to the sampling autoclave. Orange spheres denote the observed pressure immediately after sampling, blue spheres denote the pressure recovery after the system stabilised.

9 consecutive samples were taken from the $scCO_2$ filled autoclave. Every sampling resulted in a near instant pressure drop of 15-30 bar and a temperature drop of 1-2 °C, followed by a gradual recovery in pressure over approximately 2 minutes as the system stabilised and regained the set temperature of 65 °C. A final pressure loss of 5-10 bar per sampling was measured. As expected, the pressure loss is dependent on the system pressure before sampling. A fixed volume of $scCO_2$ was removed with every sample taken, so a fixed density drop was imposed on the reactor. Due to the

nonlinear relation between pressure and CO_2 density (Figure 3.17) the pressure drop when sampling will be lower at lower reactor pressure.

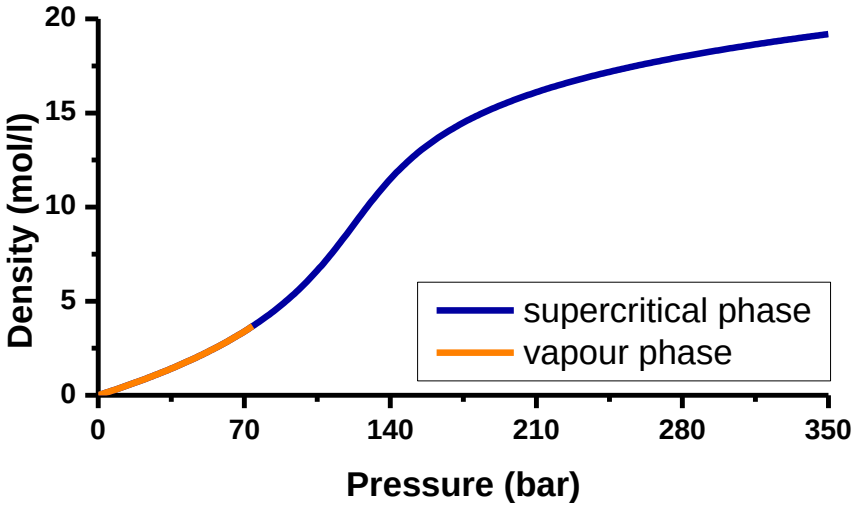


Figure 3.17 CO_2 density in function of pressure at 65 °C. produced using data from NIST [119]

With pressure during and after sampling following a predictable and reproducible trend, the system was deemed safe to use in on-line reaction sampling. After conducting initial leak tests, a test was conducted to assure that the sampling cylinder method could provide representative sampling of a monomer and polymer mixture.

A known amount of polymer was weighed and loaded into the sampling autoclave, before sealing the system and bringing it to typical reaction conditions (207 bar, 65°C). The polymer was allowed to stir in $scCO_2$ for two hours to assure a dispersion was achieved. Following this, a known amount of monomer was added via HPLC, bringing the pressure to approximately 220 bar. The system contained 1/3 polymer and 2/3 monomer, corresponding to a 33% conversion. Two samples were obtained, using the sampling cylinder system. The first sample showed a conversion of 63% while the second sample showed a conversion of 30% from ^1H NMR measurements. The first sampling clearly showed polymer build up around the edge of the ⅛ inch

tubing of the sampling cylinder system. This is likely from polymer getting stuck in the pinhole exit of the sampling base during the initial redispersion. The second sample, while slightly lower than expected, confirms that monomer could be captured and measured using the sampling cylinder system.

Due to the erroneous conversion of the first sample, the sampling methodology was tweaked, by adding the use of the sampling pipe prior to cylinder sampling. Again, a known amount of polymer was added to the autoclave before bringing the system to 207 bar and 65 °C. After 2 hours of redispersion time, monomer was added via the HPLC. The polymer-monomer mixture corresponded to 33% conversion. To clear the sampling exit of the sampling base of any lodged polymer, a sample was taken using the sampling pipe method. Following this, a sample was taken with the sampling cylinder. This was repeated twice more to assure reproducibility of the method. The conversions measured via ^{1}H NMR were 31%, 35%, and 30%, showing excellent alignment with the mixture in the autoclave. The use of the sampling pipe to clear the sampling exit of the base was shown to be crucial for reliable sampling.

3.5.3.2 On-line monitoring of the free-radical dispersion polymerisation of MMA

Having confirmed the sampling cylinder system can reliably and reproducibly sample at high pressure, sampling was attempted during a standard MMA polymerisation (10 ml MMA, 5 wt% PDMS-MA, 1 wt% AIBN), initiated via HPLC injection with an initial pressure of 250 bar. An elevated pressure was chosen to allow room for the pressure drop of sampling, as it is known the dispersion fails below 170 bar. $CDCl_3$ was used as the catching solvent in the cylinder. Samples were analysed directly using ^{1}H NMR

and samples were dried prior to resolution in THF (HPLC grade) for GPC analysis. The results of this were then be compared to the data obtained from batch experiments, and the developed sigmoidal model.

Sampling was conducted using the sampling cylinder system at 4 separate time points during the reaction. Sampling was not attempted within the first 60 minutes, to avoid disrupting the highly sensitive nucleation phase (Table 3.4).

Table 3.4 Analysis results of polymerisation reaction samples obtained using the sampling cylinder setup (Entry 1-4) and the final polymer product (Entry 5).

Entry	Reaction time (min)	Conversion (%)[a]	Mn (kDa)[b]	Mw (kDa)[b]	Đ[b]
1	65	16.4	57	138	2.43
2	86	24.8	75	195	2.60
3	158	78.7	124	299	2.41
4	183	90.0	131	306	2.34
5	226	97.1	150	365	2.43

a – determined via ^{1}H NMR (section 2.3.2), b – determined via GPC (section 2.3.1)

The obtained conversion data was compared to the sigmoidal model developed previously from batch experiments, and a close fit was seen (Figure 3.18). This is clear evidence that the sampling cylinder setup can reliably sample an ongoing polymerisation in $scCO_2$, without loss of reaction components in the sample.

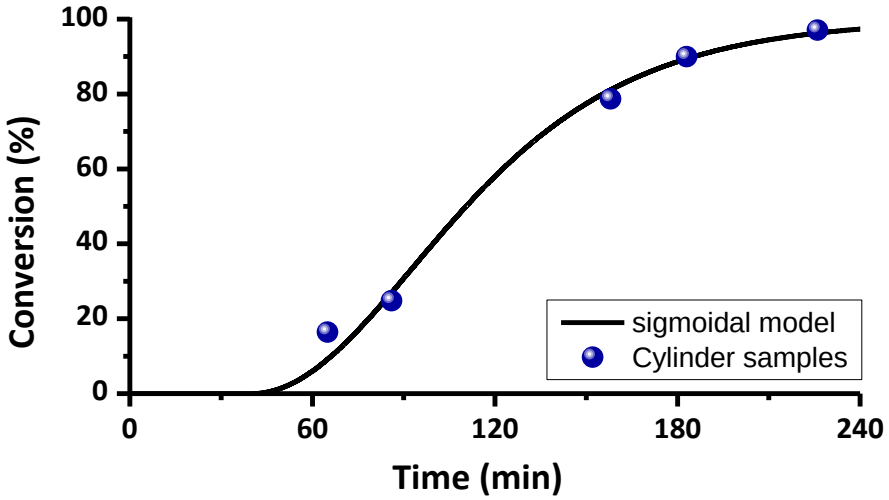


Figure 3.18 Comparison of observed conversion in function of reaction time, obtained from sampling cylinder test (Table 3.4), and fitted sigmoidal model (Figure 3.12). Reaction conditions: 10 ml of MMA, 0.468 g of PDMS-MA, 93.6 mg of AIBN, 220 bar and 65 ℃. Model fitting variables: $t_0 = 1800\ s$, $k' = 2.85 * 10^{-3}\ M^{-1}s^{-1}$.

Molecular weight trends for the cylinder samples and the previously conducted batch experiments were also compared and showed similar values throughout(Figure 3.19).

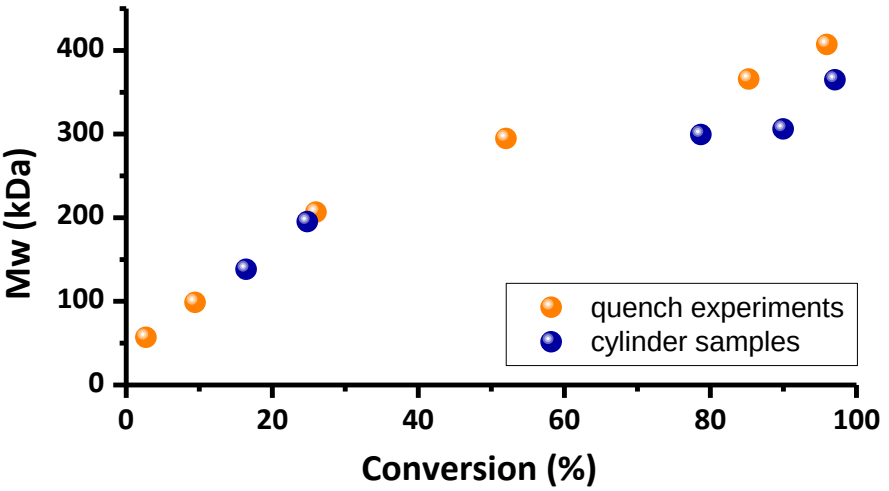


Figure 3.19 Mass average molar mass in function of conversion for the quenching experiments detailed in Table 3.1, compared to the sampling cylinder experiment detailed in Table 3.4.

Although sampling during the reaction caused large pressure variations, conversion and molecular weight progression appeared largely unaffected. The final product was also the expected free flowing white powder. To confirm the desired particle

morphology was achieved, SEM imaging was performed, showing that spherical particles were indeed formed as expected (Figure 3.20). Secondary nucleation, resulting in the formation of small particles at high conversion, was however also observed.

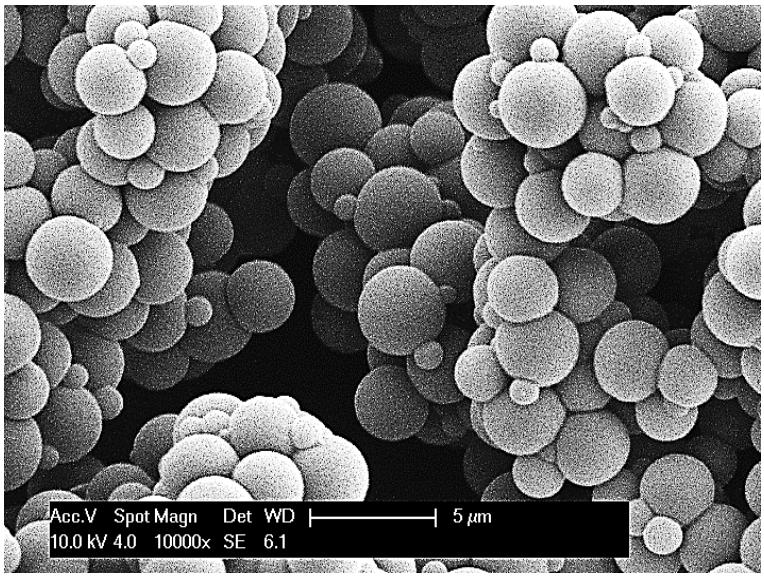


Figure 3.20 SEM image of final product obtained after sampling cylinder experiment (Table 3.4, Entry 5), showing clear spherical particles were formed. Average particle diameter of 2642 (±934) nm with a PSD of 1.23.

This unexpected occurrence was attributed to the lower pressure during the later stages of the reaction (Figure 3.21). Lower pressure may affect solubility of reaction components, inducing secondary nucleation. This observation will be expanded upon in the following chapter. This adverse pressure effect was avoided in all further reactions by adding CO_2 after sampling, to compensate for the induced pressure drop.

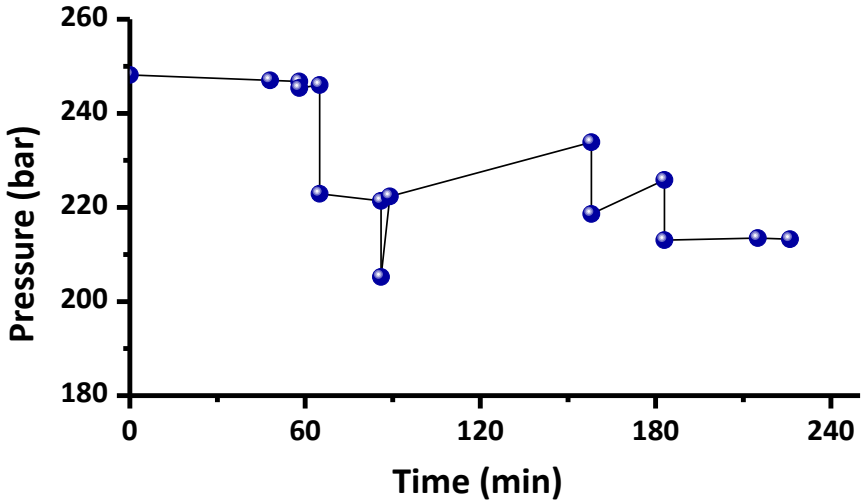


Figure 3.21 Pressure progression during the sampling cylinder experiment detailed in Table 3.4. Four clear pressure drops are seen after sampling, CO_2 was added at 87 minutes to maintain sufficient pressure in the system to maintain system stability.

The standard MMA dispersion FRP was conducted 3 times using identical reaction conditions to the previously performed batch reactions, and samples were obtained at 30-minute intervals using $CDCl_3$ as the catching solvent. To counteract any negative effects of pressure drops, 10-15 bar was added to the reaction just prior to sample acquisition, assuring a constant pressure throughout the polymerisation. Analytical results were collated (Table 3.5) and conversion was compared to batch results (Figure 3.22).

Table 3.5 Data obtained from samples of polymerisation reactions monitored using the cylinder system. Reaction conditions: 10 ml of MMA, 0.468 g of PDMS-MA, 93.6 mg of AIBN, 220 bar and 65 ℃.

Reaction time (min)	Conversion (%)[a]	M_n (kDa)[b]	M_w (kDa)[b]	Đ[b]
61	16.2	36	104	2.90
65	16.4	57	138	2.43
65	17.6	43	148	3.42
66	17.8	33	104	3.17
85	24.8	45	154	3.42
86	24.8	75	195	2.60
92	29.6	51	172	3.34
93	28.6	60	174	2.89
120	57.5	63	204	3.22
121	55.0	63	206	3.26
123	47.6	131	234	1.79
150	62.9	91	264	2.90
150	75.4	86	264	3.07
152	72.1	133	235	1.76
158	78.7	124	299	2.41
178	87.3	98	262	2.68
180	83.8	115	273	2.38
182	79.5	170	296	1.74
183	90.0	131	306	2.34
226	97.1	150	365	2.43
240	97.0	124	313	2.52
240	95.7	186	319	1.72
240	94.7	162	344	2.13

a – determined via ^{1}H NMR (section 2.3.2), b – determined via GPC (section 2.3.1)

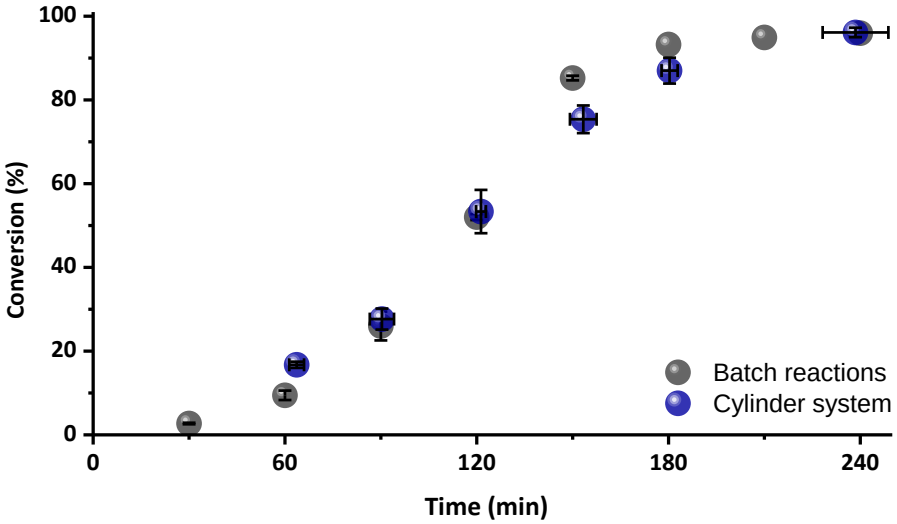


Figure 3.22 Conversion of MMA as a function of reaction time from samples obtained using the cylinder system compared to sequential batch reactions quenched by crash cooling. Error bars represent the standard deviation of experimental conversion from 3 separate reactions. Reaction conditions: 10 ml of MMA, 0.468 g of PDMS-MA, 93.6 mg of AIBN, 220 bar and 65 ℃.

A small apparent conversion discrepancy was observed after 150-180 minutes, but this is believed to be due to the partial drying of the polymer powder in the batch experiments, as discussed previously. From comparison of the average molar mass (Figure 3.23), it can be further seen that the samples obtained using the cylinder system are indeed representative of the ongoing polymerisation.

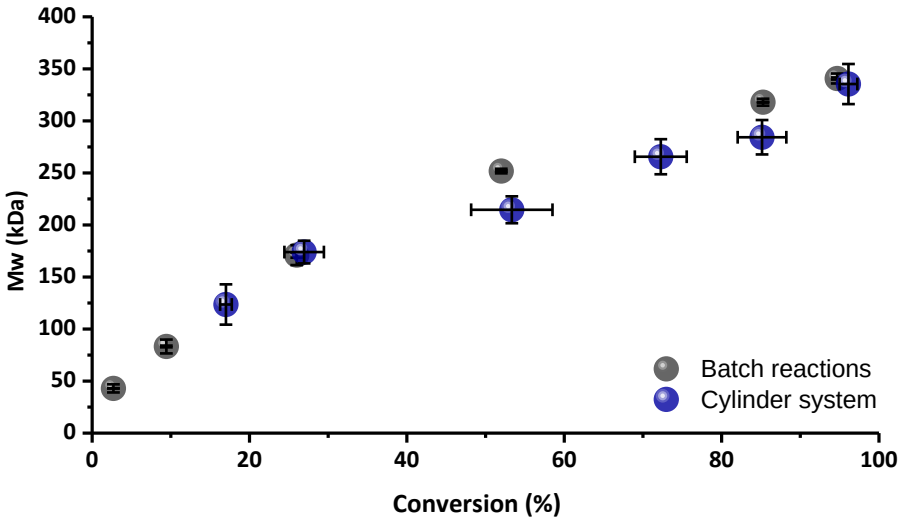


Figure 3.23 Mass average molar mass in function of conversion from samples obtained using the cylinder system compared to sequential batch reactions quenched by crash cooling. Error bars represent the standard deviation on data from 3 separate reactions. Reaction conditions: 10 ml of MMA, 0.468 g of PDMS-MA, 93.6 mg of AIBN, 220 bar and 65 °C.

The sigmoidal conversion curve obtained from the fitting of Equation 3.17 to batch experiment results, with an induction time of $t_0 = 1800\ s$ and a lumped parameter $k' = 2.85 * 10^{-3}\ M^{-1}s^{-1}$, shows excellent correlation with the obtained cylinder data (Figure 3.24). an R^2 value of 0.9797 shows that the cylinder data fits the model even better than the batch reaction data, mainly due to the apparent overestimation of conversion at 150-180 minutes that is avoided using the cylinder sampling method.

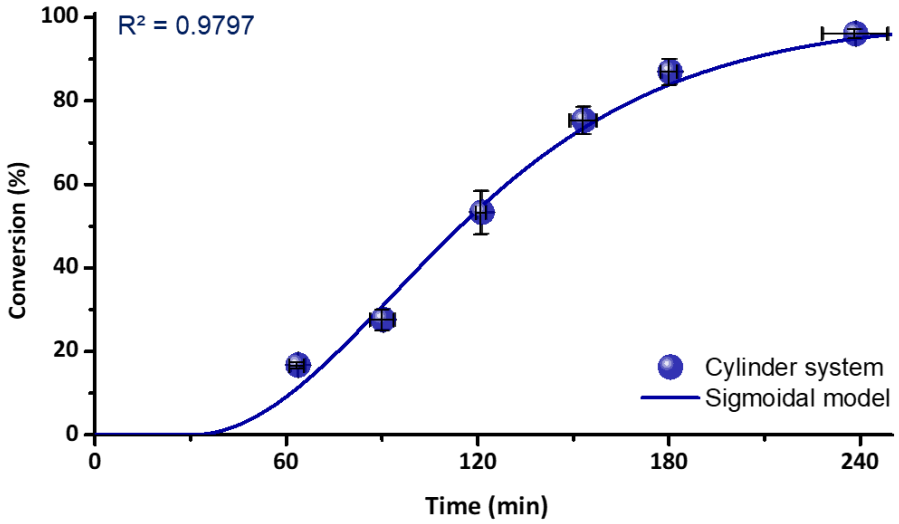


Figure 3.24 Sigmoidal model of conversion of MMA as a function of reaction time, overlayed with conversion data obtained using the cylinder system. Error bars represent the standard deviation of experimental conversion from 3 separate reactions. Reaction conditions: 10 ml of MMA, 0.468 g of PDMS-MA, 93.6 mg of AIBN, 220 bar and 65 ℃. Model fitting variables: $\boldsymbol{t_0 = 1800\ s}$, $\boldsymbol{k' = 2.85 \cdot 10^{-3}\ M^{-1}s^{-1}}$.

3.5.3.2.1 Testing the predictability of the sigmoidal model

The fitted kinetic model found through batch polymerisations and confirmed using the sampling cylinder system, can be used to predict reaction outcomes under varying conditions. The determined reduced rate constant k' is independent of initial component concentrations, allowing it to be used to predict the effect of changing initiator concentration on polymerisation progression. By maintaining the same fitting values and simply changing the initiator concentration value [I] in Equation 3.15 and Equation 3.17, a range of conversion curves were predicted for AIBN concentrations between 0.25 wt% and 2 wt% relative to MMA. In Figure 3.25 it can be seen that doubling or halving initiator concentration does not double or halve polymerisation time in this model, unlike what would be expected for a one phase FRP polymerisation.[120] The model predictions were verified using the sampling cylinder method.

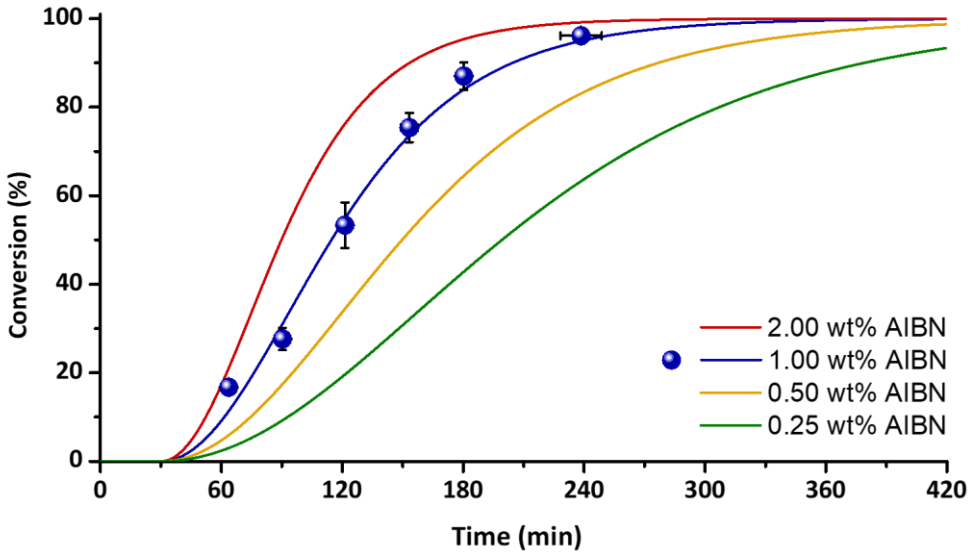


Figure 3.25 Sigmoidal model predictions of conversion of MMA as a function of reaction time for various AIBN concentrations. Lines represent model output data, while spheres represent data obtained using the cylinder system. Model fitting variables: $t_0 = 1800\ s$, $k' = 2.85 * 10^{-3}\ s^{-1}$.

While detailed verification of the model quality using the batch quench method would require 21 separate reactions (using 200 g of MMA, 10 g of PDMS-MA and 1.8 g of AIBN), our use of the new cylinder system allowed model verification in just 3 reactions (using just 28 g of MMA, 1.4 g of PDMS-MA and 260 mg of AIBN) and with a significant time saving! Analysis data from the 3 polymerisation reactions are shown in Table 3.6, covering 6 sampling points for 3 different initiator concentrations. The conversion data was overlayed onto the kinetic traces predicted by the sigmoidal model and show excellent agreement (Figure 3.26).

Table 3.6 Data obtained from samples of polymerisation reactions monitored using the cylinder system. Reaction conditions: 10 ml of MMA, 0.468 g of PDMS-MA, 23.4-187.2 mg of AIBN, 220 bar and 65 ℃.

AIBN (wt% wrt MMA)	Reaction time (min)	Conversion (%)[a]	M_n (kDa)[b]	M_w (kDa)[b]	Đ[b]
0.25	91	14.0	201	351	1.74
0.25	131	18.3	334	572	1.71
0.25	170	31.0	440	719	1.63
0.25	202	48.0	482	756	1.57
0.25	281	64.2	527	864	1.64
0.25	340	87.7	495	792	1.60
0.25	400	94.1	519	846	1.63
0.5	65	12.5	10	63	6.78
0.5	97	22.7	37	220	5.94
0.5	123	29.7	71	324	4.58
0.5	155	51.2	248	429	1.73
0.5	188	66.7	297	495	1.66
0.5	243	89.1	286	487	1.70
0.5	275	95.4	300	550	1.83
2	75	28.6	46	100	2.17
2	101	49.7	65	150	2.33
2	118	68.9	85	150	1.77
2	137	81.3	123	193	1.57
2	155	90.0	103	175	1.70
2	205	94.9	135	207	1.53
2	300	96.7	114	173	1.51

a – determined via ^{1}H NMR (section 2.3.2), b – determined via GPC(section 2.3.1)

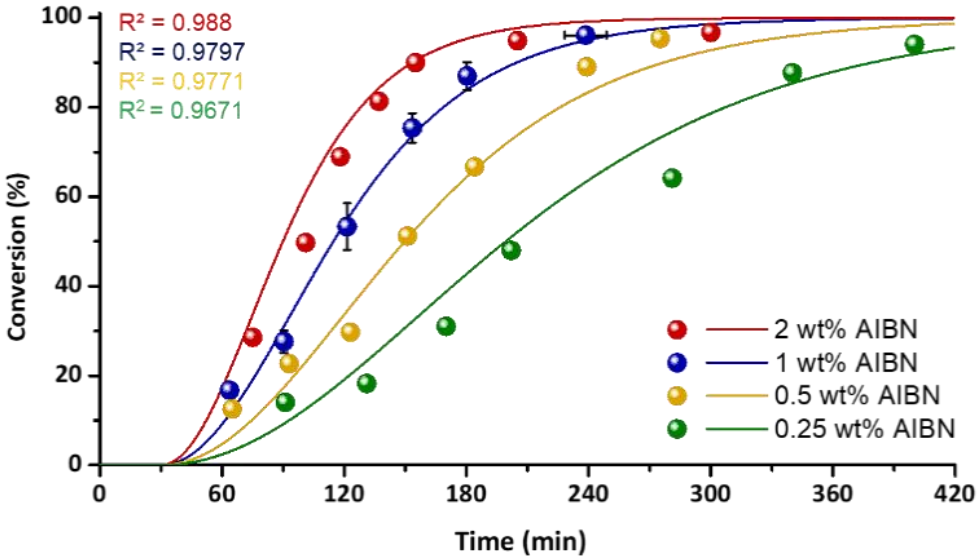


Figure 3.26. Conversion of MMA as a function of reaction time from samples obtained using the cylinder system (spheres) overlaying sigmoidal model predictions (lines) for various AIBN concentrations. Reaction conditions: 10 ml of MMA, 0.468 g of PDMS-MA, 23.4-187.2 mg of AIBN, 220 bar and 65 °C. Model fitting variables: $\boldsymbol{t_0 = 1800\ s}$, $\boldsymbol{k' = 2.85 \cdot 10^{-3}\ M^{-1}s^{-1}}$.

With R^2 values above 0.95 for all polymerisation conditions, it was shown that the model was accurate across the tested AIBN concentration range, while the cylinder system was readily capable of on-line sampling under a range of varying conditions.

3.5.3.3 Monitoring of a range of reaction systems

To initiate the broader application of the sampling cylinder system for reaction monitoring in supercritical fluids, the system suitability was tested for a selection of different polymerisation reactions using the same setup.

3.5.3.3.1 Monitoring of the RAFT controlled dispersion polymerisation of MMA

(This subsection of RAFT controlled polymerisations was conducted in collaboration with Dr Ana Alves Costa Pacheco, while she was part of the Howdle group)

The RAFT controlled dispersion polymerisation of MMA was chosen as a first test due to the similarities with the FRP dispersion polymerisation of MMA and to support an ongoing research project within the group, in need of reliable kinetics to understand CTA efficiency in $scCO_2$. The same sampling method and conditions were maintained.

Previous research into the RAFT controlled dispersion polymerisation of MMA in $scCO_2$ looked into the efficacy of four different dithiobenzoate CTAs.[121] All four CTAs presented pseudo first-order kinetics, giving experimental molar masses close to the theoretical molar mass, with a narrow dispersity of less than 1.30. These data mirrored the control seen in solution polymerisations.[121] Successive batch reactions were quenched by crash cooling the reactor at set times, where samples at low conversion were collected by dissolving them in THF followed by precipitating in cold hexane. This methodology is rather laborious, time consuming and introduces considerable error, as each data point represents a different reaction. In addition, the monitoring at low conversion is compromised by the precipitation step, where short polymer chains can be lost. The sampling cylinder method was used as a more convenient and reliable monitoring system for the RAFT controlled dispersion polymerisation of MMA using CPDT as the CTA.

The RAFT controlled polymerisation was successfully monitored using the cylinder system, confirming that CPDT provided good control over the reaction (Table 3.7). The final molar mass was found to be virtually equal to the theoretical prediction and a narrow polydispersity of $Đ = 1.20$ was achieved.

Table 3.7 Data obtained from samples of polymerisation reactions monitored using the sampling cylinder method. Reaction conditions: 10 ml of MMA, 0.468 g of PDMS-MA, 23.4-187.2 mg of AIBN, 220 bar and 65 °C.

Reaction time (h)	Conversion (%)[a]	$M_{n,th}$ (kDa)[b]	M_n (kDa)[c]	Đ[c]
2	5.7	3.33	4.8	1.16
3	7.4	4.35	5.9	1.19
5.1	14.5	8.54	8.0	1.20
6.1	21.3	12.49	10.5	1.21
8	41.2	24.19	16.2	1.16
10	56.0	32.87	23.5	1.28
24	97.8	57.46	57.3	1.20

a – determined via ^{1}H NMR (section 2.3.2), b – calculated from CPDT and monomer concentration using $M_{n,th} = \left(\frac{[MMA]}{[CPDT]} * conversion\right) * M_{MMA} + M_{CPDT}$, c – determined via GPC (section 2.3.1)

GPC analysis of samples collected throughout the reaction showed controlled growth of the polymer chain in function of time, as seen by a unimodal peak shift to lower elution times (Figure 3.27).

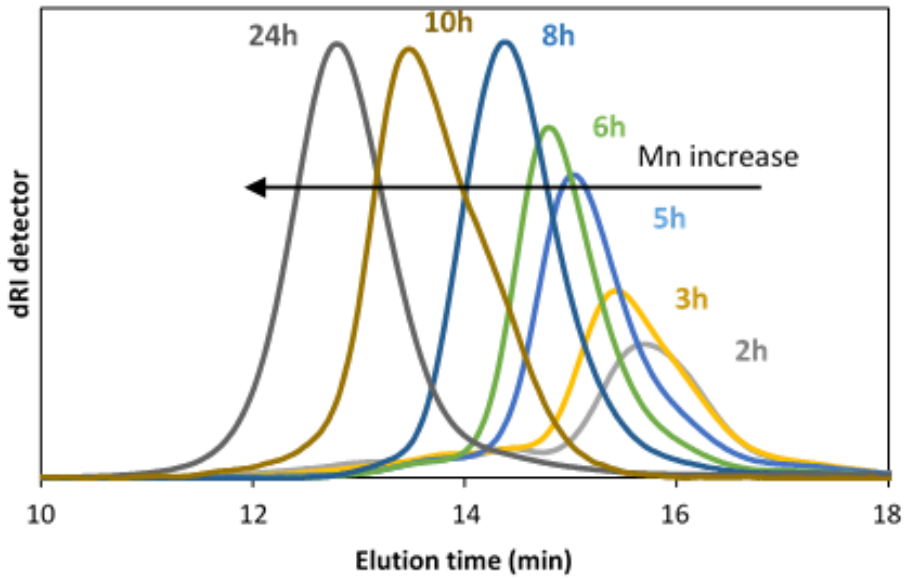


Figure 3.27 GPC traces showing the growth of PMMA in function of time in $scCO_2$ using CPDT as the chain transfer agent. Reaction conditions:10 g of MMA, 0.5 g of PDMS-MA, 0.085 mmol of AIBN, 0.17 mmol of CPDT, 275 bar and 65 °C.

The linear evolution of M_n as a function of conversion is in good agreement with pseudo-living behaviour, as the linear trend of the experimental data is closely aligned with the theoretical molecular weight increase. Livingness was further confirmed by the low dispersity observed throughout the reaction, remaining below $Đ \leq 1.30$ throughout (Figure 3.28).

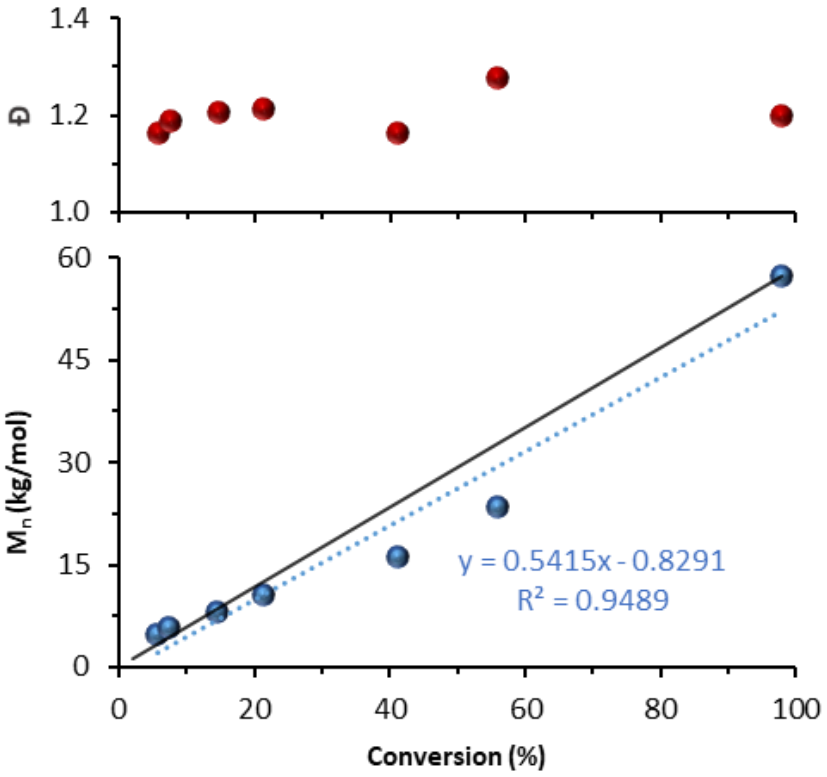


Figure 3.28 Evolution of M_n (blue) and Đ (red) as a function of conversion; solid trend line (black) is the theoretical M_n and dashed trend line (blue) is the linear fitting of experimental data. Reaction conditions: 10 g of MMA, 0.5 g of PDMS-MA, 0.085 mmol of AIBN, 0.17 mmol of CPDT, 275 bar and 65 °C.

The logarithmic monomer conversion as a function of time provided important mechanistic insight, as two distinct regimes were observed for the polymerisation. The initial regime (Figure 3.29) indicates mild retardation, which is commonly observed for RAFT polymerisation of methacrylates, although it tends to be more pronounced for polymerisation of acrylates or acrylamides.[122] From the experimental

data, an initial induction period of approximately 14 minutes was found. Gregory *et al.* previously reported induction periods of up to 12 hours for MMA polymerisation in $scCO_2$ with dithioester CTAs and no retardation.[121] However, these data were obtained from successive quenched batch reactions where precipitation of the product in cold hexane might have excluded low molecular weight chains and artificially delayed the observation of polymerisation onset. Therefore, the induction period was likely shorter. Long retardations are expected with other CTAs for example with the high stability of a dithioester intermediate radical. However, a shorter induction time should be expected for trithiocarbonate CTAs such as CPDT, owing to the less stable intermediate radicals.[123] This hypothesis aligns well with our experimental results (Figure 3.29).

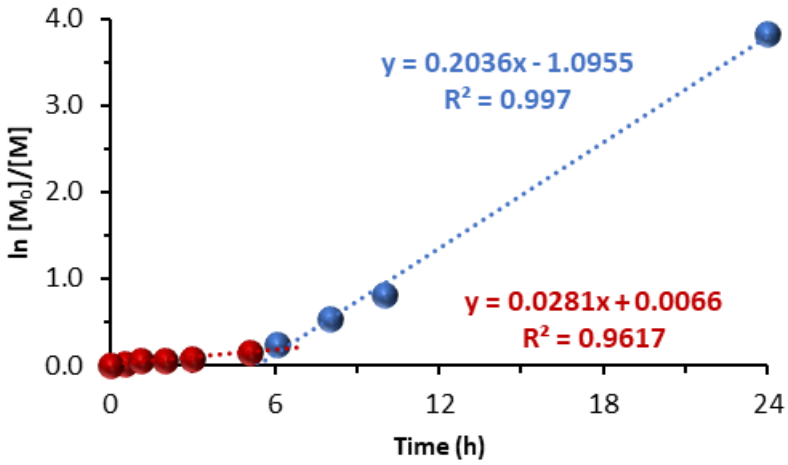


Figure 3.29. Pseudo-first-order kinetic plot of monomer conversion in function of reaction time for the dispersion polymerisation of MMA with CPDT in $scCO_2$. Two distinct reaction regimes are seen (red, blue). A 7-fold rate increase is seen between regimes.

The second regime started after 6 hours of reaction time and presents a 7-fold increase in the rate of polymerisation compared to the previous regime. The pseudo-first-order kinetic plot remained linear throughout the second regime, up to 97.80 %

conversion. Based on previous RAFT dispersion polymerisation studies, this inflection point most likely indicates the onset of micellar nucleation.[124, 125] At the onset of nucleation, as the monomer swells the nuclei, the high concentration of monomer causes a significant increase of the reaction rate. Consequently, this also indicates that the critical chain length J_{crit} was achieved at around 10 kg mol^{-1}.

Using the cylinder system, the control of CPDT over the dispersion polymerisation of MMA was confirmed by conducting a single polymerisation. The experiment also afforded insights into the mechanism of the reaction, uncovering two distinct reaction regimes associated with the onset of nucleation. The facile application of the cylinder system quickly led to findings that have provided a better understanding of the polymerisation system and opened the door for further development in the area of controlled polymerisations in $scCO_2$ in an efficient and reproducible manner.

3.5.3.3.2 Monitoring the free-radical dispersion polymerisation of styrene

The use of a different monomer for the FRP dispersion polymerisation was tested using styrene. Styrene has a much lower reactivity and very different monomer/polymer solubility in $scCO_2$ in comparison to MMA.[126, 127] The polymerisation was conducted with 2 wt% AIBN with regards to monomer, to allow the reaction to reach >95 % conversion quicker. $CDCl_3$ was again used as the sample solvent, as it is a satisfactory solvent for styrene and polystyrene, so no changes to the sampling procedure were needed.

The styrene polymerisation was monitored successfully using the cylinder setup. While the polymerisation took more than 30 hours to reach above 95% conversion, the cylinder system allowed for on-line tracking of the reaction progress, meaning high conversion could be reached on the first attempt. Initial samples confirmed the lower reactivity of this system (Figure 3.30), while further sampling allowed for real-time determination of the point at which the desired conversion was reached, after approximately 30 hours. While the polymerisation was far slower than the polymerisation of MMA, the conversion progression did show the same sigmoidal progression. Kinetic modelling was therefore performed using Equation 3.17, as done previously for the polymerisation of MMA. A good fitting of the data was achieved (Figure 3.30), showing the typical sigmoidal progression of conversion.

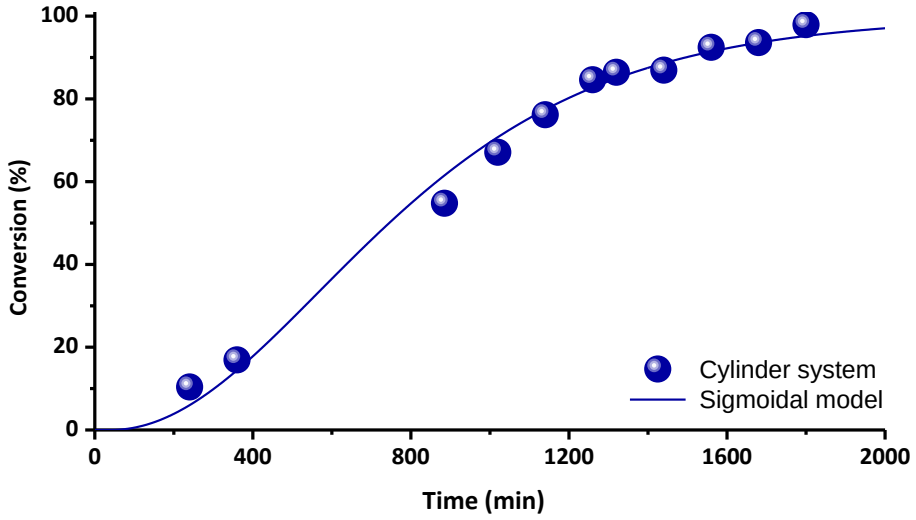


Figure 3.30 Conversion of styrene as a function of reaction time from samples obtained using the cylinder system overlaying a sigmoidal model fitting line. Reaction conditions: 10 ml of styrene, 1.818 g of PDMS-MA, 181.8 mg of AIBN, 245 bar and 65 °C. Model fitting variables: $t_0 = 1800\ s$, $k' = 2.4 \cdot 10^{-4}\ M^{-1}s^{-1}$.

3.5.3.3.3 Free radical precipitation polymerisation of acrylic acid

The next test of the sampling cylinder method was a different heterogeneous polymerisation system. The precipitation polymerisation of acrylic acid is a reaction that does not use a stabiliser to guarantee a consistent reaction mixture, as poly(acrylic acid) forms in-situ particles without the need for a stabiliser. The reaction has also been kinetically analysed previously by Ollagnier *et al.*[89] using in-situ IR spectrometry, allowing for a clear comparison of observed conversion. Acrylic acid is soluble in water, so D_2O was chosen as the solvent to add into the cylinder system. The high molar mass poly(acrylic acid) formed in this reaction is generally poorly soluble, meaning that NMR analysis would be delayed until solution was achieved. To remedy this issue, methanol was added to the D_2O as an internal standard, allowing for the loss of monomer to be tracked. A stock solution of D_2O and methanol was used throughout the experiment and an initial sample was taken to establish the ratio between acrylic acid and methanol in a fully unpolymerized sample. The relative reduction in acrylic acid with respect to methanol in subsequent samples was then used to determine conversion.

The observed conversion trend was compared to the fitted kinetic model from Ollagnier *et al*.,[89] showing that the cylinder system provides the same accurate data (Figure 3.31). Unlike the on-line IR monitoring system, the sampling cylinder method affords a scalable, reliable, and more robust solution at a far lower price.

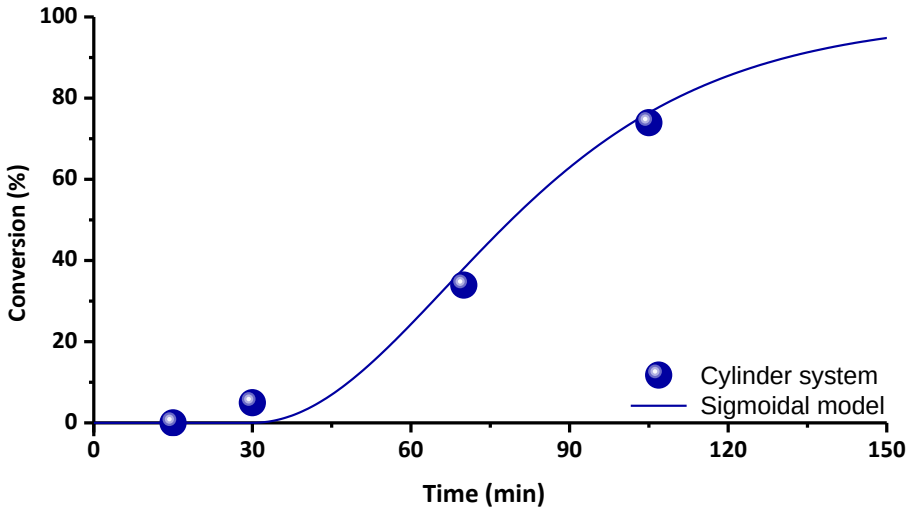


Figure 3.31 Conversion of acrylic acid as a function of reaction time from samples obtained using the cylinder system overlaying a sigmoidal model fitting line with fitting variables from Ollagnier et al.[89] Reaction conditions: 2 g of acrylic acid, 30 mg of AIBN, 160 bar and 62 °C. Model fitting variables: $t_0 = 1800\ s$, $k' = 1.60 \cdot 10^{-2}\ M^{-1}s^{-1}$.

3.5.3.3.4 Enzymatic ring-opening polymerisation of caprolactone

In an attempt to investigate the kinetics of two simultaneous competing reactions, the HEMA initiated eROP of ε-caprolactone in $scCO_2$ was studied. The hydroxyl group of HEMA can act as an initiator in ROP to yield functional polymers.[128, 129] While in the presence of Novozym 435, HEMA is known to undergo transesterification with itself, resulting in a lack of control over the polymers produced.[130, 131] Utilising the cylinder system, both transesterification and polymerisation were monitored simultaneously, showcasing that competing reactions can be monitored simultaneously in-situ. $CDCl_3$ was used as the sample solvent since it is suitable for HEMA, CL, and pCL. Analysis of the reaction mixture samples showed the expected increase in both polymerisation and transesterification in function of time (Figure 3.32).

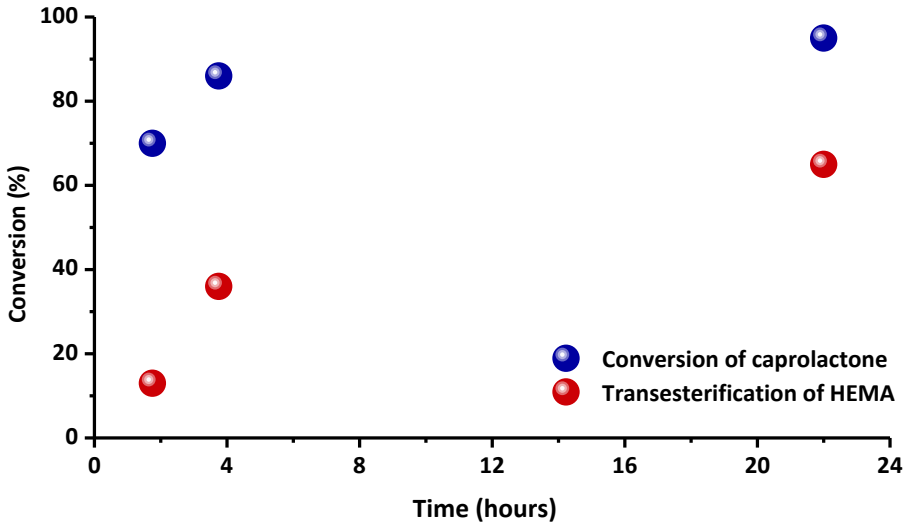


Figure 3.32 Conversion in function of reaction time for the polymerisation of caprolactone and the concurrent transesterification of HEMA. Reaction conditions: 4 g of CL, 0.18 g of HEMA, 0.4 g of Novozym 435, 207 bar and 65 °C.

While further investigation of this reaction system is beyond the scope of this research, it is clear that the new cylinder sampling system is capable of monitoring a more complex reaction mixture with two competing reactions in an expanded bulk.

3.6 Conclusions

Accessible on-line reaction monitoring is crucial for reproducible and efficient research of chemical reactions and especially polymerisations. In industry, sampling and subsequent analysis of ongoing reactions is the main method of monitoring.

In this chapter, we demonstrated the development of an inexpensive and reliable on-line sampling method for reactions in $scCO_2$, using only readily commercially available parts.[132] The efficacy of the sampling setup was first confirmed for the widely studied dispersion polymerisation of MMA, by comparing conversion and molar mass trends to known values. Kinetic modelling provided insights into the polymerisation mechanism and allowed us to predict the effect of altering component

concentrations. The rapid data gathering capabilities of the developed sampling method were highlighted by varying initiator concentration for the dispersion polymerisation of MMA, and quickly gaining large amounts of data to match the kinetic model predictions.

The wide applicability of the sampling cylinder method was then showcased by monitoring a range of very different polymerisations and reactions at various conditions. The ability to easily add an internal standard for the monitoring of acrylic acid conversion, highlighted the facile and adaptable applicability of the developed sampling cylinder method.

Chapter 4

Improving Reactor Conditions and Exploiting the Tuneable Density of $scCO_2$ in Free Radical Dispersion Polymerisations

4.1 Overview

Dispersion polymerisations of methyl methacrylate and styrene are widely employed for producing discrete, spherical polymer particles from traditional solvents, which cover a broad particle size range.[28, 32] With environmental impact becoming an ever more widespread concern, there is increasing demand for greener solvents with advantageous characteristics.[36] Supercritical carbon dioxide ($scCO_2$) offers the potential of a greener solvent for dispersion polymerisations, with uniquely tuneable solvent properties and the ability to avoid energy and cost intensive drying steps.[34] This chapter will describe the optimisation of reactor conditions for the dispersion polymerisation of MMA and styrene, focussing on agitation and loading efficiency, essential factors for commercial polymer production.[15] Further to this, the tuneable density of $scCO_2$ and its effect on the solubility of poly(dimethyl siloxane) stabilisers in dispersion polymerisations will be analysed. By varying the reactor pressure at the start of polymerisation, solvent strength can be altered without the need for cosolvent systems used in traditional solvents.[133] The effect of this on polymerisation kinetics and particle size control will be explored. Finally, this additional control mechanism will be utilised to achieve a PMMA particle size range far beyond what was previously attainable with this stabiliser, further enhancing the potential use of $scCO_2$ as a green solvent for industrial polymer production.

4.2 Introduction

Time and cost efficiency are important aspects of commercially successful industrial dispersion polymerisations. To this end, it is important to maximise production

capacity, product consistency, and reaction rate. Another important aspect of industrial dispersion polymerisations is the reliable control over particle size and a convenient method of altering it. Many efficiency and control aspects of dispersion polymerisations at a fundamental level are related to solubility and stabilisation during the polymerisation process. To progress the use of $scCO_2$ as a solvent for dispersion polymerisations, a thorough investigation of the stabilisation system and its effects within this medium is required.

4.2.1 Stabilising dispersion polymerisations

As described in Chapter 1, stabilisation plays a large role in a successful dispersion polymerisation. A schematic overview of a dispersion polymerisation (Figure 4.1), displays the transition from an initially homogeneous solution to a heterogeneous dispersion, that occurs during the polymerisation. A suitable surfactant is required to stabilise the precipitating polymer chains and form a heterogeneous solution. The surfactant is essential to avoid aggregation of the insoluble particles, allowing spherical dispersed particles to be formed.

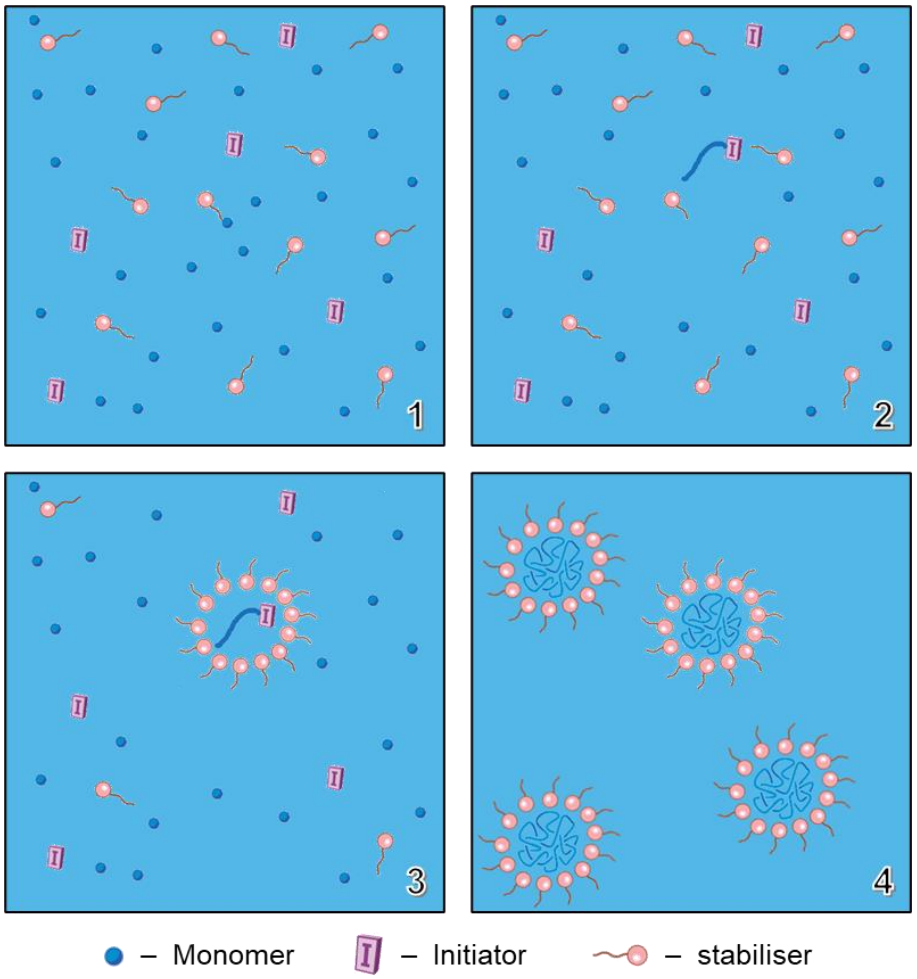


Figure 4.1 Schematic overview of the dispersion polymerisation mechanism: 1) Homogeneous solution before polymerisation 2) homogeneous solution with soluble oligomer chain 3) heterogeneous solution with insoluble oligomer chain dispersed by the stabiliser 4) heterogeneous solution of dispersed polymer particles surrounded by stabiliser.

A suitable surfactant for dispersion polymerisation needs to both associate efficiently with the growing polymer particles and display good solubility in the chosen solvent. This dual requirement means the stabiliser need to be amphipathic, containing both an anchor segment with affinity for the polymer particle surface and a solvent soluble section.[11, 27] Block copolymers or homopolymers with functional end group are widely used in dispersion systems to achieve the desired solvent and polymer philicity, and achieve the required steric stabilisation.[15, 27, 134] Beyond the chemical

structure of the stabiliser, a range of conditions will influence the stabilisation efficacy in a dispersion polymerisation, such as mixing, component concentrations and the used solvent.

4.2.2 The importance of agitation

Efficient agitation of a polymerising system can be essential to obtaining a desired consistent product, especially in heterogeneous polymerisation systems.[11] Beyond the need for agitation to improve heat dissipation, it can be required in heterogeneous polymerisations to assure a consistent mixture of phases is maintained. While suspension and emulsion polymerisations are significantly affected by reactor geometry and stirring rate, dispersion polymerisations can be largely unaffected from these factors.[135] There will generally be an upper and lower limit of agitation needed to maintain a stable dispersion, directly dependent on the stabiliser, monomer, and solvent being used. In $scCO_2$, dispersion polymerisations of MMA conducted using fluorinated polymeric stabilisers such as the acid-terminated perfluoropolyether Krytox 157 FSL have been shown to form dispersion particles without the need for any agitation.[46, 67, 68] It was however discovered that agitations above 25 RPM using a single stage vertical blade turbine impeller, would result in enough shear forces to disrupt stabilisation.[47] Excessive agitation can disrupt the steric association between growing polymer particles and the anchoring head group of a dispersion stabiliser, resulting in particle coagulation and precipitation.[136] This effect has been observed experimentally in $scCO_2$ when using Krytox 157 FSL as the stabiliser (Figure 4.2).[47]

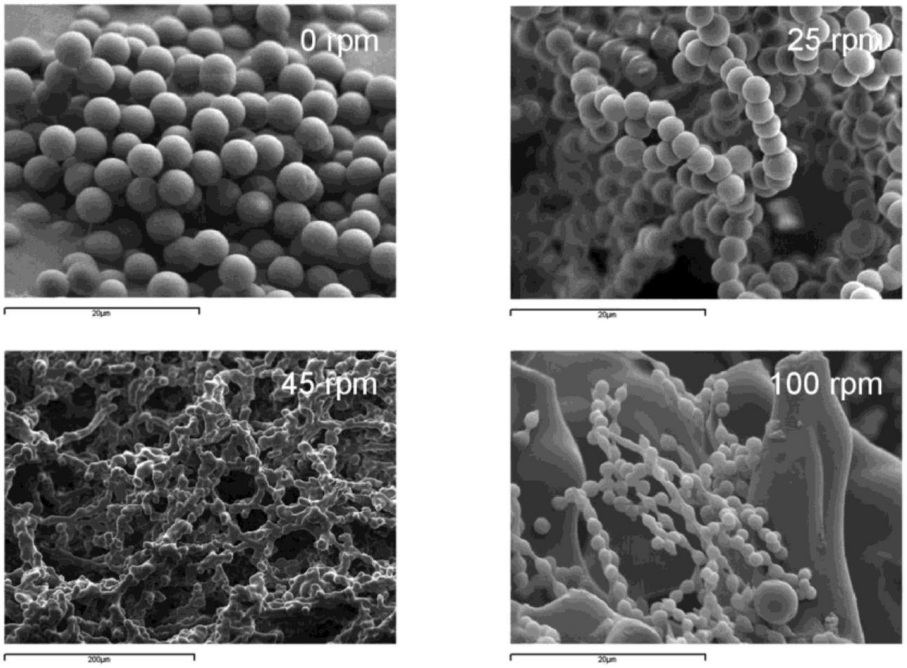


Figure 4.2 SEM pictures of polymer obtained from dispersion polymerisation of MMA in $scCO_2$ using Krytox 157 FSL as the stabiliser, varying in stirring rate (0, 25, 45, and 100 RPM), showing shear induced coagulation occurring at higher stirring rates.[47]

Other dispersion stabilisers will withstand far higher shear rates, and therefore function at higher stirring rates, but can require a minimum agitation to maintain particle separation and dispersion stability. Siloxane based stabilisers, such as PDMS-MA, are known to require more intense agitation in $scCO_2$.[137] Previous research has shown that particle stability can change with changing of agitation intensity within siloxane stabilised dispersion systems.[35, 49, 52, 137] It was reported that the dispersion polymerisation of MMA using PDMS-MA was unsuccessful without agitation, and required significantly higher stirring rates than Krytox stabilised systems to avoid precipitation and attain dispersed particles.[46, 49]

Additional to the chemical nature of the stabiliser, stirrer design and reactor dimensions are an important factor in reaching a stable dispersion system.[105, 111, 137] The amount of shear forces put into a dispersion system are dependent on impeller

and reactor dimension,[7, 27, 108, 138] and this can critically effect reaction outcome. The high pressure system used in this work for dispersion polymerisations in $scCO_2$ is a closed tank featuring a single stage pitched-blade turbine impeller.[9, 35] Previous research into the effect of blade size, shaping, and angle for pitched-blade impellers in traditional solvents has shown the possibility of two dominating flow regimes.[139] It was demonstrated that at a critical blade angle, the flow pattern present in the reactor tank will change from axial to radial (Figure 4.3). This critical angle is dependent on a host of factors, including but not limited to tank dimensions, impeller clearance, stirring direction, solvent viscosity, and homogeneity of the system being mixed.[139] For consistent mixing throughout a tank reactor, axial flow is preferred, as radial flow can result in inconsistent component concentrations above and below the pitched-blade impeller.[139, 140]

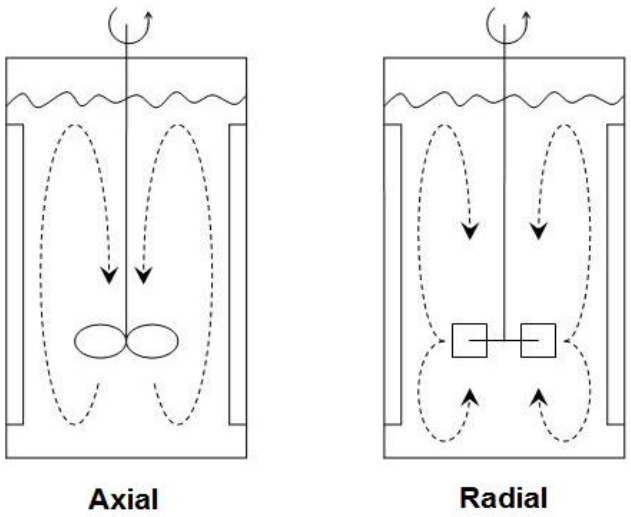


Figure 4.3 Schematic comparison of axial and radial flow patterns in a closed tank reactor.

4.2.3 The effect of component concentrations and reactor loading

Several reaction parameters can influence the average particle diameter and PSD of a dispersion polymerisation product. For atmospheric dispersion polymerisations, it is known that particle size is dependent on monomer solubility and critical chain length (J_{crit}[11, 29] / Z_{mer}[30]) in the selected solvent.[141] A short Z_{mer} length will result in increased nucleation and smaller particles, while a longer Z_{mer} length will delay particle nucleation, resulting in fewer and larger particles. The final particle size obtained in dispersion polymerisations normally increases with increasing monomer concentrations.[135, 142-144] As monomer is usually a good solvent for its own polymer, higher monomer concentration will favour an increase in Z_{mer} length during initial polymerisation. Particle size control can be achieved by altering initial monomer, stabiliser, and initiator concentrations to manipulate the nucleation process towards desired particle concentrations.[94, 138] The final particle size is directly related to the particle concentration achieved during the nucleation phase. The number of particles present in the system at the end of the nucleation phase remains constant during the so-called particle growth phase and is directly related to final particle size.[98, 99]

In $scCO_2$ the same principals of particle size control apply, as shown in detail by McAllister *et al*.[35] By varying initial PDMS-MA and MMA concentration, McAllister *et al.* were able to produce PMMA particles with an average diameter ranging from 320 nm to 3.8 μm.[35]

Beyond particle size control, the overall loading of reactants will affect the stability of dispersion polymerisations. If insufficient material is present, nucleating polymer

chains won't be surrounded by stabiliser and a dispersion will never form. Conversely, if solvent concentration is too low, or reactant concentration is too high, steric separation between particles will be lost and particles will be pushed into each other, resulting in coagulation.[27, 93, 133] In traditional solvents, the overall reactant loading limit for the dispersion polymerisation of MMA was found to be 40 vol% or higher, depending on stabiliser type.[106, 145] In $scCO_2$ meanwhile, the ultimate loading limit of MMA dispersion polymerisations has not been explicitly explored, with published reactant loadings ranging from 12 vol%[35] up to 24 vol%[52], far lower than what is achieved in traditional solvents.

4.2.4 Effect of solvent/antisolvent strength

The efficacy of the solvent to dissolve the monomer, stabiliser, and growing polymer chains will influence the outcome of dispersion polymerisations.[27] as with increased monomer concentration, a more soluble polymer chain results in a higher Z_{mer} length and the formation of larger particles.[141] The solubility of the monomer in the solvent phase compared to the dispersed polymer phase will also affect kinetics, particle size, and particle stability.[135] Finally, particle size will also depend on the ability of the solvent to dissolve the stabiliser, as the affinity of the stabiliser for surrounding nucleating particles will change.[138, 146] Using different stabilisers, with different solvent affinity, will result in different polymer particle sizes being achieved under otherwise identical conditions.[138, 146]

4.2.4.1 Mixed solvent systems

An alternative way to alter the solubility and partitioning of all components and inducing particle size variation, is through the use of a mixed solvent system.[141] The

dispersion polymerisation of MMA and styrene in traditional solvents such as dodecane or methanol can be influenced by the addition of water as an antisolvent.[106, 133, 138, 146] The water reduces the affinity of the stabiliser towards the solvent, driving it toward nucleating polymer particles, resulting in smaller particles being formed.[146] Additionally, the water can drive the monomer towards the dispersed particle phase, increasing the partition coefficient of the monomer in the system. The increased monomer concentration in the dispersed phase can then result in a higher polymerisation rate, vastly improving reaction times.[133]

4.2.4.2 Mixed solvent systems with $scCO_2$

The use of mixed solvent systems in $scCO_2$ for dispersion polymerisations remains very limited. The use of hexane to improve the solubility of PDMS-MA as a stabiliser for the polymerisation of MMA was demonstrated by Yates *et al*.[147] Conversely CO_2 was used as an antisolvent by Zetterlund and co-workers, to drive the polymerisation locus of MMA[148] and styrene[149] towards the dispersed phase and even induce an emulsion polymerisation system.[150]

4.2.4.3 Pressure influence in $scCO_2$ dispersions

An additional route to changing the solvent strength in $scCO_2$ is by altering the reaction pressure, as this will change the density and solvating power of the CO_2 solvent. This can provide a further method of particle size control and kinetic influence, without the need for a mixed solvent system. For the dispersion polymerisation of MMA with PDMS-MA stabiliser, several groups have observed that pressure did not have any significant effect on particle size[97, 98], while other groups stated a possible effect without experimental confirmation.[97, 103] With alternate

stabilisers meanwhile, it has been seen that increasing initial pressure can both increase[53, 151] and decrease[114] the final particle size, depending on the solubility of the employed stabiliser and monomer in $scCO_2$.

4.3 Aims and objectives

The goal of the research presented in this chapter is to improve reproducibility of the dispersion polymerisation of MMA in $scCO_2$ and gain an understanding of the parameters affecting the system. The gained knowledge will then be applied to achieve the dispersion polymerisation of styrene using PDMS-MA for the first time.

Reproducibility issues have often affected dispersion polymerisations in $scCO_2$. Inconsistent stirrer design and stirring rate are thought to be the origin, but a concise investigation is yet to be completed. This chapter will investigate the influence of agitation variations on product quality and aim to develop a reliable impeller design based on the vast literature available for traditional closed tank stirring in conventional solvents. The loading limits of the polymerisation in $scCO_2$ will then be tested and compared to tradition polymerisation solvents.

Previous research within the group has shown that traditional particle size control techniques used in dispersion systems are also applicable in $scCO_2$.[35] A factor that has yet to be investigated in $scCO_2$ is the altering of component solubility. In traditional solvents this is achieved by using solvent mixtures, but in $scCO_2$ this may also be achieved by altering the pressure at which the reaction is conducted. In this chapter we will investigate the exploitation of the pressure dependent solubility of PDMS-MA in $scCO_2$[43, 54] to develop a facile particle size control method for PMMA particles,

without the use of cosolvents. Observed particle size trends will be linked directly with the solubility of the used stabiliser, through a series of reactions conducted at a lower temperature and with a longer PDMS-MA chain length, as this alters the cloud point pressure. Combining this pressure-particle size dependency with existing control methods (stabiliser concentration, monomer loading)[35], we will attempt to expand the attainable particle size range of PMMA particles in $scCO_2$.

Finally in this chapter, the gained insights will be applied to the dispersion polymerisation of styrene, a reaction previously not possible with PDMS-MA as a stabiliser.

4.4 Experimental

4.4.1 Materials

Methyl methacrylate (MMA, 99 %) was obtained from Mitsubishi Chemical. 2,2'-Azobis(isobutyronitrile) (AIBN, 98 %) was purchased from Molekula. Styrene (99 %) was purchased from Sigma-Aldrich. Monomethacrylate terminated polydimethylsiloxane (PDMS-MA, 150-200 cSt, 10 000 g/mol), hexamethylcyclotrisiloxane (D_3, 99 %) and 3-(methacryloxy)propyldimethylchlorosilane (95%) were obtained from Fluorochem. N-Butyllithium (nBuLi, 2.5 M in hexane, anhydrous) was purchased from Acros organics and 2,2'-azobis(4-methoxy-2,4-dimethylvaleronitrile) (V-70) was purchased from Wako. Carbon dioxide (CO_2, SCF grade 5.5, 99.9995 %) was obtained from Air Products and Chemicals Inc. All chemicals were used as received.

4.4.2 One step dispersion polymerisation in $scCO_2$

Batch dispersion polymerisations were carried out in an in-house built high-pressure reaction vessel with an internal volume of 60 ml (max. operating conditions: 120 °C, 380 bar), detailed in section 2.2.3.

For a typical reaction, an AIBN (0.0936 g, 1 wt% relative to monomer) and PDMS-MA (0.468 g, 5 wt% relative to monomer) mixture and MMA (10 ml, 9.36 g) were degassed[109] by bubbling with argon in separate vials for 30 minutes. During this time, the autoclave was flushed with CO_2 at 2-3 bar, venting through the keyhole. After 30 minutes of degassing, 10 ml of MMA was added to the AIBN/PDMS-MA mixture using a gastight luer-lock glass syringe. The resulting solution was then transferred quantitatively into the autoclave, injected through the keyhole against a positive flow of CO_2. The key was then inserted into the autoclave, sealing it off completely from the atmosphere. At this point CO_2 was added, pressurising the system to 50 bar. Heat was then applied through the heating jacket, bringing the temperature to 35°C. CO_2 and heat were then added incrementally until the desired reaction conditions were reached (typically 65 °C and 220 bar). The point at which reaction conditions were reached was chosen as the starting point of the reaction. After 210 minutes, when polymer conversion reached >90%,[132] the heating was turned off and the system temperature was allowed to fall below 30 °C. At this point the stirring was stopped and the pressure was released slowly, returning to atmospheric conditions and yielding a fine white powdered product.

4.4.3 HPLC initiated dispersion polymerisation in $scCO_2$

To better control the initial pressure of the MMA polymerisation and avoid the reaction proceeding during the heating up process, the initiator was injected through an HPLC pump attached to the system. As AIBN is a solid powder, it could not be added to the autoclave without solvent. A stock solution of AIBN in 10 ml MMA was used to pump in the desired amount of initiator. A diagram representation of the autoclave and HPLC setup is shown in section 2.2.4. The autoclave setup allows for the addition of liquid to the autoclave setup at reaction pressure via the labelled HPLC inlet tap. This is a previously published procedure, used for a range of high-pressure polymerisations.[35, 69, 132, 152]

An AIBN in MMA stock solution and a PDMS-MA (0.468 g) and MMA (7.5 ml) mixture were degassed[109] by bubbling with argon in separate vials for 30 minutes. During this time, the autoclave was flushed with CO_2 at 2-3 bar, venting through the keyhole. After 30 minutes of degassing, the PDMS-MA and MMA mixture was then transferred quantitatively into the autoclave, injected through the keyhole against a positive flow of CO_2. The key was then inserted into the autoclave, sealing it off completely from the atmosphere. At this point CO_2 was added, pressurising the system to 50 bar. Heat was then applied through the heating jacket, bringing the temperature to 35 °C. CO_2 and heat were then added incrementally until the desired reaction conditions are reached (typically 65 °C and 200 bar), keeping the pressure approximately 20 bar below the final target pressure.

Prior to connecting the HPLC to the autoclave, the pipe system was rinsed by pumping acetone through to the autoclave connection. Following this, the degassed

MMA/AIBN stock solution was pumped through, pushing out the acetone. With the piping filled with the stock solution, the pipe was connected to the HPLC inlet tap of the autoclave (Figure 2.4). With the autoclave HPLC inlet tap closed, pressure was built up by pumping in stock solution at a slow rate. The pressure of the HPLC pump was brought up to reaction pressure, meaning that opening the HPLC inlet tap would not cause any liquid movement. The flow rate of the HPLC pump was set to 1 ml/min, the HPLC inlet tap was opened, and the pump was engaged. The desired amount of AIBN (0.0936 g) was added after 150 seconds of pumping, along with 2.5 ml of MMA. The pump was then stopped and the HPLC inlet tap was closed. This point was chosen as the starting point of the reaction. HPLC pressure was released through the internal purge system, before disconnecting the pipe from the HPLC inlet. The entire HPLC system is then flushed with 60 ml of acetone. This method of initiator addition affords a far more consistent estimation of reaction pressure during early nucleation.

4.4.4 Two step dispersion polymerisation in $scCO_2$

Two stage dispersion polymerisations were carried out in an in-house built high-pressure reaction vessel with an internal volume of 60 ml (max. operating conditions: 120 °C, 380 bar), detailed in in section 2.2.3.

For a typical reaction, An AIBN in MMA stock solution and a PDMS-MA (1.404 g, 20 wt% wrt total monomer loading) and MMA (2.5 ml) mixture were degassed[109] by bubbling with argon in separate vials for 30 minutes. During this time, the autoclave was flushed with CO_2 at 2-3 bar, venting through the keyhole. After 30 minutes of degassing, the PDMS-MA and MMA mixture was then transferred quantitatively into the autoclave, injected through the keyhole against a positive flow of CO_2. The key

was then inserted into the autoclave, sealing it off completely from the atmosphere. At this point CO_2 was added, pressurising the system to 50 bar. Heat was then applied through the heating jacket, bringing the temperature to 35 °C. CO_2 and heat were then added incrementally until the desired reaction conditions are reached (typically 65 °C and 200 bar), keeping the pressure approximately 20 bar below the final target pressure.

Prior to connecting the HPLC to the autoclave, the pipe system was rinsed by pumping acetone through to the autoclave connection. Following this, the degassed MMA/AIBN stock solution was pumped through, pushing out the acetone. With the piping filled with the stock solution, the pipe was connected to the HPLC inlet tap of the autoclave (Figure 2.4). With the autoclave HPLC inlet tap closed, pressure was built up by pumping in stock solution at a slow rate. The pressure of the HPLC pump was brought up to reaction pressure, meaning that opening the HPLC inlet tap would not cause any liquid movement. The flow rate of the HPLC pump was set to 1 ml/min, the HPLC inlet tap was opened, and the pump was engaged. The desired amount of AIBN (0.0702 g, 1 wt% wrt final monomer loading) was added after 150 seconds of pumping, along with 2.5 ml of MMA. The pump was then stopped and the HPLC inlet tap was closed. This point was chosen as the starting point of the reaction. HPLC pressure was released through the internal purge system, before disconnecting the pipe from the HPLC inlet. The entire HPLC system is then flushed with 60 ml of acetone.

After 60 minutes of reaction time, when nucleation of polymer particles forming a stable dispersion system has occurred, a further charge of MMA (2.5 ml) was added

via HPLC pump at a rate of 0.2 ml/min following the same pump procedure. After a further 210 minutes, when polymer conversion reached >90%,[132] the heating was turned off and the system temperature was allowed to fall below 30 °C. At this point the stirring was stopped and the pressure was released slowly, returning to atmospheric conditions, and yielding a fine white powdered product.

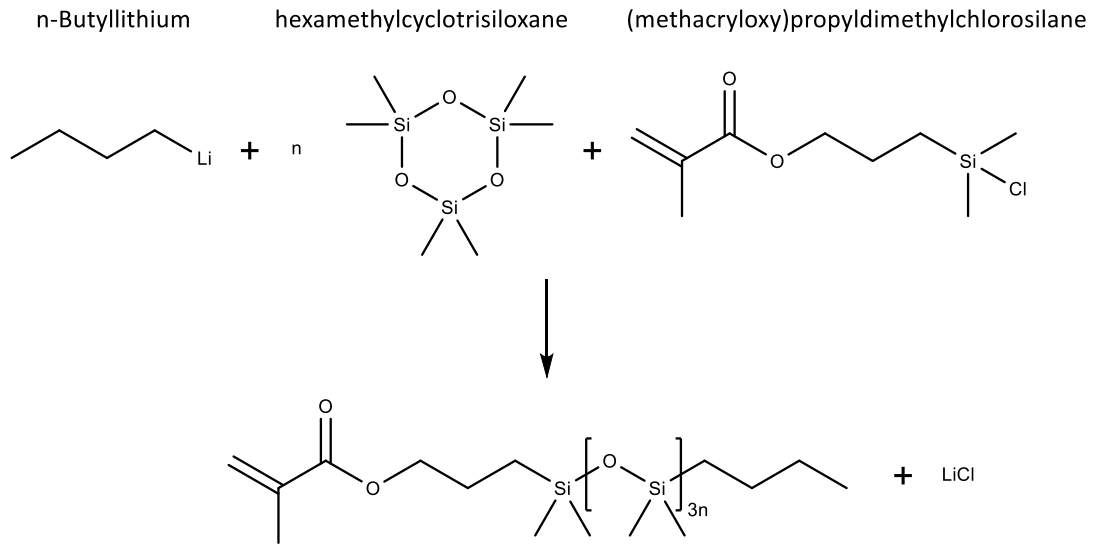
4.4.5 Solubility measurement in fixed volume viewcell

In order to visibly observe the solubility limit/cloud point of PDMS-MA in pure $scCO_2$, a fixed volume viewcell (100 ml)[153-155] was used. The viewcell setup is shown in detail in section 2.2.5. In a typical experiment, 0.5 g of sample was added to a 1 ml glass vial and inserted in the view cell. The windows were sealed and clamped to the body, and CO_2 was added up to 50 bar. The temperature was raised to the desired conditions, then CO_2 was incrementally added until the sample dissolved. At this point pressure was slowly released until a cloud point was observed, signifying the solubility limit of the sample in pure $scCO_2$. The pressure reading accuracy is $\leq$ 0.25 % of the span limit point calibration, with a linearity error of $\leq$ 0.15 % and a repeatability of ± 0.05% of the full scale (345 bar). At 317 bar, the highest pressure used in this work, this results in a pressure reading error of ± 1.51 bar (22 psi).

4.4.6 PDMS-MA synthesis through anionic polymerisation

PDMS-MA of 15 kDa was synthesised by anionic ring-opening polymerisation[49, 156] of hexamethylcyclotrisiloxane (D_3) (Scheme 4.1). Briefly, 10 g of D_3 (equal to a final 33.3% w/v solution) was dissolved in distillation dried THF (30 ml) in an oven dried round-bottom flask under an inert atmosphere of argon. The sealed system was cooled in an insulated 70 vol% water - 30 vol% methanol bath with dry ice to maintain

a temperature of -20 °C. Once the desired reaction temperature of -20 °C was reached, 220 µl of n-butyllithium (2.5 M in hexane, anhydrous) was added to initiate the polymerisation and the mixture was stirred using a magnetic flea for at least 24h. To terminate the polymer chain, 259 mg of 3-(methacryloxy)propyldimethylchlorosilane (2 mol eq. compared to n-butyllithium) was added. Lithium chloride precipitated and was removed by filtration. The polymer was purified by dropwise precipitating in MeOH at -70 °C and dried under vacuum.



Monomethacrylate terminated polydimethylsiloxane (PDMS-MA)

Scheme 4.1 Synthesis of functionally terminated polydimethylsiloxane, conducted in THF under argon atmosphere at -20 °C.

^{1}H NMR spectroscopy was used to confirm the structure of the 15 kDa product, with details shown in the results section of this chapter.

4.4.7 Free radical dispersion polymerisation of styrene

A typical reaction was conducted with styrene (9.09 g, 10 ml), PDMS-MA stabiliser (20 wt% relative to styrene, 1.818 g) and AIBN initiator (2 wt% relative to styrene, 181.8 mg) in a 60 ml high pressure autoclave. Styrene, PDMS-MA and AIBN were

degassed by bubbling with argon in an ice-bath cooled glass vial for 30 minutes, while stirring. During this time, the autoclave was flushed with CO_2 at 2-3 bar, venting through the keyhole. After 30 minutes, the reactants mixture was injected into the autoclave through the keyhole against a positive flow of CO_2. The key was then inserted into the autoclave, sealing it off from the atmosphere. At this point CO_2 was added, pressurising the system to 50 bar. Heat was then applied through the heating jacket, bringing the temperature to 65 °C. CO_2 was then added until the system pressure reached 245 bar. The moment the reaction temperature was reached was chosen as the starting point of the reaction.

4.5 Results and discussion

4.5.1 Agitation effects

Initial conditions used for MMA dispersion polymerisations were based on previous research and standard operating procedures within the group.[35, 46, 49, 55, 157] from repeated reactions it was observed however that product quality was not fully consistent. Although the majority of the formed polymer product was the expected free flowing powder (Figure 4.4), significant clumping was found fused to the base of the autoclave and caking was sometimes observed on the autoclave walls.



Figure 4.4. Free flowing powder removed from autoclave in 3 repeat experiments conducted under standard reaction conditions (10 ml MMA, 5 wt% PDMS-MA, 1 wt% AIBN, 207 bar, 65 °C) after 240 minutes of reaction time.

SEM images of the formed powder showed clear particles with consistent size and morphology (Figure 4.5).

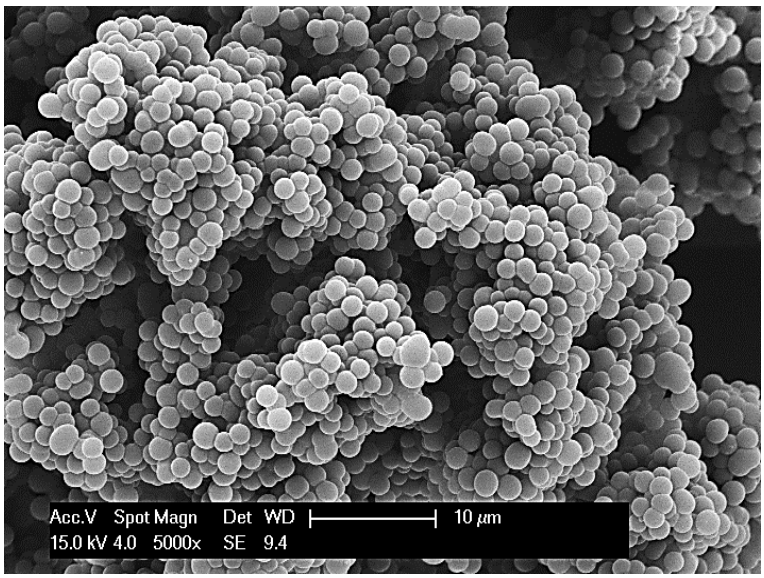


Figure 4.5. SEM image of PMMA powder synthesised from a standard reaction (10 ml MMA, 5 wt% PDMS-MA, 1 wt% AIBN).

In one reaction, a solid bell-shaped clump was found attached to the bottom of the autoclave, positioned centrally, directly under the impeller. The clump was removed and analysed (Figure 4.6).

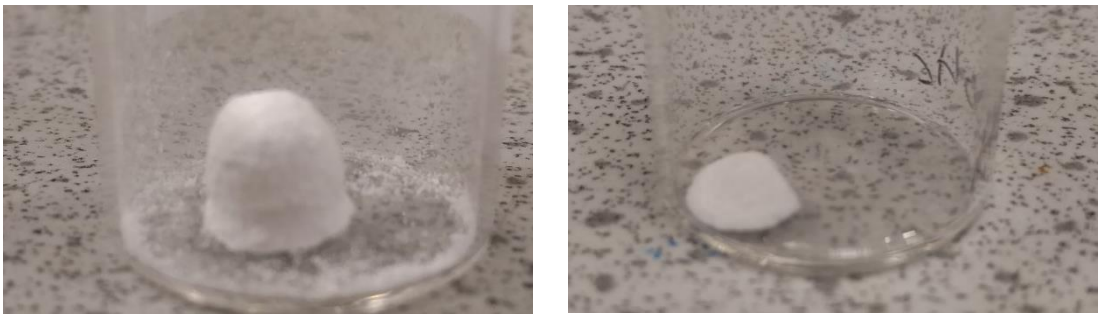


Figure 4.6. Left: bell-shaped clump, Approximately 6 mm in diameter, formed directly under the impeller and stuck to the bottom of the autoclave under standard reaction conditions. Right: Solid disk of approximately 6 mm in diameter, forming the base of the bell-shaped clump shown left.

To confirm this clump formation had resulted in reduced powder quality, SEM images were taken of the clump. Upon breaking the clump down with a spatula for SEM stub mounting, large parts reverted back to a powder. There was however a solid disk that remained, originating from the bottom of the clump (Figure 4.6, right).

SEM imaging showed that the main body of the clump was made up of the desired discrete particle structure, though possibly with slight fusing. The solid disk however, showed extensive particle fusing and was essentially a single monolithic structure (Figure 4.7).

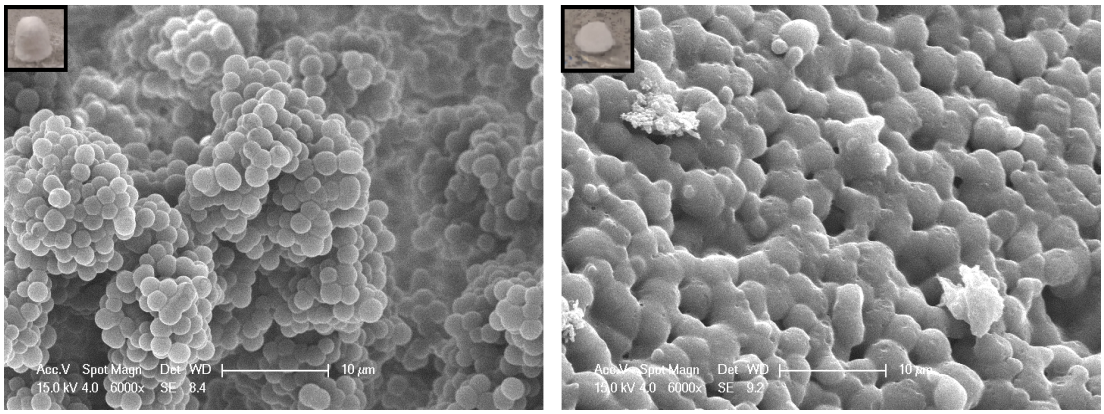


Figure 4.7. SEM images at 6 000x magnification of the clump (left) and disk (right) pictured in Figure 4.6, showing extensive particle fusion.

The observed particle fusion in the formed clump is due to dispersed PMMA particles coagulating. This can occur when there is insufficient PDMS-MA stabiliser to surround the particles, which can be caused by insufficient mixing, causing local concentration variations. Particle coagulation was seen to originate directly beneath the pitched-blade impeller which, based on literature,[139, 140] is the location of minimal agitation within the employed axial flow stirring system, linking the reduced product quality to a flawed stirrer design.

Clump formation during polymerisation was found to be a recurring issue for several autoclave setups within the research group. By comparing the impellers used when clumping occurred frequently to the impellers used when clumping rarely occurred, it was found that the blade angle was the main differentiator (Figure 4.8). The effect of impeller blade angle is in line with expectations, as increasing blade angle increases overall agitation energy and also increases agitation directly below the impeller.[139]



Figure 4.8. Two pitched blade impellers used in the autoclave setup within the group. A clear difference in blade pitch angle can be seen, with the left impeller angled at 35°and the right impeller angled to 15°.

Using a transparent autoclave filled with water and glitter, the stirrers could be compared visually. The impeller with 15° pitch angle was found to not mix the glitter efficiently and formed a visible clump directly under the stirrer (Figure 4.9, left). The impeller with higher blade pitch angle meanwhile, did not show visual accumulation of glitter directly underneath the impeller (Figure 4.9, right).



Figure 4.9. Comparison of stirring efficiency of impellers with 15° (left) and 35° (right) pitch angle, showing that the low blade angle causes accumulation under the impeller.

By increasing the pitch angle of the impeller blades, the contact volume per rotation is increased. This results in an increase in volumetric flow rate, increasing movement along an axial flow pattern. This results in increased agitation under the impeller, reducing the clumping issue. However, it is important not to increase the pitch angle too much, as this can result in a radial flow pattern (Figure 4.3).[139] A radial flow pattern is a double vortex pattern that is unsuited for polymerisation reactor mixing, as phase separation can occur between separate vortices. The critical angle for this

flow pattern transition is dependent on the viscosity of the system and the dimensions of the vessel but is usually within a range of 60-85°.[139, 140]

While testing the impellers in the clear autoclave, it was observed that the blades would intermittently touch the autoclave walls. This will naturally disturb an axial flow pattern, where the mixture is expected to flow past the impeller up or down the autoclave wall. The distance between impeller blades and the autoclave base, was also found to be highly variable, which is also a known factor in maintaining a consistent axial flow pattern.[105, 137, 139, 140] To further alleviate any stirring issues, an idealised single stage impeller was designed and produced, with improved dimension compared to previous impellers (Figure 4.10).



	Typical impeller	Optimised impeller
Shaft length	40-50 mm	60 mm
Blade diameter	30 mm	24 mm
Blade angle	15-40°	45°
Clearance from reactor floor	22.5-32.5 mm	12.5 mm

Figure 4.10 Design parameters of low pitch angle stirrer (left) originally installed in the high-pressure autoclave and the optimized stirrer (right) designed to alleviate stirring issues.

By extending the stirrer shaft, the pitched blades of the optimised stirrer were placed closer to the reactor floor, at a distance less than half the reactor diameter of 32 mm. This increased the agitation around the reactor floor, further reducing the chances of

clumping occurring.[139] The blade diameter of the optimised stirrer was also reduced to avoid blocking the axial flow pattern. The blade diameter was set at 75% of the autoclave diameter, above the 70% required to maintain lamellar flow.[139] Increasing the blade-wall distance is also important to assure the axial flow pattern is maintained as oversized stirrer blades block axial flow patterns from passing the blades into the upper areas of the reactor.

The stirring of the new optimised stirrer design was compared to the original setup, again using a transparent autoclave filled with water and glitter (Figure 4.11). From the images, it is clear that the optimised stirrer affords a more consistent distribution of glitter throughout the autoclave. This is due to the reduced blade diameter, lower floor clearance and higher blade pitch angle, combining to afford more consistent and unblocked axial flow pattern.

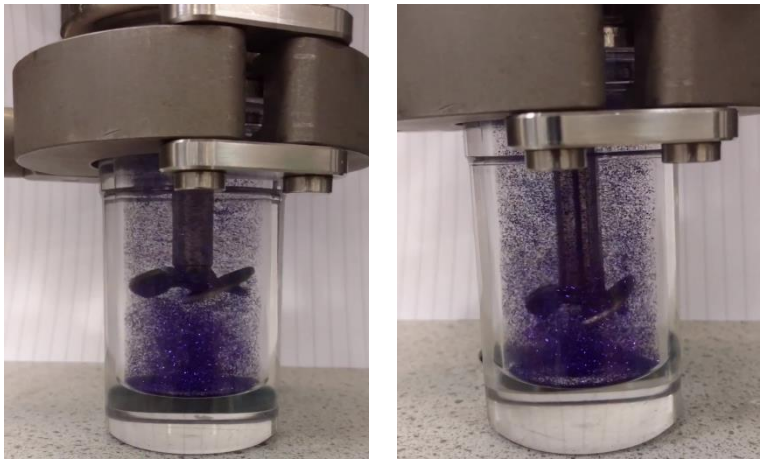


Figure 4.11 Comparison of stirring efficiency of a typical low pitch angle impeller (left) and the optimised impeller (right) at 200 rotations per minute. Improved glitter agitation and distribution and can be seen with the optimised impeller design.

While the improved agitation flow pattern will improve reaction consistency, increased agitation can have adverse effects on dispersion polymerisations, as too much movement can hinder steric stabilisation around dispersed nuclei. A standard

MMA dispersion polymerisation was performed using the optimised impeller design, to confirm that the increased agitation does not adversely affect dispersion stability. Results were then compared to previous standard reactions with the low pitch angle stirrer (Table 4.1), while SEM images confirmed the formation of discrete particles (Figure 4.12).

Table 4.1 results for MMA dispersion polymerisation reactions conducted under standard reaction conditions. Entry 1: low pitch angle impeller, Entry 2: optimised impeller.

Entry	Reaction time (min)	Conversion (%)[a]	Yield (%)	M_n (kDa)[b]	M_w (kDa)[b]	Đ[b]
1	180	93.2	82.8	167	407	2.43
2	180	92.1	82.3	151	386	2.56

a – determined via ^{1}H NMR (section 2.3.2), b – determined via GPC (section 2.3.1)

The reaction with optimised impeller design (Table 4.1, Entry 2) yielded a free-flowing powder with conversion and molecular weights in line with a previously successful standard reaction (Table 4.1, Entry 1), without any clumping or material deposited on the autoclave base. Particle size analysis was carried out on both powder samples, showing near identical average particle diameter and PSD (Figure 4.12).

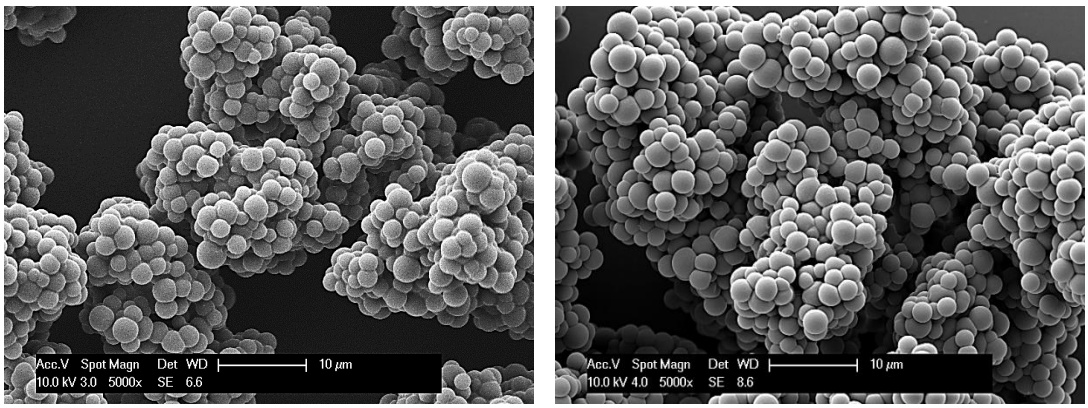


Figure 4.12 SEM images of powder obtained for polymerisations detailed in Table 4.1. Left: Entry 1 (typical impeller) - average particle diameter 2578 nm and PSD = 1.07 Right: Entry 2 (optimised impeller) - average particle diameter 2613 nm and PSD = 1.05.

With the dispersion polymerisation of MMA confirmed to proceed consistently and effectively with the optimised impeller design, the effects of varying stirring rate were explored.

From literature, it is clear that stirring rate can have a great effect on dispersion polymerisations, with insufficient stirring causing coagulation and excessive stirring causing stabiliser to detach from stabilised particles.[47, 52] By altering the stirring rate, agitation energy input during a reaction can be tuned. Standard reactions were conducted at 300 RPM previously, but the limits and effect of agitation were yet to be analysed with the optimised impeller.

To confirm the stirring rate limits of the reaction, and to explore any effects on product properties, standard reactions were conducted at various stirring speeds (Table 4.2).

Table 4.2 Results for polymerisation reactions conducted at standard conditions, varying in stirring speed.

Entry	Stirring speed (RPM)	Reaction time (min)	Conversion (%)[a]	Yield (%)	M_n (kDa)[b]	M_w (kDa)[b]	Đ[b]
1	150	240	97.0	72.5	107	281	2.62
2	300	240	95.9	85.9	168	407	2.42
3	600	240	98.2	91.7	158	383	2.43

a – determined via ^{1}H NMR (section 2.3.2), b – determined via GPC (section 2.3.1)

From the conducted experiments, it was seen that increasing stirring rate had no significant effect on the observed conversion, powder yield or polymer properties. Decreasing the stirring rate to 150 RPM however, induced a clear decrease in molecular weight averages and yield. The reason for this was a significant PMMA precipitation layer formed on the autoclave base, resulting in material being lost and effecting the ongoing polymerisation. Comparing the pressure progression of the

polymerisations (Figure 4.13), a pressure spike was observed when stirring at 150 RPM due to the formation of a precipitation layer where CO_2 is repulsed. When insufficient agitation is created within the system, dispersed particles will coagulate and expel the stabiliser, at which point they can precipitate out of the mixture. The dispersed phase of the polymerisation will then be smaller, resulting in polymerisation occurring more in the continuous phase, ultimately lowering the achieved molecular weight (Table 4.2).

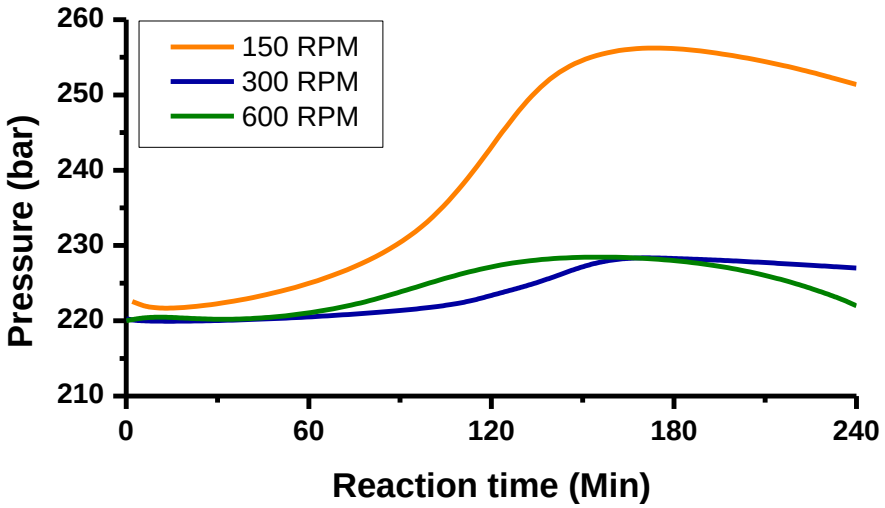


Figure 4.13 Pressure progression of reactions detailed in Table 4.2, varying in stirring rate. Reduced stirring rate induces a sharp pressure spike at the point of highest conversion rate, associated with the precipitation of insufficiently stabilised polymer.

SEM images of the obtained powders (Figure 4.14) again show that increasing the stirring rate to 600 RPM had no influence on the product formed. A reduced stirring speed of 150 RPM however, resulted a decrease in average particles size as material is lost to a precipitation phase.

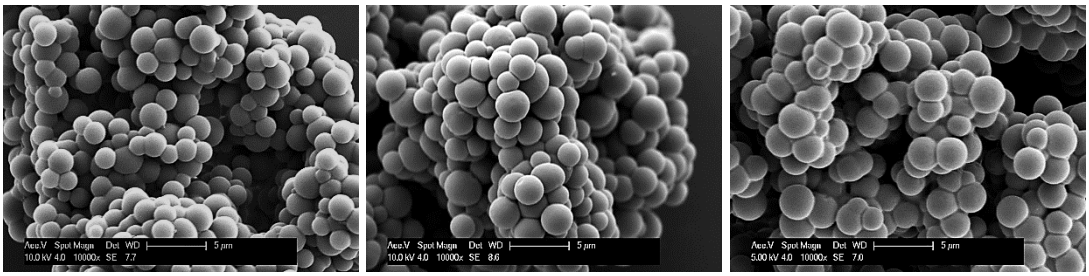


Figure 4.14 SEM images of powder product formed from standard reactions at varying stirring speeds. Left: 150 RPM (average diameter is 2062 nm, PSD=1.07), centre: 300 RPM (average diameter is 2613 nm, PSD=1.05), right: 600 RPM (average diameter is 2582 nm, PSD=1.05).

From the conducted experiments it is clear that the reaction is not sensitive to changes in stirring speed, but a minimum stirring speed is required to assure a consistent dispersion throughout. A maximum stirring speed, above which the dispersion fails due to excessive shear forces, was not found.

4.5.2 Loading Limits of dispersion polymerisation of MMA

For the commercial application of any polymerisation system, it is important to maximise production capacity. All previous dispersion polymerisations of MMA were conducted with 10 ml of monomer in what was assumed to be a 60 ml vessel. The autoclave is produced to have an internal volume of 60 ml, but the effect of the impeller and autoclave head void are unknown. Before increasing the loading, the exact volume of the autoclave setup was determined.

The volume of the used autoclave setup was determined by adding water to the setup until the volume was filled. The autoclave impeller was attached to the autoclave head, the head and base were sealed with an O-ring and the clamp, the key was inserted, and the outlet tap was attached and closed tightly. The inlet pipe was left unattached as it was used as an overflow. The HPLC pump was filled with water that

was subsequently pumped into the autoclave via the HPLC inlet until water was pushed out of the inlet pipe (Figure 4.15). The internal volume of the HPLC and inlet pipework was determined from Swagelok specification sheets of the tubing (Table 4.3).

Table 4.3 Swagelok tubing dimensions and volume filled with water during autoclave volume measurement.

External diameter (in.)[a]	Wall thickness (in.)[a]	Internal diameter (in.)	Internal radius (cm)	Internal volume (ml/m)	Length in setup (m)	Volume filled (ml)
1/16	0.02	0.0225	0.028575	0.26	0.08	0.021
1/8	0.028	0.069	0.08763	2.41	0.20	0.482

a – information from Swagelok specifications sheet

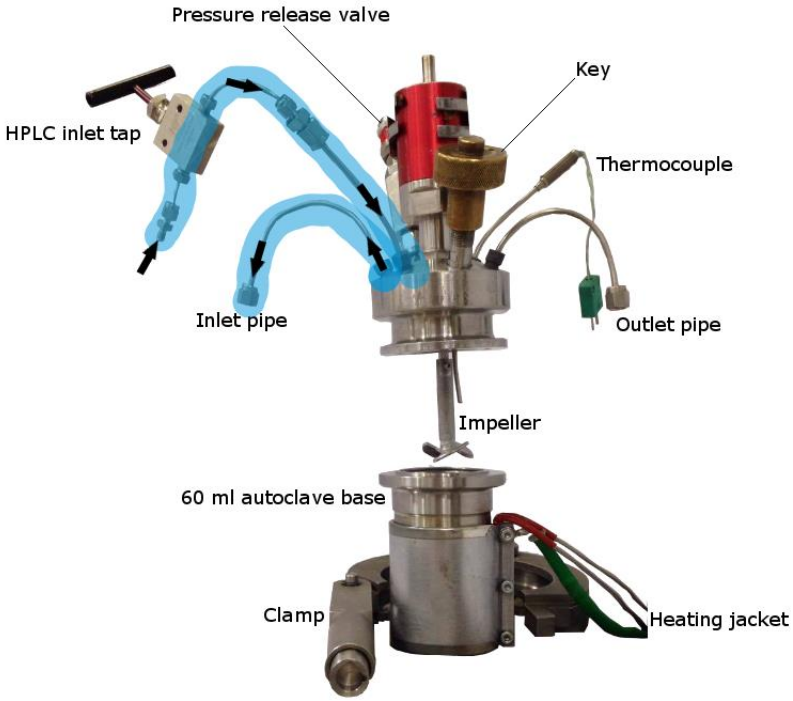


Figure 4.15 60 ml autoclave setup, with the used path for water addition during autoclave volume determination highlighted in blue.

66.75 ml of water was added via the HPLC pump before water flowed out of the inlet pipe. Subtracting 0.5 ml to compensate for the volume of the excess pipework, the actual internal volume of the autoclave was found to be 66.25 ml. This process was repeated 3 times, giving the same volume of 66.25 ml each time. This means that

monomer loading during the standard MMA dispersion polymerisation was not 16.67 % (10 ml/60 ml), but 15.09 % (10 ml/66.25 ml).

There are two loading limits relevant to this system, namely the single dose limit and the ultimate loading limit. The single dose limit is the amount of monomer that can be added initially, without causing heat dissipation issues. As was observed during stirring rate tests of the optimised impeller, this value will be dependent on agitation factors. The ultimate loading limit is more intrinsic to the polymer system and needs to be determined separate from temporary effects like heat production.

4.5.2.1 Single stage loading limit

Previous work showed that the dispersion polymerisation of MMA with a stirring speed of 300 RPM was reliable with a monomer loading of 10 ml. this was used as a reference point for increasing monomer loading and stirring speed sequentially, to find the single stage loading limit.

A series of polymerisations were conducted under identical conditions, only varying in monomer loading (and stabiliser and initiator loading, as they are relative to monomer loading) and stirring speed as needed (Table 4.4).

Table 4.4 Results for polymerisation reactions conducted at standard conditions, varying in stirring speed.

Entry	Stirring speed (RPM)	Monomer loading (ml)	Conversion (%)[a]	Yield (%)	M_n (kDa)[b]	M_w (kDa)[b]	Đ[b]
1	300	10	95.9	85.9	168	407	2.4
2	300	12.5	96.0	88.2	133	335	2.5
3	300	12.5	96.8	89.2	109	321	2.9
4	450	12.5	97.7	94.4	148	387	2.6
5	450	15	98.1	87.2	122	318	2.6
6	600	15	97.7	85.6	145	378	2.6
7	600	17.5	92.0	81.0	127	319	2.5
8	600	17.5	96.4	89.6	79	262	3.3

a – determined via ^{1}H NMR (section 2.3.2), b – determined via GPC (section 2.3.1)

Table 4.4 Entry 2 and 3 were conducted with a monomer loading of 12.5 ml, while maintaining a stirring rate of 300 RPM. A slight precipitation/coagulation was observed in the autoclave after polymerisation, confirmed by the lower molecular weight achieved in comparison to the polymerisation with a 10 ml monomer loading. This diminished product quality was also accompanied by a larger change in pressure during polymerisation (Figure 4.16).

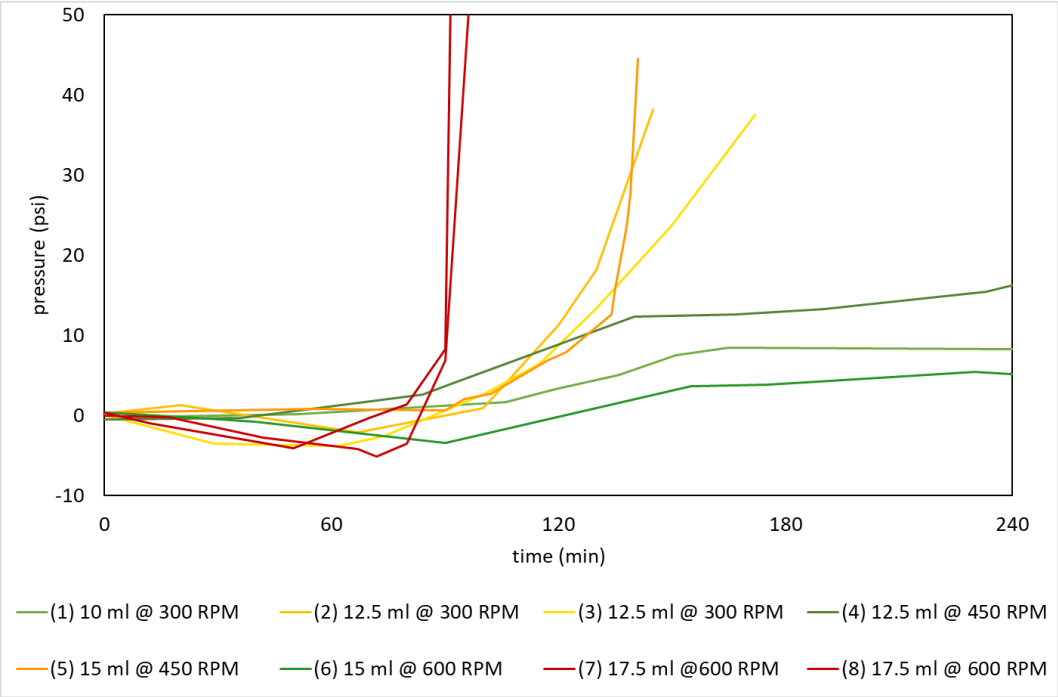


Figure 4.16 Pressure change as a function of reaction time for the MMA dispersion polymerisations detailed in Table 4.4 (Entry numbers in graph legend), showing that pressure change during polymerisation indicated reaction outcome. (green) produced good product, (yellow) some precipitation was observed, (red) monolithic, fused product was formed.

Increasing the stirring rate to 450 RPM with a 12.5 ml loading (Table 4.4, Entry 4) afforded a consistent product and pressure progression during the polymerisation, in line with the reference reaction (Table 4.4, Entry 1). From this it was clear that the one stage loading limit at 300 RPM for this reaction is below 12.5 ml, while elevating the stirring rate has increased this limit.

Increasing the loading to 15 ml with a stirring rate of 450 RPM (Table 4.4, Entry 5) resulted in a sharper pressure increase, accompanied with lower molecular weight polymer and a slight precipitation in the autoclave base. The one stage loading limit at 450 RPM was found to be between 12.5 ml and 15 ml.

Elevating the stirring rate to 600 RPM with a monomer loading of 15 ml (Table 4.4, Entry 6) allowed for a smooth and consistent reaction profile, again highlighting the effect of agitation on heat dissipation and dispersion stability. However, when increasing the loading further to 17.5 ml (Table 4.4, Entry 7 and 8), an intense pressure spike was observed after 90 minutes of reaction time. The reaction was terminated immediately as the pressure build-up was fast approaching the safety limit of the setup. After cooling the reactor and releasing the CO_2, a solid lump was found fused to the impeller shaft and autoclave base (Figure 4.17).

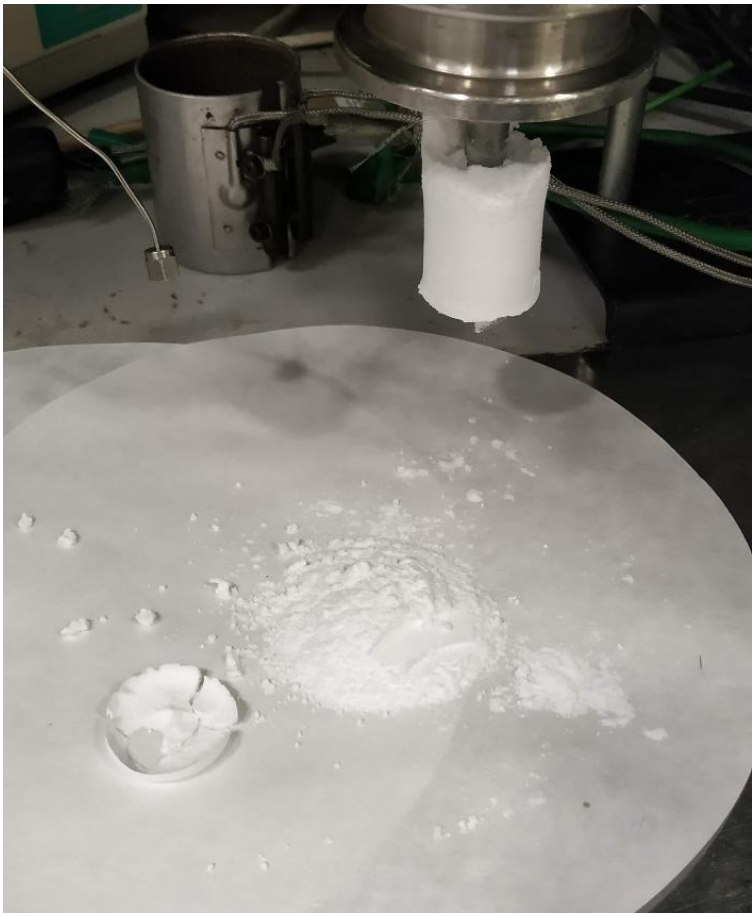


Figure 4.17 Polymer product formed with a monomer loading of 17.5 ml and stirring rate of 600 RPM (Table 4.4, Entry 7), showing a large solid block attached to the impeller and a powder-like material chopped out of the autoclave base.

The single stage loading limit at 600 RPM was found to be lower than 17.5 ml, but the pressure increase implied an ultimate volume limit may have been reached. This was then tested in subsequent experiments.

4.5.2.2 Ultimate loading limit

Based on the one stage limits researched previously, a loading of 15 ml was known to be attainable while 17.5 ml resulted in reaction failure. A two-stage reaction method was employed to find the ultimate loading limit (Figure 4.18). First, a monomer loading of 12.5 ml was polymerised, before adding an additional 5 ml of monomer after the initial monomer was consumed, all at a stirring rate of 600 RPM. Through this method, the polymerisation rate was kept sufficiently low throughout that any failure would be due to the ultimate loading limit of the PMMA dispersion.

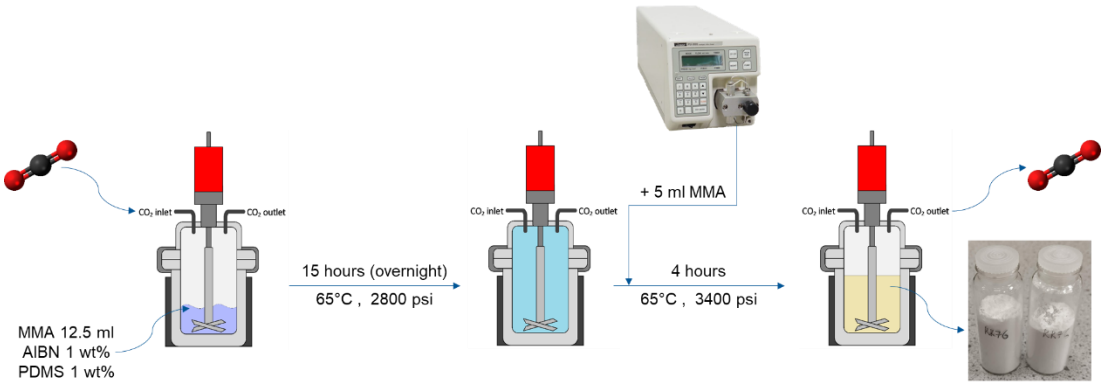


Figure 4.18 Two-stage reaction outline, with stage one containing 12.5 ml of MMA and stage two adding 5 ml of monomer to the autoclave.

Despite employing a two-stage method, the polymerisation pressure spiked intensely, shortly after injecting 5 ml of MMA for the second polymerisation step.

The monomer loading of the first stage was reduced to 12 ml (for a total loading of 17 ml), and the polymerisation procedure was repeated (Figure 4.18). At a total loading of 17 ml, the reaction produced a free-flowing polymer powder without any

precipitation or adverse pressure fluctuations during the polymerisation. GPC confirmed the molecular weight was in line with expectations, and SEM showed the expected particles were formed. With the autoclave volume being 66.25 ml, the ultimate monomer loading limit of the MMA dispersion polymerisation was found to be 25.7±0.4 vol%, with the uncertainty arising from the accuracy of the syringe used to add the first monomer loading (±0.25 ml). Including the PDMS-MA stabiliser (density = 0.97 g/ml) and AIBN (density = 1.1 g/ml), the ultimate reactant loading was 27.1±0.4 vol%. In traditional solvents such as dodecane or ethanol, the attainable solid content for an equivalent dispersion polymerisation is 40 vol% or even higher.[106, 145] While the ultimate loading limit in $scCO_2$ is lower, the definition of a clear working window is essential for safe and reliable polymer production.

4.5.3 Influence of pressure on the dispersion polymerisation of MMA

During previously conducted dispersion polymerisation monitoring experiments (Chapter 3), It was observed that particle size varied depending on reactor pressure. This was investigated further and linked to the utilised stabiliser. The solubility of the PDMS-MA stabiliser was investigated prior to an in-depth study of the effect of various parameters on the dispersion polymerisation of MMA.

4.5.3.1 Solubility of commercial PDMS-MA (10 kDa) at 65 °C

The solubility of PDMS-MA (10 kDa) was determined using a fixed volume viewcell at 65 °C. This is the standard temperature for MMA polymerisations in $scCO_2$ found

widely in literature using AIBN as the initiator.[98, 103, 132] From the viewcell study, the cloud point was determined to be 248 bar (3600 psi) (Figure 4.19). This is in agreement with previous literature findings for the same compound,[39, 43, 98, 158] confirming the reliability of this method. The viewcell study was conducted in triplicate with varying amounts of PDMS-MA (0.5-2.5 g), with the cloud point again being found at 248 bar (3600 psi). within the stabiliser loading range used within this study, no change of cloud point was observed, and the solubility pressure of PDMS-MA is therefore assumed constant.



140 bar **255 bar** **248 bar**

Figure 4.19 Images of PDMS-MA (10 000 g/mol) in $scCO_2$ at 65 °C. (left) undissolved sample highlighted in the vial, (centre) sample is fully dissolved and the system is transparent, (right) the sample has crashed out of solution and the system becomes turbid at the cloud point of PDMS-MA.

To determine the effect of PDMS-MA solubility on the polymerisation of MMA in $scCO_2$, a series of polymerisations were conducted at pressures around the cloud/solubility point of 248 bar.

4.5.3.2 MMA dispersion polymerisation with commercial PDMS-MA (10 kDa)

4.5.3.2.1 Effect of pressure on particle size

Changing the pressure at which the polymerisation is conducted, will alter the solubility of all components present in the system.[43] The effect of this on the product quality was studied by conducting successive standard polymerisation reactions at varying initial reactor pressure (Table 4.5, Table 4.6). To ensure polymerisation did not occur prior to reaching the desired pressure, all reactions were initiated via HPLC addition of the initiator, as described above.

Table 4.5 Particle sizing results for polymerisation reactions conducted at standard conditions after 180 minutes of reaction time, varying in initial reactor pressure.

Entry	Initial pressure (bar)	$d_n \pm \sigma$ (nm)[a]	PSD[a]
1	145	-	-
2	172	1683 ± 238	1.057
3	193	2183 ± 315	1.062
4	220	2614 ± 340	1.051
5	248	3292 ± 312	1.022
6	275	2837 ± 122	1.005
7	317	2943 ± 133	1.006

a – determined via SEM particle sizing

Table 4.6 Results for polymerisation reactions conducted at standard conditions after 180 minutes of reaction time, varying in initial reactor pressure.

Entry	Initial pressure (bar)	Conversion (%)[a]	Yield (%)	M_n (kDa)[b]	M_w (kDa)[b]	Đ[b]
1	145	22.7	57	24	110	4.5
2	172	92.4	86	150	392	2.6
3	193	94.7	87	166	398	2.4
4	220	92.1	82	151	386	2.5
5	248	93.5	85	154	366	2.4
6	275	90.7	73	135	306	2.3
7	317	89.9	76	144	315	2.2

a – determined via ^{1}H NMR (section 2.3.2), b – determined via GPC (section 2.3.1)

At 145 bar (Table 4.5, Entry 1), the polymerisation reaction did not proceed via a stable dispersion. Based on previous literature studies on the solubility of PDMS-MA in a CO_2-MMA mixture[43, 99, 159] this was an expected result. At 145 bar, the PDMS-MA stabiliser is insoluble in the MMA-CO_2 solvent[43, 99, 159], resulting in a kinetically slower precipitation polymerisation system. Despite MMA working as a cosolvent for the PDMS-MA stabiliser, at 145 bar the stabiliser remains undissolved and incapable of stabilising the targeted dispersion. The formed and analysed product was a viscous liquid with precipitated polymer covering the reactor base. Due to low conversion, volatile monomer was lost, and yield was significantly lower.

Reactions conducted at pressures from 172 bar to 248 bar (Table 4.5, Entry 2-5) showed consistent high conversion and yield, with molecular weight averages broadly unchanged (Table 4.6). The product formed during these reactions was a consistent, free-flowing powder that was easy to remove after opening the autoclave. Reactions performed above 248 bar (Table 4.5, Entry 6-7) however, showed a decline in powder quality. Although a large portion of the product was an easy to handle, free-flowing powder, a significant deposit was formed on the reactor

wall and floor (Figure 4.20). This naturally resulted in a decreased yield of particle powder, as irremovable precipitated product remained in the reactor.



Figure 4.20 Deposit left in reactor base after standard polymerisation reaction at 275 bar (Table 4.5, Entry 6) due to a loss of dispersion stability, resulting in a 5-10% drop in yield.

While PDMS-MA is only soluble above 248 bar in pure $scCO_2$, for reactions conducted at initial pressures between 172-248 bar (Table 4.5, Entry 2-5), the stabiliser is soluble due to the presence of MMA as a cosolvent capable of associating with the methacrylate end group of PDMS-MA.[43, 98, 99] This inherent association between monomer/polymer and stabiliser, assures an efficient stabilisation of the dispersion system. At initial pressures above 248 bar, PDMS-MA is fully soluble in $scCO_2$ without the need for MMA association. This results in a reduced stabilising affinity, as PDMS-MA is less inclined to accumulate around growing particles and can remain free in the solvent. When the stabiliser is not effective in sustaining all the polymer particles in the continuous phase, the polymer chains will precipitate when reaching a threshold molecular weight, and this will result in the observed precipitated layer of polymer covering the autoclave walls.

SEM imaging of the formed powder products was performed (Figure 4.21) and particle size was measured (Table 4.5). Graphically, a clear trend in particle size linked to the solubility of the PDMS-MA stabiliser was observed (Figure 4.22).

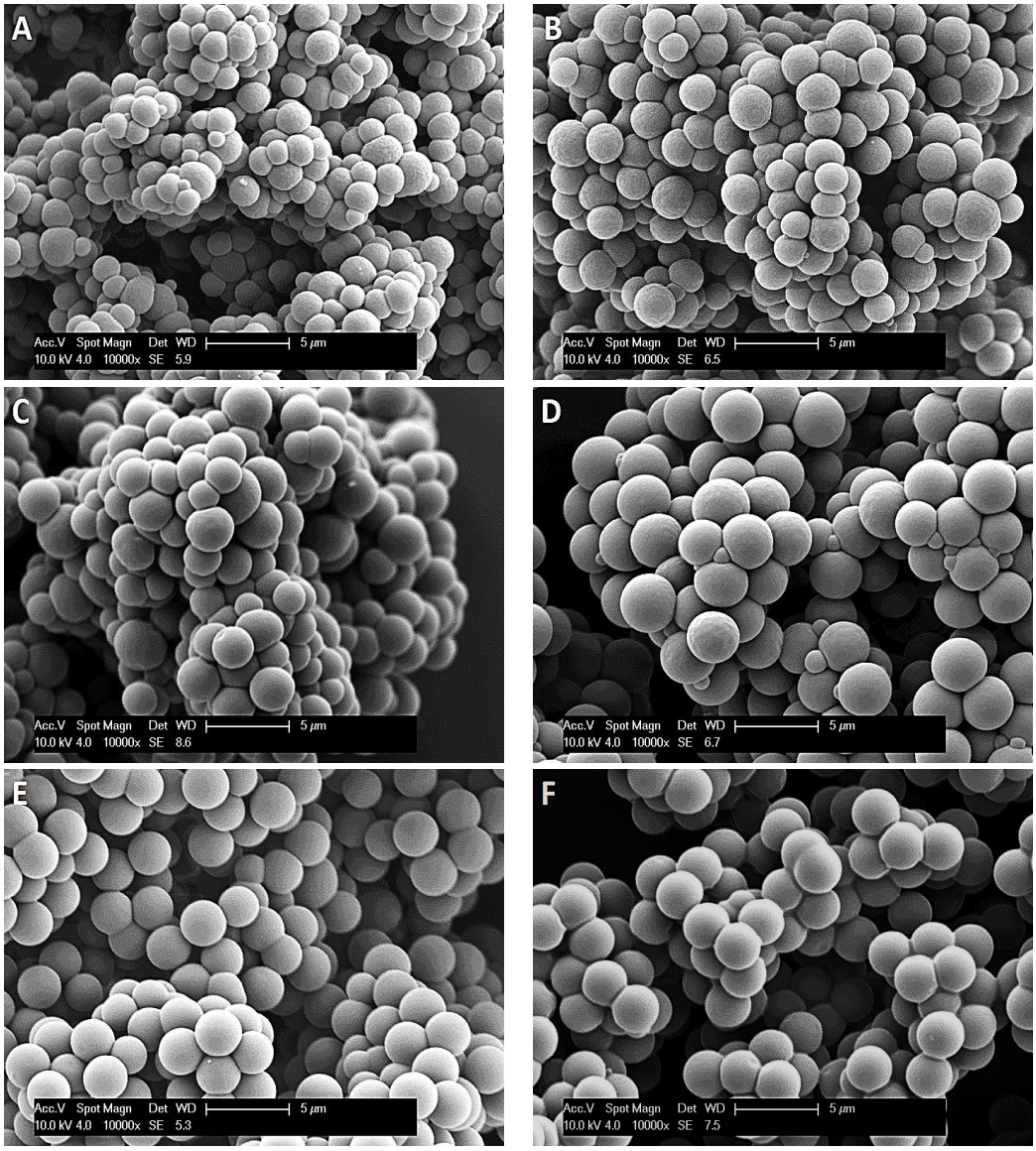


Figure 4.21 SEM images of powder formed under varying initial reactor pressure. A) 172 bar (Table 4.5, Entry 2), B) 193 bar (Table 4.5, Entry 3), C) 220 bar (Table 4.5, Entry 4), D) 248 bar (Table 4.5, Entry 5), E) 275 bar (Table 4.5, Entry 6), F) 317 bar (Table 4.5, Entry 7).

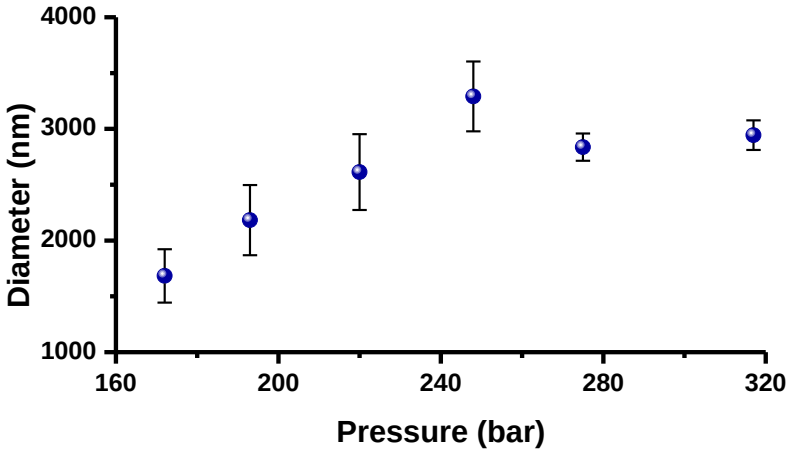


Figure 4.22 average particle diameter (d_n) in function of initial autoclave pressure, for the reactions detailed in Table 4.5. Error bars represent the standard deviation (σ). A linear increase in d_n with increasing pressure can be seen within the successful working range of the reaction (172-248 bar).

For reactions conducted with 10 ml of MMA at initial pressures of 172-248 bar (Table 4.5, Entry 2-5), a linear increase in average particle diameter was observed. As initial pressure was increased, the solubility of PDMS-MA during the reaction altered. The association of PDMS-MA around a nucleated particle became less favourable at higher pressure, kinetically slowing the stabilisation process. As nuclei had more time to agglomerate prior to stabilisation, fewer, but larger, particles were formed. While larger particles were achieved with increasing pressure, this ultimately led to reduced polymer quality when further increasing pressure beyond the cloud point of the stabiliser in pure $scCO_2$, as the association of PDMS-MA around the particles was insufficient to maintain a fully stable dispersion for all nuclei. Partial incorporation of the PDMS-MA stabiliser as a copolymer into the PMMA particle was not observed. Based on previous work,[49] it is known that the stabiliser is mainly attached physically to the particles, and it can be removed by washing, regardless of pressure and component loading.

To assure that this observation was not linked to changing the concentration of reactants and solvent due to the density increase of $scCO_2$, the polymerisations were repeated with a constant mole fraction.

4.5.3.2.2 Pressure dilution effect

The density of CO_2 as a function of pressure was determined using NIST data[119] (Figure 4.23). From this, the mole fraction of MMA in a standard reaction at 220 bar was determined to be 8.65 mol%. Using the CO_2 density data, the amount of MMA required to reach 8.65 mol% was calculated, and MMA polymerisations were conducted as previously with a fixed mol% of reactants (Table 4.7).

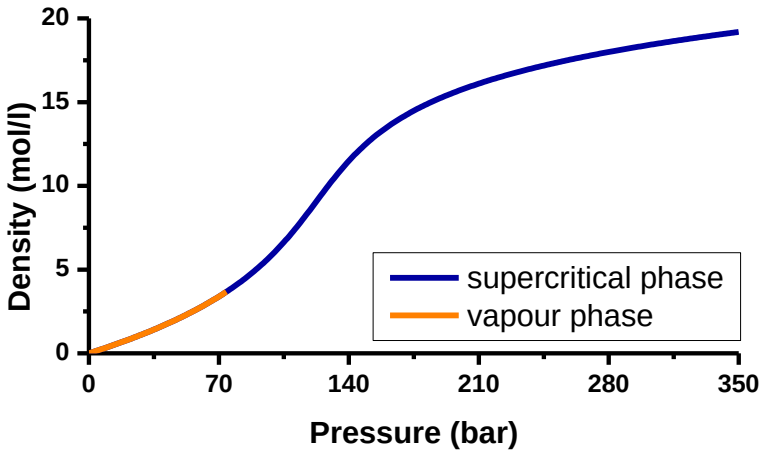


Figure 4.23 CO_2 density in function of pressure at 65 °C. produced using data from NIST.[119]

Table 4.7 Results of polymerisation reactions (5 wt% PDMS-MA, 1 wt% AIBN) conducted at constant mol%, varying in initial pressure.

Entry	Initial pressure (bar)	MMA (ml)	Conversion (%)[a]	Yield (%)	d_n (nm)[b]	σ (nm)[b]	PSD [b]
1	172	8.70	78.9	58	-	-	-
2	193	9.35	84.9	73	2015	346	1.081
3	220	10.00	92.1	82	2614	340	1.051
4	248	10.50	94.7	86	3186	171	1.008
5	275	10.85	93.4	80	2953	197	1.010

a – determined via ^1H NMR (section 2.3.2), b – determined via SEM particle sizing (section 2.3.3)

At 172 bar (Table 4.7, Entry 1), using only 8.7 ml of MMA due to the lower density of CO_2, the reaction yielded an inconsistent, sticky and chunky powder. Due to the reduced amount of MMA used in the reaction, PDMS-MA was insufficiently soluble to afford a consistent dispersion during the reaction. A mix of particles and non-descript material was observed within the product under SEM (Figure 4.24).

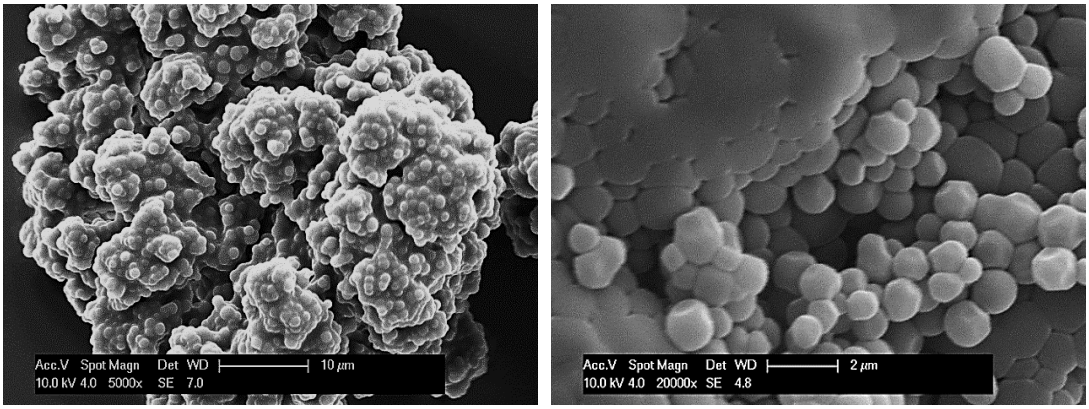


Figure 4.24 SEM images of obtained powder product at reaction pressure of 172 bar, with 8.7 ml of MMA (Table 4.7, Entry 1).

The reaction performed at 275 bar (Table 4.7, Entry 5) again formed a deposit within the autoclave, as observed previously (Figure 4.20), due to the precipitation of insufficiently stabilised PMMA.

The reactions performed at 193-248 bar (Table 4.7, Entry 2-4) produced a consistent free-flowing powder that was analysed via SEM (Figure 4.25). The particle size trend again showed a clear increase in average diameter with increasing initial pressure (Figure 4.26).

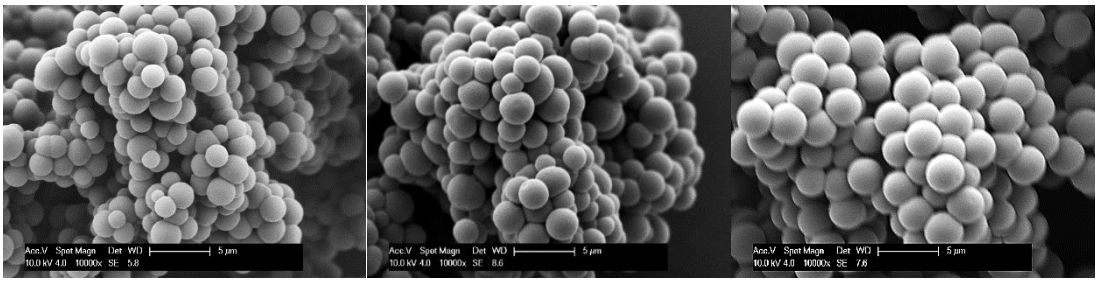


Figure 4.25 SEM images of powder formed during constant mole fraction experiments at varying pressure. Left: 193 bar (Table 4.7, Entry 2), centre: 220 (Table 4.7, Entry 3), right: 248 bar (Table 4.7, Entry 4).

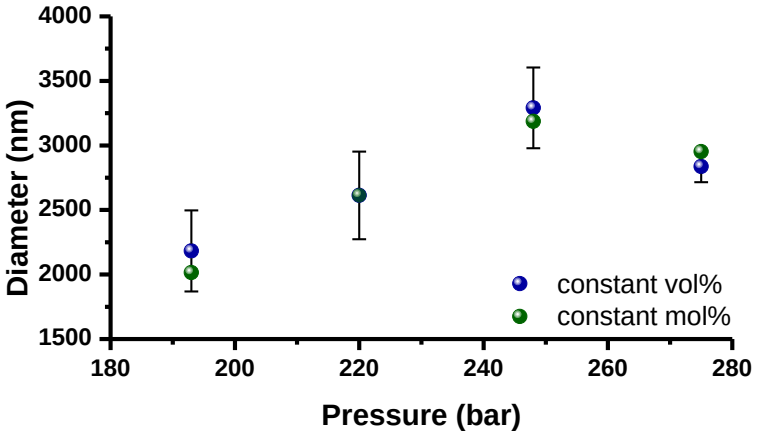


Figure 4.26 Average particle diameter (d_n) as a function of initial autoclave pressure, for the reactions detailed in Table 4.7 compared to reactions conducted with constant monomer volume. The change in component volumes, to achieve constant mol% in comparison to CO_2, has no discernible effect on particle size control.

From the obtained particle size data, it is clear that dilution from added CO_2 at increasing pressure had no measurable effect on particle size and component solubility within the pressure range of the polymerisation.

4.5.3.2.3 Influence of temperature on solubility and efficacy of the stabiliser

To confirm that the particle size effect is directly linked to the solubility of the stabiliser in $scCO_2$, the polymerisations were repeated at a lower temperature using V-70 as the initiator. By changing the operating temperature from 65 °C to 40 °C, the

density of CO_2 as a function of pressure changes significantly, as does the solubility of PDMS-MA. The density of the CO_2 solvent as a function of pressure at 40 °C and 65 °C were compared, showing the higher density at lower temperature (Figure 4.27). The solubility of PMDS-MA (10 kDa) at 40 °C was determined using the fixed volume viewcell and compared to results at 65 °C (Figure 4.28).

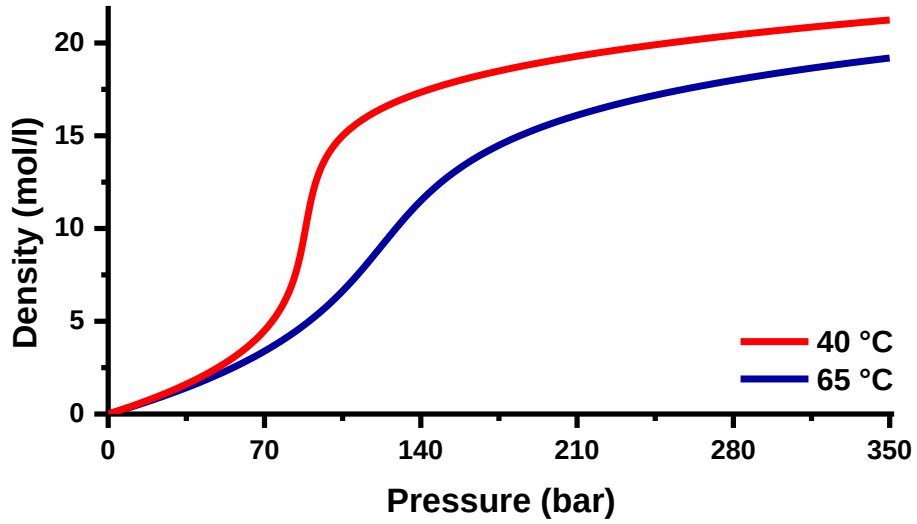


Figure 4.27 CO_2 density as a function of pressure at 40 °C and 65 °C showing the increased density at lower temperature. Produced using data from NIST.[119]

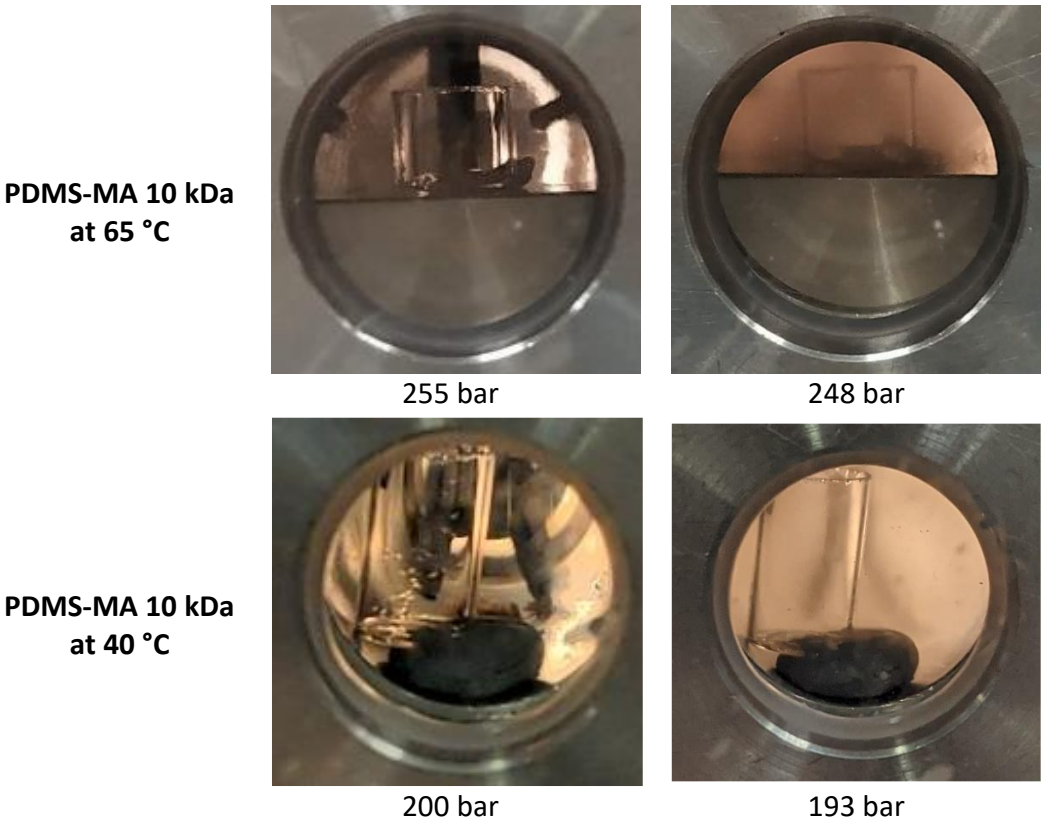


Figure 4.28 Images of PDMS-MA (10 000 g/mol) in $scCO_2$ at 65 °C (top) and 40 °C (bottom). The cloud point was found at 248 bar and 193 bar respectively. The left images show a clear homogeneous mixture, while the right-hand images show a clouded mixture due to PDMS-MA becoming insoluble.

The cloud point at 40 °C was found to be 193 bar, which corresponds to a CO_2 density of 18.93 mol/l,[119] compared to 248 bar and 17.26 mol/l[119] at 65 °C. To confirm that the solubility of PDMS-MA is the determining factor in the observed particle size trend, a series of MMA polymerisations were conducted around the cloud point of 193 bar at 40 °C (Table 4.8). The particle size data is compared graphically to the trend observed at 65 °C (Figure 4.29).

Table 4.8 Particle sizing results for polymerisation reactions conducted at 40 °C, varying in initial reactor pressure.

Entry	Initial pressure (bar)	Conversion (%)[a]	Yield (%)	$d_n \pm \sigma$ (nm)[b]	PSD [b]
1	138	98.8	91	1877 ± 380	1.11
2	165	98.3	90	2425 ± 375	1.06
3	193	97.6	91	3051 ± 323	1.03
4	220	95.1	82	2695 ± 156	1.01

a – determined via ^{1}H NMR (section 2.3.2), b – determined via SEM particle sizing (section 2.3.3)

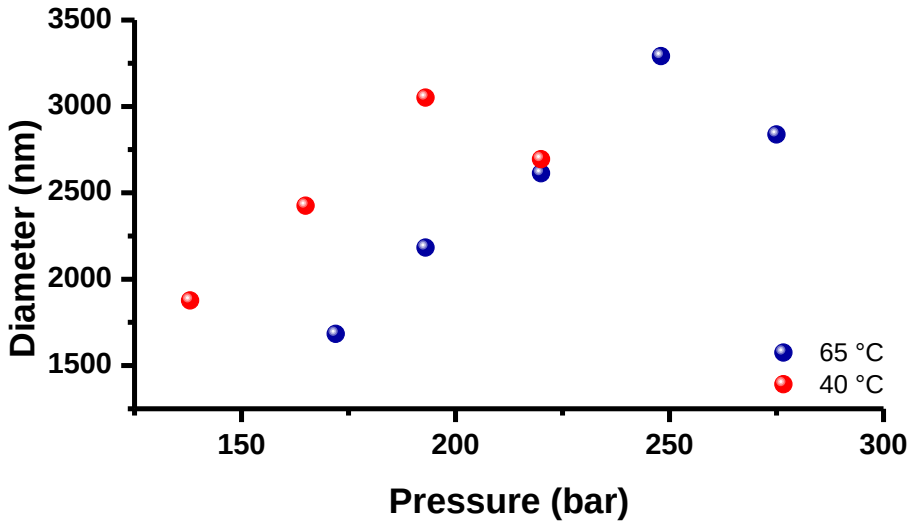


Figure 4.29 Average particle diameter (d_n) in function of initial autoclave pressure, for the MMA dispersion polymerisations conducted at 40 °C (red) (Table 4.8) and 65 °C (blue) (Table 4.5). A linear increase in particle size, with a maximum at the cloud point of the stabiliser, can be seen at both reaction temperatures.

At 40 °C, we again observe an increasing particle size trend up to the cloud point of PDMS-MA at reaction conditions. Meanwhile, polymerisations above the cloud point show partial precipitation of PMMA. This results in a lower product yield due to the diminished stabilising affinity of the PDMS-MA, reinforcing the trend observed at 65 °C. While the solvent density at 40 °C is higher than at 65 °C, it appears to have no noticeable effect on the polymerisation system. The determining factor for particle size and product consistency seems to be the solubility of the PDMS-MA stabiliser,

it's partitioning towards PMMA, and the linked affinity to surround the insoluble particles.

4.5.3.3 Influence of stabiliser chain length

(The synthesis of PDMS-MA was conducted in collaboration with Mathieu Souhil, a summer student visiting the Howdle group)

PDMS-MA of 15 kDa chain length was synthesised following the procedure detailed in section 4.4.6. ^{1}H NMR was used to confirm the structure and determine the chain length of the molecule (Figure 4.30). The hydrogen singlet at 0.1 ppm originating from CH_3 groups on the siloxane chain was compared to the hydrogen singlet at 6.1 ppm originating from the methacrylate double bond in the end group, to determine an approximate chain length of 183 units. While this was slightly lower than the targeted 190 units, the main goal was to synthesise a stabiliser with a lower solubility in CO_2, and thus a different stabilisation window in comparison to the commercial 10 kDa PDMS-MA.

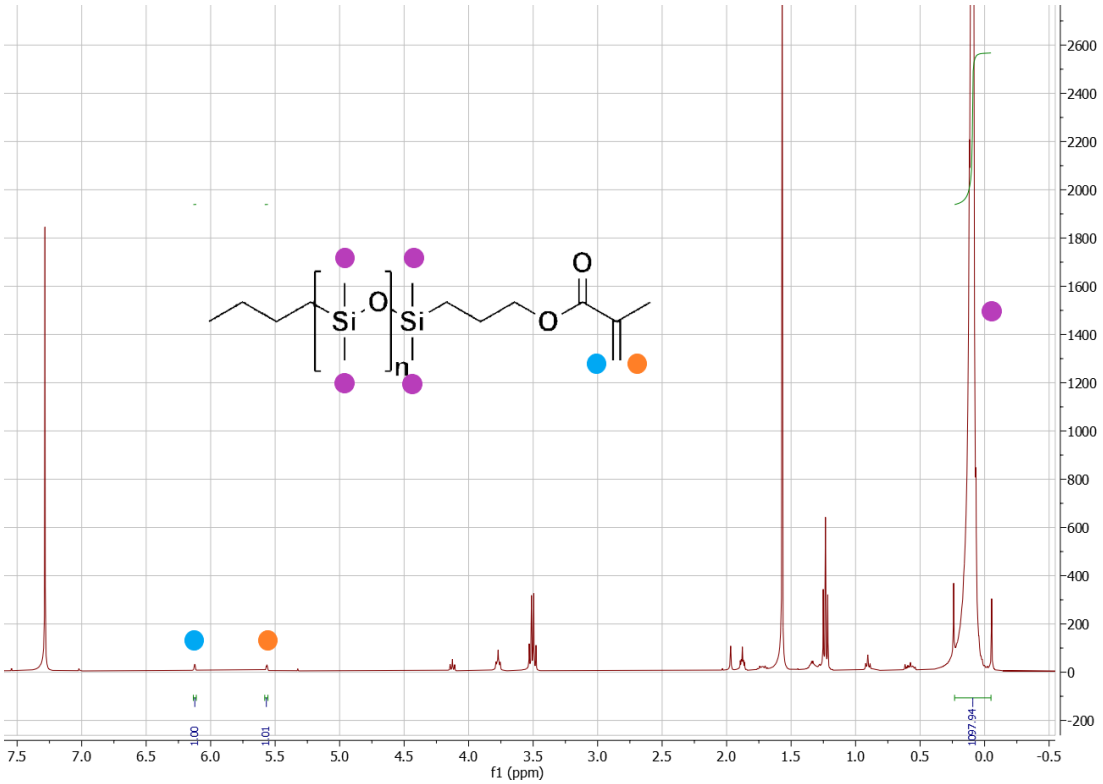


Figure 4.30 Annotated ^{1}H NMR of PDMS-MA (15 kDa) showing the chain to be approximately 183 (target: 190) units long, calculated by dividing the purple labelled peak volume by 6 when the blue peak volume is set to 1. Orange: hydrogen singlet of methacrylate double bond in end group, Blue: hydrogen singlet of methacrylate double bond in end group, purple: hydrogen singlet from CH_3 groups on siloxane chain δ: (ppm in $CDCl_3$) 6.10 (s, 1H) and 5.54 (s, 1H) [$=CH_2$], 4.10 (t, 2H) [$Si–CH_2–CH_2–CH_2–O$], 1.94 (s, 3H) [$–C(=CH_2)–CH_3$], 1.70 (m, 2H) [$Si–CH_2–CH_2–CH_2–O$], 1.25 (m, 6H) [$CH_3–(CH_2)_3–Si$], 0.88 (t, 2H) [$Si–CH_2–CH_2–CH_2–O$], 0.57 (m, 3H) [$CH_3–CH_2$], 0.13 (s) [$O–Si(CH_3)_2–CH_2$] and 0.07 (s, 1140H) [$O–Si(CH_3)_2–O$].

From the viewcell solubility experiment (Figure 4.31), it was found that 15 kDa PDMS-MA solubilises at 269 bar at 65 °C. This was sufficiently higher than the commercial PDMS-MA (10 kDa), to allow for an altered particle size trend.

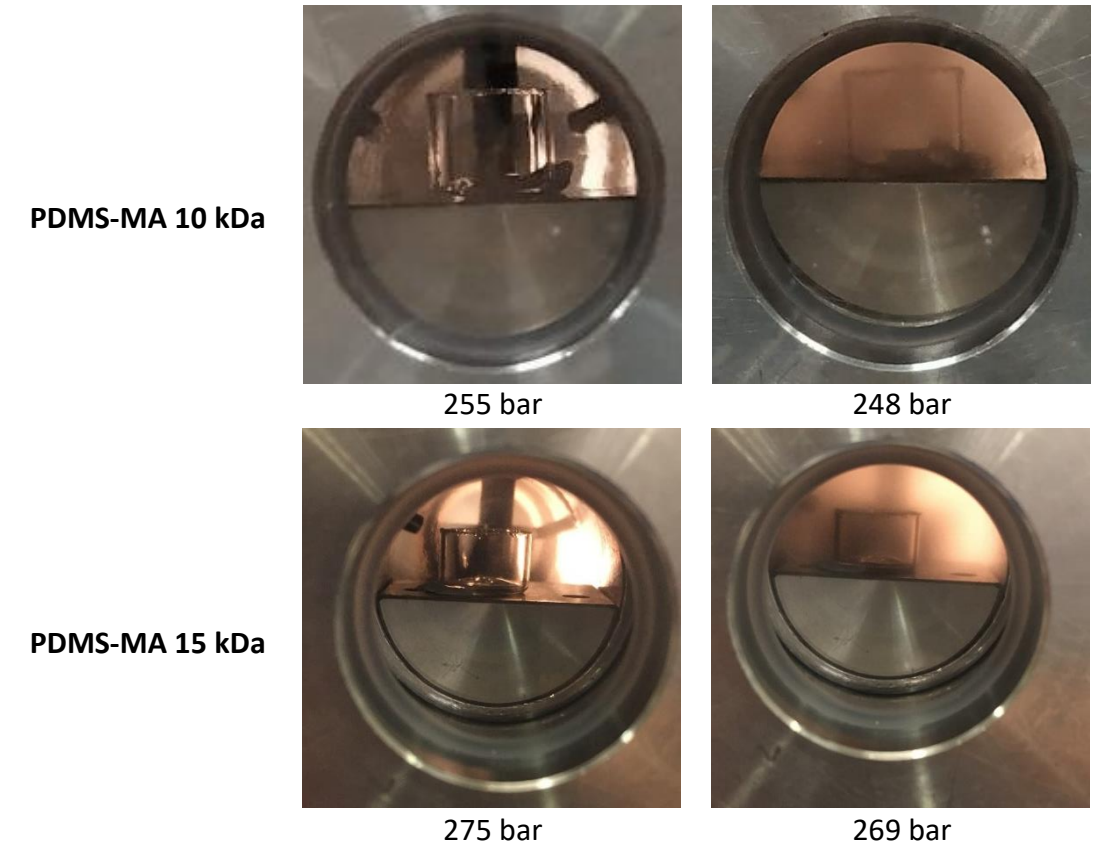


Figure 4.31 Images of PDMS-MA in $scCO_2$ at 65 °C, comparing the solubility limit of 10 kg/mol (top) and 15 kg/mol (bottom), found to be 248 bar and 269 bar respectively. The left images show a clear homogeneous mixture, while the right-hand images show a clouded mixture due to PDMS-MA becoming insoluble.

A series of MMA polymerisations were then performed around the solubility point of 269 bar, and the particle size trend was analysed. Experimental results (Table 4.9) and the particle size trend were compared (Figure 4.32) to the trend observed with the commercial 10 kDa PDMS-MA.

Table 4.9 Particle sizing results for polymerisation reactions conducted at 65 °C with PDMS-MA (15 kDa), varying in initial reactor pressure.

Entry	Initial pressure (bar)	Conversion (%)[a]	Yield (%)	$d_n \pm \sigma$ (nm)[b]	PSD [b]
1	186	96.0	89	1681 ± 307	1.03
2	207	97.1	87	2153 ± 281	1.05
3	227	97.0	79	2434 ± 775	1.23
4	248	95.8	93	2693 ± 207	1.02
5	269	97.0	91	3259 ± 231	1.01
6	289	97.4	79	2944 ± 133	1.01

a – determined via ^{1}H NMR (section 2.3.2), b – determined via SEM particle sizing (section 2.3.3)

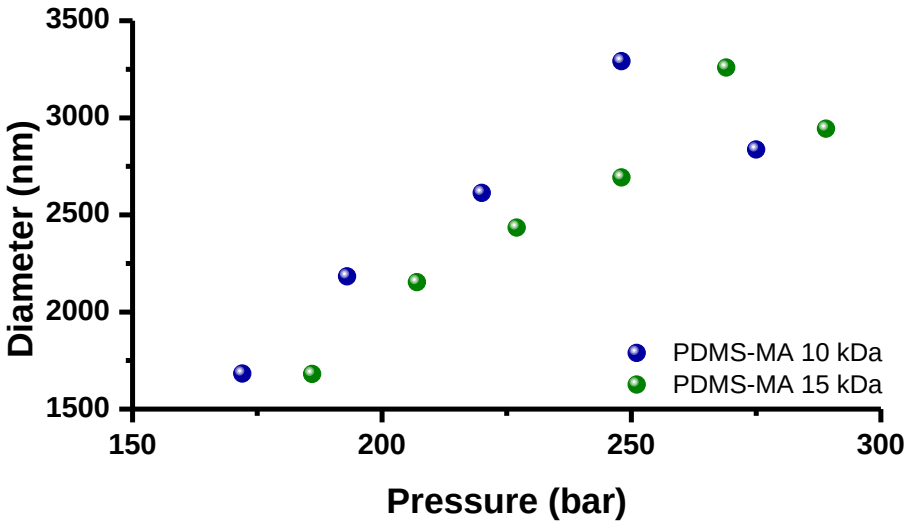


Figure 4.32 Average particle diameter (d_n) in function of initial autoclave pressure, for the MMA dispersion polymerisations with 15 kDa PDMS-MA (green)(Table 4.9) and 10 kDa PDMS-MA (blue)(Table 4.5). A linear increase in particle size, with a maximum at the cloud point of the stabiliser, can be seen for both PDMS-MA chain lengths.

The particle size trend again shows a clear link with the solubility of the stabiliser, with the highest particle size achieved at the solubility pressure of the stabiliser. Reactions above the solubility pressure result in partial precipitation and loss of material, while reactions at lower pressure give progressively smaller particles.

4.5.3.4 Expanding the attainable particle size range

Previous research by McAllister *et al.*[35] produced PMMA particles of 0.32-3.81 µm in diameter, all conducted at a pressure of 207 bar. The smallest particles were produced by using an initial loading of 5 ml MMA and 20 wt% PDMS-MA, followed by a later injection of 2.5 ml of MMA. The largest particles were produced by reducing the amount of PDMS-MA stabiliser used in the reaction to 1 wt% with respect to monomer loading and using 10 ml of MMA.

By utilising the pressure-particle size relationship defined above, the particle size range achieved by McAllister *et al*. using PDMS-MA stabiliser was expanded upon. By lowering the starting pressure to produce smaller particles or increasing the pressure to form larger particles, a significantly larger particle size range was achieved.

The smallest particles were produced by using an initial loading of 5 ml MMA and 20 wt% PDMS-MA at a pressure of 190 bar. The largest particles on the other hand, were produced by reducing the amount of stabiliser used in the reaction to 1 wt% relative to monomer loading and using 10 ml of MMA at an elevated pressure of 248 bar. Both reactions produced a consistent free flowing powder, which was analysed for particle size via SEM. Obtained images (Figure 4.33) show the vast range of particle size that can be covered using identical reactants. The experiments successfully expanded significantly upon the previously obtained particle sizes using identical reactants (Table 4.10).[35]

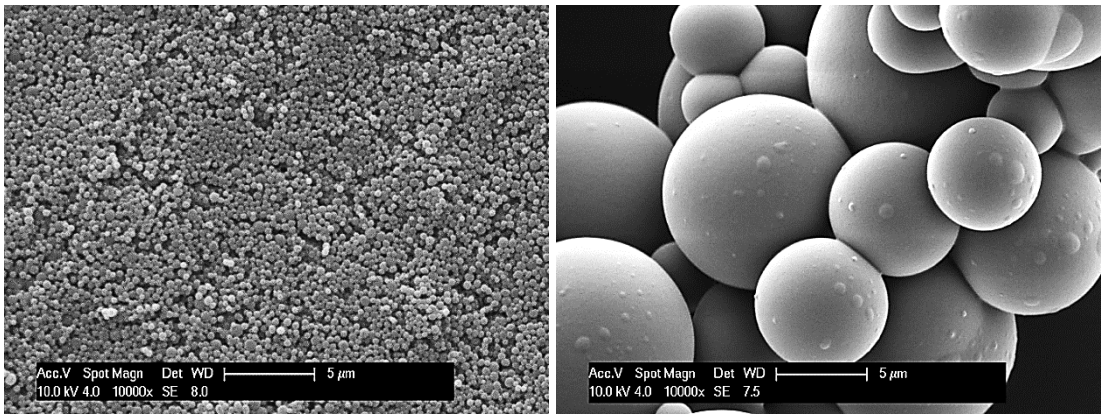


Figure 4.33 SEM image of smallest particles produced at 190 bar and the largest particles produced at 248 bar, expanding on previously reached particle size extremes using PDMS-MA in $scCO_2$.

Table 4.10 Particle size data of smallest and largest particles shown in Figure 4.33 (Entry 1-2), compared to previous extremes produced by Tom McAllister et al. (Entry 3-4).

Entry	Source	Initial pressure (bar)	Yield (%)	d_n (nm)[a]	PSD[a]
1	This work	190	83	265	1.05
2	This work	248	73	7144	1.52
3	McAllister *et al.*[35]	207	89	317	1.10
4	McAllister *et al.*[35]	207	75	3807	1.25

a – Determined via SEM particle sizing

By altering the initial reactor pressure, the attainable average PMMA particle size range in $scCO_2$ using PDMS-MA was significantly expanded from 0.32-3.81 µm to 0.26-7.14 µm.

4.5.4 Dispersion polymerisation of styrene with PDMS-MA stabiliser

Reaction conditions for the dispersion polymerisation of styrene with PDMS-MA stabiliser were chosen based on literature and previous findings from the optimisation of the dispersion polymerisation of MMA. From literature it is known that styrene polymerises significantly slower than MMA,[126, 127, 133, 145] thus requiring

higher temperatures or increased initiator loading. As higher temperatures would involve a change in solvent density and stabiliser solubility, it was chosen to maintain a working temperature of 65 °C and increase initiator loading to 2wt% with regards to monomer loading. Initial reactions were conducted at 248 bar, the solubility/cloud point of the PDMS-MA stabiliser, to assure optimal stabilisation conditions. Stabiliser loading was held at 20 wt% with regards to monomer throughout, the highest loading used previously.

Polymerisation rate was monitored through the sampling cylinder method developed in Chapter 3 (Figure 4.35). Conversion was calculated from NMR using Equation 4.1, with peak assignments shown in Figure 4.34.

$$x_{styrene} = \frac{I_{blue(7.50-6.25)} - 6 * I_{orange(5.65-5.85)}}{I_{blue(7.50-6.25)} - I_{orange(5.65-5.85)}}$$

Equation 4.1

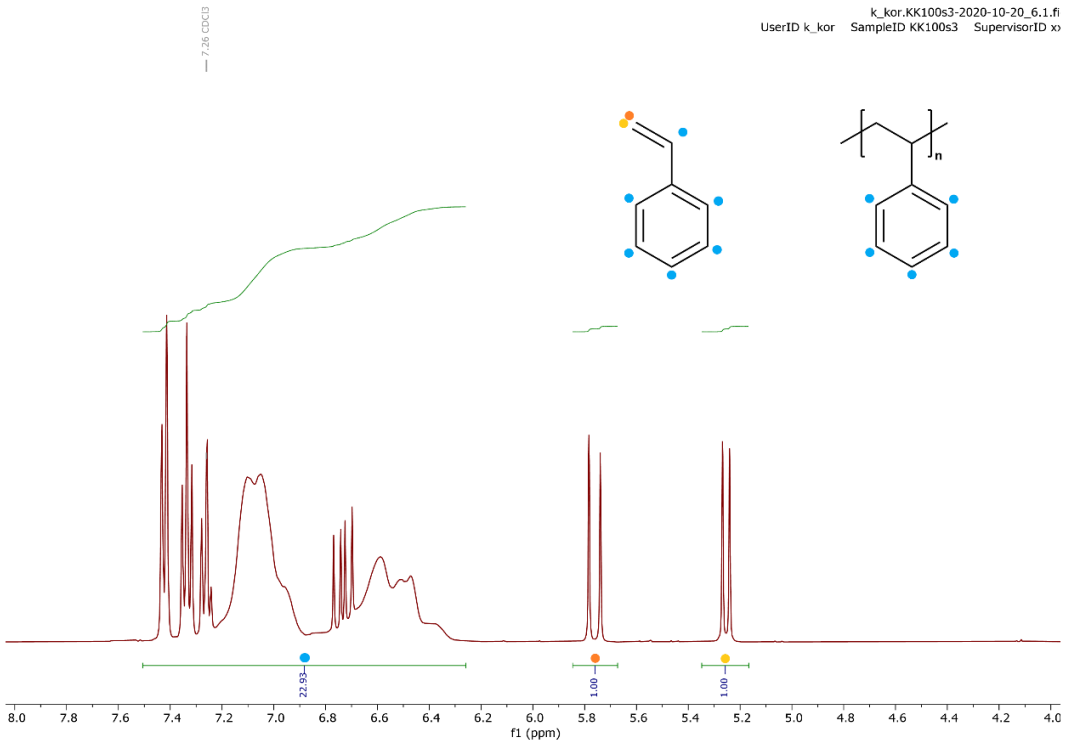


Figure 4.34 Annotated ^{1}H NMR of styrene and polystyrene mixture obtained after 19 hours (1440 minutes) of reaction time. Reaction conditions: 10 ml of styrene, 1.818 g (20 wt% wrt monomer) of PDMS-MA, 181.8 mg (2 wt% wrt monomer) of AIBN, 248 bar and 65 °C.

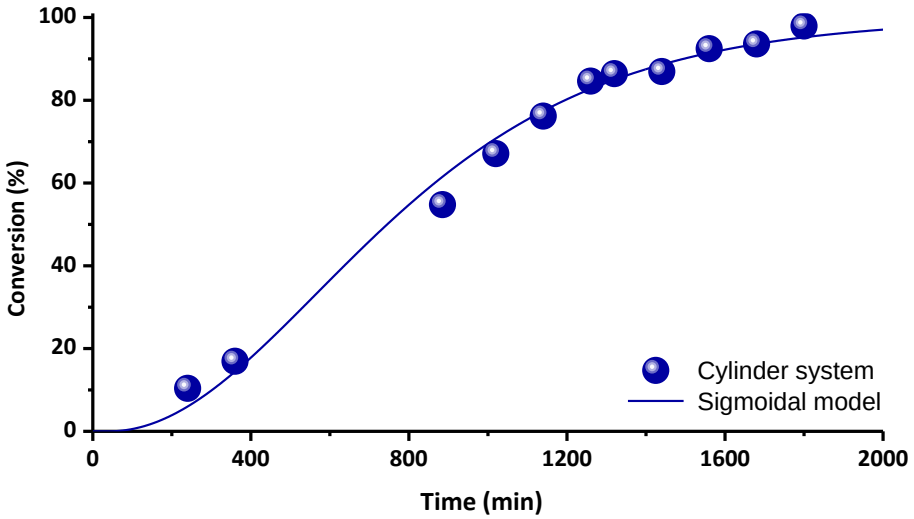


Figure 4.35 Conversion of styrene as a function of reaction time from samples obtained using the cylinder system overlaying a sigmoidal model fitting line. Reaction conditions: 10 ml of styrene, 1.818 g (20 wt% wrt monomer) of PDMS-MA, 181.8 mg (2 wt% wrt monomer) of AIBN, 248 bar and 65 °C. Model fitting variables: $\boldsymbol{t_0 = 1800\ s}$, $\boldsymbol{k' = 2.4 \cdot 10^{-4}\ M^{-1}s^{-1}}$.

The polymerisation was found to proceed successfully, though at a significantly slower rate compared to the dispersion polymerisation of MMA. Through SEM imaging (Figure 4.36), it was found that particles of 335±64 nm were formed. Unlike previously formed PMMA particles, the formed PS particles readily suspended in heptane to allow for DLS analysis. This more robust particle sizing method was employed to confirm an average particle size of 356 nm, in line with SEM analysis results.

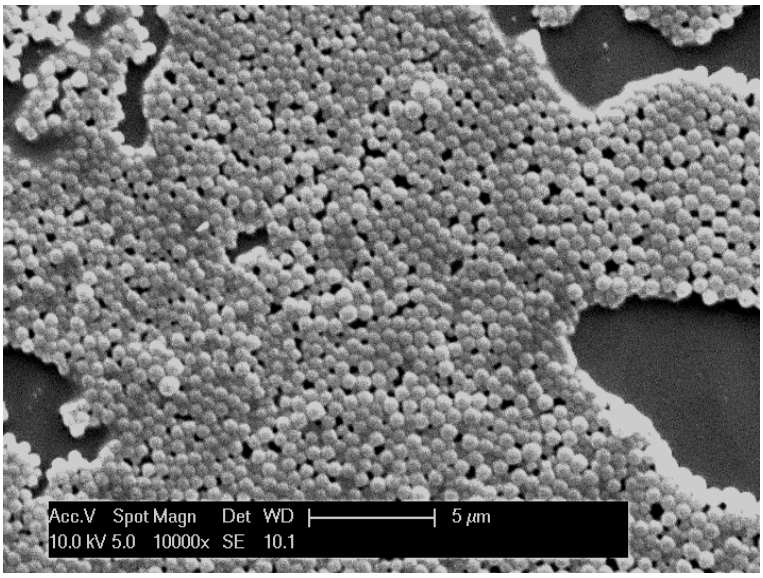


Figure 4.36 SEM image of PS particles of formed through dispersion polymerisation of styrene. Reaction conditions: 10 ml of styrene, 1.818 g (20 wt% wrt monomer) of PDMS-MA, 181.8 mg (2 wt% wrt monomer) of AIBN, 248 bar and 65 °C. Particle size was measured using Fiji(ImageJ) and found to be 335±64 nm.

GPC showed a M_n of 31 kDa and a M_w of 65 kDa. This is in line with kinetic observations, as the reaction is proceeding more significantly in the solvent phase, resulting in shorter chains being formed. While molecular weight is low, DSC nevertheless confirmed a glass transition around 97 °C (Figure 4.37), in line with expectations for PS. Due to this low molecular weight however, a further increase in

initiator loading was not considered, as further chain length reduction could lead to a reduction in glass transition temperature.

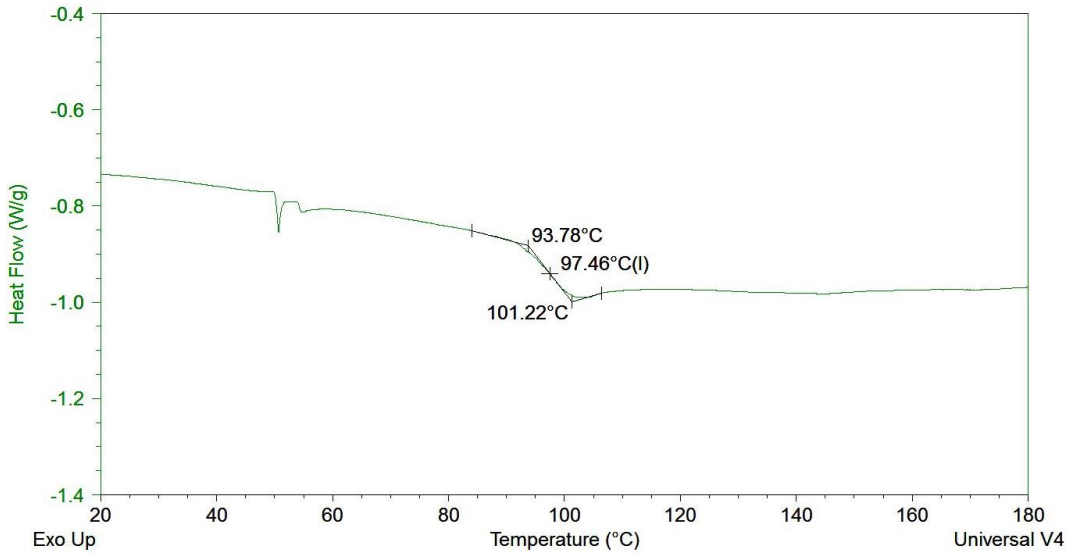


Figure 4.37 DSC trace of PS particles shown in Figure 4.36, showing a glass transition around 97 °C.

4.5.4.1 Cosolvent effect on polymerisation kinetics

From literature, the addition of an antisolvent for the polymer has been shown to potentially improve polymerisation rate by pushing the reaction locus towards the dispersed particle phase.[133] This effect has yet to be observed in $scCO_2$, but the slow polymerisation rate of styrene would be an ideal candidate to investigate. Methanol was chosen as a solvent, due to its good miscibility with $scCO_2$ and its antisolvent properties towards PS.[5, 9, 29, 149]

Two polymerisations were conducted using methanol as a cosolvent, with 10 vol% and 20 vol% methanol with respect to overall autoclave volume, and conversion was monitored using the sampling cylinder method. 1 ml of THF was added along with 4 ml $CDCl_3$ in the cylinder, as it was found that THF was needed to avoid precipitation of the polymer during ^1H NMR.

It was concluded that 10 vol% and 20 vol% methanol had no beneficial impact on the polymerisation kinetics (Figure 4.38).

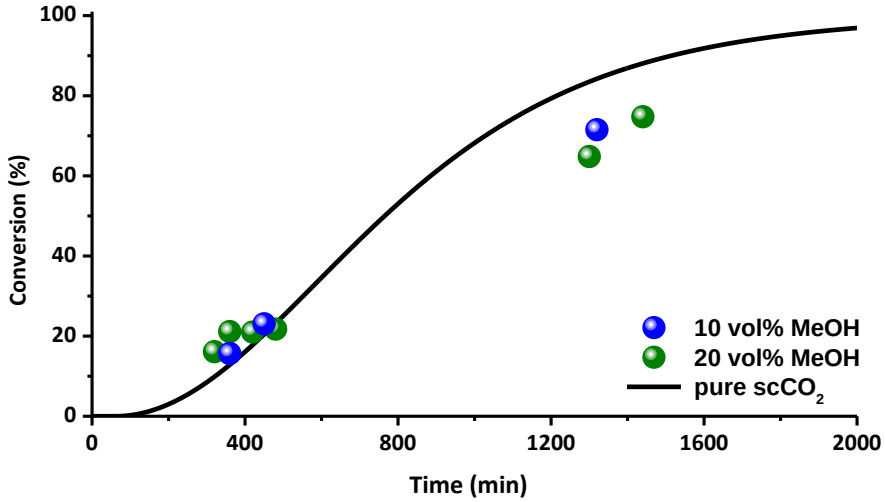


Figure 4.38 Conversion of styrene as a function of reaction time from samples obtained using the cylinder system for the polymerisations using 10% and 20% methanol as a cosolvent, overlayed with a sigmoidal model fitting line of conversion without cosolvent. Model fitting variables: $t_0 = 1800\ s$, $k' = 2.4 \cdot 10^{-4}\ M^{-1}s^{-1}$.

Despite the solubility of styrene and PS in methanol, the polymerisation kinetics were not improved by using a cosolvent. Unlike in conventional solvents, the use of an anti-solvent did not drive the polymerisation locus into the dispersed particle phase. Indeed, a lower conversion was achieved after 30 hours of reaction time with both 10 and 20 vol% of methanol present.

4.5.4.2 Effect of pressure on particle size control

The pressure-particle size relation discovered for the dispersion polymerisation of MMA, was found to be related to the solubility of the PDMS-MA and the fact that MMA functions as a cosolvent for the stabiliser. This resulted in smaller particles being formed at lower pressures, where the stabiliser would associate more closely with the monomer and polymer. Previous dispersion polymerisations of PS were

conducted at 248 bar, so a series of polymerisations were conducted at lower pressures to investigate the possible particle size effect.

It was however quickly found that the dispersion polymerisation fails below 241 bar, due to the lack of stabiliser solubility. From this it is clear that styrene has no solubilising effect on PDMS-MA, reducing the working window for this polymerisation to 240-250 bar.

4.5.4.3 Loading limit of polymerisation

Due to the lower polymerisation rate of styrene compared to MMA, heat dissipation was not considered as a loading limiting factor. The ultimate loading limit of reactants for the dispersion polymerisation of MMA was previously found to be 27.11 vol%. For the dispersion polymerisation of styrene, using 20 wt% PDMS-MA, a total loading of 27.11 vol% corresponds to 14.9 ml of styrene. The polymerisation was first conducted using 15 ml of styrene, 20 wt% PDMS-MA, and 2 wt% AIBN, following the standard polymerisation procedure employed previously.

During polymerisation, there was a pressure increase of approximately 30 bar overnight, and the reaction had reached 92% conversion (from ^{1}H NMR) in just 22 hours. The reaction afforded a monolithic aggregate, filling the entire autoclave, that was broken down into a powder with relative ease. From SEM imaging (Figure 4.39) it is clear that the excessive loading had induced some particle agglomeration, resulting in the formation of a second particle size population.

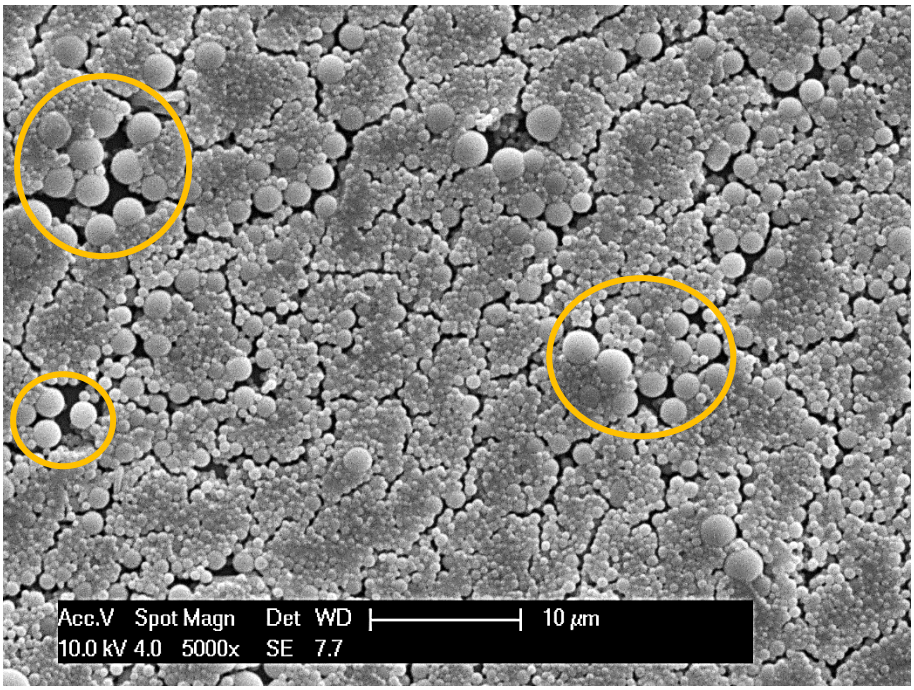


Figure 4.39 SEM image of PS particles of formed through dispersion polymerisation of styrene. Reaction conditions: 15 ml of styrene, 2.727 g (20 wt% wrt monomer) of PDMS-MA, 272.7 mg (2 wt% wrt monomer) of AIBN, 248 bar and 65 °C. Particles of the expected size (335±64 nm, Figure 4.36) can be seen alongside a significant population of large particles (circled in yellow).

The polymerisation was repeated with a 14 ml styrene loading, which should proceed smoothly based on the loading limit determined for the dispersion polymerisation of MMA. During the styrene polymerisation, pressure increased steadily with conversion, with a final increase of 15 bar after 40 hours of reaction time. Conversion was found to be 98% (from ^{1}H NMR), with a 92% yield of a free-flowing powder. SEM imaging (Figure 4.40) showed particles of 345±61 nm in diameter were formed, without any aggregates of second particle size populations. This is in line with particles obtained during initial reactions at a 10 ml monomer loading (Figure 4.36, 335±64 nm).

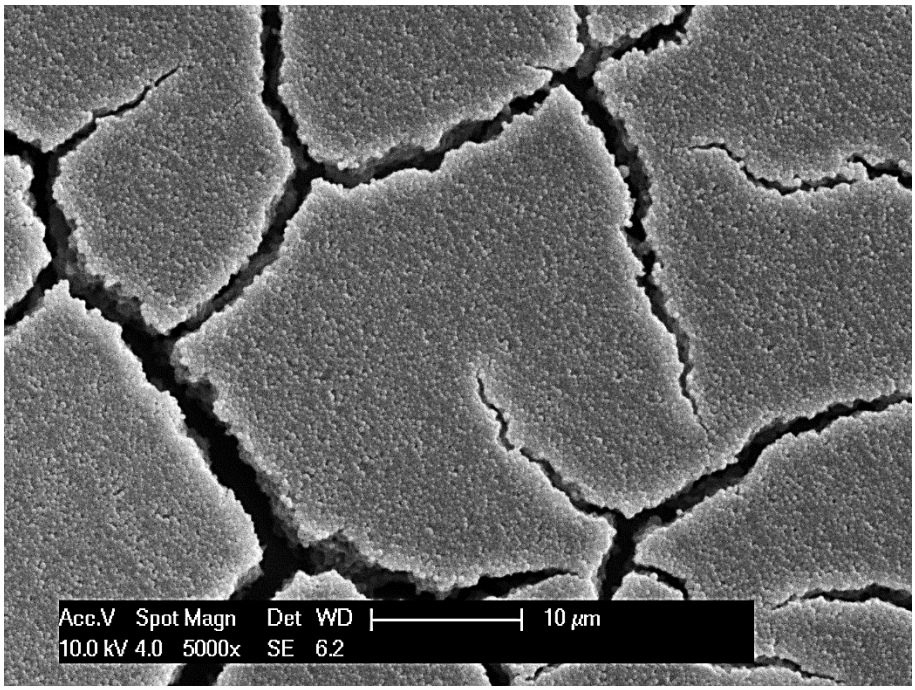


Figure 4.40 SEM image of PS particles of formed through dispersion polymerisation of styrene. Reaction conditions: 14 ml of styrene, 2.545 g (20 wt% wrt monomer) of PDMS-MA, 254.5 mg (2 wt% wrt monomer) of AIBN, 248 bar and 65 °C. Particles of 345±61 nm in diameter (compared to 335±64 nm, Figure 4.36) were formed.

The loading limit for the dispersion polymerisation of styrene was found to be identical to the loading limit found for the polymerisation of MMA.

4.6 Conclusions

In moving towards the commercial application of $scCO_2$ as a solvent for dispersion polymerisations, control and efficiency of the system is essential. In this chapter, we aimed to solve the issue of inconsistent reproducibility of the dispersion polymerisation of MMA and found the issue to be variable agitation. By optimising the dimensions of the impeller, consistent agitation was assured, and reproducible polymer products were formed. After determining the volume of the reactor, the maximum achievable reactant loading was determined experimentally. While the found solid content of 27% is lower than for dispersion polymerisations in traditional

solvents, where 40% and higher is attainable,[145] it gives a clear working window for the dispersion polymerisation of MMA in $scCO_2$.

Another important aspect of commercial dispersion polymerisations is predictable and tuneable particle size control. Through detailed control and optimisation of the system, we were able to observe unique pressure dependent behaviour. We were then able to exploit the unique pressure tuneability of the green $scCO_2$ solvent to achieve intricate particle size control for the dispersion polymerisation of MMA. By altering the initial polymerisation pressure, we were able to affect the solubility of the PDMS-MA stabiliser and its affinity to surround nucleating PMMA particles during the polymerisation. This phenomenon was studied in detail to map out the effect of pressure on particle size, giving further insight into the polymerisation system. Finally, this knowledge was exploited to significantly expand the attainable average particle size range[35] to 0.26-7.14 µm for PMMA particles stabilised with PDMS-MA.[160]

Moving on to the dispersion polymerisation of styrene, this reaction was achieved for the first time in CO_2 using PDMS-MA as the stabiliser. It was however found that there was no exploitable affinity to the PDMS-MA stabiliser, meaning tuneable particle size control with pressure was not possible. With the lower reactivity of styrene, kinetics improvement was attempted by using methanol as a cosolvent. It was found however, that this had no beneficial effects on the polymerisation rate. The highest attainable solid content for the dispersion polymerisation of styrene was again found to be 27%, as observed with MMA. This again gives a clear working window for any dispersion polymerisations stabilised with PDMS-MA.

Chapter 5

Production of Core Shell Particles for Impact Modification

5.1 Overview

Polymer particles with core-shell morphologies have a wide range of applications, such as surface coatings, printing, catalysis, impact modifiers, pollution control, sensing, and drug delivery among many.[66, 161-164] Core-shell particles are of special interest due to their superior properties not possessed by the individual components, as combined characteristics of core and shell material can impart new functionality to the particle.[66] Core-shell particles are broadly in the nano and micro size range, prepared through heterogeneous polymerisation techniques such as emulsion and dispersion among others.[66, 165-168] This chapter will display the first ever production of core-shell particles via dispersion polymerisation in supercritical carbon dioxide. Using previously garnered knowledge on polymerisation control in $scCO_2$, polystyrene particles will be synthesised as core material prior to the addition of a PMMA shell. Size variations of both core and shell phase will be explored, to create a tailored framework for PS:PMMA core-shell particle production. The addition of property altering components will also be explored, such as cross-linkers and hydrophilic monomers, to induce enhanced particle properties. A wide range of analytical techniques will be utilised to demonstrate the attained particle morphology.

5.2 Introduction

Throughout the plastics industry, materials are added to “pure” polymer materials in order to improve product quality and induce desirable properties. [56] These are known as polymer additives and they perform a range of roles in a plastic product often split

into two categories; modifying specific properties (mechanical strength, colour, transparency, heat or UV resistance, conductivity, bacterial resistance) and modifying processing characteristics (curing, miscibility, ductility, mouldability, lubriciousness and slippiness, recyclability).[58] Polymer additives often convey several benefits at once. For example carbon black is widely used as a pigment, but also functions as a light shield, as a conductivity enhancer, and as a reinforcement.[58] While many pigment and filler additives are small molecules, additives for processability enhancement or property alteration can be polymers themselves.[59] Polymeric polymer additives can deliver a range of enhancements, though detailed polymer knowledge is required to understand the effect of macromolecules in a complex plastic mixture. Polymer particles with core-shell morphology are of special interest as additives and smart materials due to the combined characteristics of core and shell material, imparting new functionality to the overall particle that is not possessed by the individual components.[66] Core-shell particles are used in a wide range of applications, such as surface coatings, printing, catalysis, impact modifiers, pollution control, sensing, and drug delivery among many.[66, 161-164] These particles are broadly in the nano and micro size range and are prepared through emulsion, dispersion, or precipitation polymerisation techniques.[66, 165-168]

5.2.1 Structure and applications of core-shell particles

A simple two-component core-shell particle (Figure 5.1) consists of a gas, liquid, or solid core, covered with a solid polymer shell.[66, 161] a wide range of monomers have been used in core-shell particle synthesis, including methyl methacrylate (MMA), butyl (meth)acrylate (B(M)A), (meth)acrylic acid ((M)AA), styrene (St), divinylbenzene

(DVB), N-isopropylacrylamide (NIPAM), ethyleneglycol dimethacrylate (EGDMA), and N,N'-methylenebisacrylamide (MBA).[66, 169]

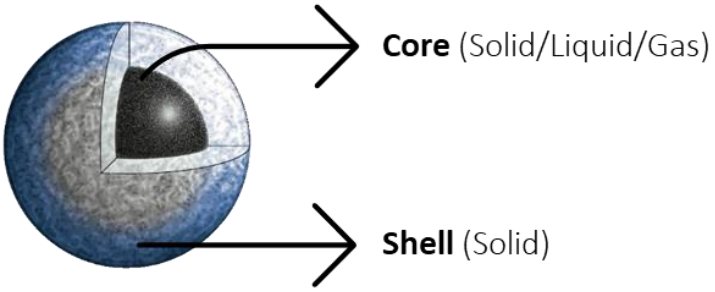


Figure 5.1 A 3D representative illustration of core-shell particle architecture.[170]

While a singular core-shell structure can provide a range of advantageous characteristics, more advanced core-shell morphologies can be of interest. A selection of core-shell structures used in the agriculture sector (Figure 5.2) highlight the wide range of synthesis and application possibilities for core-shell particles, with possible end applications in this field include controlled agrochemical release, enhanced crop protection, soil decontamination, and disease detection.[171]

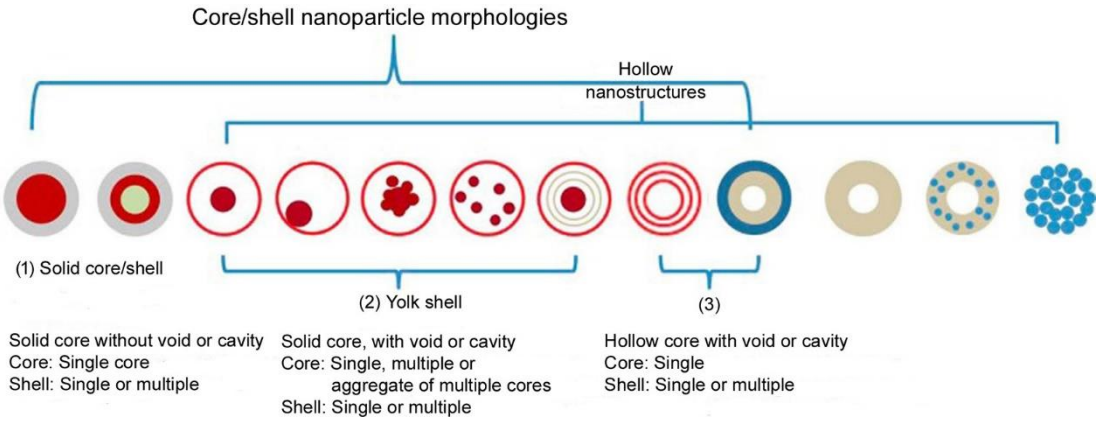


Figure 5.2 Schematic depiction of different kinds of core-shell nanoparticle morphologies used in the agricultural sector.[171]

The combination of tailored core-shell morphology and the use of stimuli sensitive polymers,[172] such as polyNIPAM,[173] is well studied in microgel research. The

structural features of microgel core-shell particles are of interest in biomaterial applications, such as drug delivery and regenerative medicine.[169, 174]

5.2.1.1 Core-shell particles as impact modifiers

While core-shell particles with wide ranging morphologies and materials find applications in a plethora of fields, special attention will be paid to their application as impact modifiers in thermoplastics. The goal of impact modifiers is to compensate for inherent brittleness, or temperature induced embrittlement, notch sensitivity, and crack propagation, observed in many commodity plastics.[57]

Impact absorption relies on incorporating nanometre-sized, crosslinked rubbery particles throughout a plastic matrix.[60-63] The addition of a compatibilising polymeric layer onto the impact modifier particle is required to ensure the particles incorporate evenly into the matrix during product manufacturing.[167] Impact modifiers therefore have a typical two-component core-shell structure, with a rubbery core and a hard polymeric shell (Figure 5.3). The core material is typically an acrylic monomer such as butyl acrylate or a mixture of styrene and butadiene. Acrylic cores provide better weather resistance and stability, while butadiene-based cores perform better at low temperature applications and show better dispersibility in commercially valuable engineering plastics such as polycarbonate alloys.[27, 66, 175]

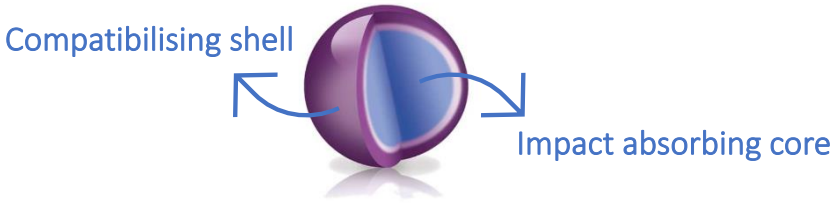


Figure 5.3 typical structure of a core-shell impact modifier, consisting of an impact modifying core and a compatibilising polymer shell that is soluble in the target matrix.

Plastics initially deform under stress through microscopic crazing and shear banding. Crazing is a phenomenon that precedes fracture in brittle plastics and occurs under hydrostatic stress and is associated with a volume increase.[176, 177] Shear banding occurs in narrow zones of intense strain and tends to occur during compressive stress associated with volume contraction.[27, 178, 179] Shear banding and crazing can occur simultaneously upon impact or stretching and can be distinguished by the different angle compared to the imposed stress. Crazes appear perpendicular to the applied stress, while shear bands develop at an angle (Figure 5.4).[176] macroscopic breaks and deformations occur when crazes link up and expand to form cracks prior to yield (Figure 5.5) or when shear bands accumulate and propagate.[65, 178]

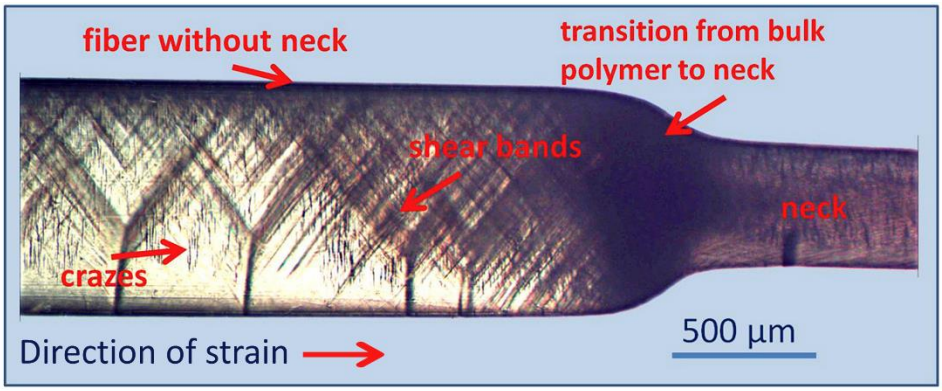


Figure 5.4 Microscopic image of poly ethylene terephthalate fibre under tensile drawing, showing the formation of perpendicular crazes and angled shear bands with respect to the direction of strain.[176]

Impact modifying particles prevent craze and shear band accumulation by acting as a nucleation point under stress. The result of this is a large number of small crazes and shear bands dissipated throughout the material, delaying the accumulation of these defects into macroscopic damage (Figure 5.5).

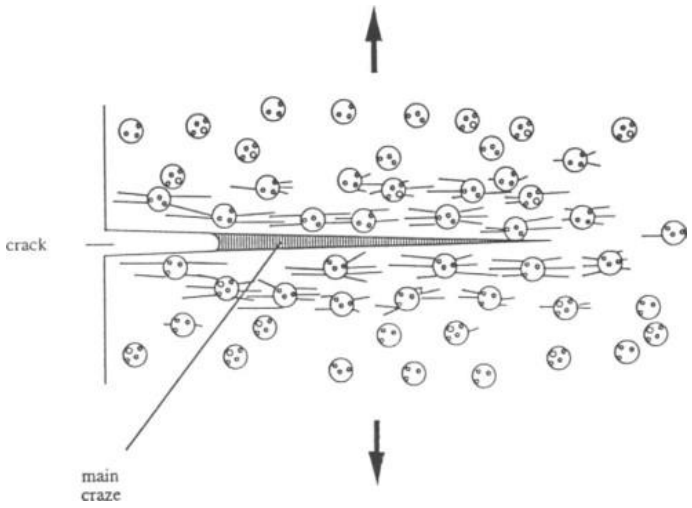


Figure 5.5 Representation of craze proliferation to form a macroscopic crack in a polymer material. Subsidiary crazes are shown forming around rubber impact absorbing particles introduced into the material, delaying crack formation.[178]

The production of core-shell particles for impact modification, exploited commercially by Kaneka, was explored during a summer placement, with details available in the appendix.

5.2.2 Core-shell particle synthesis in $scCO_2$

While synthesis of core-shell polymer particles is widely researched in conventional solvents, their synthesis in $scCO_2$ remains largely unexplored. Cao Li-Qin *et al.* synthesised poly(NIPAM) microgel particles in $scCO_2$ using complex stabiliser molecules that functioned as a stabilising shell.[165, 180] They used both carboxymethyl starch[180] and a poly(dimethyl siloxane)-graft-poly(acrylic acid) stabiliser[165] to form poly(NIPAM) particles with a functional corona. While they did produce microgel particles with temperature and pH responsiveness, the "shell" is in fact the stabiliser from the emulsion system, meaning they have no control over layer thickness and do not have true core-shell morphology.

The synthesis of particles with spherical and lamellar morphology using RAFT controlled dispersion polymerisation in $scCO_2$ has been studied within the Howdle group.[69, 181-186] Using a two-stage polymerisation reaction, block copolymers of immiscible monomers are created. The different monomers phase-separate within dispersed particles to form particles with intricate morphologies, this was confirmed via TEM and small angle X-ray scattering (SAXS) (Figure 5.6). While a range of internal morphologies can be achieved using this method, the domain sizes are significantly smaller than typically seen in core-shell particles. For impact modification, larger domains are required to achieve the favourable properties of both core and shell phases.[15, 27, 117]

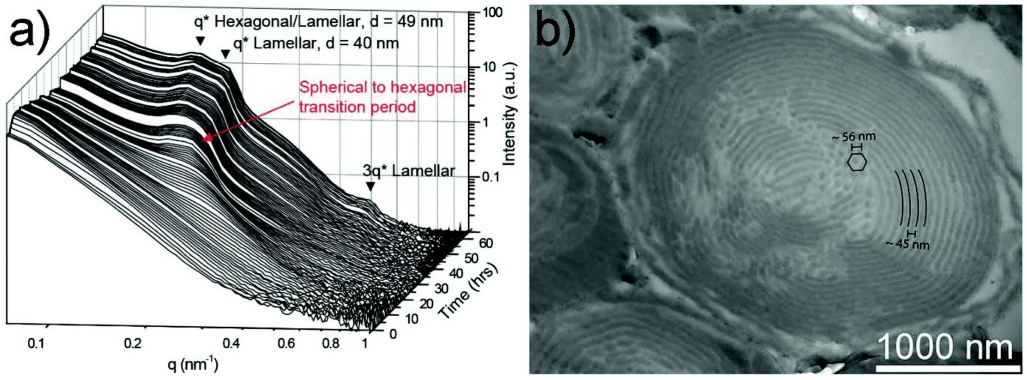


Figure 5.6 (a) Time-resolved in-situ SAXS profiles collected throughout the dispersion polymerisation of PMMA(25)-PS(50) in $scCO_2$. The time between the individual profiles included is approximately 30 minutes. (b) TEM images of representative cross-sectioned PMMA(25)-PS(50) microparticles synthesised in the X-ray autoclave and collected at the end of the reaction. The majority of microparticles exhibit a coexisting mix of both lamellar and hexagonal morphologies. The PS domains appear dark due to staining with RuO_4. [69]

Particles with internal morphology where also synthesised by McAllister *et al.* through a three-stage free radical dispersion polymerisation of MMA followed by dimethylaminoethyl methacrylate (DMAEMA), resulting in “pomegranate like”

microparticles (Figure 5.7).[187] This same particle structure was again achieved by Haddleton *et al.* using MMA followed by benzyl acrylate (BzA) or butyl acrylate (BA).[157]

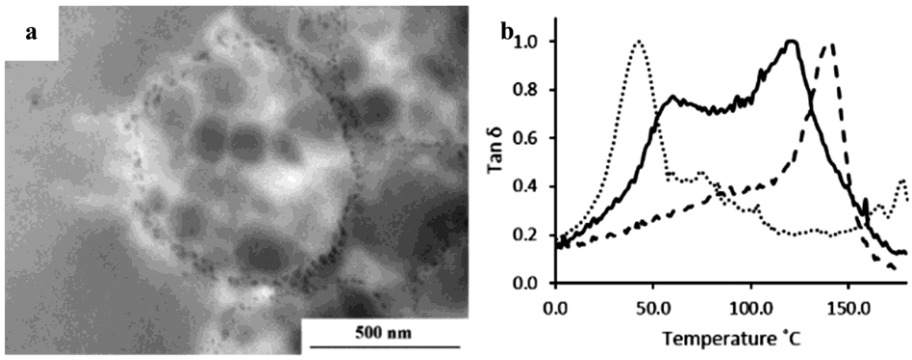


Figure 5.7 (a) TEM image of the stained section of PMMA particles synthesised by three-stage dispersion polymerisation in $scCO_2$ incorporating 37 wt% DMAEMA and (b) the accompanying DMA tan δ trace. The tan δ traces for the PDMAEMA (dotted line) and PMMA (dashed line) are also shown for reference. The double-peaks demonstrate that there are two separate polymer domains within the particles, and these are clearly visible in the TEM images.

While slightly larger domains were achieved using DMAEMA, the use of BA or BzA resulted in domains of 20-40 nm in diameter, which is too small for impact modification.[60, 65] Additionally, necessary crosslinking of the impact absorbing phase[27, 56] was not introduced which could severely disrupt the observed formation of the domains.

5.3 Aims and objectives

The goal of the research presented in this chapter is to develop a method to produce true core-shell particles using free radical dispersion polymerisation in $scCO_2$.

To build up a broader understanding of core-shell systems and impact modifiers, a placement project at Kaneka will be outlined. This will give a better insight into the

production and processing of impact modifiers in a commercial setting. The production of core-shell acrylic impact modifiers with a functional additive will be explored, highlighting the effect of small changes on the free radical emulsion polymerisation system.

Building on from knowledge gained in previous chapters, the production of PS:PMMA core-shell particles will be pursued. Variation of core and shell thickness will be explored, creating a robust framework for tailored particle synthesis. The ability to introduce crosslinking in both phases will be analysed, allowing for selective phase solubility as well as added functionality. Finally, further addition of functional comonomers and the effect on particle stability will be outlined.

5.4 Experimental

5.4.1 Materials

Methyl methacrylate (MMA, 99 %) was obtained from Mitsubishi Chemical. 2,2'-Azobis(isobutyronitrile) (AIBN, 98 %) was purchased from Molekula. Styrene (99 %), 2-hydroxyethylmethacrylate(HEMA, 97%), and divinylbenzene (DVB, 85%) were purchased from Sigma-Aldrich. Monomethacrylate terminated polydimethylsiloxane (PDMS-MA, 150-200 cSt, 10 000 g/mol) was obtained from Fluorochem. Butyl acrylate (BA, 99 %) was acquired from BASF. N-isopropyl acrylamide (NIPAM, 99 %) was purchased from Acros. Carbon dioxide (CO_2, SCF grade 5.5, 99.9995 %) was obtained from Air Products and Chemicals Inc. All chemicals were used as received.

5.4.2 Free radical dispersion polymerisation of styrene with DVB

The reaction was conducted with styrene (6-10 g), DVB (0-10 wt% relative to styrene), PDMS-MA stabiliser (5-20 wt% relative to styrene) and AIBN initiator (2 wt% relative to styrene) in a 60 ml high pressure autoclave. Styrene, DVB, PDMS-MA, and AIBN were degassed by bubbling with argon in a vial kept on ice for 30 minutes. During this time, the autoclave was flushed with CO_2 at 2-3 bar, venting through the keyhole. After 30 minutes, the mixture was injected into the autoclave through the keyhole against a positive flow of CO_2. The key was then inserted into the autoclave, sealing it off from the atmosphere. At this point CO_2 was added, pressurising the system to 50 bar. Heat was then applied through the heating jacket, bringing the temperature to 65 °C. CO_2 was then added until the system pressure reached 245 bar. The moment the reaction temperature was reached was chosen as the starting point of the reaction.

5.4.3 Redispersion of PS particles in $scCO_2$

PS particles (0.75-5 g) were added to the autoclave base prior to reactor assembly. CO_2 was added to the sealed vessel, up to 30 bar, before slowly releasing CO_2 down to a reactor pressure of 10 bar. This pressure cycle was repeated 5 times, to remove oxygen present in the vessel without dispersing the PS powder. After this, CO_2 was added, pressurising the system to 50 bar, and the stirring was engaged at 400 RPM. Heat was then applied through the heating jacket, bringing the temperature to 35 °C. CO_2 and heat were then added incrementally until the desired reaction conditions of

65 °C and 245 bar were reached. After at least 15 hours, the PS particles form a stable dispersion in $scCO_2$.

5.4.4 Preparation of PS:PMMA core-shell particles in $scCO_2$

PS particles were redispersed following the above procedure. A stock solution of MMA, with 1 wt% AIBN relative to MMA, was degassed by bubbling with argon for 30 minutes. Prior to connecting the HPLC to the autoclave, the pipe system was rinsed by pumping acetone through to the autoclave connection. Following this, the degassed MMA with AIBN stock solution was pumped through, pushing out the acetone. With the piping filled with the stock solution, the pipe was connected to the HPLC inlet tap of the autoclave. With the autoclave HPLC inlet tap closed, pressure was built up by pumping in stock solution at a slow rate. The pressure of the HPLC pump was brought up to the reactor pressure (245 bar), meaning that opening the HPLC inlet tap would not cause any liquid movement. The flow rate of the HPLC pump was set to 0.1 ml/min, the HPLC inlet tap was opened, and the pump was engaged. The desired amount of MMA was added (assuring that the added mass of MMA remained below the mass of polymer in the reactor), at which point the pump was stopped and the HPLC inlet tap was closed. HPLC pressure was released through the internal purge system, before disconnecting the pipe from the HPLC inlet. The entire HPLC system is then flushed with 60 ml of acetone. 240 minutes after HPLC injection, when MMA conversion is ≥90%, a further injection of MMA with AIBN can be conducted following the same procedure, again assuring that the added mass of MMA remains below the mass of polymer in the reactor. 240 minutes after the final MMA injection, the reaction time needed to reach >95% conversion of MMA, the

heating was turned off and the system temperature was allowed to fall below 30 °C. At this point the stirring was stopped and the pressure was released slowly, returning to atmospheric conditions, and yielding a fine white powdered product.

5.5 Results and discussion

5.5.1 PS:PMMA Core-shell particle synthesis

Having demonstrated the ability to form PS and PMMA particles using PDMS-MA in $scCO_2$, styrene and MMA were chosen for the production of core-shell particles. The first targeted structure was a 1:1 PS:PMMA core-shell particle, using PS particles as a core to deposit a PMMA shell onto. All PS to PMMA ratios are expressed as mass ratios. It was elected to produce the particles in a two-pot process (Figure 5.8), as this allowed for a better controlled working pressure and better tailoring of relative core and shell size. A two-pot reaction process has been used successfully within the group in the past for RAFT controlled dispersion polymerisations in $scCO_2$.[69, 183, 185, 186]

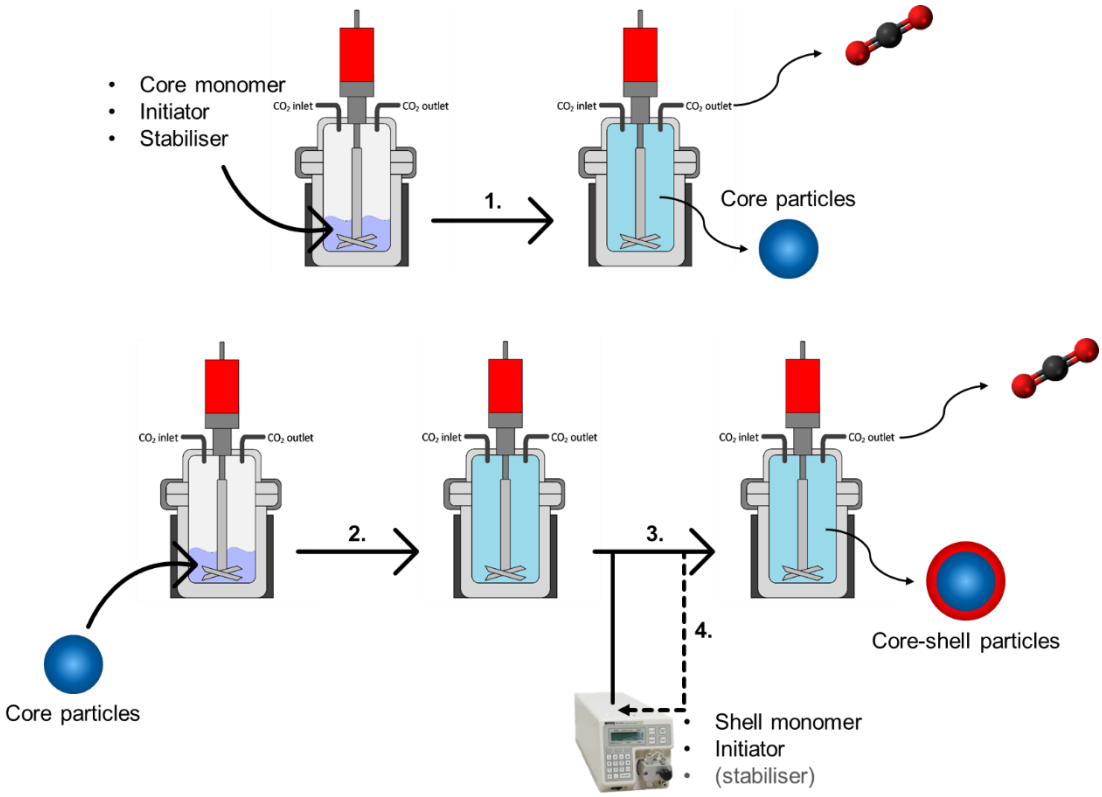


Figure 5.8 Graphical outline of the two-pot core-shell synthesis process, showing the production and collection of core particles, followed by the redispersion of core particles and the synthesis of the shell material. 1.) dispersion polymerisation of core monomer, 2.) redispersion of core particles in $scCO_2$, 3.) polymerisation of shell monomer, 4.) optional polymerisation of additional shell monomer.

With the synthesis of PS particles achieved in chapter 4, the redispersion of these particles was tested. Previous work has shown that PMMA particles can be redispersed at 220 bar for at least 2 hours.[69] The redispersion stability of PS particles with 20 wt% PDMS-MA was tested by redispersing the particles at various pressures and timeframes, prior to injecting 5 ml styrene along with 2 wt% AIBN (Table 5.1). Based on previous kinetics data, the injected styrene was allowed to polymerise for 30 hours prior to product collection. Because of the high initial PDMS-MA loading, it was elected to not add additional stabiliser to aid redispersion.

Table 5.1 Reaction conditions and product outcomes for the redispersion and growth of PS particles in $scCO_2$.

Entry	Redispersion time (hours)	Redispersion pressure (bar)	Final product consistency
1	2	220	Liquid/solid mixture
2	15	220	Liquid/solid mixture
3	2	241	Liquid/solid mixture
4	15	241	Powder

It was found that the PS particles require at least 241 bar to redisperse, which is identical to the previously determined minimum pressure for the dispersion polymerisation of styrene. Additionally, it was found that the redispersion of PS was significantly slower than that of PMMA. While PMMA can be redispersed in 2 hours, PS particles needed to be left overnight (15 hours) to regain a stable dispersion (Table 5.1, Entry 4). This is thought to be caused by the reduced diffusivity of $scCO_2$ in PS compared to PMMA, slowing down redispersion.[188]

Having shown the ability to redisperse and grow PS particles in $scCO_2$, the addition of PMMA was attempted following the same overall procedure (Figure 5.8). After overnight redispersion of 5 g of PS particles (300 nm diameter), a mixture of 5 ml MMA with 1 wt% AIBN was injected at 0.1 ml/min using the HPLC pump system. MMA polymerisation was allowed to proceed for 4 hours after injection, prior to recovery of a dry free-flowing powder (Figure 5.9). The product was then analysed extensively to determine the morphology of the formed material.

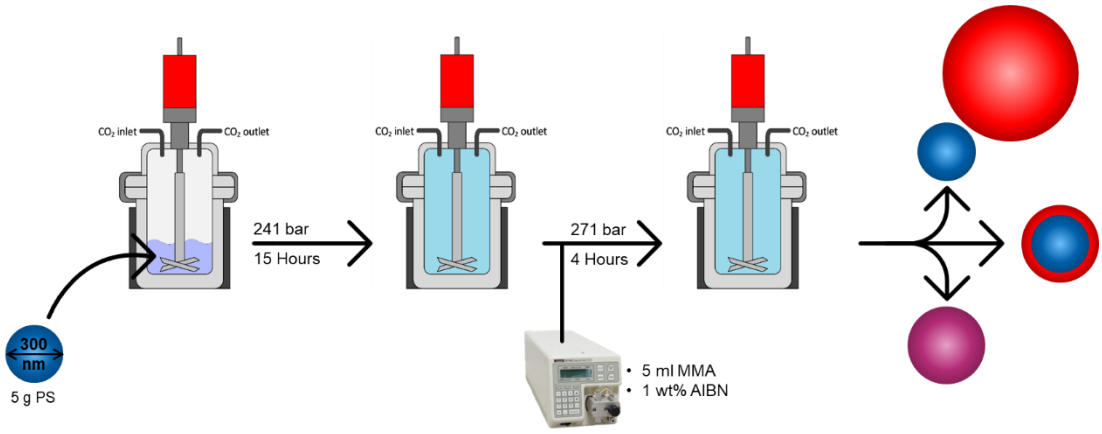


Figure 5.9 Reaction scheme for the synthesis of 1:1 PS:PMMA core-shell particles in $scCO_2$, showing possible reaction outcomes on the right (blend, core-shell, separate particles).

Three possible outcomes from the polymerisation reaction were hypothesised, namely the formation of the desired core-shell particles, the formation of particles consisting of a PS/PMMA blend, or the formation of PMMA particles separate to the present PS particles.

NMR analysis of the formed powder confirmed that high conversion of MMA had been achieved, while there was no residual styrene present in the product. A high yield of ~90% also confirmed a successful polymerisation had taken place (Table 5.2).

Table 5.2 Results for the two-pot polymerisation of styrene followed by MMA to form PS:PMMA 1:1 core-shell particles (Figure 5.8). Entry 1: PS core particles, Entry 2: core-shell particles made from Entry 1 material.

Entry	Conv. (%)[a]	Yield (%)	M_n (kDa)[b]	M_w (kDa)[b]	Đ[b]	$d_n \pm \sigma$ (nm)[c]	d_z (nm)[d]	PDI[d]
1	95.4	89.1	31	65	2.1	305±61	316	0.206
2	100/92.4*	91.4	39	98	2.5	401±135	383	0.247

*a – determined via ^1H NMR (section 2.3.2), b – determined via GPC (section 2.3.1), c – determined via SEM particle sizing (section 2.3.3), d – determined via DLS (section2.3.5), * – conversion of styrene and MMA respectively*

SEM and DLS analysis showed the formation of uniform particles of approximately 400 nm, 100 nm larger than the PS core particles (Table 5.2). The amount of PDMS-MA present during polymerisation of the MMA shell was 10 wt% of the total monomer in the system. Under these conditions any formed PMMA particles would be around 2 µm in diameter, but this is not observed in SEM or DLS, inferring all PMMA material is in the same particle as the PS (Figure 5.10).

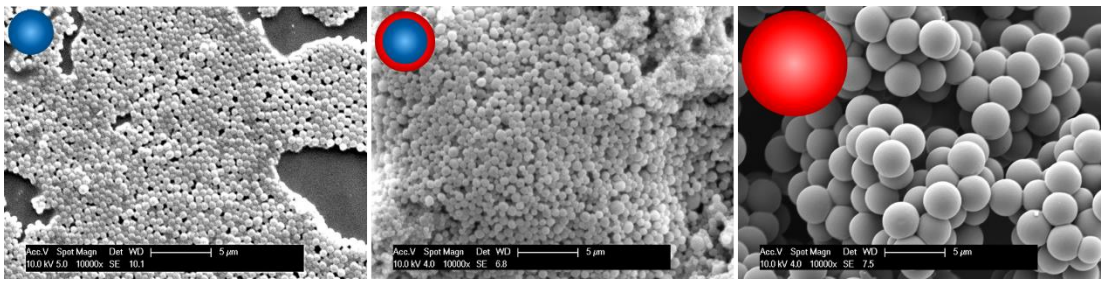


Figure 5.10 SEM images at 10 000 times magnification of PS core particles (left), core-shell particles (middle), and PMMA particles (right), showing the increase in average particle diameter when adding a PMMA shell to the PS core, without the formation of separate PMMA particles.

Thermal properties of the product were investigated using DSC and compared to the PS core material and PMMA particles produced previously (Figure 5.11). As DSC traces are acquired on a second heating run to remove plastic history, no structural data information can be gained. Nevertheless, it can be seen that PS and PMMA polymers are present separately in the core-shell product, with glass transitions appearing round 95 and 125 °C.

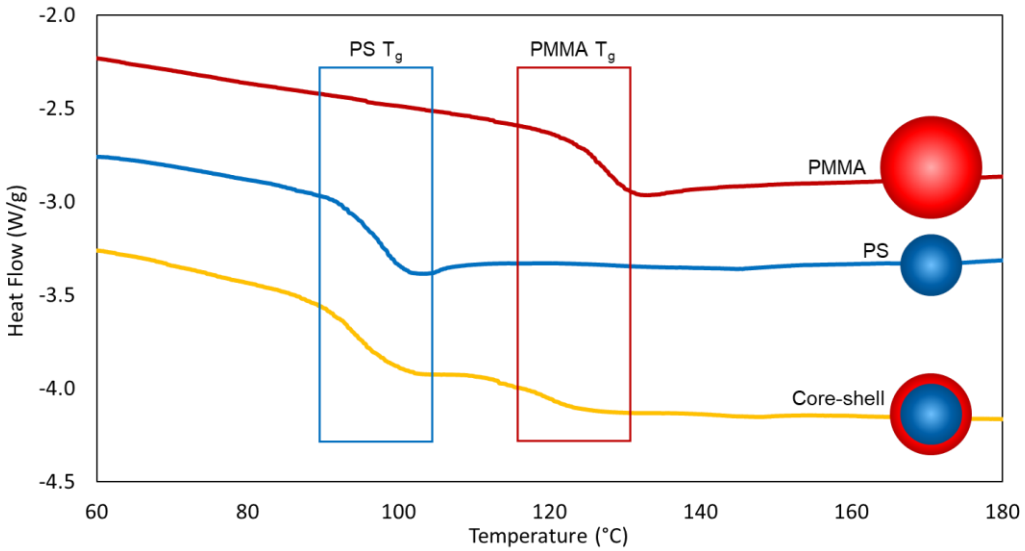


Figure 5.11 DSC traces of PS, PMMA, and the synthesised PS:PMMA core-shell material, with overlay boxes highlighting the glass transition zone of PS (blue) and PMMA (red).

DMA analysis, unlike DSC, is performed on the product without a prior heating cycle to remove plastic memory, allowing for the analysis of the particle structure. It showed a clear dual transition in the modulus as a function of temperature for the core-shell material, with glass transition temperatures typical for PS and PMMA, confirming that they are present as separate phases in the synthesised powder (Figure 5.12). For comparison, a PS-co-PMMA particle powder was made following the standard 1 stage polymerisation method (50/50 PS to MMA ratio), resulting in particles with copolymer chains showing a glass transition between that of pure PS and pure PMMA.

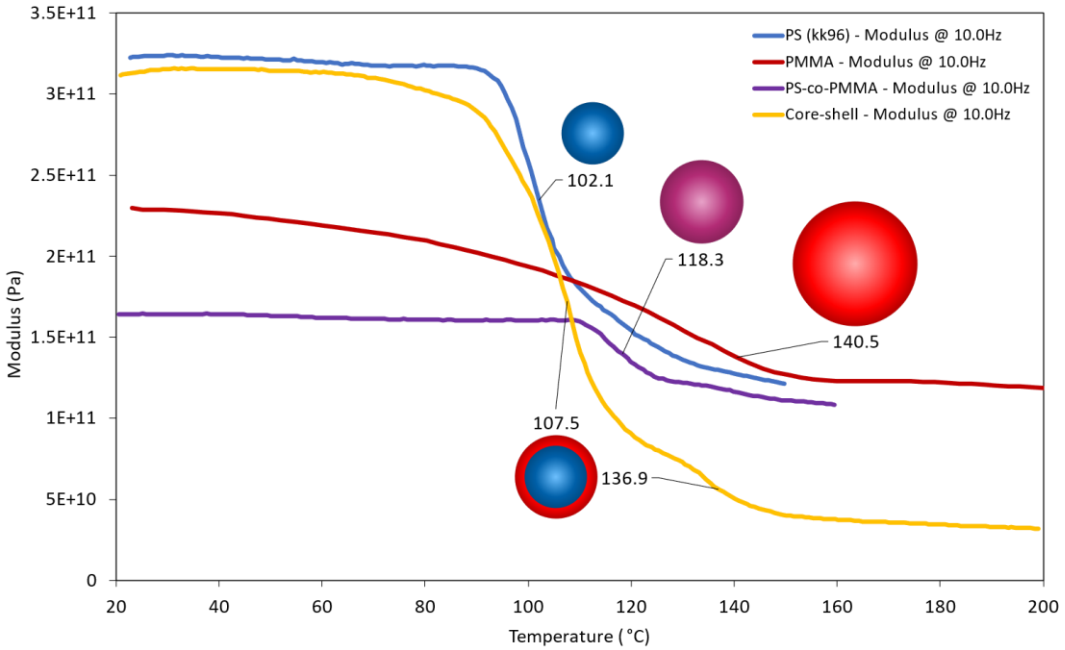


Figure 5.12 Modulus as a function of temperature for polymer powders, measured using DMA, for PS core particles (blue), PMMA particles (red), PS-co-PMMA blend particles (purple), and PS:PMMA core-shell particles (yellow). Glass transition temperature values are labelled on the curve alongside the particle structures, with blue representing PS and red representing PMMA.

While it is more customary to use the tan δ maximum to determine T_g in DMA analysis, the use of modulus was required in this case. The tan δ curve of the core-shell material did not show a clear transition for PMMA, as this signal was drowned out by the prior softening of PS. This was demonstrated to be the case by analysing a 50/50 physical blend of PS and PMMA particles by DMA, where the PMMA signal was also not visible in the tan δ trace but could be seen in the modulus trace (Figure 5.13).

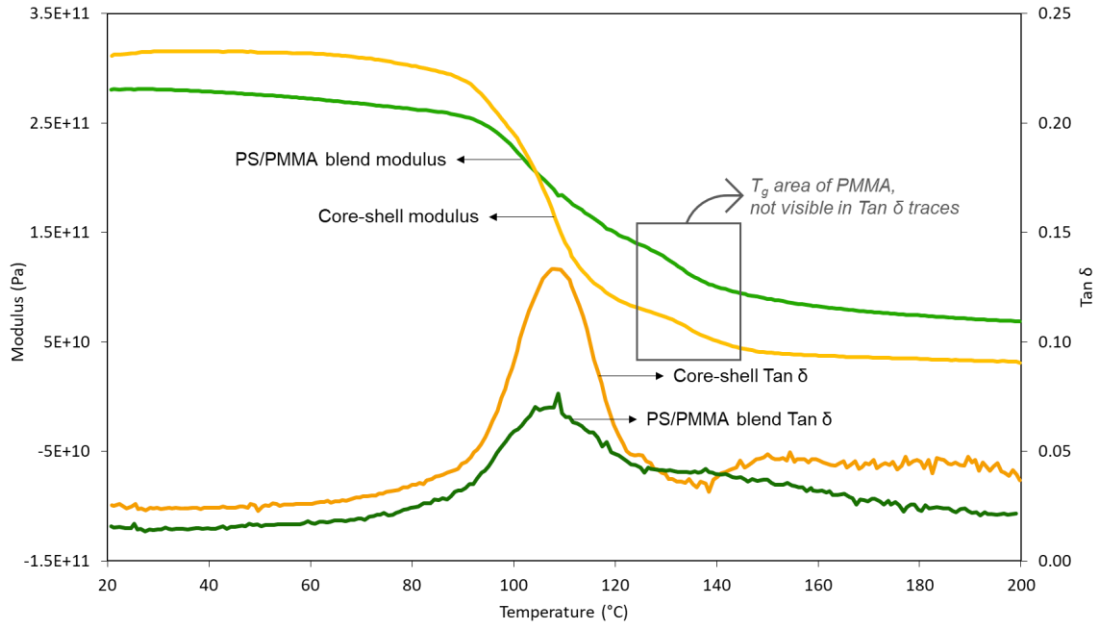


Figure 5.13 Modulus and tan δ as a function of temperature, measured using DMA, for a 1:1 PS:PMMA core-shell material (yellow) and a 50/50 physical blend of PS and PMMA particles (green). The T_g of PS, around 100 °C, is visible in both tan δ and modulus traces, while the PMMA T_g, around 135 °C, is only visible in the modulus traces.

SEM showed PS and PMMA were within the same particle and DMA showed that PS and PMMA were in separate phases, indicating the desired core-shell morphology was formed. To acquire more visual proof, core-shell particles were embedded in resin, sectioned into 100 nm thin slices, stained with ruthenium vapour, and imaged via TEM. From the obtained images a clear core-shell morphology was found, confirming the first ever production of the core-shell particles via dispersion polymerisation in $scCO_2$ (Figure 5.14).

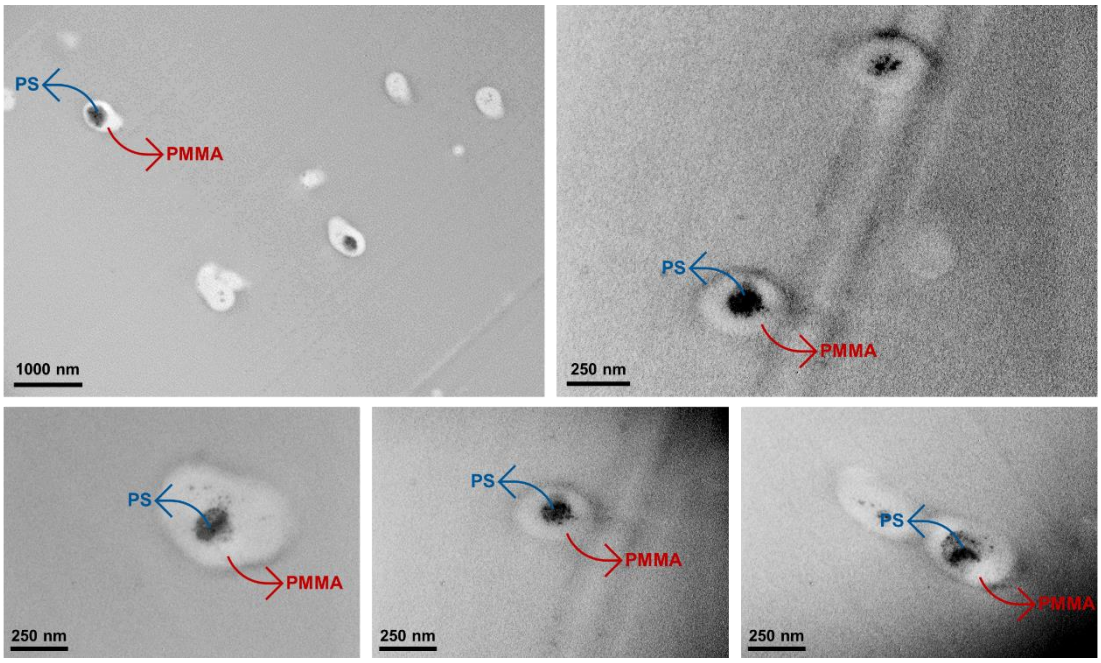


Figure 5.14 TEM images of 1:1 PS:PMMA core-shell particle sections, stained with RuO_4. Staining is hosted in the aromatic ring of styrene, causing it to appear black in the images.

The polymerisation kinetics of the shell formation were monitored using the sampling cylinder system, developed in Chapter 3. The end of monomer injection was chosen as time 0, but due to the injection of monomer (5 ml at 0.1 ml/min) taking 50 minutes, detailed kinetic analysis was not attempted. It was however noted that polymerisation does proceed via similar kinetic behaviour to the simple dispersion polymerisation of PMMA, showing a sigmoidal progression (Figure 5.15). This shows that the PMMA is formed mainly in the dispersed particle phase, and not deposited onto the PS particles from the continuous phase, which would result in far lower conversion rates. GPC analysis of the shell material separately, further confirming the reaction mechanics, will be discussed later in this chapter.

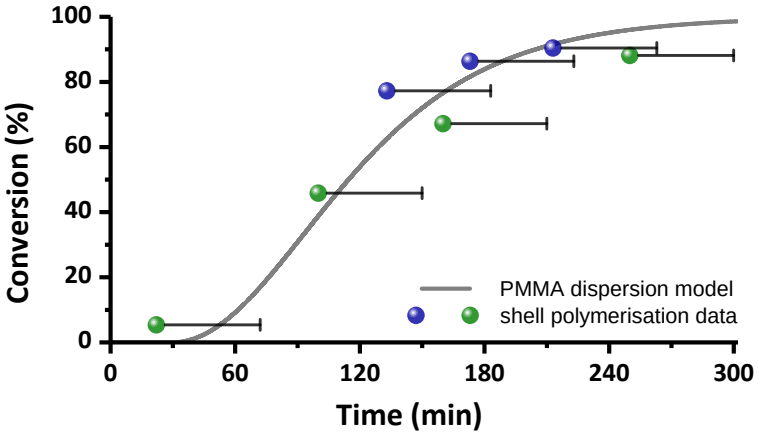


Figure 5.15 MMA conversion as a function of time for the shell forming step in core-shell particle synthesis (green, blue, two repeat reactions), compared to the conversion model of the dispersion polymerisation of PMMA in $scCO_2$. The error bars on the core-shell data represent the 50-minute injection time of monomer before reaction time 0.

5.5.2 Varying shell thickness

(This work was conducted in collaboration with Morgan Reynolds-Green during his time as a Master student in the Howdle group)

With the synthesis of a 1:1 PS:PMMA achieved, the addition of more shell material was attempted using the same overall reaction procedure. First, the synthesis of a 1:2 PS:PMMA core-shell product was attempted by simply doubling the monomer injected after redispersion (Figure 5.16).All PS:PMMA ratios are expressed as mass ratios. While injecting MMA into the PS dispersion, the pressure increase from the amount of added material meant the safety limit (310 bar) was reached. To avoid this in the future, the injection volume should be kept below 6.5 ml when starting pressure is at 241 bar.

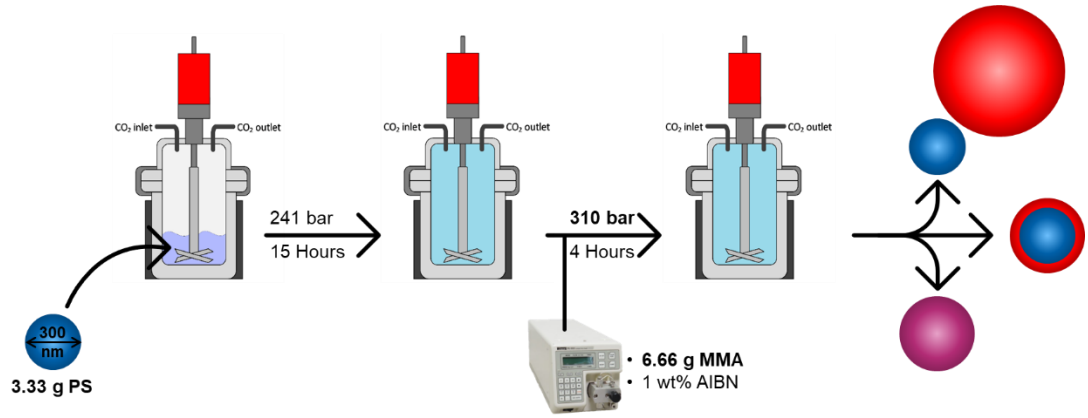


Figure 5.16 Reaction scheme for the synthesis of 1:2 PS:PMMA core-shell particles in $scCO_2$, showing possible reaction outcomes on the right (blend, core-shell, separate particles).

To confirm the formation of particles with core-shell material, SEM was first conducted. However, this showed that PMMA had in fact reacted separately to the core PS particles, resulting in the formation of large PMMA particles alongside PS and core-shell particles (Figure 5.17). The distribution seen in SEM was also confirmed by DLS, where two populations were observed (Figure 5.18). As PMMA particles tend to crash out of the heptane dispersion used for DLS, the size values are of limited value.

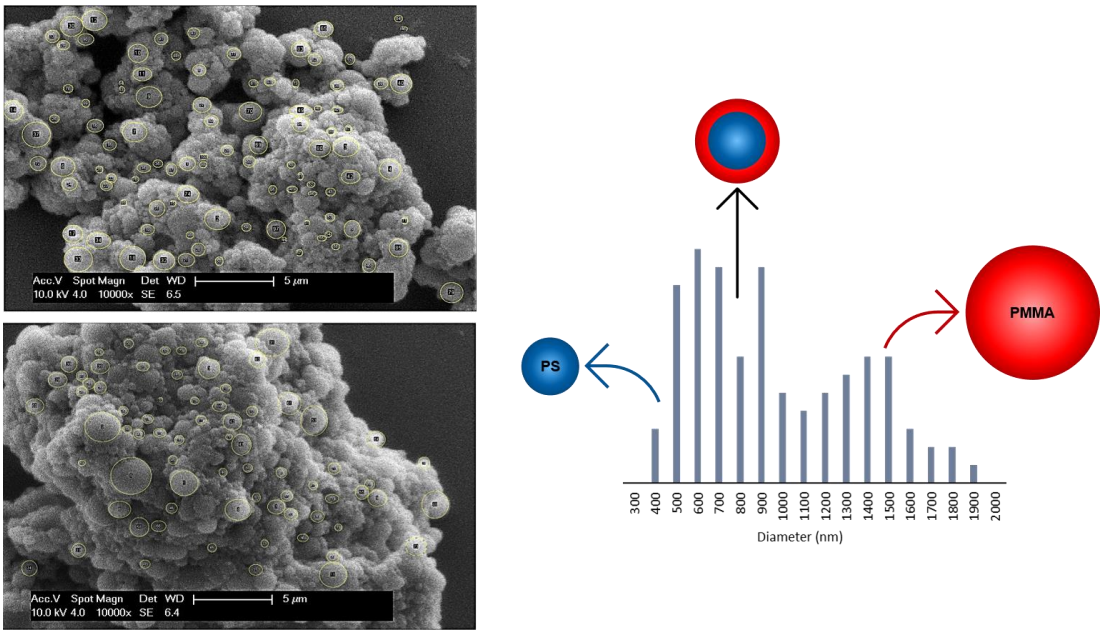


Figure 5.17 (left) SEM images of failed 2:1 PS:PMMA particle synthesis product, with particle diameter measurements shown as yellow circle overlays. (right) Measured particle size distribution intensities, showing a significant population above 1000 nm, typical of unwanted PMMA particles.

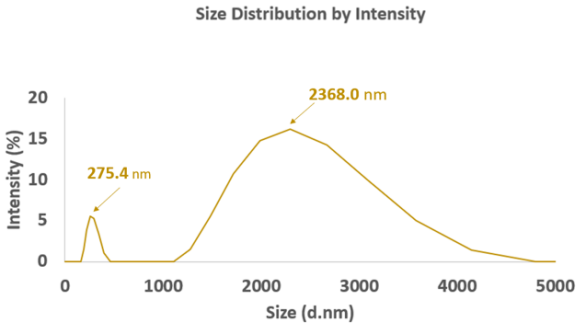
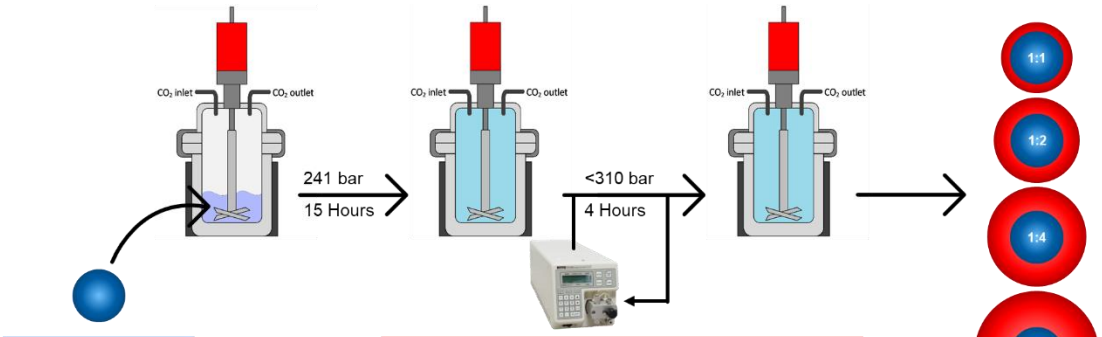


Figure 5.18 DLS analysis of failed 2:1 PS:PMMA particle synthesis product, showing dual size distribution at size ranges typical of PS and PMMA respectively.

Subsequent syntheses were modified to avoid separate particle formation and to remain within safe pressure parameters. The maximum weight of reagents injected was limited to 6.00 g, to limit the final pressure reached. The MMA addition was split into multiple steps, based on the successful 1:1 core-shell synthesis and the failed 1:2 core-shell reaction. The initial injection was kept lower in mass than that of the redispersed particles already present in the autoclave. It was hypothesised that core-

shell morphology was not achieved as the greater proportion of MMA present favoured the formation of discrete particles. As the 1:1 core-shell system had already been synthesised it was thought that the higher core to shell ratios could be synthesised by building up the shell in stages. Multiple injections, with a reaction time of at least 4 hours between injections, should allow for PMMA shell to form upon the PS core and for the reaction to complete before the second loading is added, thus avoiding the formation of discrete PMMA particles.

To assure consistent core size across all samples, core-shell particles of varying shell thickness were synthesised using a single batch of PS core material. Alongside a 1:1 core-shell product, the multi-stage shell growth method was used to produce 1:2, 1:4, and 1:8 PS:PMMA core-shell particles, with tuned PS core loadings and injection amounts (Figure 5.19).



Core-shell ratio	PS (g)
1:1	5
1:2	3
1:4	1.5
1:8	0.75

Core-shell ratio	1. MMA (g)	2. MMA (g)	3. MMA (g)	4. MMA (g)
1:1	5	-	-	-
1:2	2	4	-	-
1:4	1.5	2	2.5	-
1:8	0.75	1.25	2	2

Figure 5.19 Reaction scheme for the synthesis of 1:1, 1:2, 1:4, and 1:8 PS:PMMA core-shell particles in $scCO_2$, with up to 4 stages of MMA injection. All MMA injections contain 1 wt% AIBN and 5 wt% PDMS-MA.

All reactions yielded a free-flowing powder, implying successful polymerisation (Figure 5.20).

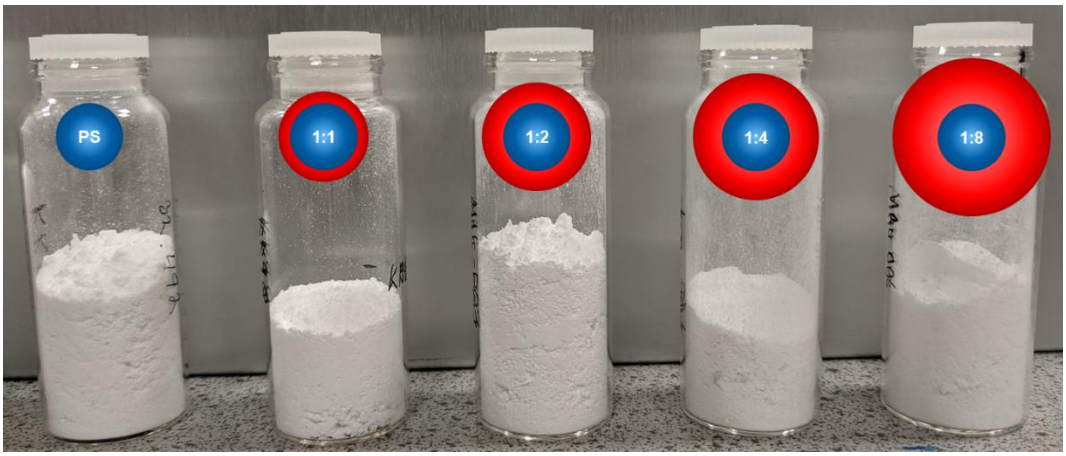


Figure 5.20 image of formed powders through the two-pot multi-stage polymerisation of styrene followed by MMA to form PS:PMMA core-shell particles of varying shell thickness (Figure 5.19).

The final conversion of the injected MMA and the achieved ratio of PS:PMMA was calculated using ^{1}H NMR (section 2.3.2). To find the conversion of MMA, the unreacted vinyl peak (Figure 5.21, 1H, s, δ = 5.56 ppm, H-10) was compared to the polymer peak (Figure 5.21, 3H, s, δ = 3.60 ppm, H-6). To find the ratio of PS:PMMA, the PS aromatic peaks (Figure 5.21, 5H, m, δ = 7.25-6.20 ppm, H-3, 4, 5) were compared to the PMMA peak (Figure 5.21, 3H, s, δ = 3.60 ppm, H-6). Residual styrene was not visible in the spectra. ^{1}H NMR confirmed high conversion and that the desired ratios were achieved while GPC showed the formation of polymer (Table 5.3).

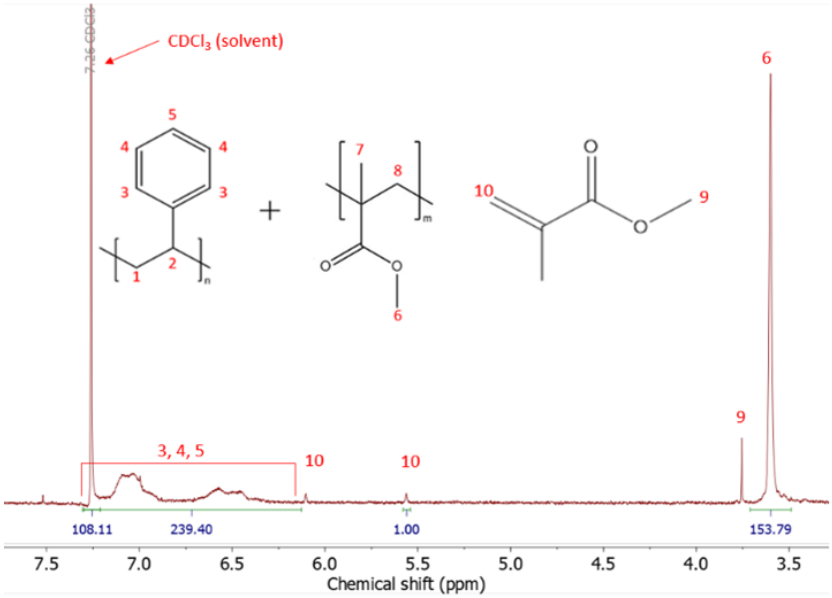


Figure 5.21 ^{1}H NMR spectrum for 1:2 core-shell product. Integration values shown were used to calculate percentage conversion and the ratio of PS:PMMA present (Table 5.3).

Table 5.3 Results for the two-pot multi-stage polymerisation of styrene followed by MMA to form PS:PMMA core-shell particles of varying shell thickness (Figure 5.19). Entry 1: PS core particles, Entry 2-5: core-shell particles made from Entry 1 material.

Entry	Targeted PS:PMMA mass ratio	PS:PMMA mass ratio[a]	MMA conversion (%)[a]	M_n (kDa)[b]	Đ[b]
1	-	-	-	17	2.9
2	1:1	1:1.3	92.5	36	2.4
3	1:2	1:2.0	98.1	40	2.8
4	1:4	1:3.7	97.7	44	2.1
5	1:8	1:8.1	98.5	50	2.0

a – determined via ^{1}H NMR (section 2.3.2, Figure 5.21), b – determined via GPC (section 2.3.1)

The number-averaged molecular mass (M_n) and dispersity (Đ) show a trending increase with increasing PMMA content (Table 5.3). The GPC traces of the materials show a decrease in intensity above 13 minutes as more PMMA is added, along with a shift to shorter elution times overall (Figure 5.22). Unfortunately, due to the significant overlap of the PS and PMMA signals for the core-shell systems, along with

the broad dispersity typical of free radical polymerisations, deeper analysis of the GPC data was impossible.

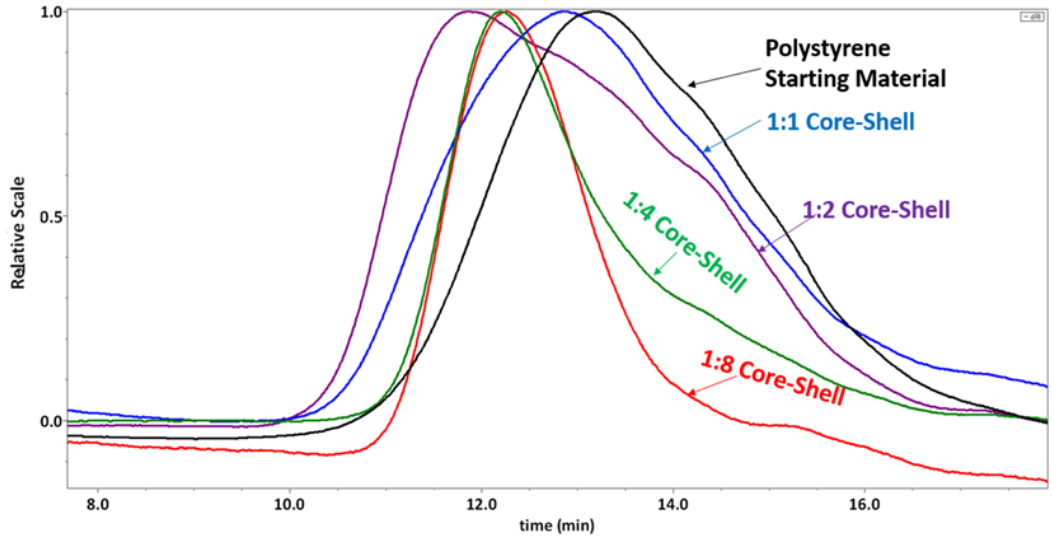


Figure 5.22 GPC traces of PS and core-shell materials of varying PMMA shell thickness (Table 5.3), showing a general decrease in elution time with increased PMMA content.

The particle size of the formed products was analysed using SEM and DLS. SEM imaging showed a consistent particle size increase with increasing shell thickness, but more importantly no discernible formation of separate PMMA particles (Figure 5.23). DLS analysis further confirmed the success of the core-shell syntheses, as a single particle size population was seen for all samples (Figure 5.24).

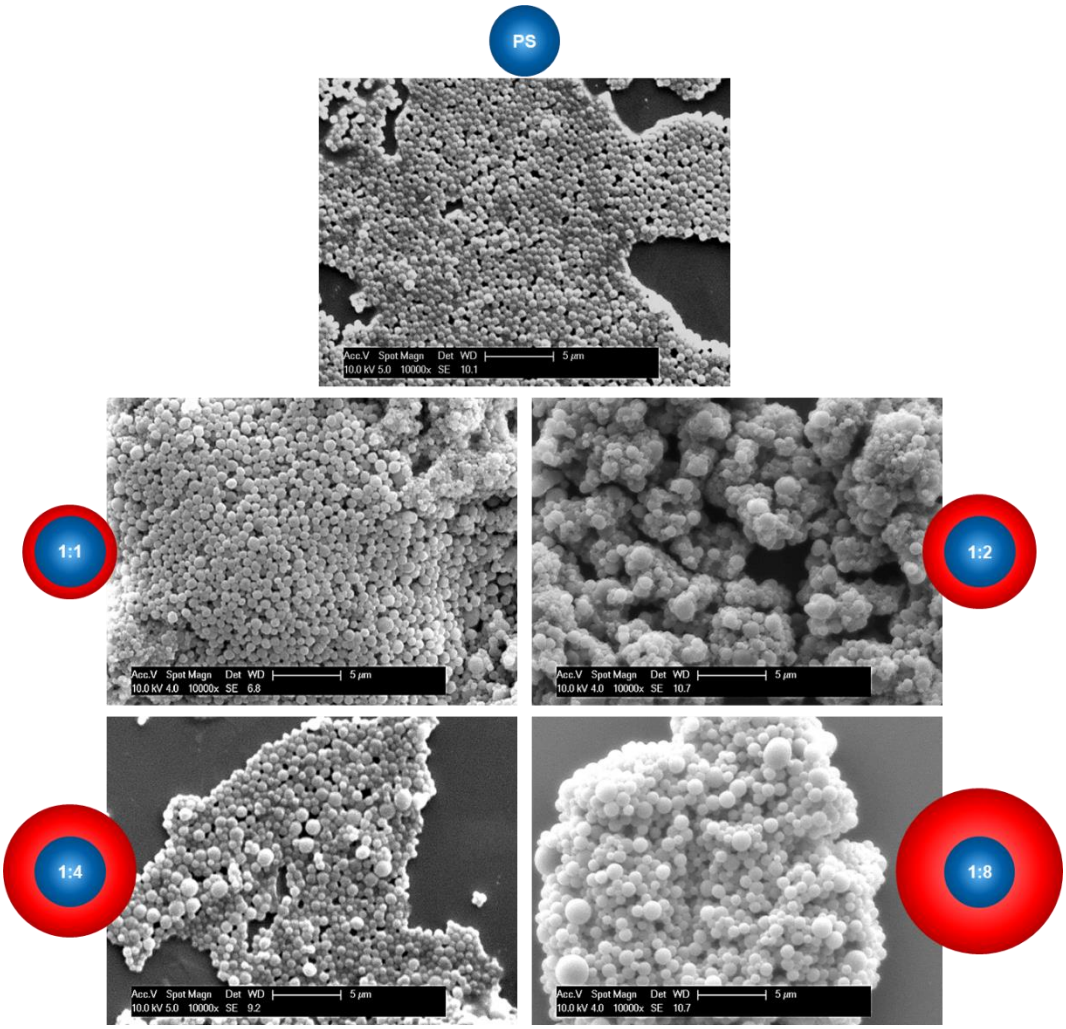


Figure 5.23 SEM images of PS starting material and core-shell particles synthesised using multi-stage injection method (Figure 5.19), showing an increase in particle size with increasing shell thickness.

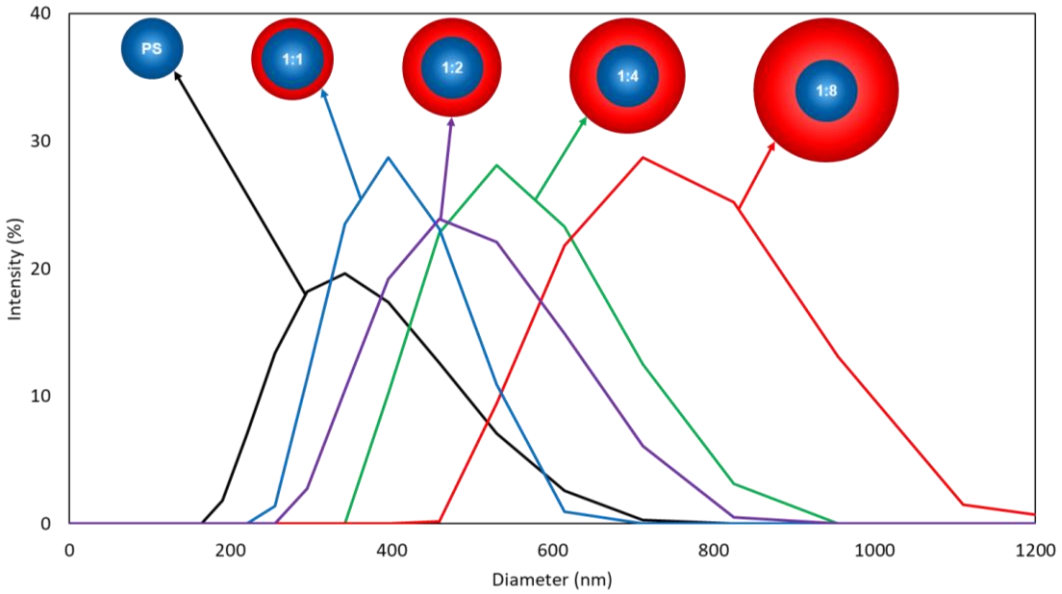


Figure 5.24 DLS derived size distribution by intensity of PS starting material and core-shell particles synthesised using multi-stage injection method (Figure 5.19), showing only single particle size populations and a consistent increase in diameter with increasing shell thickness.

The observed particle size trend was compared to the theoretical particle size growth expected from the added material. By assuming perfect spheres and a consistent density throughout the particles, a diameter prediction was created from the initial PS core particles (Figure 5.25). This prediction lined up consistently with the collected SEM and DLS particle diameter data, confirming the successful addition of PMMA onto the PS core particles up to a 1:8 core to shell ratio (Table 5.4).

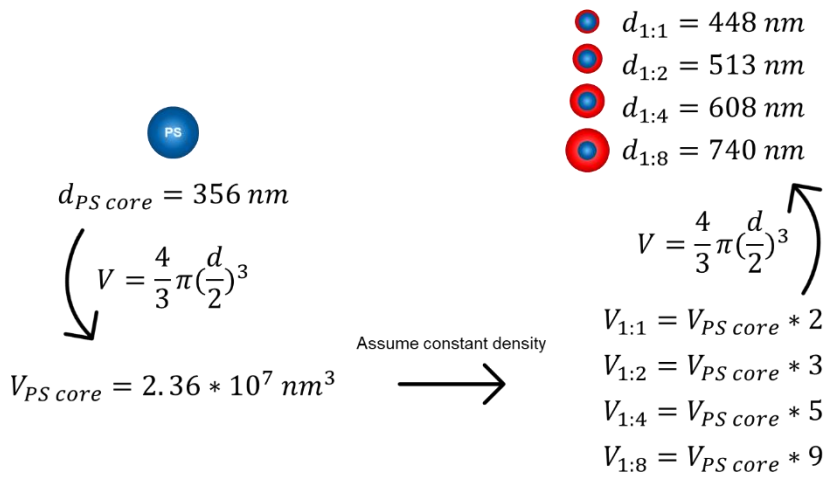


Figure 5.25 Prediction method of particle diameter of core-shell particles from core diameter, assuming particles are perfect spheres and have a constant density throughout all particles.

Table 5.4 Calculated and measured average particle sizes of the PS starting material and core-shell particles synthesised using multi-stage injection method (Figure 5.19). Entry 1: PS core particles, Entry 2-5: core-shell particles made from Entry 1 material.

Entry	Targeted PS:PMMA core-shell ratio	Diameter (nm)[a]	Diameter (nm)[b]	Diameter prediction (nm)[c]
1	-	373	356	356[d]
2	1:1	470	401	448
3	1:2	509	486	513
4	1:4	641	552	608
5	1:8	736	740	740

a – determined via SEM, b – determined via DLS, c – calculated assuming spherical particles of constant density (added mass = increase in sphere volume), d – assumed from DLS data as starting point for calculation

Having confirmed that all PMMA had added to the PS particles for all attempted PS:PMMA ratios, DMA analysis was utilised to confirm the formation of a core-shell morphology. As shown previously, separate transitions for PS and PMMA can be hard to determine, though comparison to physical blends of PS and PMMA particles can give better context to acquired data. Corresponding physical blends with 1:2, 1:4, and 1:8 PS:PMMA mass ratios were prepared and analysed via DMA alongside the synthesised core-shell products. From tan δ traces of the core-shell materials a

maximum was observed at 108 °C for all mass ratios (1:1,1:2,1:4, and 1:8) (Figure 5.26). While this is slightly higher than the tan δ maximum of PS (103 °C), this is in line with observations of the corresponding physical blends of PS and PMMA. The overlap of the softening zone of PS and PMMA causes an apparent shift of their respective tan δ maxima in physical blends, and this is mimicked in the core-shell materials (Figure 5.27). Core-shell materials with higher PMMA loading (1:4 and 1:8) exhibited a second tan δ maximum around 130 °C, corresponding to the PMMA shell.

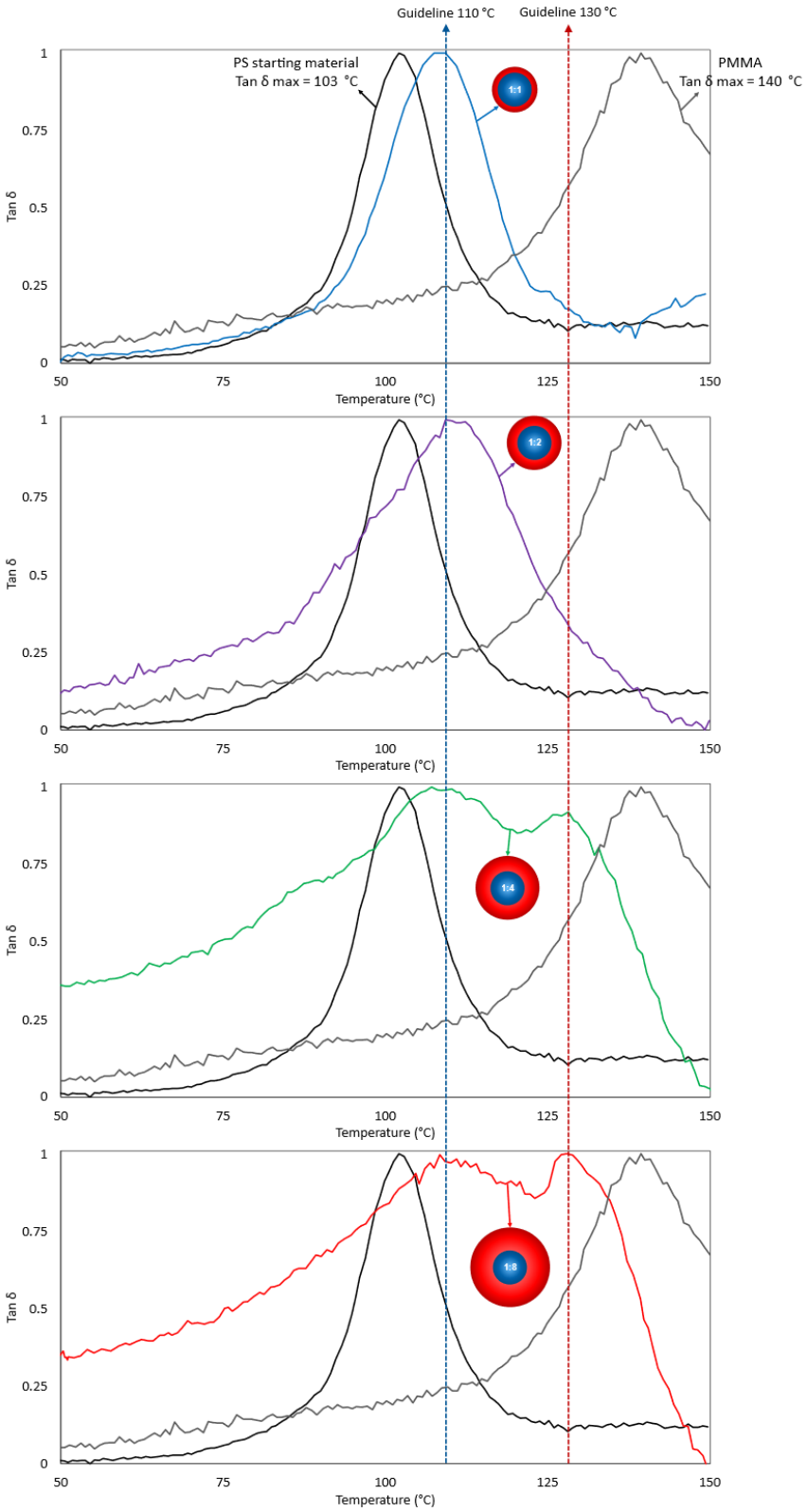


Figure 5.26 DMA obtained tan δ traces of core-shell particles synthesised using multi-stage injection method (Figure 5.19), with guidelines at 110 and 130 °C. All core-shell materials show a tan δ maximum around 110 °C, corresponding to the PS core material. 1:4 and 1:8 core-shell particles show a second tan δ maximum around 130 °C, originating from the PMMA shell. PS and PMMA traces are shown for reference.

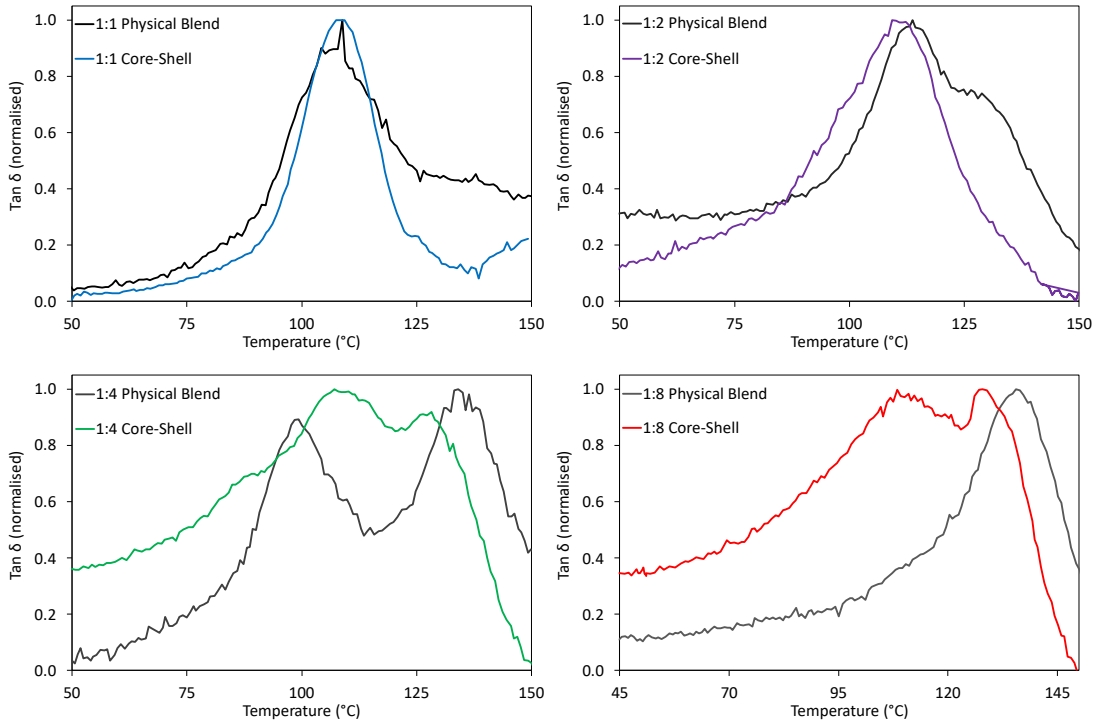


Figure 5.27 DMA obtained tan δ traces of core-shell particles synthesised using multi-stage injection method (Figure 5.19), with their corresponding physical blends. The similarity of the respective traces highlights the phase separation present in the core-shell particles and the difficulty of obtaining separate tan δ maxima for separate materials.

As with the previous DMA analysis of 1:1 mass ratio PS:PMMA core-shell particles, the modulus was able to provide better visual confirmation of the two discrete phases present in the core-shell materials. It was found that increasing PMMA content caused a reduction in the modulus drop seen around 100 °C, along with an increase in modulus drop around 130 °C (Figure 5.28). This again shows that separate phases are being formed, regardless of the volume of shell added to the PS core material.

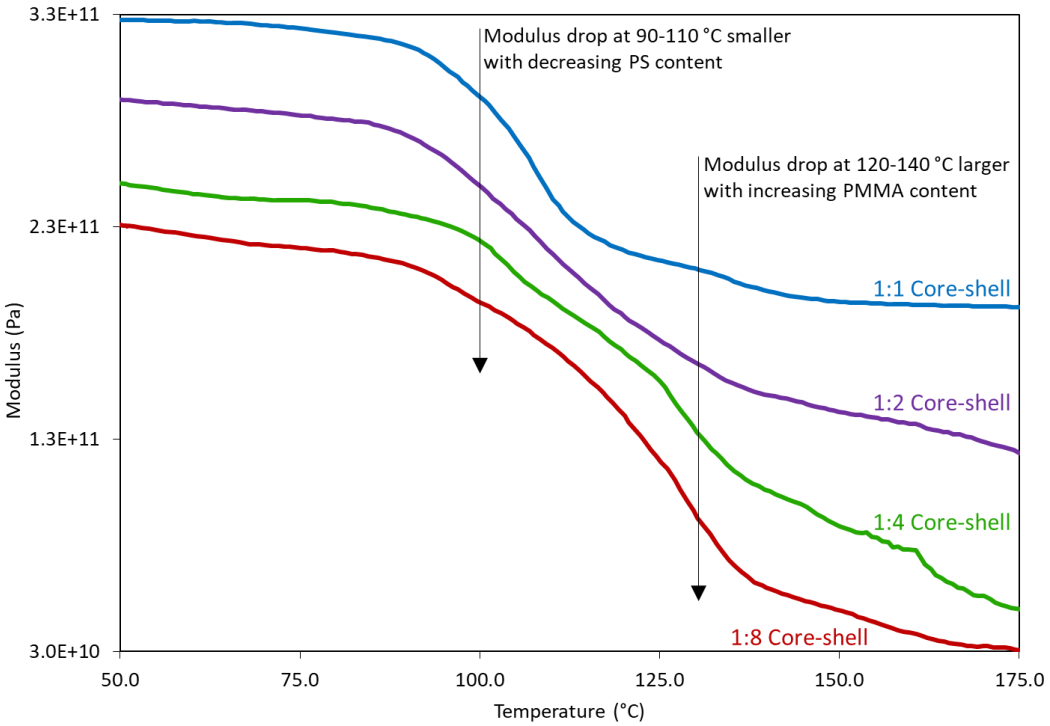


Figure 5.28 Modulus as a function of temperature of core-shell particles synthesised using multi-stage injection method (Figure 5.19). the modulus decreases around 100 °C are due to the PS core material, while the modulus decreases around 130 °C is due to the PMMA shell material. The intensity of the modulus changes is correlated to the amount of the core and shell material present in the sample.

It should be noted that the measured tan δ maxima and Modulus drop temperatures for the core-shell materials are slightly offset from the values of the pure polymer material. The typical PS signal at 103 °C appears at 108 °C for the core-shell material, while the PMMA signal at 140 °C is seen around 130 °C for the core-shell particles, regardless of core to shell ratio. While this narrowing of the gap between PS and PMMA transition temperatures is also observed to a certain degree in the physical blend samples, it may be enhanced by interface effects in the core-shell materials. A slight tapering between the PS and PMMA layers could also contribute to this observation, as slight blending at the core-shell interface could broaden the glass transitions of both PS and PMMA.

5.5.2.1 Alternative analysis methods

To provide an alternative method of core-shell structure analysis, ToF-SIMS, AFM, and nanoIR analyses were attempted through collaborations.

ToF-SIMS analysis is used to provide chemical information of a sample surface, and a chemical profile into the depths of a sample. By sputtering the sample surface with a laser, top layers can be removed to expose subsequent layers within a sample, that can then be analysed separately. ToF-SIMS analysis was attempted on PS:PMMA core-shell particles of varying core to shell mass ratio (1:1, 1:2, 1:4, 1:8), looking for characteristic ions of the present polymers (Figure 5.29). comparing the different samples, it was found that with increasing PMMA shell thickness, a higher ratio of MMA was found. Conversely, less PS was present in these particles, as expected. Sadly, more detailed information about the core-shell morphology was not attained. This was attributed to the fact that sputtering into the particles was occurring too quickly, resulting in a steady state measurement before any shell and core information could be gathered separately. Improved sample preparation, to form a consistent monolayer across the measured area, may be able to alleviate this issue in future work.

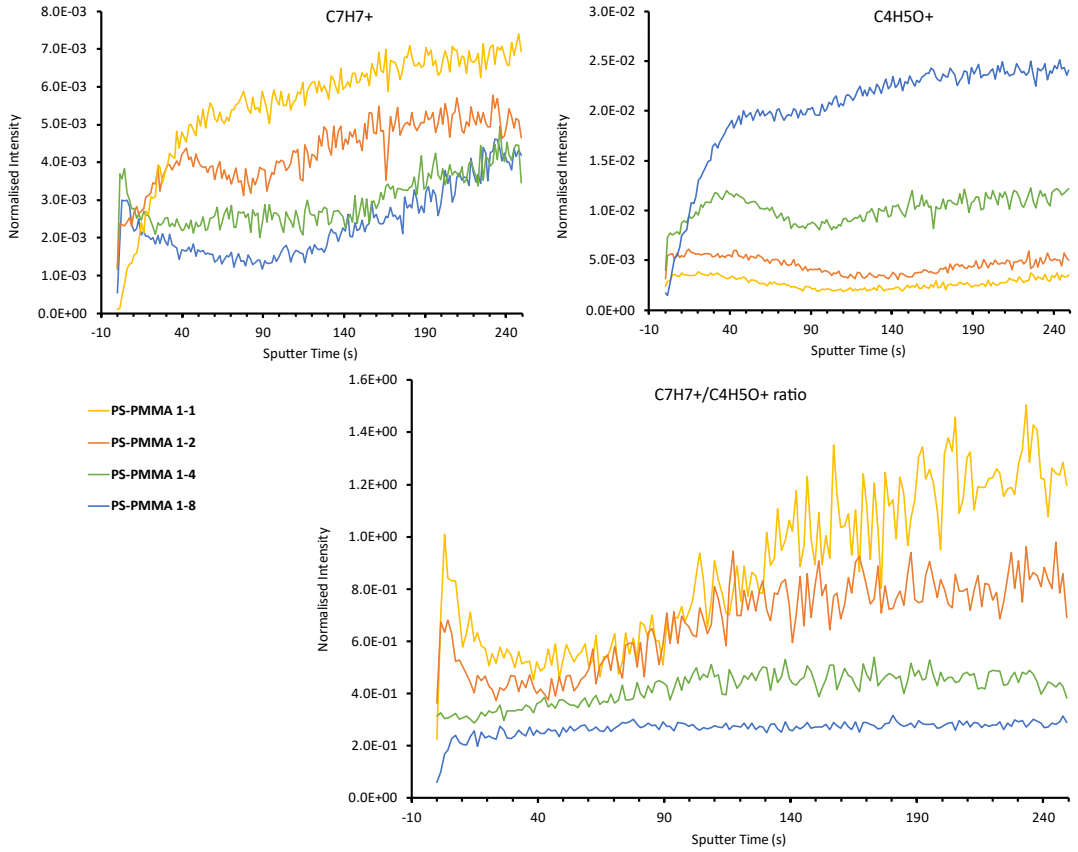


Figure 5.29 ToF-SIMS data output shown as Intensity as a function of sputter time for $C_7H_7^+$(top left, styrene), $C_4H_5O^+$(top right, MMA), and $C_7H_7^+$/ $C_4H_5O^+$(bottom, styrene/MMA ratio), for the produced PS:PMMA core-shell particles. While no morphology information can be extracted, the relative amounts of MMA and styrene present in the samples is consistent with expectations.

In a collaboration with Bruker (Karlsruhe), a novel nanoIR analysis was attempted. This analysis method combines the special resolution of AFM with the chemical information of IR, which should allow us to distinguish between PMMA and PS on the nm scale. Core-shell particles with a PS:PMMA mass ratio of 1:1 and 1:8 were analysed using this technique, first by AFM, and then by photothermal AFM-IR in point specta mode, and finally in IR band ratio mode. After confirming the presence of particles with optical microscopy, AFM was used to locate a single particle for detailed analysis (Figure 5.30). IR spectra were then acquired at different spots across the particles (Figure 5.31). Despite stable measurement conditions, the IR spectra

appeared to show PS and PMMA equally present at all locations. A definitive reason for this was not discovered, but sample preparation issues or AFM tip contamination are suspected to be the cause.

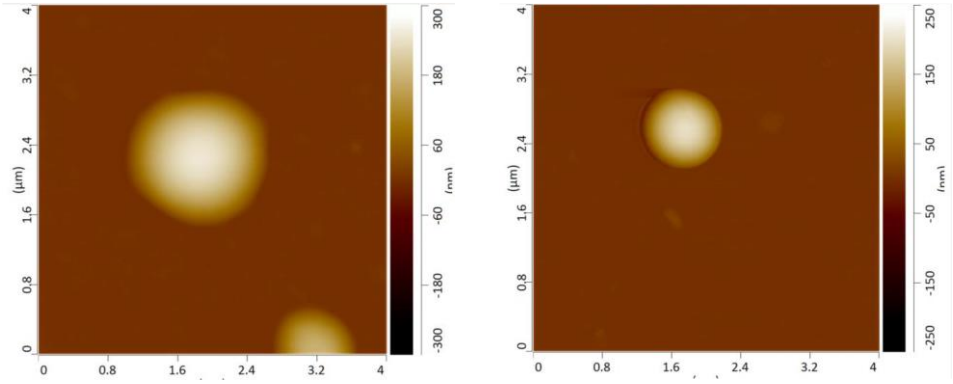


Figure 5.30 AFM image of PS:PMMA core-shell particle with a 1:1 mass ratio (left) and a 1:8 mass ratio (right).

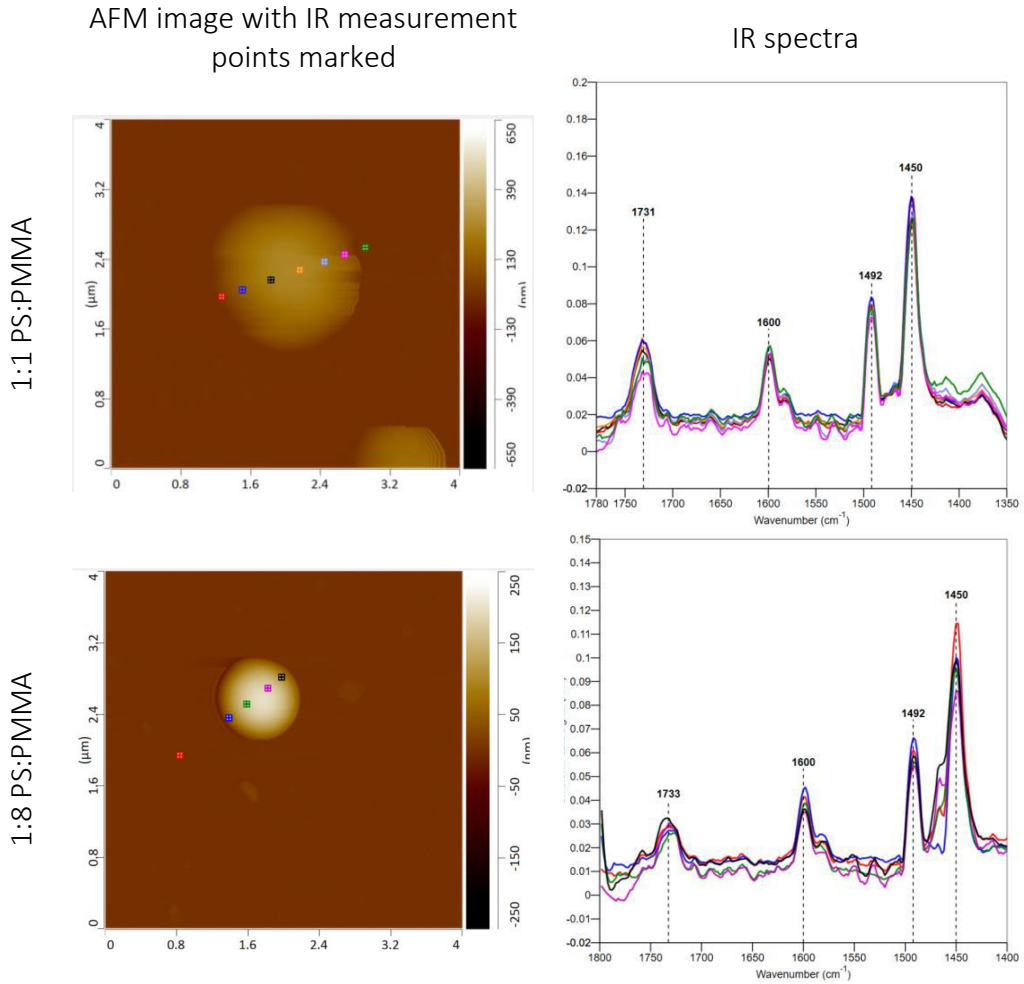


Figure 5.31 photothermal AFM-IR spectroscopy data for 1:1 (top) and 1:8 (bottom) PS:PMMA core-shell particles.

IR band ratio imaging was also conducted, using the IR peaks at wavenumbers 1730 cm^{-1} and 1492 cm^{-1} to represent PMMA (carbonyl stretch) and PS (ring C=C vibrations) respectively (Figure 5.32). The band ratio images show significant amounts of PS and PMMA in varying ratios present away from the core-shell particle. this is further evidence of a contamination that is obscuring all measurements, either due to sample preparation or probe contamination. While very preliminary conclusions from Bruker were that slight differences on the particles appear to show the presence of a PMMA shell structure, the evidence for this is too limited at this time. Future work into optimising sample preparation, could result in clearer data, allowing for the use of what appears to be a very high-resolution analysis technique.

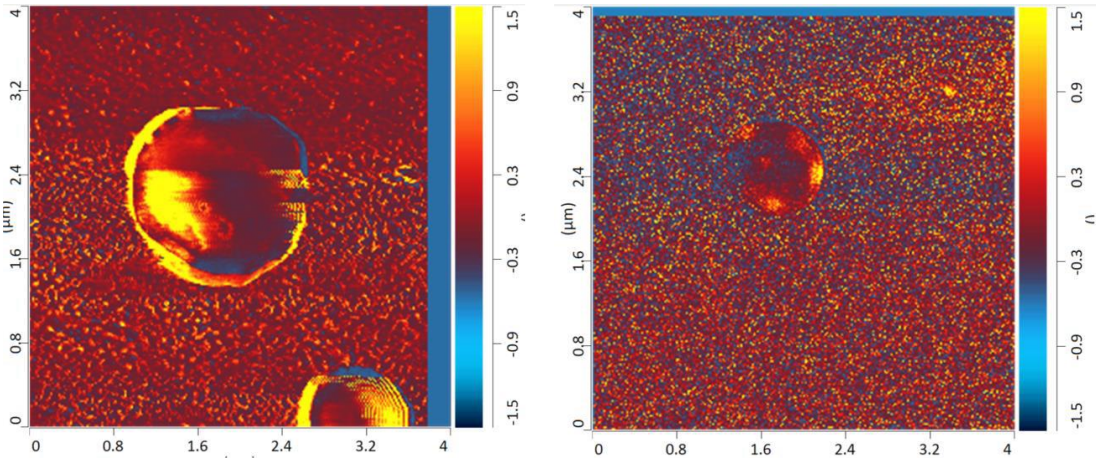


Figure 5.32 photothermal IR band ratio imaging (1730/1492 cm^{-1}) showing the ratio of PMMA to PS, for a 1:1 (left) and 1:8 (right) PS:PMMA core-shell particle. Yellow represents the highest PMMA concentration, while blue represents areas of higher PS concentration.

5.5.3 Varying core size and material

After demonstrating control over shell thickness, we then attempted to vary the size of the PS core. By using 5 wt% PDMS-MA with respect to the monomer for the core synthesis step, larger PS core particles were attained (Figure 5.33). It must be noted

that the attainable particle size range for PS is far lower than that of PMMA. With 5 wt% PDMS-MA, PMMA particles of 3.3 µm were achieved, while PS particles of 795 nm were formed under identical conditions.

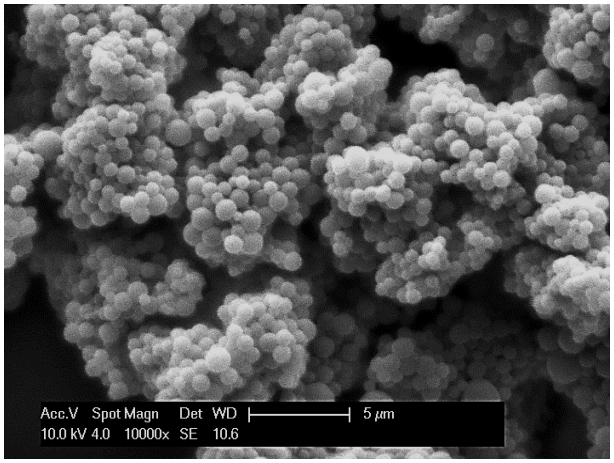


Figure 5.33 SEM image of PS particles synthesised using 5 wt% PDMS-MA with respect to styrene. An average particle size of 795±274 nm was measured from the image.

These 800 nm PS particles were then redispersed overnight, before injection of MMA to afford 1:1 PS:PMMA core-shell particles, following the same procedure as previously (Figure 5.9). SEM imaging of the formed core-shell material confirmed the shell growth, with an average particle diameter increase of 65 nm and no second population formation (Figure 5.34).

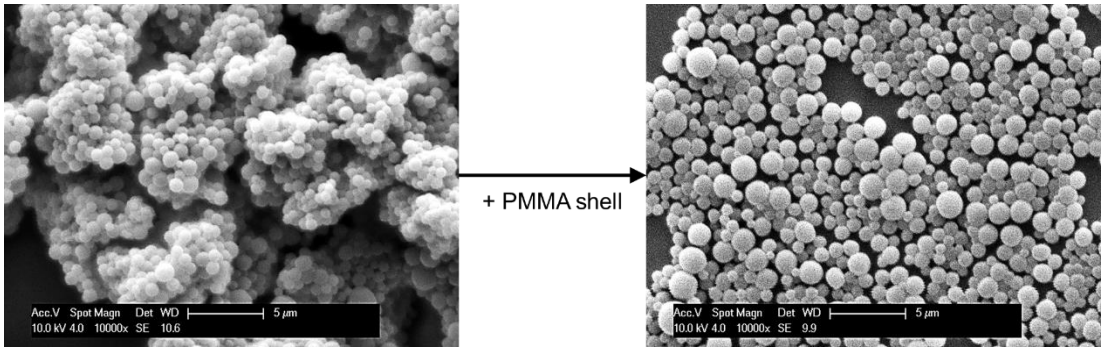


Figure 5.34 SEM images of PS core material (left, 795±274 nm) and 1:1 core-shell material (right, 960±265 nm).

Next, the synthesis of 1:1 PMMA:PS core-shell particles was attempted. PMMA core material was first synthesised using 5 wt% PDMS-MA, to produce particles of 2990±252 nm diameter. following the same procedure as previously (Figure 5.9), styrene was injected and allowed to polymerise to high conversion. After 26 hours, ^{1}H NMR confirmed a styrene conversion of ~92%. SEM analysis however, showed that the shell formation had failed, with separate PS particles of <500 nm present alongside the 3 µm PMMA particles (Figure 5.35).

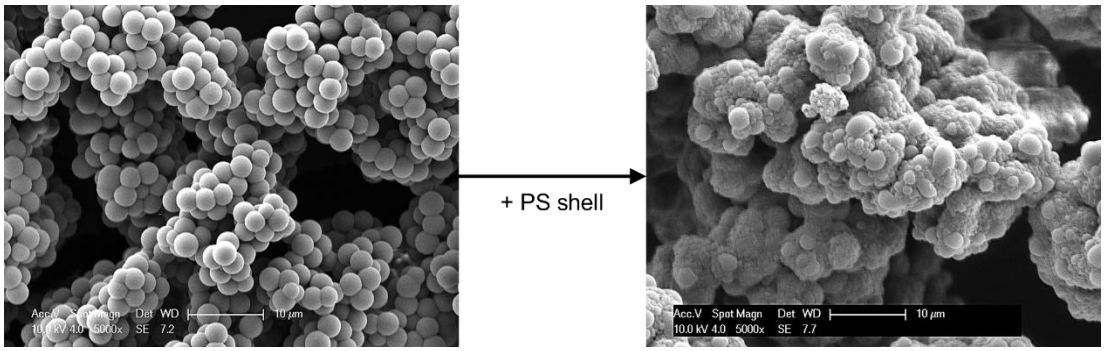


Figure 5.35 SEM images of PMMA core material (left, 2990±252 nm) and a mixture of PS and PMMA particles after a failed attempt at producing 1:1 PMMA:PS core-shell particles (right).

As the PMMA core particle size used was quite large, PMMA:PS core-shell synthesis was retried with PMMA particles of 296±53 nm diameter, mimicking the previously successful production of PS:PMMA core-shell particles. However, SEM again showed that separate PS particles were formed, confirming that shell formation had failed. Successful shell addition should result in particle diameters around 400 nm, but broad particle diameters were observed in the formed product (Figure 5.36).

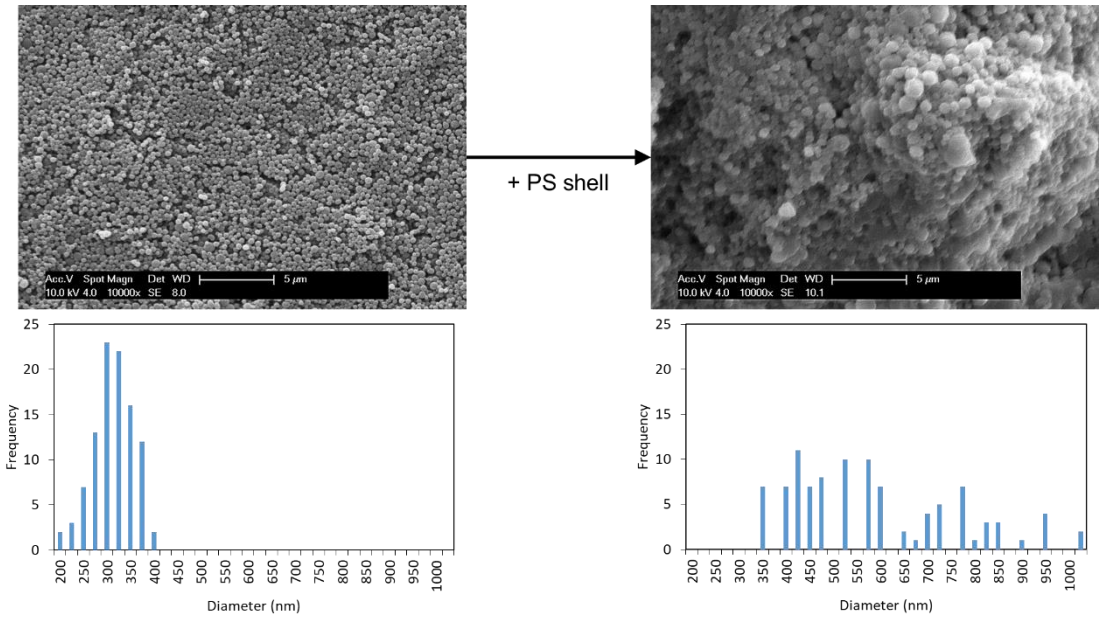


Figure 5.36 5.37 SEM images of PMMA core material (left, 296±53 nm) and a mixture of PS and PMMA particles after a failed attempt at producing 1:1 PMMA:PS core-shell particles (right). Histograms of measured particle diameters show the narrow size distribution prior to shell synthesis (bottom left), and the loss of size control after PS addition (bottom right).

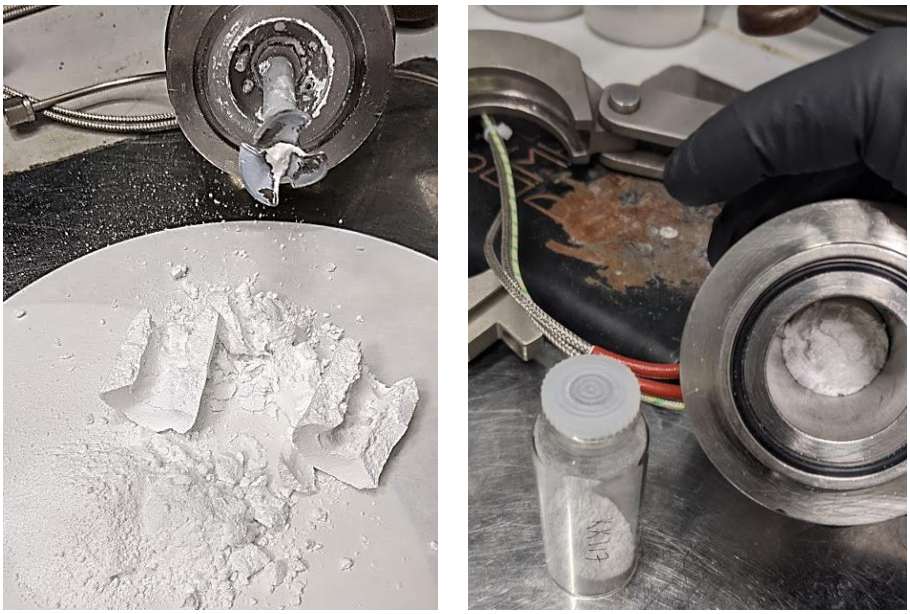
Based on the successful core-shell synthesis of PS:PMMA previously, the failure to form PMMA:PS core-shell particles must be attributed to the PMMA core material and its incompatibility towards hosting a PS/styrene phase on its surface. It is hypothesised that this is due to the higher solubility of $scCO_2$ in PMMA compared to PS at reaction conditions.[188] The softer PMMA, interpenetrated with CO_2, is more mobile under reaction conditions, allowing for more movement within a particle. The more solid PS may form a more stable scaffold for PMMA addition, while the more plasticized PMMA particle is less favourable for PS. Further investigation into this could be conducted by introducing crosslinker into the core, reducing the swellability and possibly allowing for the addition of a PS shell onto PMMA.

5.5.4 The addition of crosslinking to core-shell particles

For many core-shell particle applications, including impact modification, a crosslinked core is required. Divinyl benzene (DVB) was chosen as the crosslinking agent for the styrene core of the PS:PMMA core-shell particles synthesised previously, because of its chemical compatibility with styrene. By simply adding 0.25-5 wt% (with regards to styrene) of DVB at the beginning of the core polymerisation, crosslinked, insoluble material was formed. It was however found that using ≥2 wt% DVB resulted in loss of dispersion control and induced the Trommsdorf effect after 6 to 7 hours (Table 5.5). This time coincides with the point at which monomer moves into the dispersed phase for the polymerisation of styrene and can polymerise quicker, causing more heat production. This runaway reaction causes an extreme pressure spike to above 400 bar (ending the reaction on safety grounds), while the formed monolithic structures have conversions well above 90% based on solid content measurement. By lowering the overall loading and the amount of DVB, it was possible to achieve a free flowing yet insoluble PS particle powder without the occurrence of the Trommsdorf effect (Figure 5.38).

Table 5.5 Reaction conditions and outcomes for styrene polymerisations conducted at 248 bar, with 20 wt% PDMS-MA and 2 wt% AIBN with regards to styrene.

Entry	Styrene (g)	DVB wt% (wrt styrene)	reaction time (hours)	Final product consistency
1	10	10	6	Monolith
2	10	5	6	Monolith
3	7	2	7	Powder/Monolith mix
4	6	0.5	26	Powder
5	7	0.75	26	Powder



Monolith powder

Figure 5.38 Visual comparison of PS-co-DVB reaction products. (left) Monolithic structure produced with 2 wt% DVB, (right) powder produced with 0.75 wt% DVB.

SEM analysis of the formed PS particles showed that the desired 300 nm particles had been formed, though image quality was severely hampered as the crosslinked particles charged under the electron beam (Figure 5.39).

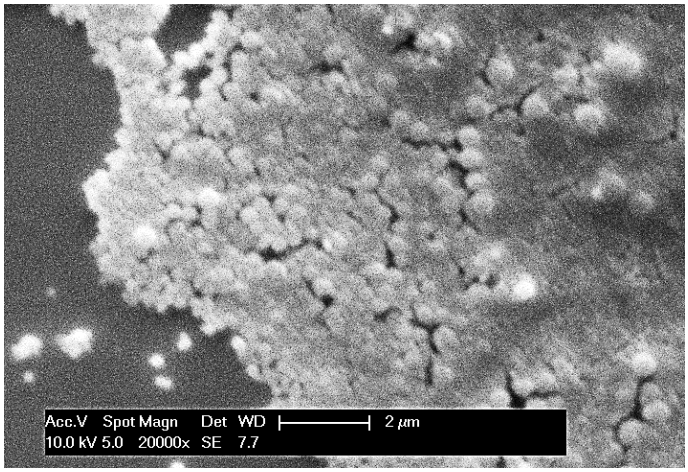


Figure 5.39 SEM image of crosslinked, insoluble, PS particles, showing an average particle diameter of around 300 nm.

A PMMA shell was added to the crosslinked PS core, following the same procedure as used previously (Figure 5.9), to form a 1:1 PS-co-DVB:PMMA core-shell. SEM again confirmed the formation of the desired particles, with an average particle diameter

around 400 nm (Figure 5.40). Robust particle size analysis was not performed as the SEM quality was insufficient and DLS was not possible, because the crosslinked particles did not disperse in heptane. We suspect the dense crosslinking prevents the particles from swelling in the DLS solvent, so the particles simple sink to the bottom of the cuvette.

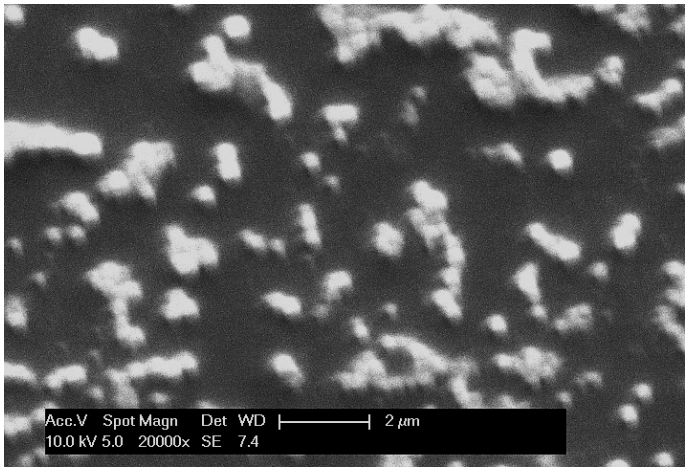


Figure 5.40 SEM image of 1:1 PS-co-DVB:PMMA core-shell particles, showing an average particle diameter of around 400 nm.

A great analytical advantage of having an insoluble PS core, was that the PMMA shell could be dissolved and analysed separately, giving further insight into the reaction system. The formed PS-co-DVB:PMMA core-shell particles were stirred in THF for 1 hour, dissolving the PMMA shell, then pushed through a 200 nm filter to remove the insoluble PS cores. A GPC trace of the shell was then compared to previous GPC traces of PS and PMMA (Figure 5.41). From this it was confirmed that the PMMA shell in the core-shell particle reached the same average molar mass as simple PMMA particles. This, along with the previously measured polymerisation kinetics, showed that the polymerisation of MMA occurred predominantly in the dispersed phase in a high monomer concentration environment.

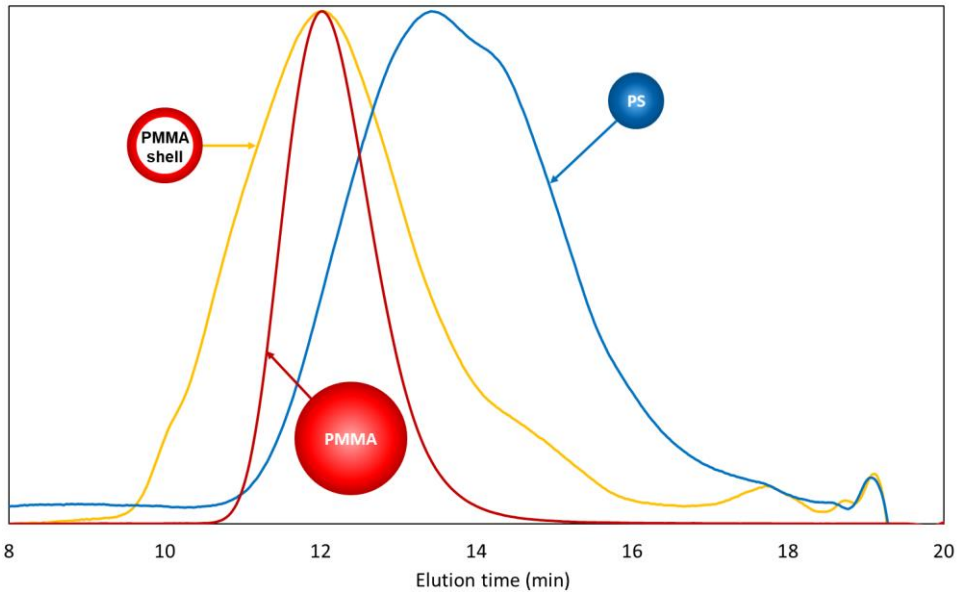


Figure 5.41 Refractive index intensity as a function of elution time, from GPC, showing the average molar mass of PMMA shell material overlapping with that of PMMA particles, eluting well before PS.

Some core-shell applications, such as smart release systems for precision farming, can benefit from cross-linking in the shell to maintain structural integrity as the core interacts with the environment.[171] As a simple proof-of-concept, shell crosslinking was attempted for the 1:1 PS:PMMA core-shell particles. Allyl methacrylate (AMA), having very good chemical compatibility with MMA, was chosen as the crosslinking agent for the PMMA shell. Following the same reaction procedure as before, 5 wt% AMA was added to the monomer injection step (Figure 5.9) to form 1:1 PS:PMMA-co-AMA core-shell particles.

The PS:PMMA-co-AMA core-shell particles were stirred in $CDCl_3$ for 3 days, to dissolve the PS core material. ^1H NMR analysis of the solution showed only a minimal PMMA signal, around 1% in size compared to PS, confirming the crosslinking of the PMMA phase was successful. Additionally, it was found that adding the particles to $CDCl_3$ for

5 minutes prior to ^{1}H NMR analysis showed very low amounts of PS, implying that it is indeed constrained by the crosslinked PMMA material, delaying its dissolution.

SEM analysis of the PS:PMMA-co-AMA core-shell product, was again slightly challenging due to the sample charging under the electron beam. However, images were obtained showing particles of the expected size range (Figure 5.42). Particles did show slight coagulation, though this may be avoided by lowering the crosslinker loading from 5 wt% down to 0.5 wt%, as seen with the core crosslinking reactions.

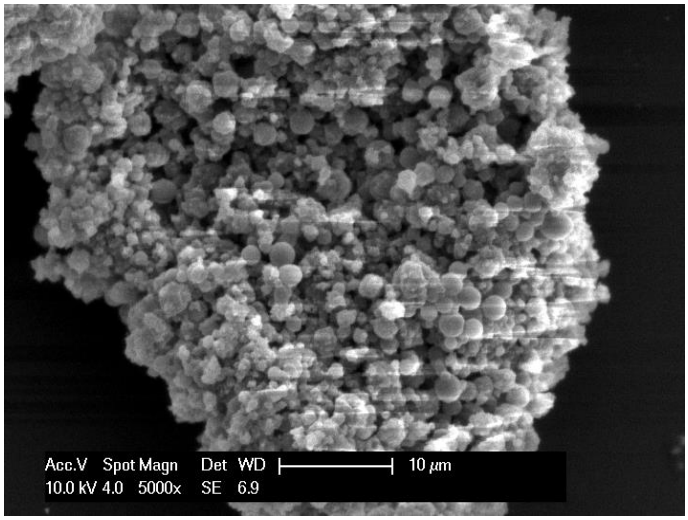


Figure 5.42 SEM image of 1:1 PS:PMMA-co-AMA core-shell particles, showing discrete core-shell particles alongside some coagulation.

5.5.5 The use of alternate monomers in core-shell particles

To provide a starting point for further research into smart core-shell particle synthesis in $scCO_2$, a range of co-monomers were added to the basic core-shell synthesis method (Figure 5.43).

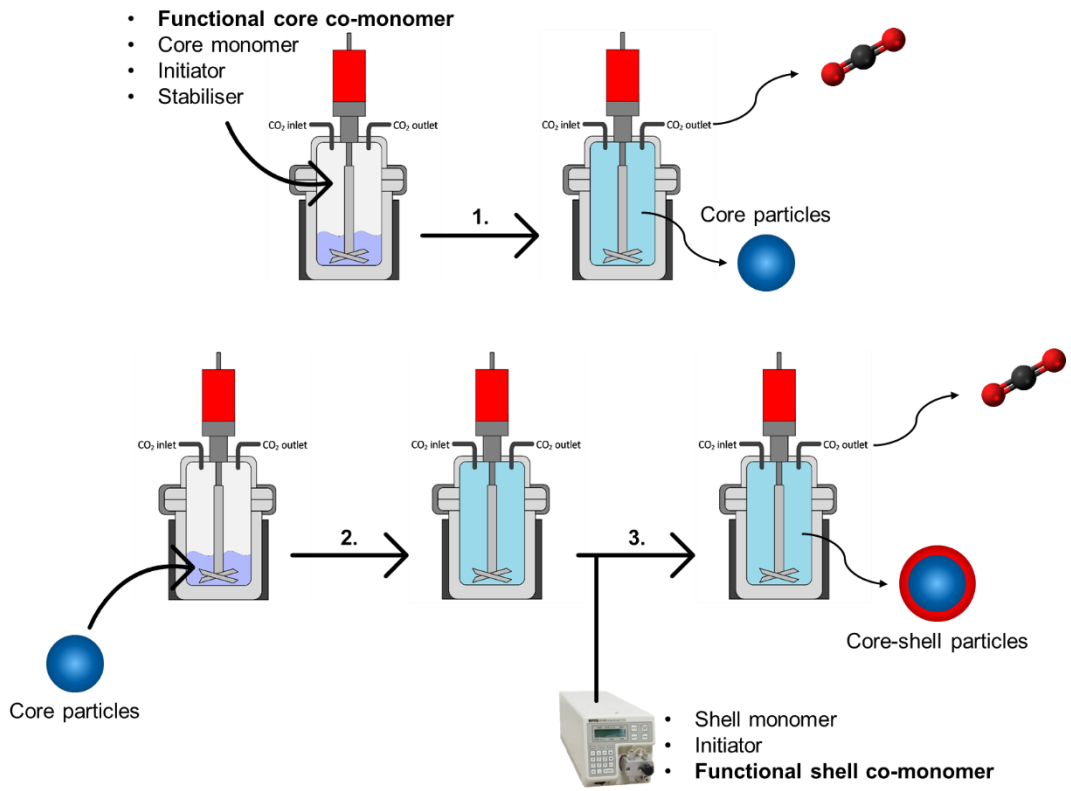


Figure 5.43 Graphical outline of the two-pot core-shell synthesis process with added functional co-monomers, showing the production and collection of core particles, followed by the redispersion of core particles and the synthesis of the shell material. 1.) Dispersion polymerisation of core monomer mixture, 2.) redispersion of core particles in $scCO_2$, 3.) polymerisation of shell monomer mixture.

For impact modification purposes, the incorporation of a soft polymer is needed in the core. Butyl acrylate (BA), the typical monomer of choice in industrial impact modifier production, was chosen to add to the core production step (Figure 5.43, 1.). However, it was found that the addition of just 5 wt% BA, along with 0.5 wt% DVB, with regards to styrene was sufficient to inhibit particle formation, resulting in a gel like grainy paste after 48 hours of polymerisation time (Figure 5.44, left). SEM imaging showed no visible particle formation had occurred, with the formation of large smooth grains of ~0.5 mm diameter (Figure 5.44, right).



Figure 5.44 (left) Image of PS with 5 wt% BA and 0.5 wt% DVB with regards to styrene product, showing a grainy gel formed around the stirrer shaft. (right) SEM images of PS with 5 wt% BA and 0.5 wt% DVB, confirming no nanoparticles were formed.

As BA was found to disrupt the PS particle formation, we attempted to form a crosslinked BA layer between the crosslinked PS core and PMMA shell. This was done by redispersing 4 g of crosslinked PS particles, injecting 4 g of BA and 0.5 wt% AMA with regards to monomer, before injecting 2g of MMA with 1 wt% AIBN relative to MMA to form the shell. The product formed was a paste of PS particles in PBA and PMMA material, that was insoluble for any NMR analysis (Figure 5.45). From solid content analysis, conversion was estimated to be around 80 percent. SEM analysis showed the presence of PS particles embedded in unstructured polymer, showing the loss of core-shell control with the addition of BA into the method (Figure 5.45). We hypothesise that the low T_g of BA (-70 °C)[189] and its higher plasticisation in $scCO_2$[39] make the polymer to unstable to settle into a core-shell structure.[101]

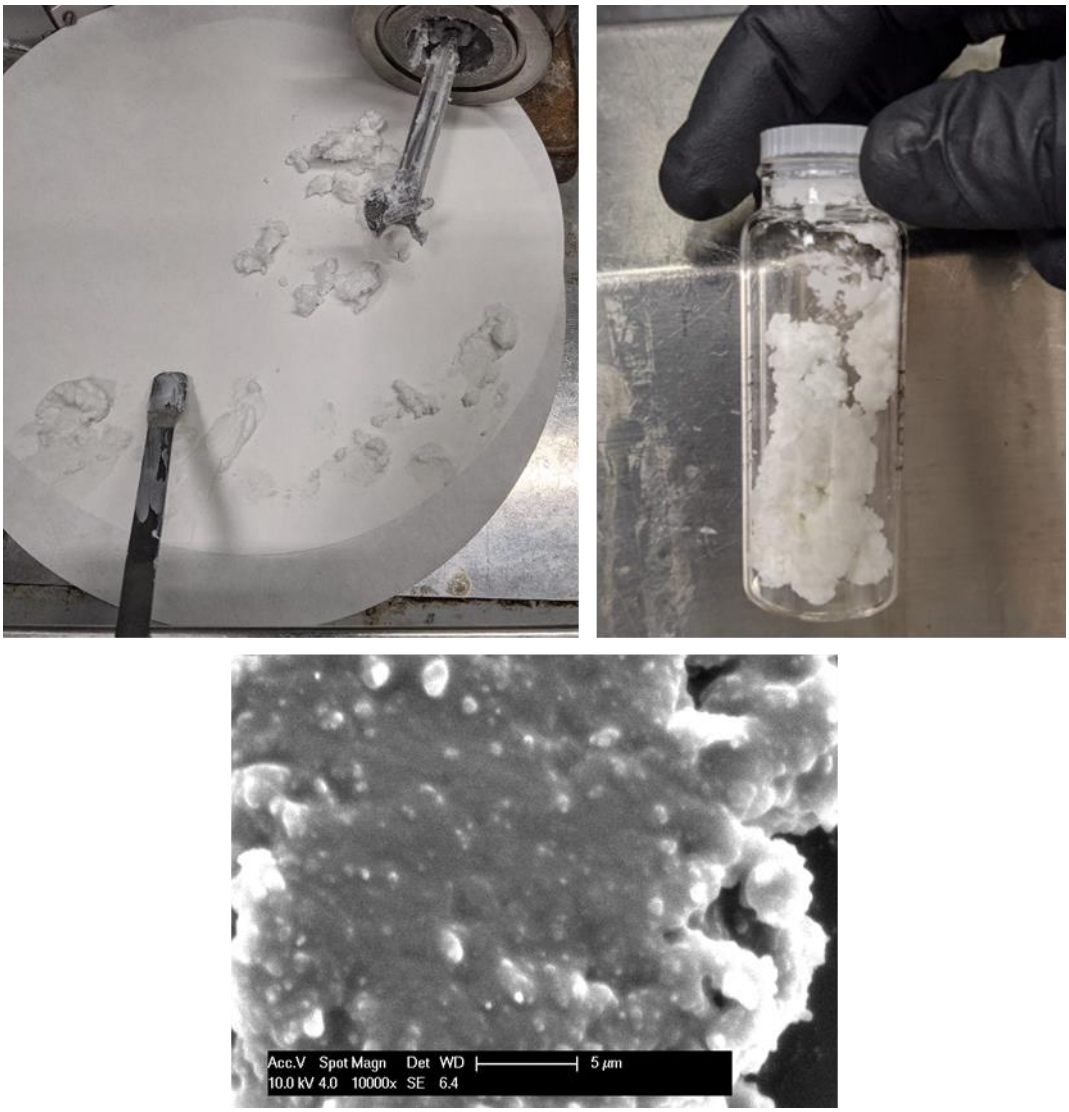


Figure 5.45 (top) Pictures showing the formed paste of 4 g of crosslinked PS particles, with 4 g of BA with 1 wt% AIBN and 0.5 wt% AMA with regards to monomer, and 2g of MMA. (bottom) SEM image of the formed product, showing crosslinked PS particles in an unstructured polymer matrix of PBA and PMMA.

To provide the potential for adding responsiveness to the shell of the synthesised PS:PMMA core-shell particles, desirable for agricultural and drug delivery applications, the addition of a water-soluble component was explored. First, the addition of 10 wt% HEMA to the MMA injection was attempted. We hoped that the higher T_g of PHEMA (60 °C)[190] compared to PBA would allow for core-shell formation.

This however resulted in large agglomerates forming instead of the desired core-shell system (Figure 5.46).

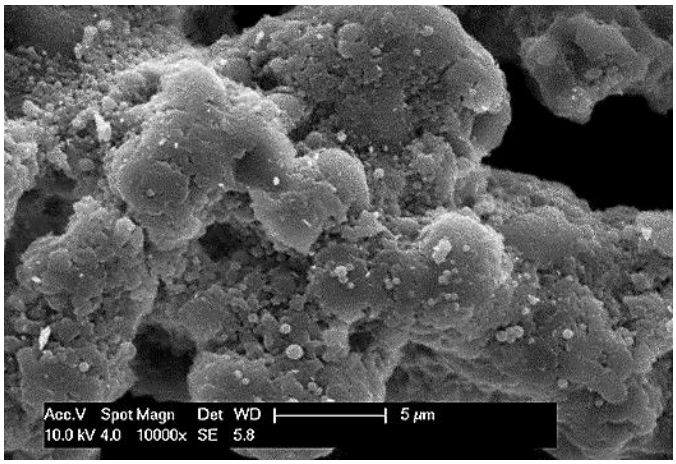


Figure 5.46 SEM image of PS Particles within an unstructured matrix of MMA with 10 wt% HEMA, showing that HEMA addition has disrupted the core-shell particle formation seen previously with this reaction method.

To maintain core-shell morphology with the addition of a functional monomer, the functional element may need to be more susceptible to PDMS-MA stabilisation. BA and HEMA both form unstructured polymer monoliths in the presence of PDMS-MA, while PS and PMMA can form stable particles. A copolymer particle of PS and PMMA could also be synthesised, showing that adding a compatible comonomer can work. To that end, the homopolymerisation of NIPAM with 20 wt% PDMS-MA was attempted, to assess its viability as a functional monomer in the core-shell method. NIPAM is widely researched in the nanogel field, possessing temperature dependent water solubility. Additionally, the T_g of PNIPAM is 132 °C,[191] well above that of BA and HEMA, and near that of PMMA, .

NIPAM was first confirmed to be soluble in $scCO_2$ above 125 bar and 65 °C (Figure 5.47). NIPAM was polymerised following the standard dispersion polymerisation

procedure (10g NIPAM, 20 wt% PDMS-MA, 1 wt% AIBN) and was found via NMR to reach conversion >90% after 4 hours of reaction time (Figure 5.48).



Figure 5.47 viewcell images of NIPAM in $scCO_2$, showing the solid material in the cell (left), the material dissolved at 130 bar (middle), and the cloud point of NIPAM at 125 bar and 65 °C (right).

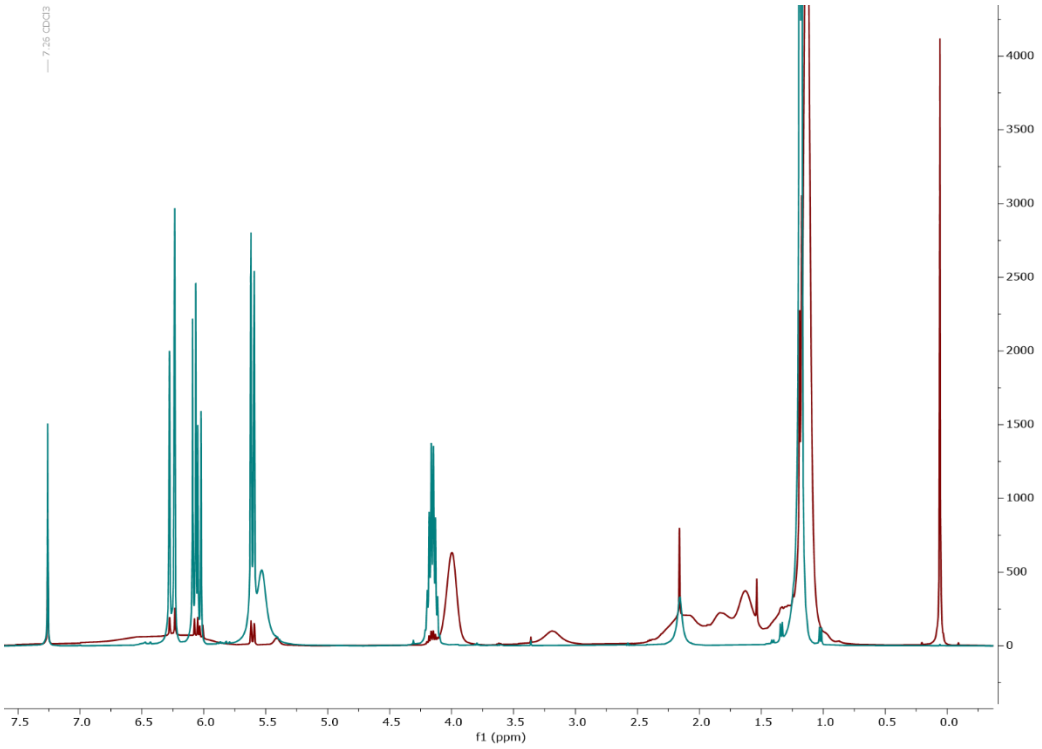


Figure 5.48 NMR spectrum of NIPAM (blue) and PNIPAM (red). Conversion can be determined from the peak at 4.2 ppm originating from the monomer and the peak at 4.0 ppm from the polymer.

SEM of the product showed that while particles had been formed, there was significant fusing (Figure 5.49).

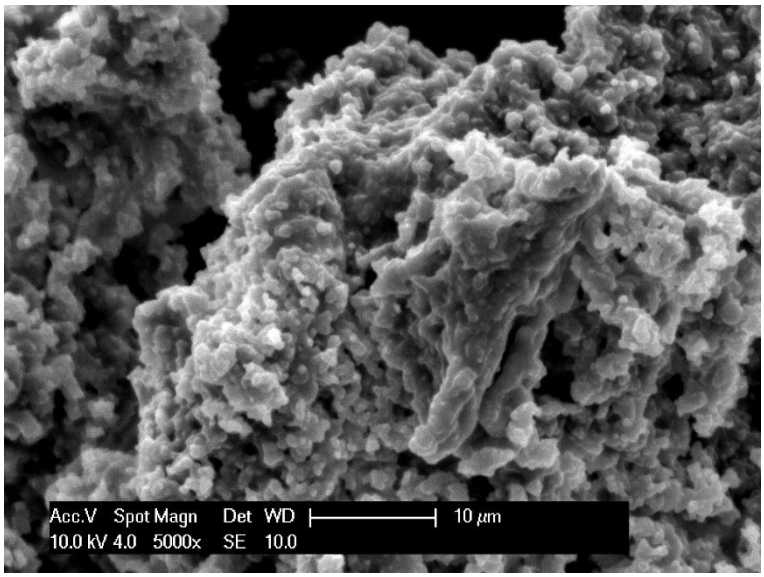


Figure 5.49 SEM image of PNIPAM particles produced in $scCO_2$ using 20 wt% PDMS-MA as stabiliser.

The formed PNIPAM was shown to dissolve in water, as well as display its characteristic temperature dependent solubility, crashing out of water at 40 °C (Figure 5.50).

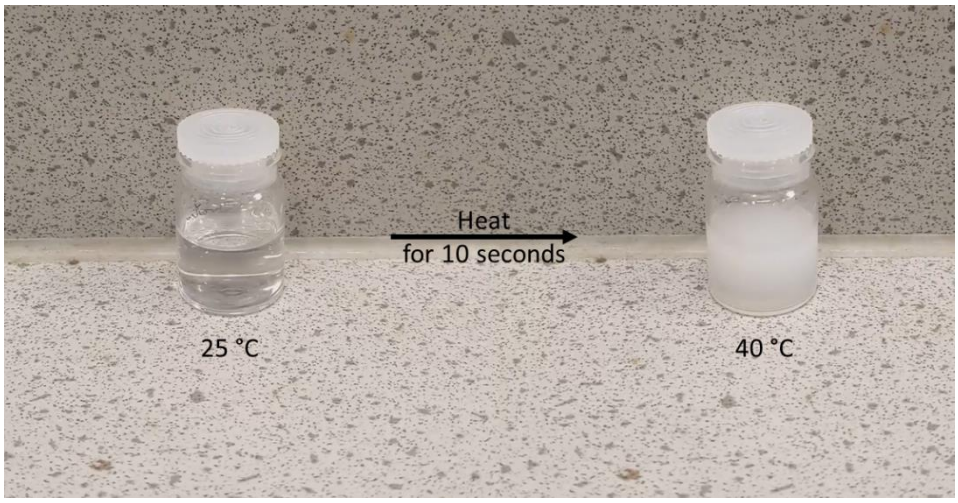


Figure 5.50 PNIPAM dissolved in water (left) and PNIPAM crashing out of solution upon heating above 40 °C.

As NIPAM was found to be more suitable for the dispersion conditions used throughout this work, its copolymerisation with MMA was conducted. This again

produced a free-flowing powder, with SEM confirming the production of discrete particles (Figure 5.51).

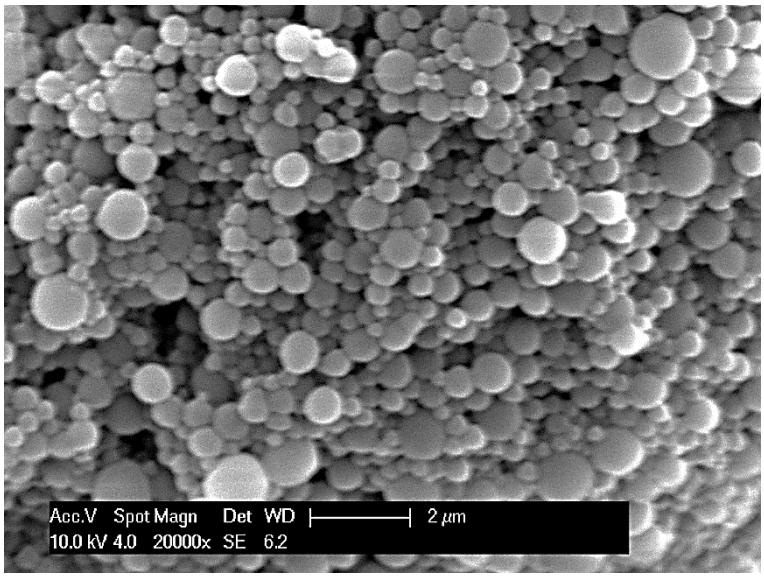


Figure 5.51 SEM image of P(NIPAM-co-MMA), confirming the formation of discrete particles.

With NIPAM showing the potential to form stable dispersion particles in $scCO_2$, and PNIPAM being a desired polymer within core-shell nanogel research, further work towards the incorporation of this molecule in the core-shell system could provide a route towards the commercialisation of the developed core-shell synthesis method.

5.6 Conclusions

The production of core-shell structured particles has many challenges but opens the door to a wide range of valuable applications. In this chapter we showed the first ever synthesis of multi material core-shell particles in $scCO_2$. Building on previously gained knowledge, the redispersion of PS particles and subsequent addition of a PMMA shell was achieved. The method was then developed further to allow for large variations in both core and shell thickness, allowing the production of tailored particles within a broad particle size range.

The capacity to add crosslinking, affecting phase stability and solubility, was shown in both core and shell layers, again expanding on the valuable structures that can be attained with the developed method. The effect of more chemically different comonomers was briefly explored, demonstrating the sensitivity of the system to this. While the introduction of some useful comonomers at ≥10 wt% disrupted the formation of the core-shell particles, the successful inclusion of crosslinkers ≤1 wt% shows the system can include small amounts of guest molecules without loss of morphology control. Additionally, the production of P(MMA-co-S) and P(MMA-co-NIPAM) particles shows the potential for achieving substantial blending of suitable monomer species within the dispersion system.

Chapter 6

Conclusions and Future Work

6.1 Conclusions

The aim of this thesis was to assess the commercial viability of using $scCO_2$ as a solvent in dispersion polymerisations. More specifically, the goal was to assess and assure reproducibility, then explore the possibility of producing dispersion particles with useful core-shell morphology for commercial applications.

After the introductory chapter, three main goals were set out to achieve the overall aim:

- Develop a reliable and universally applicable monitoring system to assess reproducibility of dispersion polymerisations.
- Improve polymerisation reproducibility and reaction conditions to maximise reactor output.
- Apply knowledge to develop core-shell particles through dispersion polymerisation.

Chapter 3 addressed the first point by first outlining reaction monitoring in conventional solvents and the lack of equivalent monitoring capability in $scCO_2$. A novel and reliable monitoring system for polymerisations in $scCO_2$ was then developed to address this shortcoming, through the on-line collection of a representative reaction sample. This sampling system was tested on a range of known polymerisations, displaying its versatile applicability. A kinetic description of the free radical dispersion polymerisation of MMA was developed from the acquired monitoring data, giving a better insight into the polymerisation mechanism and locus (Figure 6.1).

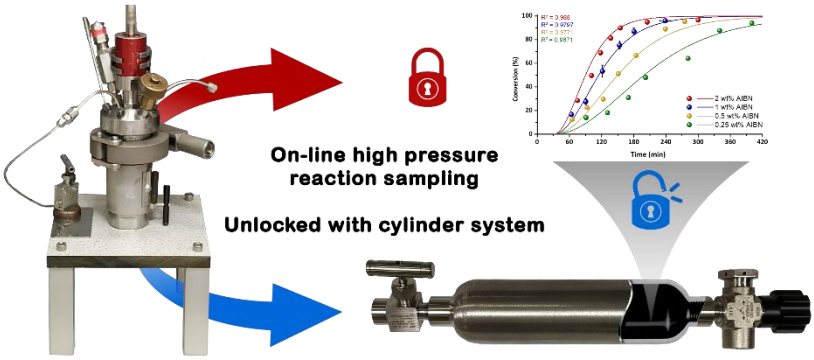


Figure 6.1 Graphical abstract of Chapter 3, highlighting the sampling cylinder system developed for on-line reaction monitoring in $scCO_2$ and the kinetic insights this has unlocked.

Chapter 4 built on the knowledge gained in Chapter 3 to address the second point of optimising free radical dispersion polymerisations and maximising reactor output in $scCO_2$. The effect of component concentrations and solvent strength on dispersion polymerisations was analysed, and the autoclave setup was altered to improve reproducibility. The effect of the uniquely variable density of supercritical fluids was exploited to unlock a different way of controlling particle size in a dispersion, ultimately leading to a vast expansion of the attainable particle size range and giving more intricate control and understanding (Figure 6.2).

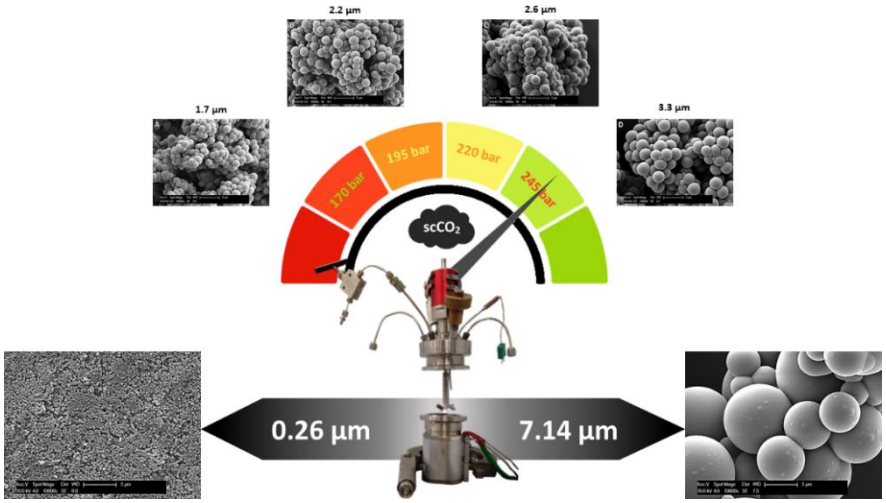


Figure 6.2 Graphical abstract of Chapter 4, highlighting the effect of pressure on particle size and the attainable particle size range in the free radical dispersion polymerisation of MMA.

Finally, Chapter 5 addressed the last point of producing core-shell particles in $scCO_2$, exploiting the gained knowledge of previous chapters to produce true core-shell polymer particles in $scCO_2$ for the first time (Figure 6.3).

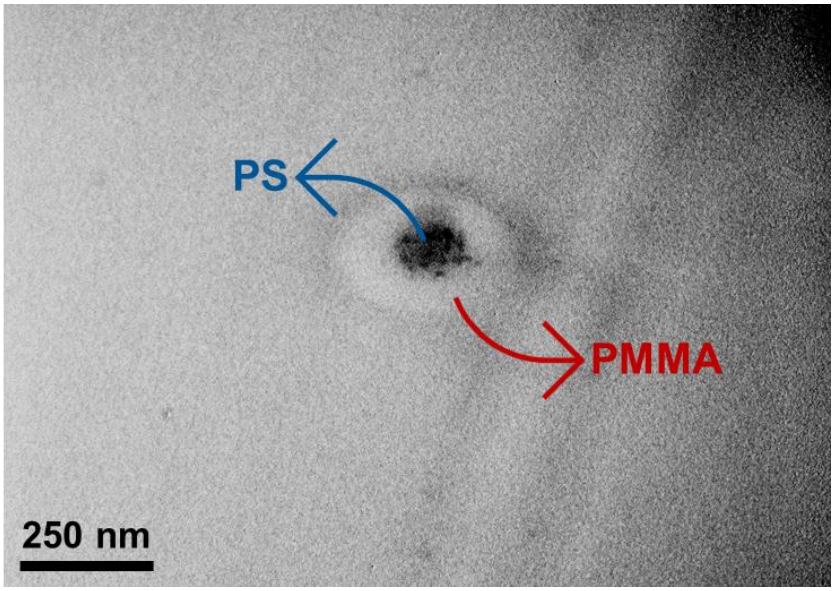


Figure 6.3 TEM image of 1:1 mass ratio PS:PMMA core-shell particle section, stained with RuO_4, showing the desired core-shell morphology. Staining is hosted in the aromatic ring of styrene, causing it to appear black in the images.

PS:PMMA core-shell particles of varying size and layer thickness were synthesised and analysed in detail (Figure 6.4). The possibilities and limitations of the core-shell polymerisation technique were then explored through the introduction of comonomers in both phases of the core-shell system. While limitations of the system were outlined, a clear framework for successful synthesis was found, highlighting the potential to produce core-shell particles with unique properties for commercial avenues.

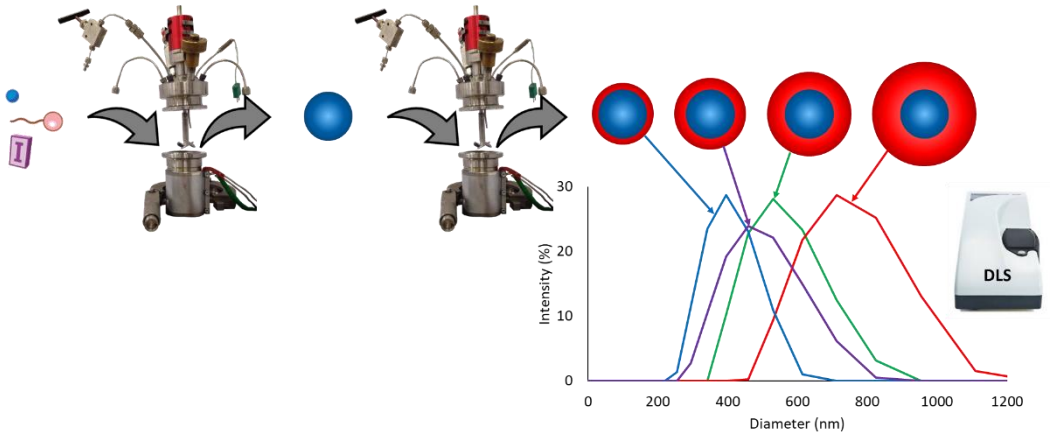


Figure 6.4 Graphical abstract of chapter 5, highlighting the first ever production of core-shell particles in $scCO_2$ and the ability to produce particles with varied feature size.

6.2 Future work

Significant strides towards the use of $scCO_2$ as a solvent for core-shell particle synthesis were achieved in this thesis. More work is however needed to convince industry of the implementation of such a novel system.

Firstly, further research will be needed into the precise synthesis of functionalised core-shell particles with specific target applications in mind, such as microgels for drug delivery or tailored agricultural systems. While this thesis provides a solid framework for core-shell particle synthesis, impact modifier synthesis with soft polymer species proved unattainable. Further research into temperature responsive NIPAM containing core-shell particles could provide an exciting new avenue towards commercial core-shell particle production.

Achieving core-shell structures with alternate monomers and functionalities may also require the use of different stabilisers, tailored to the monomers and the end application simultaneously. The use of stabilisers containing stimuli responsive

monomers such as acrylic acid could add further unique properties to core-shell particles, further enhancing their commercial applicability and value.

Secondly, while the process of producing PS:PMMA core-shell particles was proven to be controllable, it is still quite slow. The two-pot method allows for better analysis of the core particles prior to shell addition but delays the process significantly, due to the collection and redispersion of the core particles. Optimisation of this process would be key to maximising output and profitability in commercial applications, and this will be important for any further research in this area. The developed sampling system could help in this regard, as separate collection of core material for analysis can largely be bypassed. It has been shown that the core particles can be produced with 6 g of styrene, and it has been shown that there is space to inject a further 6 g of material within the safe working parameters of the reactor. The one-pot production of 1:1 core-shell particles should therefore be possible but would require investigation and optimisation.

Finally, from a fundamental chemistry side, in-situ SAXS or SANS analysis of the shell polymerisation step could provide clear kinetic analysis of its growth. This might give more insight into the polymerisation system and the parameters affecting it, and it could show the potential for making thinner shell layers required in many applications.

Appendix

Placement at Kaneka Belgium NV

The following section will summarise a research project into the production of a functionally enhanced core-shell impact modifier through free radical emulsion polymerisation. The work was conducted during a 10-week placement at Kaneka in the summer of 2020.

Project aim

The goal of this project is to improve the impact resistance of PVC window profiles by altering the core-shell structure of an acrylic impact modifier (AIM) currently used in this application. The current AIM consists of a crosslinked PBA core with a PMMA shell and confers good impact improvement in the bulk of PVC window profiles, though a clear weakness has been identified at the corner weld in the final product (Figure 0.1).

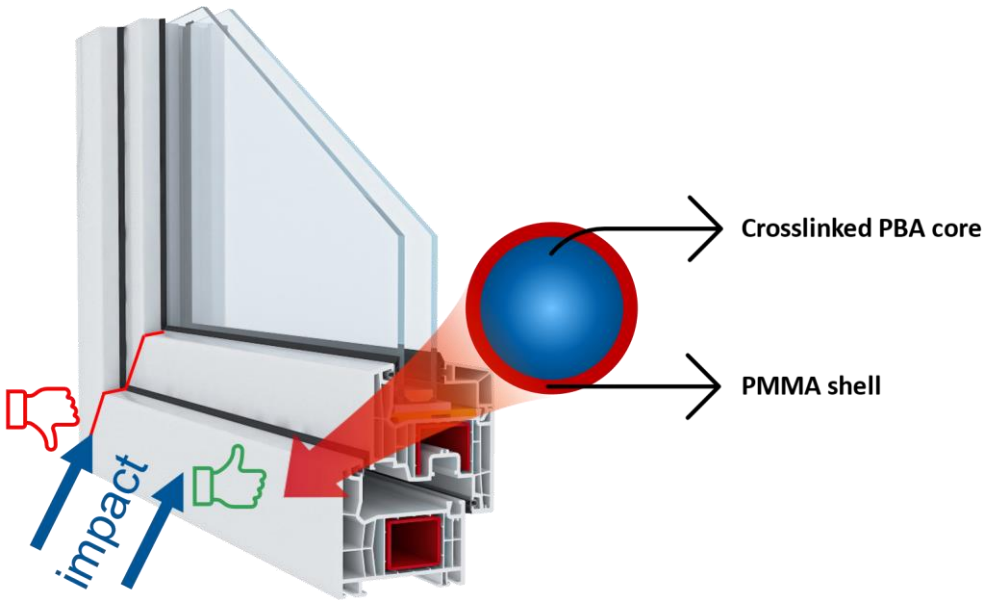


Figure 0.1 Representation of a PBA:PMMA core-shell impact modifier incorporated into a PVC based window profile, highlighting the improved impact resistance of the bulk material and the weakness at the weld point.

This weakness is thought to be caused by the high temperatures used to form the corner weld after extrusion, resulting in the remelting of the PVC matrix. As the PMMA shell of the impact modifier has already dissipated during extrusion, the exposed PBA core can dislodge during welding, resulting in a loss of impact resistance.

The proposed solution for this dislodging is the incorporation of a functional monomer, that will be referred to as monomer X, onto the outer layer of the PBA core, that can react with PVC at elevated temperature, thus anchoring the impact modifier into position upon welding.

Production of PBA:P(X):PMMA core-shell particles for impact modification

Due to the higher cost of monomer X compared to BA and MMA, the amount of monomer added to the base recipe needed to be minimised. It was decided that an interlayer containing <10 wt% of monomer X would be added between core and shell. A first series of polymerisations was conducted to test the effect of varying monomer X concentration. Following this, a series of polymerisations was conducted to test the effect of varying the copolymer material in the layer containing monomer X. In total 6 novel impact modifiers were produced, alongside 2 reference impact modifiers following the current commercial recipe (Figure 0.2).

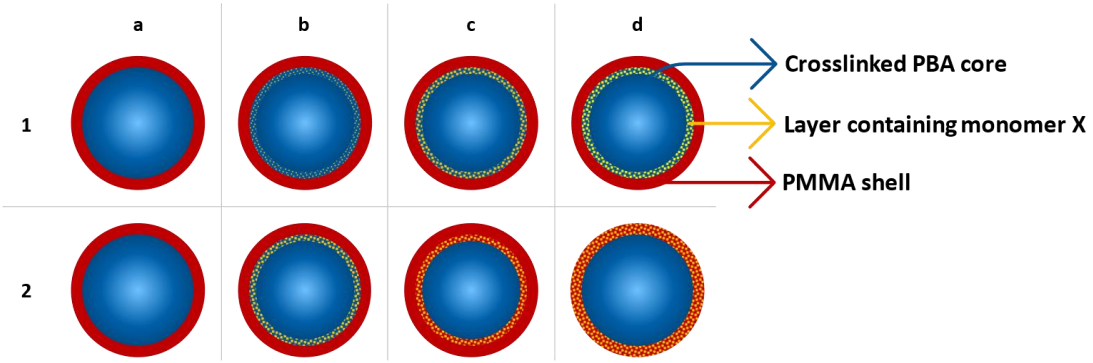


Figure 0.2 Synthesised impact modifier structures. Red: PMMA, Blue: PBA, yellow: P(X). 1.a: reference impact modifier, 1.b-1.d: 1.a with monomer X incorporated at increasing wt% loadings in outer core layer, 2.a: reference impact modifier, 2.b: 2.a with P(BA-co-X) as outer core material, 2.c: 2.a with P(MMA-co-X) as outer core material, 2.d: 2.a with P(MMA-co-X) as shell material.

Latex synthesis through emulsion polymerisation

In a typical emulsion polymerisation, water and stabiliser were added to a 5 l glass reactor with mechanical stirring and a baffle system, to assure turbulent mixing (Figure 0.3). The headspace of the reactor was kept under nitrogen flow to avoid oxygen ingress. After heating to reaction conditions, a first loading of BA and crosslinker was added. Initiator was added to the reactor, forming PBA core particles. During polymerisation, additional BA was injected to grow the formed particles further (semi-batch process). When polymer conversion was sufficiently high, the functional layer containing monomer X was formed by injecting the desired monomer mixture. Finally, MMA was injected to form the shell, followed by several initiator doses to remove residual monomer to attain a stable latex.



Figure 0.3 Emulsion polymerisation setup, featuring 4 glass reactors with mechanical stirring in a heated water bath. Monomer injection systems can be seen on either side of the reactor vessel.

Polymer latex analysis

Polymerisation monitoring was achieved through simple solid content analysis preceding every injection stage of the polymerisation. Solid content was determined by removing a known volume of the reacting latex, depositing it in a weighted cotton pad, drying of the sample, and weighing the amount of formed solid. This will give a clear estimate of conversion, indicating if the emulsion system functioned correctly.

Gas chromatography (GC) was used to determine residual monomer content prior to every monomer injection. This formed an essential part of the research, as residual monomers will induce blending/grafting between successive layers in the core-shell particle. It is essential for particle stability and end application performance that there is a slight grafting between layers, as it assures particle integrity. The addition of monomer X into the polymerisation had profound effects on the residual monomer content, meaning reaction times needed to be changed to assure similar grafting of the functionalised core-shell particles.

UV analysis was used to determine final particle size. Using a known standard curve, serial dilutions of the latex were analysed for absorbance at a fixed wavelength using a UV spectrometer.

Latex drying to attain impact modifying powder

Because impact modifiers are sold as a dry powder, the latex needs to be dried after emulsion polymerisation. There are two techniques used commercially for this, spray drying and chemical coagulation. Spray drying is a very energy intensive procedure, where the latex is sprayed in a large, heated chamber to evaporate the solvent. Chemical coagulation is a more intricate method, where destabilising chemicals are added to the latex, causing the stable emulsion to collapse. This results in the sedimentation of particle clusters, that can then be restabilised and recovered through centrifugation.

During chemical coagulation it is essential to form particle clusters of the correct size, as over-coagulation will result in a grainy product that cannot perform in the end application. The final cluster size must also be sufficiently large to avoid static build-up in the bulk powder after drying.

The chemical coagulation process was found to be generally unaffected by the addition of monomer X into the core-shell latex recipe. The main factor was found to be the time between onset of coagulation and the addition of the restabilising component. It was observed that waiting longer resulted in the formation of 800-micron sized clusters, that cannot disperse during final processing (Figure 0.4). clusters below 400 micron were desired and could be achieved with the functionalised core-shell particles.

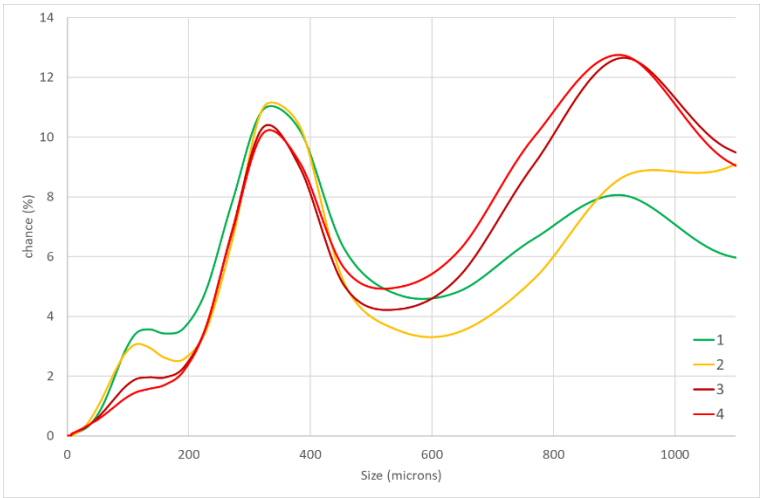


Figure 0.4 Particle size analysis of latexes treated by chemical coagulation at increasing coagulation times (1 to 4), showing that longer coagulation time results in increased cluster formation above 500 micron.

After chemical coagulation, the core-shell powders were recovered by centrifuging the mixture, then drying the solid until residual moisture content was below a desired threshold. The dry core-shell material was then put through a blender to achieve a free-flowing powder, ready for incorporation in commercial PVC blends(Figure 0.5).

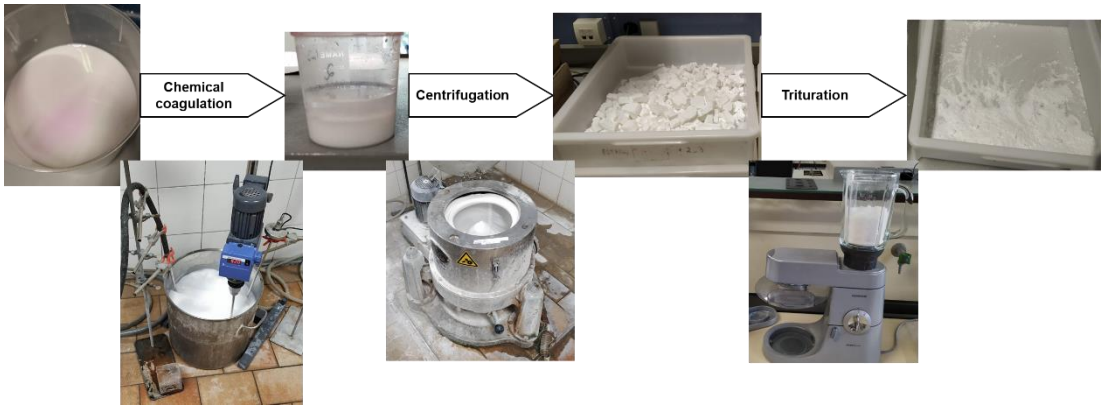


Figure 0.5 Summary of process to achieve free-flowing powder from latex, showing chemical coagulation to form clustered sediments (left), centrifugation to remove water (centre), and trituration to break down the formed solid into a fine powder (right).

Production of commercial PVC thick film blends

Commercial PVC blends for window profiles contain a range of additives, such as impact modifiers, processing aids, stabilisers, plasticisers, lubricants, and fillers. Dosing of various additives depends on end-application, but impact modifiers typically make up less than 10 wt% of the final material. Within the research department at Kaneka, commercial blends are reproduced and extruded into thick films using a Thermo scientific HAAKE PolyLab QC extruder system fitted with a single slot sheet die (Figure 0.6).



Figure 0.6 Thermo scientific HAAKE PolyLab QC extruder with sheet/thick film die. Plastic mixture is added to the hopper, feeding into the heated extruder chamber, where the plastic is pushed out through the die to form thick films of the plastic blend.

Prior to thick film production, the effect of novel additives on the melt extrusion process must be tested. PVC is known to show a gelling effect in the melt phase under extrusion, and this can be heavily affected by additives in the system.[166, 167, 192-194] Gelling of molten PVC results in a large viscosity increase, that would harm the extrusion process, and must be avoided (Figure 0.7).

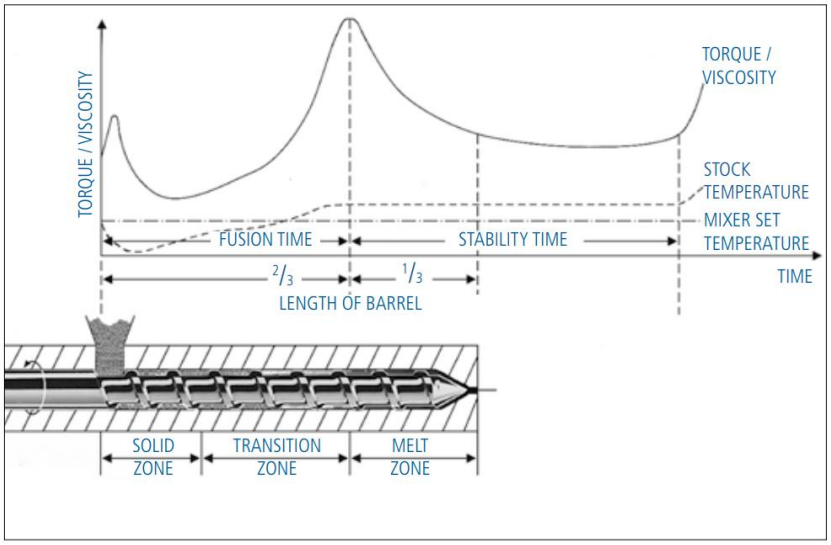


Figure 0.7 Viscosity as a function of time in a production extruder, showing the different phases observed during extrusion. The initial fusion time must be overcome during extrusion to assure a homogeneous product, while the stability time may not be exceeded, as the viscosity spike thereafter will reduce the product quality.

The time/temperature at which gelling occurs can be analysed via Rheometry in a Brabender Plastograph EC Plus (Figure 0.8). By measuring the torque experienced by rotating mixing blades surrounded by the sample, while heating at a constant rate, melting, mixing, and subsequent gelling can be observed.

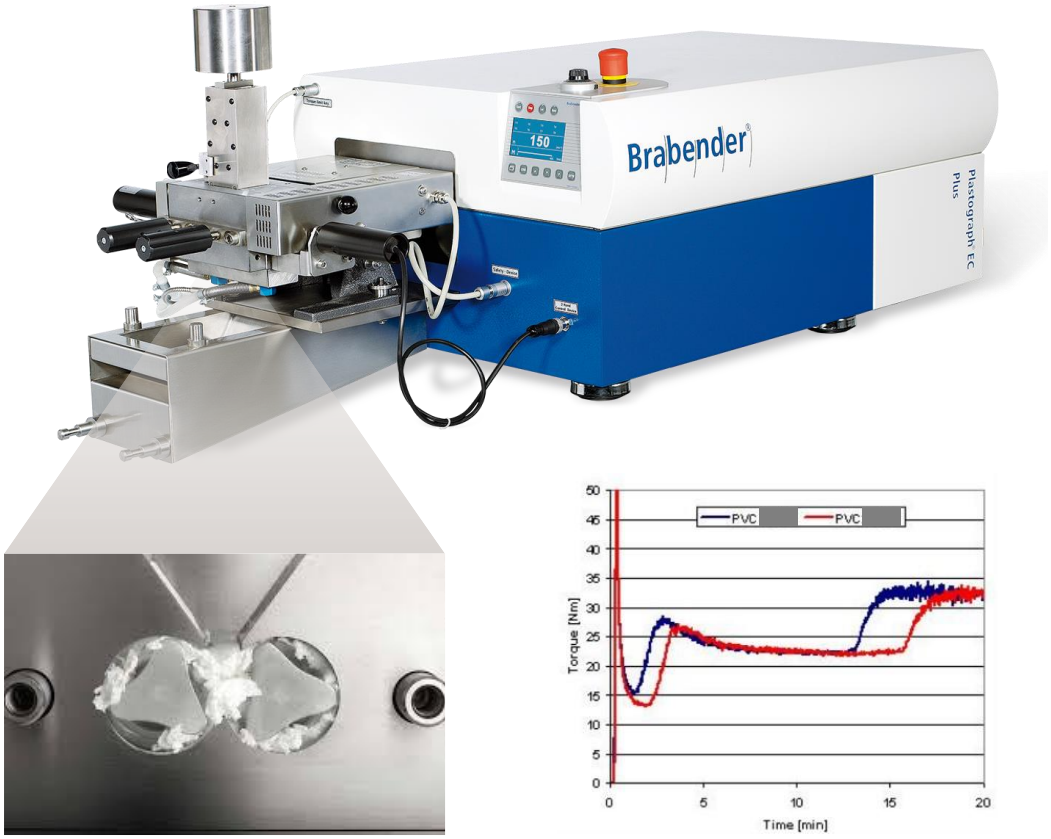


Figure 0.8 Brabender Plastograph EC Plus, with inset view of mixing blades (left). Second inset shows a typical trace of torque in function of time for PVC blends, showing effect of varying additives (right).

The formed core-shell impact modifiers with monomer X functionalisation (Figure 0.2) were incorporated into PVC test films, following a commercial standard blend recipe for PVC window profiles. Brabender gelation tests were conducted to assure the correct extrusion conditions were used, prior to the production of thick films containing functionalised impact modifier (Figure 0.9).



Figure 0.9 8 series of PVC thick films, containing the synthesised functionalised impact modifier particles (Figure 0.2), produced using a Thermo scientific HAAKE PolyLab QC extruder (Figure 0.6), in commercial standard blends.

Testing of thick films

The bulk impact resistance of the formed thick films was first tested by Charpy V notch impact test (Figure 0.10). During this test, a weighted hammer is swung through a thick film sample and the stress and strain of the sample at break are measured.

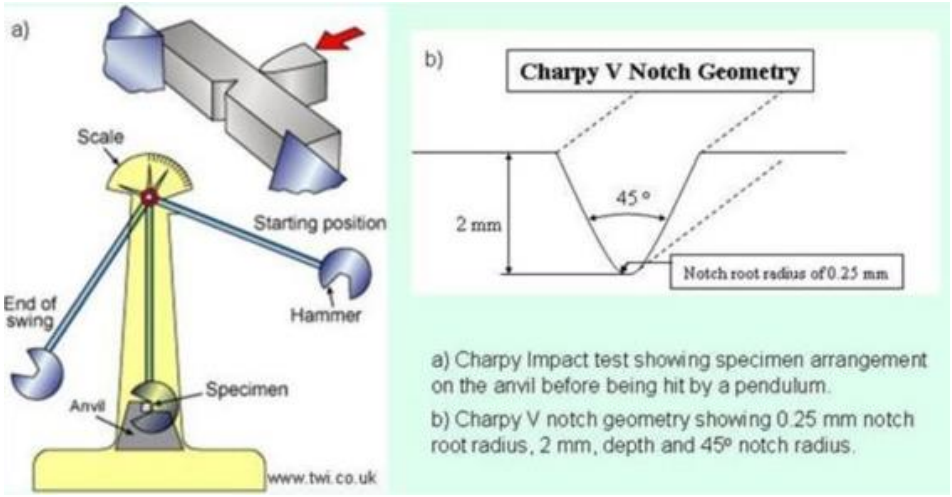


Figure 0.10 graphical summary of a Charpy V notch impact test, showing analytical setup (a), and typical notch geometry (b).[195]

SEM was also used to analyse thick films of PVC after Charpy impact testing. The break surface was cut from the film and mounted on an SEM stub using carbon tape (Figure 0.11). To avoid charge build-up, a gold coating was applied to samples prior to imaging with a JEOL JSM-6010LA analytical scanning electron microscope. SEM provided visual insight into the anchoring efficiency of the impact modifier particles at break, essential for good impact absorption.

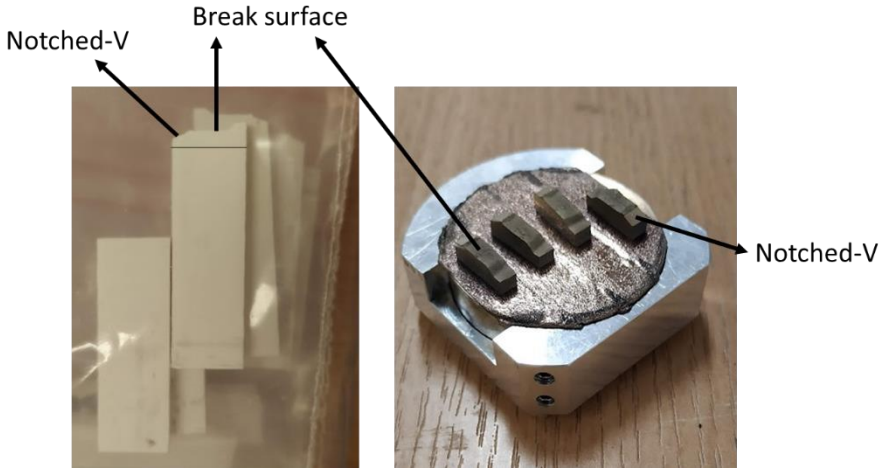


Figure 0.11 Thick films containing functionalised impact modifier after Charpy V notch impact test (left), and break surface samples mounted for SEM analysis (right).

Finally, identical film samples were welded together using a profile welder at 250 °C and analysed using the Charpy impact test on the weld area (Figure 0.12). The welded films break apart at the weld point, as this is the weakest point of the sample.

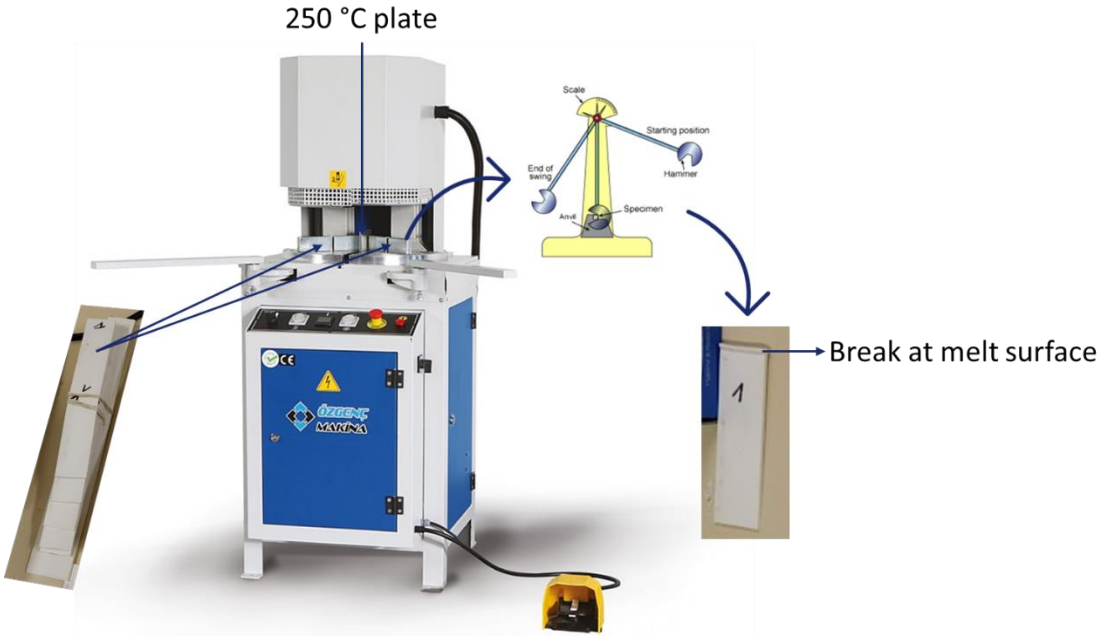


Figure 0.12 PVC film welding and analysis. From left to right: 2 identical films are placed in the PVC welder and welded together at 250 °C by contact with a heated plate. The welded film is then mounted in a Charpy impact test, where the film will break at the melt surface as this is the weakest point.

Charpy impact analysis of the films containing functionalised impact modifier containing monomer X showed a higher stress and strain at break compared to samples with the current commercial impact modifier (Figure 0.13). While the added functional layer improved impact resistance, the amount of functional monomer added had no apparent effect.

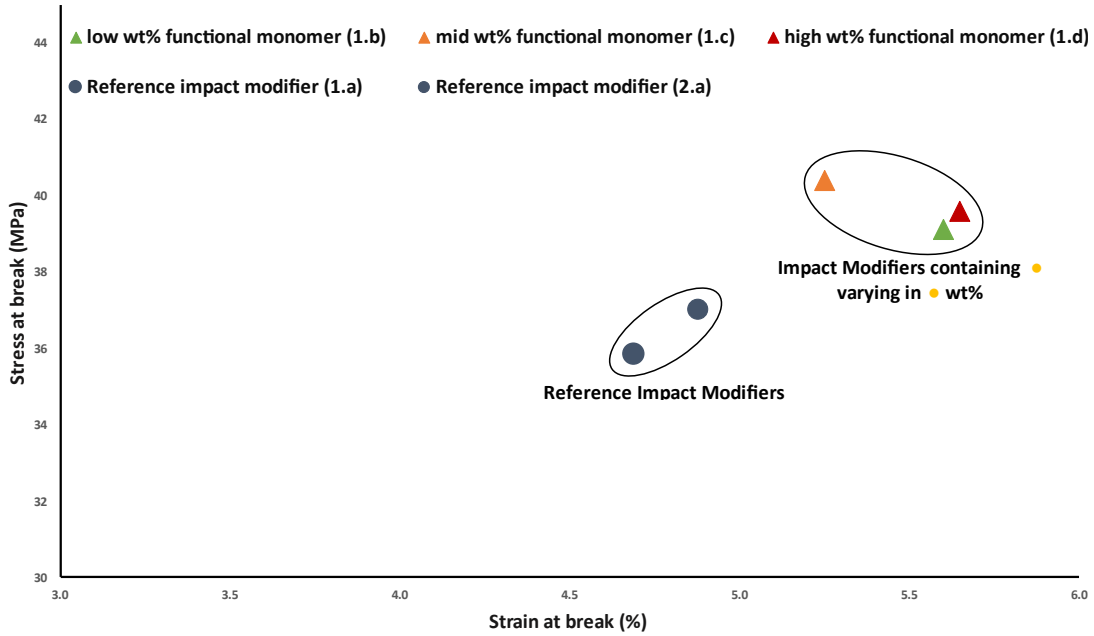


Figure 0.13 Measured stress and strain at break for PVC films with monomer X functionalised core-shell impact modifier particles (Figure 0.2). 1.a and 2.a are identical commercial impact modifiers, while 1.b, 1.c, and 1.d contain functionalised core-shell impact modifiers varying in monomer X wt%.

Placement conclusions

The goals of the placement overall were achieved, as novel impact modifiers with added functionality were produced and tested in a commercial product. From the impact test results it was concluded that the inclusion of a minimum amount of monomer X was sufficient to induce better anchoring of the impact absorbing particles in the PVC matrix, and the research had commercial potential pending further testing.

Beyond the project itself, a clear insight into commercial impact modifier production was gained. The intricate complexity of the process was notable, such as the amount of separate monomer additions in the performed emulsion polymerisations, the array of stabilisers and initiators used in a single recipe, the complex and sensitive drying process, and the complex compounding and extrusion methods. Conversely,

it must be noted that a plethora of different recipes are used to produce core-shell particles, highlighting that a vast range of core-shell particle structures can find a commercially viable market.

Reaction list

In the following table is a summary of reactions discussed in the thesis, including lab code, notable reaction conditions and analysis output, to aid with auditing and continuation of any work. The first column contains a link to the location in the thesis where the data is discussed, while the second column contains the code used for the reaction in lab notes and sample storage. Any analytical values were determined following the respective procedures detailed during Chapter 2 in section 2.3.

Thesis location	lab code	polymer/monomer (g)	AIBN (wt%)	PDMS-MA (wt%)	Temp. (°C)	Pressure (psi)	Stirrer rate (RPM)	HPLC initiator?	sampling?	water quench?	Conversion (%)	M_n (kg/mol)	M_w (kg/mol)	yield (%)	d_n (nm)	PSD/σ (nm)
Table 3.2 - 1	kk006	MMA - 9.36	1	5	65	3000	300	N	Y	N	98.2	105	355	89		
Table 3.2 - 2	kk007	MMA - 9.36	1	5	65	3000	300	Y	Y	N	90.4	139	387	82		
Table 3.2 - 3	kk008	MMA - 9.36	1	5	65	3000	300	Y	Y	N	96.6	161	406	85		
Table 3.1 - 1	kk009	MMA - 9.36	1	5	65	3000	300	Y	N	30 min	2.6	20	37			
Table 3.1- 4	kk010	MMA - 9.36	1	5	65	3000	300	Y	N	60 min	10.7	33	89			
Table 3.1 - 5	kk011	MMA - 9.36	1	5	65	3000	300	Y	N	60 min	9.1	35	87			
Table 3.1 - 7	kk013	MMA - 9.36	1	5	65	3000	300	Y	N	90 min	29.1	65	183			
Table 3.1 - 13	kk014	MMA - 9.36	1	5	65	3000	300	Y	N	150 min	84.8	133	323	76		
Table 3.1 - 2	kk015	MMA - 9.36	1	5	65	3000	300	Y	N	30 min	2.6	19	48			
Table 3.1 - 8	kk016	MMA - 9.36	1	5	65	3000	300	Y	N	90 min	22.3	49	157			
Table 3.1 - 14	kk017	MMA - 9.36	1	5	65	3000	300	Y	N	150 min	85.1	120	318	79		
Table 3.1 - 10	kk018	MMA - 9.36	1	5	65	3000	300	Y	N	120 min	52.5	86	254			
Table 3.1 - 15	kk019	MMA - 9.36	1	5	65	3000	300	Y	N	150 min	85.9	124	313	85	2049	1.07
Table 3.1 - 3	kk020	MMA - 9.36	1	5	65	3000	300	Y	N	30 min	2.9	20	43			
Table 3.1 - 9	kk021	MMA - 9.36	1	5	65	3000	300	Y	N	90 min	26.6	58	173			
Table 3.1 - 6	kk022	MMA - 9.36	1	5	65	3000	300	Y	N	60 min	8.5	28	73			
Table 3.1 - 11	kk023	MMA - 9.36	1	5	65	3000	300	Y	N	120 min	51.2	85	248			
Table 3.1 - 12	kk024	MMA - 9.36	1	5	65	3000	300	Y	N	120 min	52.3	93	252			
Table 4.3	kk025	N	N	N	65	14	0	N	N	N						
Table 3.1 - 17	kk027	MMA - 9.36	1	5	65	3000	300	Y	N	210 min	94.9	158	334		2566	1.11
Table 3.1 - 18 **Table 4.2 - 2**	kk028	MMA - 9.36	1	5	65	3000	300	Y	N	240 min	96.0	168	343		2562	1.05
Table 3.1 - 16	kk029	MMA - 9.36	1	5	65	3000	300	Y	N	180 min	93.2	167	346	83	2578	1.07
Table 4.5 - 4 **Table 4.6 - 4**	kk032	MMA - 9.36	1	5	65	3000	300	Y	N	180 min	92.1	151	386	82	2613	1.05
Table 4.5 - 2 **Table 4.6 - 2**	kk033	MMA - 9.36	1	5	65	2500	300	Y	N	180 min	92.4	150	392	86	1683	1.057
Table 4.5 - 1 **Table 4.6 - 1**	kk034	MMA - 9.36	1	5	65	2100	300	Y	N	180 min	22.7	24	110	57		
Table 4.5 - 3 **Table 4.6 - 3**	kk035	MMA - 9.36	1	5	65	2800	300	Y	N	180 min	94.7	166	398	87	2183	1.061
Table 4.5 - 5	kk036	MMA - 9.36	1	5	65	3600	300	Y	N	180 min	93.5	154	366	85	3292	1.022

Thesis location	lab code	polymer/monomer (g)	AIBN (wt%)	PDMS-MA (wt%)	Temp. (°C)	Pressure (psi)	Stirrer rate (RPM)	HPLC initiator?	sampling?	water quench?	Conversion (%)	M_n (kg/mol)	M_w (kg/mol)	yield (%)	d_n (nm)	PSD/σ (nm)
Table 4.5 - 6 Table 4.6 - 6	kk037	MMA - 9.36	1	5	65	4000	300	Y	N	180 min	90.7	135	306	73	2837	1.005
Table 4.7 - 1	kk038	MMA - 8.14	1	5	65	2500	300	Y	N	180 min	78.9	115	279	58		
Table 4.7 - 2	kk039	MMA - 8.75	1	5	65	2800	300	Y	N	180 min	84.9	141	370	73	2015	1.08
Table 4.7 - 4	kk040	MMA - 9.83	1	5	65	3600	300	Y	N	180 min	94.7	167	371	86	3186	1.008
Table 4.7 - 5	kk041	MMA - 10.16	1	5	65	4000	300	Y	N	180 min	93.4	145	336	80	2952	1.009
Table 4.5 - 7 Table 4.6 - 7	kk043	MMA - 9.36	1	5	65	4600	300	Y	N	180 min	89.9	144	315	76	2994	1.006
Table 4.10 - 2	kk048	MMA - 9.36	1	1	65	3600	300	Y	N	N	85.7	102	245	73	7144	1.52
Table 4.10 - 1	kk050	MMA - 4.68+2.34	1	20	65	2750	300	Y	N	N	93.0	89	204	83	265	1.05
Table 4.2 - 1	kk051	MMA - 9.36	1	5	65	3200	150	N	N	N	97.0	107	281	73	2062	1.07
Figure 4.19	kk052	N	N	Y	65	4000	300	N	N	N						
Table 4.2 - 3	kk053	MMA - 9.36	1	5	65	3200	600	N	N	N	98.2	158	383	92	2582	1.05
Figure 3.16	kk058	N	N	N	65	3000+	300	N	Y	N						
Table 3.4	kk063	MMA - 9.36	1	5	65	3500	300	Y	Y	N	97.1	150	365	73	2643	1.23
Table 4.4 - 2	kk064	MMA - 11.7	1	5	65	3300	300	Y	N	N	96.0	133	335	88	3263	1.04
Table 4.4 - 3	kk065	MMA - 11.7	1	5	65	3200	300	Y	N	N	96.8	109	321	89	3315	1.014
Table 4.4 - 4	kk066	MMA - 11.7	1	5	65	3200	450	Y	N	N	97.7	148	387	94	3247	1.012
Table 4.4 - 5	kk068	MMA - 14.04	1	5	65	3200	450	Y	N	N	98.1	122	318	87	2844	1.024
Table 3.5	kk069	MMA - 9.36	1	5	65	3200	300	Y	Y	N	97.0	124	313	78	2084	1.27
Table 3.5	kk070	MMA - 9.36	1	5	65	3200	300	Y	Y	N	95.7	186	319		2271	1.27
Table 4.4 - 7	kk071	MMA - 16.38	1	5	65	3200	600	Y	N	N	92.0	127	319	81	2844	1.02
Table 4.4 - 6	kk072	MMA - 14.04	1	5	65	3200	600	Y	N	N	97.7	145	378	86	2989	1.02
Table 4.4 - 8	kk073	MMA - 16.38	1	5	65	3200	600	Y	N	N	96.4	79	262	90	monolith	
Table 3.5	kk074	MMA - 9.36	1	5	65	3200	300	Y	Y	N	94.7	162	344	78	2297	1.17
Figure 4.18	kk075	MMA - 11.7+4.68	1	5	65	2800-3300	600	N	N	N	99.5	174	425	90	monolith	
Figure 4.18	kk076	MMA - 11.23+4.68	1	5	65	2900-3500	600	N	N	N	98.9	137	390	90	2409	1.04
Table 4.9 - 5	kk077	MMA - 9.36	1	5	65	3900	300	Y	N	N	97.0			91	3259	1.01
Table 4.9 - 3	kk078	MMA - 9.36	1	5	65	3300	300	Y	N	N	97.0			79	2434	1.22

Thesis location	lab code	polymer/monomer (g)	AIBN (wt%)	PDMS-MA (wt%)	Temp. (°C)	Pressure (psi)	Stirrer rate (RPM)	HPLC initiator?	sampling?	water quench?	Conversion (%)	M_n (kg/mol)	M_w (kg/mol)	yield (%)	d_n (nm)	PSD/σ (nm)
Table 4.9 - 6	kk079	MMA - 9.36	1	5	65	4200	300	Y	N	N	97.4			79	2944	1.006
Figure 3.31	kk080	AA - 2	2	0	65	2500	400	N	Y	N	95.0			91	3056	1.05
Table 3.6 - 8-14	kk086	MMA - 9.36	0.5	5	65	3200	400	Y	Y	N	95.4	300	550	75	2589	1.18/662
Table 3.6 - 1-7	kk089	MMA - 9.36	0.25	5	65	3200	400	Y	Y	N	94.1	519	846	75	2088	1.11/388
Table 3.6 - 15-21	kk090	MMA - 9.36	2	5	65	3200	400	Y	Y	N	96.7	114	173	74	1772	1.32/601
Figure 3.30 **Table 5.2 - 1**	kk097	St - 10	2	20	65	3500	400	N	Y	N	95.39	31	65	89	305	1.08/61
Table 5.1 - 4 **Table 5.2 - 2**	kk098	PS (kk096) – 5 MMA - 5	1	0	65	3500-4000	400	N	N	N	92.45 (MMA)	39	98	91	401	1.15/135
Figure 4.39	kk105	St - 13.635	2	20	65	3500	400	N	N	N	92.1			85	335/1250	2 populations
Figure 5.15	kk106	PS (kk104) – 5 MMA - 5	1	0	65	3500	400	N	Y	N						
Figure 4.40	kk107	St - 12.72	2	20	65	3500	400	N	N	N	98.0			92	345	1.06
Figure 5.15	kk108	PS (kk107) – 5 MMA - 5	1	0	65	3500	400	N	Y	N	94.5			75		
Table 5.3 - 1	kk111	St - 12.72	2	20	65	3500	400	N	N	N	97.9	18	50		373	77
Figure 5.16 **Figure 5.17**	mrg02	PS (kk111) – 1 MMA - 2	1	0	65	3500-4600	400	N	N	N	99.5				600/1500	2 populations
Table 5.3 - 3	mrg03	PS (kk111) – 1 MMA - 2	1	0	65	3500-4500	400	N	N	N	98.1	39	114		486	173
Table 5.3 - 4	mrg04	PS (kk111) – 1 MMA - 4	1	0	65	3500-4500	400	N	N	N	97.7	44	95		552	151
Table 5.3 - 5	mrg06	PS (kk111) – 1 MMA - 8	1	0	65	3500-4500	400	N	N	N	98.5	50	99		740	173
Figure 4.38	kk113	St – 10 10 vol% MeOH	2	20	65	3500	400	N	Y	N	91.9			69		
Figure 4.38	kk114	St – 10 20 vol% MeOH	2	20	65	3500	400	N	Y	N						
Table 5.5 - 1	kk115	St – 10 DVB - 1	2	20	65	3500	400	N	N	N					Monolith	
Table 5.5 - 2	kk116	St – 10 DVB 0.5	2	20	65	3500	400	N	N	N					Monolith	
Table 5.5 - 4	kk117	St - 6 DVB 0.03	2	20	65	3500	400	N	N	N					~300	
Figure 5.40	kk118	PS (kk117) - 5 MMA – 5	2	20	65	3500-4000	400	N	N	N					~400	
Table 5.5 - 5	kk119	St - 7 DVB - 0.0525	2	20	65	3500	400	N	N	N					~300	

Thesis location	lab code	polymer/monomer (g)	AIBN (wt%)	PDMS-MA (wt%)	Temp. (°C)	Pressure (psi)	Stirrer rate (RPM)	HPLC initiator?	sampling?	water quench?	Conversion (%)	M_n (kg/mol)	M_w (kg/mol)	yield (%)	d_n (nm)	PSD/σ (nm)
Figure 5.35	kk121	PMMA (kk072) – 5 St - 5	2	20	65	3500-4000	400	N	N	N					3000/200	2 populations
Table 4.8 - 4	kk124	MMA - 10	1(V70)	5	40	3200	400	N	N	N	95.1			82	2695	1.01
Table 4.8 - 1	kk126	MMA - 10	1(V70)	5	40	2000	400	N	N	N	98.8			91	1877	1.11
Figure 5.49	kk128	NIPAM - 10	1	20	65	3000-4000	400	N	N	N	93.8			87		
Figure 5.33	kk130	St - 10	2	5	65	3500	400	N	N	N	96.1				795	274
Table 4.8 - 2	kk133	MMA - 10	1(V70)	5	40	2400	400	N	N	N	98.3			90	2425	1.06
Table 4.8- 3	kk134	MMA - 10	V70 - 1	5	40	2800	400	N	N	N	97.6			91	3051	1.03
Figure 5.34	kk136	PS (kk130) - 5, MMA - 5	1	0	65	3500-4000	400	N	N	N					960	265
Figure 5.36	kk137	PMMA (kk050) - 5, St - 5	2	0	65	3500-4000	400	N	N	N						
Figure 5.42	kk138	PS (kk107) - 5, MMA - 5, AMA - 0.25	1	0	65	3500-4000	400	N	N	N						
Figure 5.12 (copolymer)	kk141	MMA - 5, St - 5	1.5	10	65	3500	400	N	N	N						
Figure 5.51	kk143	NIPAM - 5, MMA - 5	1	20	65	3500	400	N	N	N						

Chapter 7

References

1. Geyer, R.; Jambeck, J. R.; Law, K. L., Production, use, and fate of all plastics ever made. *Science Advances* 2017, *3* (7), e1700782.
2. Organisation for Economic Co-operation and Development(OECD), *Global Plastics Outlook*. 2022.
3. Millner, A.; Ollivier, H., Beliefs, Politics, and Environmental Policy. *Review of Environmental Economics and Policy* 2016, *10* (2), 226-244.
4. Wälti, S., Intergovernmental Management of Environmental Policy in the United States and the EU. In *Transatlantic Environment and Energy Politics: Comparative and International Perspectives*, Routledge: London, 2013; p 57-70.
5. Peach, J.; Eastoe, J., Supercritical carbon dioxide: a solvent like no other. *Beilstein J Org Chem* 2014, *10*, 1878-1895.
6. Boyère, C.; Jérôme, C.; Debuigne, A., Input of supercritical carbon dioxide to polymer synthesis: An overview. *European Polymer Journal* 2014, *61*, 45-63.
7. Richez, A. P.; Yow, H. N.; Biggs, S.; Cayre, O. J., Dispersion polymerization in non-polar solvent: Evolution toward emerging applications. *Progress in Polymer Science* 2013, *38* (6), 897-931.
8. Cooper, A. I., Polymer synthesis and processing using supercritical carbon dioxide. *Journal of Materials Chemistry* 2000, *10* (2), 207-234.
9. Kendall, J.; Canelas, D.; Young, J.; Desimone, J., Polymerizations in supercritical carbon dioxide. In *Chem. Rev.*, 1999; Vol. 99, p 543-563.
10. Wypych, G., Introduction. In *Handbook of Polymers (Second Edition)*, Wypych, G., Ed. ChemTec Publishing: 2016; p 1-2.
11. Hiemenz, P. C.; Lodge, T. P., *Polymer Chemistry, Second Edition*. CRC Press: 2007; p 608.
12. Mueller, P. A.; Storti, G.; Morbidelli, M., The reaction locus in supercritical carbon dioxide dispersion polymerization. The case of poly(methyl methacrylate). *Chemical Engineering Science* 2005, *60* (2), 377-397.
13. Zammit, M. D.; Davis, T. P.; Haddleton, D. M.; Suddaby, K. G., Evaluation of the Mode of Termination for a Thermally Initiated Free-Radical Polymerization via Matrix-Assisted Laser Desorption Ionization Time-of-Flight Mass Spectrometry. *Macromolecules* 1997, *30* (7), 1915-1920.
14. Guan, Z.; Combes, J. R.; Menceloglu, Y. Z.; DeSimone, J. M., Homogeneous free radical polymerizations in supercritical carbon dioxide: 2. Thermal decomposition of 2,2'-azobis(isobutyronitrile). *Macromolecules* 1993, *26* (11), 2663-2669.
15. Nesvadba, P., Radical Polymerization in Industry. In *Encyclopedia of Radicals in Chemistry, Biology and Materials*, John Wiley & Sons, Ltd.: 2012; p 1-36.
16. Szwarc, M., 'Living' Polymers. *Nature* 1956, *178* (4543), 1168-1169.
17. Braunecker, W. A.; Matyjaszewski, K., Controlled/living radical polymerization: Features, developments, and perspectives. *Progress in Polymer Science* 2007, *32* (1), 93-146.
18. Moad, G.; Rizzardo, E., Chapter 1 The History of Nitroxide-mediated Polymerization. In *Nitroxide Mediated Polymerization: From Fundamentals to Applications in Materials Science*, The Royal Society of Chemistry: 2016; p 1-44.
19. Nicolas, J.; Guillaneuf, Y.; Lefay, C.; Bertin, D.; Gigmes, D.; Charleux, B., Nitroxide-mediated polymerization. *Progress in Polymer Science* 2013, *38* (1), 63-235.

20. Matyjaszewski, K.; Spanswick, J., Atom Transfer Radical Polymerization (ATRP). In *Reference Module in Materials Science and Materials Engineering*, Elsevier: 2016.
21. Matyjaszewski, K.; Xia, J., Atom Transfer Radical Polymerization. *Chemical Reviews* 2001, *101* (9), 2921-2990.
22. Keddie, D. J., A guide to the synthesis of block copolymers using reversible-addition fragmentation chain transfer (RAFT) polymerization. *Chemical Society Reviews* 2014, *43* (2), 496-505.
23. Chernikova, E. V.; Sivtsov, E. V., Reversible addition-fragmentation chain-transfer polymerization: Fundamentals and use in practice. *Polymer Science, Series B* 2017, *59* (2), 117-146.
24. Perrier, S., 50th Anniversary Perspective: RAFT Polymerization—A User Guide. *Macromolecules* 2017, *50* (19), 7433-7447.
25. Goto, A.; Fukuda, T., Kinetics of living radical polymerization. *Progress in Polymer Science* 2004, *29* (4), 329-385.
26. Chai, X. S.; Schork, F. J.; DeCinque, A.; Wilson, K., Measurement of the Solubilities of Vinylic Monomers in Water. *Industrial & Engineering Chemistry Research* 2005, *44* (14), 5256-5258.
27. Lovell, P. A.; El-Aasser, M. S., *Emulsion Polymerization and Emulsion Polymers*. Wiley: 1997.
28. Mark, H. F.; Kroschwitz, J. I., *Encyclopedia of polymer science and engineering*. Wiley: 1985.
29. Jiang, S.; Sudol, E. D.; Dimonie, V. L.; El-Aasser, M. S., Kinetics of dispersion polymerization: Effect of medium composition. *Journal of Polymer Science Part A: Polymer Chemistry* 2008, *46* (11), 3638-3647.
30. Reed, W. F.; Alb, A. M., *Monitoring Polymerization Reactions: From Fundamentals to Applications*. 2014; Vol. 9780470917381, p 1-473.
31. Szabo, T. L., Chapter 2 - Molecular structures and polymer manufacture. In *Plastics (Third Edition)*, Szabo, T. L., Ed. Butterworth-Heinemann: Oxford, 2005; p 21-54.
32. Brandrup, J.; Immergut, E. H.; Grulke, E. A.; Abe, A.; Bloch, D. R., *Polymer handbook*. Wiley New York: 1999; Vol. 89.
33. Minato, H.; Iwakawa, M., Generation of Free Radicals at Subzero Temperatures. IV.1 On the Mechanism of Generation of Free Radicals from the Sodium Formaldehyde Sulfoxylate—Iron—Hydroperoxide System. *Polymer Journal* 1974, *6*, 234.
34. Krishna Mohan, S., Green solvents for polymerization of methyl methacrylate to poly(methyl methacrylate). In *Green Solvents I: Properties and Applications in Chemistry*, 2012; p 251-298.
35. McAllister, T. D.; Farrand, L. D.; Howdle, S. M., Improved Particle Size Control for the Dispersion Polymerization of Methyl methacrylate in Supercritical Carbon Dioxide. *Macromolecular Chemistry and Physics* 2016, *217* (20), 2294-2301.
36. Metz, B.; Davidson, O.; de Coninck, H.; Loos, M.; Meyer, L., IPCC Special Report on Carbon Dioxide Capture and Storage. In *Annex 1: Properties of CO_2 and carbon-based fuels*, IPCC: Cambridge, UK, 2005; p 387-388.
37. DeSimone, J. M.; Guan, Z.; Elsbernd, C. S., Synthesis of Fluoropolymers in Supercritical Carbon Dioxide. *Science* 1992, *257* (5072), 945-947.

38. Sabine, B.; Michael, B.; Christoph, I.; Almut, W., Homogeneous free-radical polymerization of styrene in supercritical CO2. *Macromolecular Rapid Communications* 1999, *20* (1), 26-32.
39. Rindfleisch, F.; DiNoia, T. P.; McHugh, M. A., Solubility of Polymers and Copolymers in Supercritical CO2. *The Journal of Physical Chemistry* 1996, *100* (38), 15581-15587.
40. Domingo, C.; Vega, A.; Fanovich, M. A.; Elvira, C.; Subra, P., Behavior of poly(methyl methacrylate)–based systems in supercritical CO2 and CO2 plus cosolvent: Solubility measurements and process assessment. *Journal of Applied Polymer Science* 2003, *90* (13), 3652-3659.
41. Romack, T. J.; Maury, E. E.; DeSimone, J. M., Precipitation Polymerization of Acrylic Acid in Supercritical Carbon Dioxide. *Macromolecules* 1995, *28* (4), 912-915.
42. D., H. D.; V., P. M., Emulsion copolymerization of D,L-lactide and glycolide in supercritical carbon dioxide. *Journal of Polymer Science Part A: Polymer Chemistry* 2001, *39* (4), 562-570.
43. Santos, T. M. M.; Rebelatto, E. A.; Chaves, B. B.; Lanza, M.; Oliveira, J. V.; Albuquerque, E. C. M. C.; Vieira de Melo, S. A. B., High pressure phase equilibrium data for carbon dioxide, methyl methacrylate and poly (dimethylsiloxane) systems. *The Journal of Supercritical Fluids* 2019, *143*, 346-352.
44. DeSimone, J. M.; Maury, E. E.; Menceloglu, Y. Z.; McClain, J. B.; Romack, T. J.; Combes, J. R., Dispersion Polymerizations in Supercritical Carbon Dioxide. *Science* 1994, *265* (5170), 356-359.
45. Hsiao, Y.-L.; Maury, E. E.; DeSimone, J. M.; Mawson, S.; Johnston, K. P., Dispersion Polymerization of Methyl Methacrylate Stabilized with Poly(1,1-dihydroperfluorooctyl acrylate) in Supercritical Carbon Dioxide. *Macromolecules* 1995, *28* (24), 8159-8166.
46. Christian, P.; Giles, M. R.; Griffiths, R. M. T.; Irvine, D. J.; Major, R. C.; Howdle, S. M., Free Radical Polymerization of Methyl Methacrylate in Supercritical Carbon Dioxide Using a Pseudo-Graft Stabilizer: Effect of Monomer, Initiator, and Stabilizer Concentrations. *Macromolecules* 2000, *33* (25), 9222-9227.
47. Rosell, A.; Storti, G.; Morbidelli, M.; Bratton, D.; Howdle, S. M., Dispersion Polymerization of Methyl Methacrylate in Supercritical Carbon Dioxide Using a Pseudo-Graft Stabilizer: Role of Reactor Mixing. *Macromolecules* 2004, *37* (8), 2996-3004.
48. Shaffer, K. A.; Jones, T. A.; Canelas, D. A.; DeSimone, J. M.; Wilkinson, S. P., Dispersion Polymerizations in Carbon Dioxide Using Siloxane-Based Stabilizers. *Macromolecules* 1996, *29* (7), 2704-2706.
49. Giles, M. R.; Hay, J. N.; Howdle, S. M.; Winder, R. J., Macromonomer surfactants for the polymerisation of methyl methacrylate in supercritical CO2. *Polymer* 2000, *41* (18), 6715-6721.
50. Christian, P.; Giles, M. R.; Howdle, S. M.; Major, R. C.; Hay, J. N., The wall effect: how metal/radical interactions can affect polymerisations in supercritical carbon dioxide. *Polymer* 2000, *41* (4), 1251-1256.
51. Wang, W.; Griffiths, R. M. T.; Giles, M. R.; Williams, P.; Howdle, S. M., Monitoring dispersion polymerisations of methyl methacrylate in supercritical carbon dioxide. *European Polymer Journal* 2003, *39* (3), 423-428.

52. Oliveira, P. F.; Machado, R. A. F.; Barth, D.; Acosta, E. D., Dispersion polymerization of methyl methacrylate in supercritical carbon dioxide using vinyl terminated poly(dimethylsiloxane). *Chemical Engineering and Processing: Process Intensification* 2016, *103*, 46-52.
53. Han, S. H.; Park, K. K.; Lee, S. H., Polymerization of methyl methacrylate in carbon dioxide using glycidyl methacrylate linked reactive stabilizer: Effect of pressure, reaction time, and mixing. *Macromolecular Research* 2009, *17* (1), 51-57.
54. Wang, R.; Cheung, H. M., A new PDMS macromonomer stabilizer for dispersion polymerization of styrene in supercritical carbon dioxide. *Journal of Applied Polymer Science* 2004, *93* (2), 545-549.
55. Giles, M. R.; Howdle, S. M., New unsaturated surfactants for the dispersion polymerisation of methyl methacrylate in supercritical carbon dioxide. *European Polymer Journal* 2001, *37* (7), 1347-1351.
56. Flick, E. W., *Plastics additives: an industrial guide [electronic resource]*. 2nd ed. ed.; Park Ridge, N.J., U.S.A. : Noyes: Park Ridge, N.J., U.S.A., 1993.
57. Ash, M.; Ash, I., *Handbook of plastics and rubber additives [electronic resource]*. 2nd ed.; Synapse Information Resources: Endicott, N.Y., 2013.
58. Murphy, J., *Additives for plastics handbook [electronic resource]*. 2nd ed.; Elsevier Advanced Technology: Oxford, UK/New York, NY, 2001.
59. Wensing, M.; Uhde, E.; Salthammer, T., Plastics additives in the indoor environment—flame retardants and plasticizers. *Science of The Total Environment* 2005, *339* (1), 19-40.
60. Bucknall, C. B., Blends containing core-shell impact modifiers Part 1. Structure and tensile deformation mechanisms (IUPAC Technical Report). *Pure and Applied Chemistry* 2001, *73* (6), 897-912.
61. Bucknall, C. B.; Ajroldi, G., Blends containing core–shell impact modifiers. Part 3 – Effects of temperature on tensile impact behaviour. *Plastics, Rubber and Composites* 2001, *30* (8), 377-383.
62. Bucknall, C. B., Blends containing core–shell impact modifiers. Part 5 – Ductile–brittle transition temperatures in impact and slow bending. *Plastics, Rubber and Composites* 2004, *33* (6), 242-248.
63. Bucknall, C. B.; Altstädt, V., Blends containing core–shell impact modifiers. Part 4 – Fatigue crack growth behaviour. 2004, *33* (6), 234-241.
64. Jansen, B. J. P.; Rastogi, S.; Meijer, H. E. H.; Lemstra, P. J., Rubber-Modified Glassy Amorphous Polymers Prepared via Chemically Induced Phase Separation. 3. Influence of the Strain Rate on the Microscopic Deformation Mechanism. *Macromolecules* 1999, *32* (19), 6283-6289.
65. Meijer, H. E. H.; Govaert, L. E., Mechanical performance of polymer systems: The relation between structure and properties. *Progress in Polymer Science* 2005, *30* (8), 915-938.
66. Ramli, R. A.; Laftah, W. A.; Hashim, S., Core–shell polymers: a review. *RSC Advances* 2013, *3* (36), 15543.
67. Christian, P.; Giles, M. R.; Griffiths, R. M. T.; Irvine, D. J.; Major, R. C.; Howdle, S. M., Free radical polymerization of methyl methacrylate in supercritical carbon dioxide using a pseudo-graft stabilizer: effect of monomer, initiator, and stabilizer concentrations. *Macromolecules* 2000, *33* (25), 9222-9227.

68. Giles, M. R.; Griffiths, R. M. T.; Irvine, D. J.; Howdle, S. M., The polymerisation of functionalised methacrylate monomers in supercritical carbon dioxide. *European Polymer Journal* 2003, *39* (9), 1785-1790.
69. Alauhdin, M.; Bennett, T. M.; He, G.; Bassett, S. P.; Portale, G.; Bras, W.; Hermida-Merino, D.; Howdle, S. M., Monitoring morphology evolution within block copolymer microparticles during dispersion polymerisation in supercritical carbon dioxide: a high pressure SAXS study. *Polymer Chemistry* 2019, *10* (7), 860-871.
70. Galia, A.; Giaconia, A.; Iaia, V.; Filardo, G., Synthesis of hydrophilic polymers in supercritical carbon dioxide in the presence of a siloxane-based macromonomer surfactant: Heterogeneous polymerization of 1-vinyl-2 pyrrolidone. *Journal of Polymer Science Part A: Polymer Chemistry* 2004, *42* (1), 173-185.
71. Kobayashi, S.; Uyama, H.; Yamamoto, I.; Matsumoto, Y., Preparation of Monodispersed Poly(methyl methacrylate) Particle in the Size of Micron Range. *Polymer Journal* 1990, *22*, 759.
72. Allen, T., Chapter 2 - Data presentation and interpretation. In *Powder Sampling and Particle Size Determination*, Allen, T., Ed. Elsevier: Amsterdam, 2003; p 56-141.
73. Yamashita, C.; Chung, M. M. S.; dos Santos, C.; Mayer, C. R. M.; Moraes, I. C. F.; Branco, I. G., Microencapsulation of an anthocyanin-rich blackberry (Rubus spp.) by-product extract by freeze-drying. *LWT* 2017, *84*, 256-262.
74. Mathurin, J.; Deniset-Besseau, A.; Bazin, D.; Dartois, E.; Wagner, M.; Dazzi, A., Photothermal AFM-IR spectroscopy and imaging: Status, challenges, and trends. *Journal of Applied Physics* 2022, *131* (1), 010901.
75. Haven, J. J.; Junkers, T., Online Monitoring of Polymerizations: Current Status. *European Journal of Organic Chemistry* 2017, *2017*, 6474-6482.
76. Gladden, L. F., Nuclear Magnetic Resonance in Chemical Engineering - Principles and Applications. *Chemical Engineering Science* 1994, *49* (20), 3339-3408.
77. Embirucu, M.; Lima, E. L.; Pinto, J. C., Survey of advanced control of polymerization reactors. *Polym. Eng. Sci.* 1996, *36* (4), 433-447.
78. Alb, A. M.; Reed, W. F., Fundamental Measurements in Online Polymerization Reaction Monitoring and Control with a Focus on ACOMP. *Macromolecular Reaction Engineering* 2010, *4* (8), 470-485.
79. Siesler, H. W., Near Infrared Spectroscopy for Polymer Reaction and Process Control: Synthesis, Processing and Recycling. *NIR news* 1995, *6* (1), 3-6.
80. van den Broek, W. H. A. M.; Derks, E. P. P. A.; van de Ven, E. W.; Wienke, D.; Geladi, P.; Buydens, L. M. C., Plastic identification by remote sensing spectroscopic NIR imaging using kernel partial least squares (KPLS). *Chemometrics and Intelligent Laboratory Systems* 1996, *35* (2), 187-197.
81. Vedula, S.; Hansen, M. G., In-line fiber-optic near-infrared spectroscopy: Monitoring of rheological properties in an extrusion process. Part II. *Journal of Applied Polymer Science* 1998, *68* (6), 873-889.
82. Lachenal, G.; Stevenson, I.; Celette, N., Near-infrared transmittance spectroscopy for radiochemical ageing of EPDM. *Analyst* 2001, *126* (12), 2201-2206.
83. Shield, S. R.; Ghebremeskel, G. N., Use of mid- and near-infrared techniques as tools for characterizing blends of copolymers of styrene–butadiene and acrylonitrile–butadiene. *Journal of Applied Polymer Science* 2003, *88* (7), 1653-1658.

84. Rohe, T.; Becker, W.; Kölle, S.; Eisenreich, N.; Eyerer, P., Near infrared (NIR) spectroscopy for in-line monitoring of polymer extrusion processes. *Talanta* 1999, *50* (2), 283-90.
85. Nagata, T.; Ohshima, M.; Tanigaki, M., In-line monitoring of polyethylene density using near infrared (NIR) spectroscopy. *Polymer Engineering & Science* 2000, *40* (5), 1107-1113.
86. Levere, M. E.; Willoughby, I.; O'Donohue, S.; de Cuendias, A.; Grice, A. J.; Fidge, C.; Becer, C. R.; Haddleton, D. M., Assessment of SET-LRP in DMSO using online monitoring and Rapid GPC. *Polymer Chemistry* 2010, *1* (7), 1086-1094.
87. Florenzano, F. H.; Strelitzki, R.; Reed, W. F., Absolute, On-Line Monitoring of Molar Mass during Polymerization Reactions. *Macromolecules* 1998, *31* (21), 7226-7238.
88. McAfee, T.; Jarand, C. W.; Zekoski, T.; Montgomery, R.; Reed, W. F., Coupling of NMR to ACOMP for Terpolymerization Monitoring and Control. *Macromolecular Reaction Engineering* 2019, *13* (6), 1900039.
89. Ollagnier, J.; Tassaing, T.; Harrisson, S.; Destarac, M., Application of online infrared spectroscopy to study the kinetics of precipitation polymerization of acrylic acid in supercritical carbon dioxide. *React. Chem. Eng.* 2016, *1* (4), 372-378.
90. Richards, J. R.; Congalidis, J. P., Measurement and control of polymerization reactors. *Computers & Chemical Engineering* 2006, *30* (10), 1447-1463.
91. Grignard, B.; Gilbert, B.; Malherbe, C.; Jérôme, C.; Detrembleur, C., Online Monitoring of Heterogeneous Polymerizations in Supercritical Carbon Dioxide by Raman Spectroscopy. *ChemPhysChem* 2012, *13* (11), 2666-2670.
92. Howdle, S. M.; Stanley, K.; Popov, V. K.; Bagratashvili, V. N., Can High-Pressure Raman Spectroscopy Be Simplified? A Microscale Optical-Fiber Capillary Cell for the Study of Supercritical Fluids. *Appl. Spectrosc.* 1994, *48* (2), 214-218.
93. Lacroix-Desmazes, P.; Guyot, A., Reactive surfactants in heterophase polymerization. *Colloid and Polymer Science* 1996, *274* (12), 1129-1136.
94. Shen, S.; Sudol, E. D.; El-Aasser, M. S., Dispersion polymerization of methyl methacrylate: Mechanism of particle formation. *Journal of Polymer Science Part A: Polymer Chemistry* 1994, *32* (6), 1087-1100.
95. Penders, M. H. G. M.; Vrij, A., A turbidity study on colloidal silica particles in concentrated suspensions using the polydisperse adhesive hard sphere model. *The Journal of Chemical Physics* 1990, *93* (5), 3704-3711.
96. Fehrenbacher, U.; Ballauff, M., Kinetics of the early stage of dispersion polymerization in supercritical CO 2 as monitored by turbidimetry. 2. Particle formation and locus of polymerization. *Macromolecules* 2002, *35* (9), 3653-3661.
97. Li, G.; Yates, M. Z.; Johnston, K. P.; Howdle, S. M., In-Situ Investigation on the Mechanism of Dispersion Polymerization in Supercritical Carbon Dioxide. *Macromolecules* 2000, *33* (11), 4008-4014.
98. O'Neill, M. L.; Yates, M. Z.; Johnston, K. P.; Smith, C. D.; Wilkinson, S. P., Dispersion Polymerization in Supercritical CO2 with a Siloxane-Based Macromonomer: 1. The Particle Growth Regime. *Macromolecules* 1998, *31* (9), 2838-2847.
99. O'Neill, M. L.; Yates, M. Z.; Johnston, K. P.; Smith, C. D.; Wilkinson, S. P., Dispersion Polymerization in Supercritical CO2 with Siloxane-Based Macromonomer. 2. The Particle Formation Regime. *Macromolecules* 1998, *31* (9), 2848-2856.

100. Mantelis, C. A.; Meyer, T., Supercritical reaction calorimetry: Versatile tool for measuring heat transfer properties and monitoring chemical reactions in supercritical fluids. *Industrial and Engineering Chemistry Research* 2008, *47* (10), 3372-3379.
101. Jiang, S.; Sudol, E. D.; Dimonie, V. L.; El-Aasser, M. S., Kinetics of dispersion polymerization of methyl methacrylate and n-butyl acrylate: Effect of initiator concentration. *Macromolecules* 2007, *40* (14), 4910-4916.
102. Thurecht, K. J.; Villarroya, S.; Zhou, J.; Howdle, S. M.; Heise, A.; Degeus, M.; Wyatt, M. F., Kinetics of enzymatic ring-opening polymerization of ε-caprolactone in supercritical carbon dioxide. *Macromolecules* 2006, *39* (23), 7967-7972.
103. Mueller, P. A.; Storti, G.; Morbidelli, M., Detailed modelling of MMA dispersion polymerization in supercritical carbon dioxide. *Chemical Engineering Science* 2005, *60* (7), 1911.
104. Chatzidoukas, C.; Pladis, P.; Kiparissides, C., Mathematical modeling of dispersion polymerization of methyl methacrylate in supercritical carbon dioxide. *Industrial and Engineering Chemistry Research* 2003, *42* (4), 743-751.
105. Mantelis, C. A.; Meyer, T., Reaction monitoring of the MMA polymerization at marginal dispersion stability. *AIChE Journal* 2008, *54* (2), 529-536.
106. Barrett, K. E. J.; Thomas, H. R., Kinetics of dispersion polymerization of soluble monomers. I. Methyl methacrylate. *Journal of Polymer Science Part A-1: Polymer Chemistry* 1969, *7* (9), 2621-2650.
107. Bilgin, S.; Tomovska, R.; Asua, J. M., Surfactant-free high solids content polymer dispersions. *Polymer* 2017, *117*, 64-75.
108. Paquet, D. A.; Ray, W. H., Tubular reactors for emulsion polymerization: I. Experimental investigation. *AIChE Journal* 1994, *40* (1), 73-87.
109. Bhanu, V. A.; Kishore, K., Role of oxygen in polymerization reactions. *Chemical Reviews* 1991, *91* (2), 99-117.
110. Loeker, F. C.; Duxbury, C. J.; Kumar, R.; Gao, W.; Gross, R. A.; Howdle, S. M., Enzyme-Catalyzed Ring-Opening Polymerization of ε-Caprolactone in Supercritical Carbon Dioxide. *Macromolecules* 2004, *37* (7), 2450-2453.
111. Mueller, P. A.; Storti, G.; Morbidelli, M.; Mantelis, C. A.; Meyer, T., Dispersion Polymerization of Methyl Methacrylate in Supercritical Carbon Dioxide: Control of Molecular Weight Distribution by Adjusting Particle Surface Area. *Macromolecular Symposia* 2007, *259* (1), 218-225.
112. Hoefling, T. A.; Enick, R. M.; Beckman, E. J., Microemulsions in near-critical and supercritical carbon dioxide. *The Journal of Physical Chemistry* 1991, *95* (19), 7127-7129.
113. Liu, T.; Desimone, J. M.; Roberts, G. W., Kinetics of the precipitation polymerization of acrylic acid in supercritical carbon dioxide: The locus of polymerization. *Chemical Engineering Science* 2006, *61* (10), 3129-3139.
114. Yuvaraj, H.; Hwang, H. S.; Kim, W. S.; Kim, H. G.; Jeong, E. D.; Lim, K. T., Dispersion polymerization of methyl methacrylate in supercritical CO2 in the presence of non-fluorous random copolymers. *European Polymer Journal* 2008, *44* (7), 2253-2261.
115. Chernyshev, A. V.; Soini, A. E.; Maltsev, V. P.; Soini, E., A model of complete classical treatment of dispersion radical polymerization kinetics. *Macromolecules* 1998, *31* (19), 6455-6460.

116. Porter, M. D.; Skinner, G. B., The steady-state approximation in free-radical calculations. A numerical example. *Journal of Chemical Education* 1976, *53* (6), 366.
117. Edmondson, S.; Gilbert, M., Chapter 2 - The Chemical Nature of Plastics Polymerization. In *Brydson's Plastics Materials (Eighth Edition)*, Butterworth-Heinemann: 2017; p 19-37.
118. Kukulj, D.; Davis, T. P.; Gilbert, R. G., Chain Transfer to Monomer in the Free-Radical Polymerizations of Methyl Methacrylate, Styrene, and α-Methylstyrene. *Macromolecules* 1998, *31* (4), 994-999.
119. NIST CO_2 data. https://webbook.nist.gov/cgi/inchi/InChI%3D1S/CO2/c2-1-3 (accessed 04/02/2021).
120. Shen, J.; Tian, Y.; Wang, G.; Yang, M., Modelling and kinetic study on radical polymerization of methyl methacrylate in bulk, 1. Propagation and termination rate coefficients and initiation efficiency. *Die Makromolekulare Chemie* 1991, *192* (11), 2669-2685.
121. Gregory, A. M.; Thurecht, K. J.; Howdle, S. M., Controlled dispersion polymerization of methyl methacrylate in supercritical carbon dioxide via RAFT. *Macromolecules* 2008, *41* (4), 1215-1222.
122. Moad, G.; Rizzardo, E.; Thang, S. H., Towards living radical polymerisation. *Acc. Chem. Res.* 2008, *41* (1133-1142).
123. Moad, G.; Rizzardo, E.; Thang, S. H., Living Radical Polymerization by RAFT Process. *Aust. J. Chem* 2005, *58*, 379-410.
124. Blanazs, A.; Madsen, J.; Battaglia, G.; Ryan, A. J.; Armes, S. P., Mechanistic insights for block copolymer morphologies: how do worms form vesicles? *J. Am. Chem. Soc.* 2011, *133* (41), 16581-7.
125. Fielding, L. A.; Derry, M. J.; Ladmiral, V.; Rosselgong, J.; Rodrigues, A. M.; Ratcliffe, L. P. D.; Sugihara, S.; Armes, S. P., RAFT dispersion polymerization in non-polar solvents: facile production of block copolymer spheres, worms and vesicles in n-alkanes. *Chemical Science* 2013, *4* (5), 2081.
126. Canelas, D. A.; Betts, D. E.; DeSimone, J. M., Dispersion Polymerization of Styrene in Supercritical Carbon Dioxide: Importance of Effective Surfactants. *Macromolecules* 1996, *29* (8), 2818-2821.
127. Ewing, A. V.; Kazarian, S. G., Current trends and opportunities for the applications of in situ vibrational spectroscopy to investigate the supercritical fluid processing of polymers. *The Journal of Supercritical Fluids* 2018, *134*, 88-95.
128. Dubois, P.; Jerome, R.; Teyssie, P., Macromolecular engineering of polylactones and polylactides. 3. Synthesis, characterization, and applications of poly(iε-caprolactone) macromonomers. *Macromolecules* 1991, *24* (5), 977-981.
129. Englezou, G.; Kortsen, K.; Pacheco, A. A. C.; Cavanagh, R.; Lentz, J. C.; Krumins, E.; Sanders-Velez, C.; Howdle, S. M.; Nedoma, A. J.; Taresco, V., 2-Methyltetrahydrofuran (2-MeTHF) as a versatile green solvent for the synthesis of amphiphilic copolymers via ROP, FRP, and RAFT tandem polymerizations. *Journal of Polymer Science* 2020.
130. Takwa, M.; Xiao, Y.; Simpson, N.; Malmström, E.; Hult, K.; Koning, C. E.; Heise, A.; Martinelle, M., Lipase Catalyzed HEMA Initiated Ring-Opening Polymerization: In Situ Formation of Mixed Polyester Methacrylates by Transesterification. *Biomacromolecules* 2008, *9* (2), 704-710.

131. Xiao, Y.; Takwa, M.; Hult, K.; Koning, C. E.; Heise, A.; Martinelle, M., Systematic Comparison of HEA and HEMA as Initiators in Enzymatic Ring-Opening Polymerizations. *Macromolecular Bioscience* 2009, *9* (7), 713-720.
132. Kortsen, K.; Pacheco, A. A. C.; Lentz, J. C.; Taresco, V.; Howdle, S. M., On-line polymerisation monitoring in scCO2: a reliable and inexpensive sampling method in high pressure applications. *The Journal of Supercritical Fluids* 2020, 105047.
133. Uyama, H.; Kobayashi, S., Dispersion polymerization of styrene in aqueous alcohol solution: Effects of reaction parameters on the polymer particle formation. *Polymer International* 1994, *34* (3), 339-344.
134. Kawaguchi, S.; Ito, K.; Okubo, M., Dispersion Polymerization. *Polymer Particles* 2005, *175*, 299-328.
135. Lovell, P. A.; El-Aasser, M. S., *Emulsion polymerization and emulsion polymers / edited by Peter A. Lovell and Mohamed S. El-Aasser*. Chichester : J. Wiley: Chichester, 1997.
136. Kroupa, M.; Vonka, M.; Kosek, J., Modeling the Mechanism of Coagulum Formation in Dispersions. *Langmuir* 2014, *30* (10), 2693-2702.
137. Mantelis, C. A.; Barbey, R.; Fortini, S.; Meyer, T., Free-Radical Dispersion Polymerization of Methyl Methacrylate in Supercritical Carbon Dioxide: A Parametric Analysis with Reaction Calorimetry. *Macromolecular Reaction Engineering* 2007, *1* (1), 78-85.
138. Richez, A. P.; Farrand, L.; Goulding, M.; Wilson, J. H.; Lawson, S.; Biggs, S.; Cayre, O. J., Poly(dimethylsiloxane)-Stabilized Polymer Particles from Radical Dispersion Polymerization in Nonpolar Solvent: Influence of Stabilizer Properties and Monomer Type. *Langmuir* 2014, *30* (5), 1220-1228.
139. Tsui, Y.-Y.; Chou, J.-R.; Hu, Y.-C., Blade Angle Effects on the Flow in a Tank Agitated by the Pitched-Blade Turbine. *Journal of Fluids Engineering* 2006, *128* (4), 774-782.
140. Gabriele, A.; Nienow, A. W.; Simmons, M. J. H., Use of angle resolved PIV to estimate local specific energy dissipation rates for up- and down-pumping pitched blade agitators in a stirred tank. *Chemical Engineering Science* 2009, *64* (1), 126-143.
141. Zhang, X.; Shen, S.; Fan, L., Uniform Polystyrene Particles by Dispersion Polymerization in Different Dispersion Medium. *Polymer Bulletin* 2008, *61* (1), 19-26.
142. Antl, L.; Goodwin, J. W.; Hill, R. D.; Ottewill, R. H.; Owens, S. M.; Papworth, S.; Waters, J. A., The preparation of poly(methyl methacrylate) latices in non-aqueous media. *Colloids and Surfaces* 1986, *17* (1), 67-78.
143. Chen, Y.; Chen, Y.-L., Aqueous dispersions of polyurethane anionomers: Effects of countercation. *Journal of Applied Polymer Science* 1992, *46* (3), 435-443.
144. Lok, K. P.; Ober, C. K., Particle size control in dispersion polymerization of polystyrene. *Canadian Journal of Chemistry* 1985, *63* (1), 209-216.
145. Tseng, C. M.; Lu, Y. Y.; El-Aasser, M. S.; Vanderhoff, J. W., Uniform polymer particles by dispersion polymerization in alcohol. *Journal of Polymer Science Part A: Polymer Chemistry* 1986, *24* (11), 2995-3007.
146. Watanabe, S.; Kobayashi, T.; Sumitomo, H.; Murata, M.; Masuda, Y., Preparation of monodisperse PMMA particles by dispersion polymerization of MMA using poly(styrene-co-methacrylic acid) copolymer as a steric stabilizer. *Polymer Bulletin* 2010, *65* (6), 543-550.

147. Yates, M. Z.; O'Neil, M. L.; Johnston, K. P., Emulsion Stabilization and Flocculation in CO2. 2. Dynamic Light Scattering. *Macromolecules* 1997, *30* (17), 5060-5067.
148. Pu, D. W.; Soh, M.; Zetterlund, P. B.; Lucien, F. P., Exploiting the homogeneous expansion limit of CO2-expanded media for the synthesis of polymeric nanoparticles. *The Journal of Supercritical Fluids* 2013, *78*, 89-94.
149. Pu, D. W.; Devitt, M. P.; Thickett, S. C.; Lucien, F. P.; Zetterlund, P. B., Dispersion polymerization of styrene in CO2-expanded ethanol. *Polymer* 2013, *54* (25), 6689-6694.
150. Pu, D. W.; Lucien, F. P.; Zetterlund, P. B., Radical polymerization of CO2-induced emulsions: A novel route to polymeric nanoparticles. *Journal of Polymer Science Part A: Polymer Chemistry* 2011, *49* (20), 4307-4311.
151. Lepilleur, C.; Beckman, E. J., Dispersion Polymerization of Methyl Methacrylate in Supercritical CO2. *Macromolecules* 1997, *30* (4), 745-756.
152. Pacheco, A. A. C.; da Silva Filho, A. F.; Kortsen, K.; Hanson-Heine, M. W. D.; Taresco, V.; Hirst, J. D.; Lansalot, M.; D'Agosto, F.; Howdle, S. M., Influence of structure and solubility of chain transfer agents on the RAFT control of dispersion polymerisation in scCO2. *Chemical Science* 2021, *12* (3), 1016-1030.
153. Goddard, A. R.; Pérez-Nieto, S.; Passos, T. M.; Quilty, B.; Carmichael, K.; Irvine, D. J.; Howdle, S. M., Controlled polymerisation and purification of branched poly(lactic acid) surfactants in supercritical carbon dioxide. *Green Chemistry* 2016, *18* (17), 4772-4786.
154. Licence, P.; Dellar, M. P.; Wilson, R. G. M.; Fields, P. A.; Litchfield, D.; Woods, H. M.; Poliakoff, M.; Howdle, S. M., Large-aperture variable-volume view cell for the determination of phase-equilibria in high pressure systems and supercritical fluids. *Review of Scientific Instruments* 2004, *75* (10), 3233-3236.
155. Curia, S.; De Focatiis, D. S. A.; Howdle, S. M., High-pressure rheological analysis of CO2-induced melting point depression and viscosity reduction of poly(ε-caprolactone). *Polymer* 2015, *69*, 17-24.
156. Smith, S. D.; DeSimone, J. M.; Huang, H.; York, G.; Dwight, D. W.; Wilkes, G. L.; McGrath, J. E., Synthesis and characterization of poly(methyl methacrylate)-g-poly(dimethylsiloxane)copolymers. I. Bulk and surface characterization. *Macromolecules* 1992, *25* (10), 2575-2581.
157. Haddleton, A. J.; Bennett, T. M.; Chen, X.; Atkinson, R. L.; Taresco, V.; Howdle, S. M., Synthesis of two-phase polymer particles in supercritical carbon dioxide. *Polymer Chemistry* 2020, *11* (31), 5029-5039.
158. Melnichenko, Y. B.; Kiran, E.; Wignall, G. D.; Heath, K. D.; Salaniwal, S.; Cochran, H. D.; Stamm, M., Pressure- and Temperature-Induced Transitions in Solutions of Poly(dimethylsiloxane) in Supercritical Carbon Dioxide. *Macromolecules* 1999, *32* (16), 5344-5347.
159. Uzun, N. I.; Akgün, M.; Baran, N.; Deniz, S.; Dinçer, S., Methyl Methacrylate + Carbon Dioxide Phase Equilibria at High Pressures. *Journal of Chemical & Engineering Data* 2005, *50* (4), 1144-1147.
160. Kortsen, K.; Fowler, H. R.; Jacob, P. L.; Krumins, E.; Lentz, J. C.; Souhil, M. R. A.; Taresco, V.; Howdle, S. M., Exploiting the tuneable density of scCO2 to improve particle size control for dispersion polymerisations in the presence of poly(dimethyl siloxane) stabilisers. *European Polymer Journal* 2022, 111108.

161. Jones, C. D.; Lyon, L. A., Shell-Restricted Swelling and Core Compression in Poly(N-isopropylacrylamide) Core–Shell Microgels. *Macromolecules* 2003, *36* (6), 1988-1993.
162. Downey, J. S.; Frank, R. S.; Li, W.-H.; Stöver, H. D. H., Growth Mechanism of Poly(divinylbenzene) Microspheres in Precipitation Polymerization. *Macromolecules* 1999, *32* (9), 2838-2844.
163. Sasa, N.; Yamaoka, T., Surface-activated photopolymer microgels. *Advanced Materials* 1994, *6* (5), 417-421.
164. Khan, A. K.; Ray, B. C.; Dolui, S. K., Preparation of core-shell emulsion polymer and optimization of shell composition with respect to opacity of paint film. *Progress in Organic Coatings* 2008, *62* (1), 65-70.
165. Cao, L.-Q.; Chen, L.-P.; Cui, P.-Y.; Wang, J.-D., Synthesis of PNIPA/PDMS-g-PAA core-shell composites in supercritical carbon dioxide. *Journal of Applied Polymer Science* 2008, *108* (6), 3843-3850.
166. Fu, X.; Bao, L.; Lei, J.; Wang, J., Preparation and characterization of a core-shell impact modifier based on (Acrylates and styrene)-grafted ground tire rubber and its poly(vinyl chloride) composites. *Journal of Vinyl and Additive Technology* 2016, *22* (4), 452-459.
167. Lee, J.-S.; Chang, F.-C., Effect of the core-shell impact modifier shell thickness on toughening PVC. *Polym. Eng. Sci.* 2004, *44* (10), 1885-1889.
168. Schärtl, W., Crosslinked Spherical Nanoparticles with Core–Shell Topology. *Advanced Materials* 2000, *12* (24), 1899-1908.
169. Saunders, B. R.; Vincent, B., Microgel particles as model colloids: theory, properties and applications. *Advances in Colloid and Interface Science* 1999, *80* (1), 1-25.
170. Brandes, H. Tips for Maximising the Performance of Core-Shell Columns. https://www.chromatographyonline.com/view/tips-for-maximizing-the-performance-of-core-shell-columns (accessed 28/07/2022).
171. Dhiman, S.; Yadav, A.; Debnath, N.; Das, S., Application of Core/Shell Nanoparticles in Smart Farming: A Paradigm Shift for Making the Agriculture Sector More Sustainable. *Journal of Agricultural and Food Chemistry* 2021, *69* (11), 3267-3283.
172. Meesorn, W.; Calvino, C.; Natterodt, J. C.; Zoppe, J. O.; Weder, C., Bio-Inspired, Self-Toughening Polymers Enabled by Plasticizer-Releasing Microcapsules. *Advanced Materials* 2019, *31* (14), 1807212.
173. Shieh, Y.-T.; Lin, P.-Y.; Kuo, S.-W., Sequence length distribution affects the lower critical solution temperature, glass transition temperature, and CO2-responsiveness of N-isopropylacrylamide/methacrylic acid copolymers. *Polymer* 2018, *143*, 258-270.
174. Saunders, B. R.; Laajam, N.; Daly, E.; Teow, S.; Hu, X.; Stepto, R., Microgels: From responsive polymer colloids to biomaterials. *Adv Colloid Interface Sci* 2009, *147-148*, 251-62.
175. SpecialChem Selection of Impact Modifiers for Polymers. https://polymer-additives.specialchem.com/selection-guide/impact-modifiers-for-polymers (accessed 01/08/2022).

176. Kechekyan, P. A.; Arzhakova, O. V.; Kechekyan, A. S.; Dolgova, A. A.; Volynskii, A. L., The effect of characteristic self-generated defects on the mechanical behavior of poly(ethylene terephthalate) fibers and films. *Polymer* 2019, *176*, 11-19.
177. Van Krevelen, D. W.; Te Nijenhuis, K., Chapter 13 - Mechanical Properties of Solid Polymers. In *Properties of Polymers (Fourth Edition)*, Van Krevelen, D. W.; Te Nijenhuis, K., Eds. Elsevier: Amsterdam, 2009; p 383-503.
178. Windle, A. H., CHAPTER 32 - A METALLURGIST'S GUIDE TO POLYMERS. In *Physical Metallurgy (Fourth Edition)*, Cahn, R. W.; Haasen†, P., Eds. North-Holland: Oxford, 1996; p 2663-2740.
179. Young, R. J.; Lovell, P. A., Introduction to Polymers. 2011.
180. Cao, L.; Chen, L.; Chen, X.; Zuo, L.; Li, Z., Synthesis of smart core–shell polymer in supercritical carbon dioxide. *Polymer* 2006, *47* (13), 4588-4595.
181. Jennings, J.; Beija, M.; Richez, A. P.; Cooper, S. D.; Mignot, P. E.; Thurecht, K. J.; Jack, K. S.; Howdle, S. M., One-Pot Synthesis of Block Copolymers in Supercritical Carbon Dioxide: A Simple Versatile Route to Nanostructured Microparticles. *Journal of the American Chemical Society* 2012, *134* (10), 4772-4781.
182. Jennings, J.; He, G.; Howdle, S. M.; Zetterlund, P. B., Block copolymer synthesis by controlled/living radical polymerisation in heterogeneous systems. *Chemical Society Reviews* 2016, *45* (18), 5055-5084.
183. Larder, R. R.; Krumins, E.; Jacob, P. L.; Kortsen, K.; Cavanagh, R.; Jiang, L.; Vuotto, C.; Francolini, I.; Tuck, C.; Taresco, V.; Howdle, S. M., Antimicrobial 'inks' for 3D printing: block copolymer-silver nanoparticle composites synthesised using supercritical CO2. *Polymer Chemistry* 2022.
184. He, G.; Bennett, T. M.; Alauhdin, M.; Fay, M. W.; Liu, X.; Schwab, S. T.; Sun, C.-g.; Howdle, S. M., A facile route to bespoke macro- and mesoporous block copolymer microparticles. *Polymer Chemistry* 2018, *9* (27), 3808-3819.
185. Bennett, T. M.; He, G.; Larder, R. R.; Fischer, M. G.; Rance, G. A.; Fay, M. W.; Pearce, A. K.; Parmenter, C. D. J.; Steiner, U.; Howdle, S. M., Clean Block Copolymer Microparticles from Supercritical CO2: Universal Templates for the Facile and Scalable Fabrication of Hierarchical Mesostructured Metal Oxides. *Nano Letters* 2018, *18* (12), 7560-7569.
186. He, G.; Bennett, T. M.; Alias, K.; Jiang, L.; Schwab, S. T.; Alauhdin, M.; Howdle, S. M., In situ crosslinking of nanostructured block copolymer microparticles in supercritical carbon dioxide. *Polymer Chemistry* 2019, *10* (29), 3960-3972.
187. McAllister, T. D.; Bennett, T. M.; Petrillo, C.; Topping, C.; Farrand, L. D.; Smith, N.; Howdle, S. M., Highly coloured and electrophoretically active polymer microparticles via staggered dispersion polymerisation in supercritical carbon dioxide and dodecane. *Journal of Materials Chemistry C* 2019, *7* (39), 12194-12203.
188. Azimi, H. R.; Rezaei, M., Solubility and diffusivity of carbon dioxide in St-MMA copolymers. *The Journal of Chemical Thermodynamics* 2013, *58*, 279-287.
189. Fioretto, D.; Livi, A.; Rolla, P. A.; Socino, G.; Verdini, L., The dynamics of poly(n-butyl acrylate) above the glass transition. *Journal of Physics: Condensed Matter* 1994, *6* (28), 5295-5302.
190. Pathmanathan, K.; Johari, G. P., Dielectric and conductivity relaxations in poly(hema) and of water in its hydrogel. *Journal of Polymer Science Part B: Polymer Physics* 1990, *28* (5), 675-689.

191. Bauri, K.; Roy, S. G.; Arora, S.; Dey, R. K.; Goswami, A.; Madras, G.; De, P., Thermal degradation kinetics of thermoresponsive poly(N-isopropylacrylamide-co-N,N-dimethylacrylamide) copolymers prepared via RAFT polymerization. *Journal of Thermal Analysis and Calorimetry* 2013, *111* (1), 753-761.
192. Fekete, E.; Földes, E.; Pukánszky, B., Effect of molecular interactions on the miscibility and structure of polymer blends. *European Polymer Journal* 2005, *41* (4), 727-736.
193. Effler, L. J.; Berard, M. T., Enhanced impact modifier for rigid PVC formulations. *Journal of Vinyl and Additive Technology* 2003, *9* (1), 19-25.
194. Jiang, H. Y.; Liu, B. J.; Deng, Y. J.; Ma, J. Y.; Cao, C. L.; Zhang, H. X., High-efficiency impact modifier prepared by coagulation emulsion polymerization through internal voiding toughening mechanism. *Polymers for Advanced Technologies* 2015, *26* (2), 182-189.
195. Shant, R.; Kyada, T.; Goyal, R.; Kathayat, T. S., Understanding the Delamination and Its Effect on Charpy Impact Energy in Thick Wall Linepipe Steel. *Journal of Materials and Metallurgical Engineering* 2014, *4*, 31-39.